

UNIVERSITÉ DU QUÉBEC

THÈSE PRÉSENTÉE À
L'UNIVERSITÉ DU QUÉBEC À TROIS-RIVIÈRES

COMME EXIGENCE PARTIELLE
DU DOCTORAT EN GÉNIE ÉLECTRIQUE

PAR
SIMON HISSEM

CONTRIBUTION À LA CONCEPTION DE CONTRÔLEUR POUR DES SYSTÈMES
DE TYPE BOÎTES NOIRES ET DES SYSTÈMES À HAUT DEGRÉ DE FONCTIONS
DE TRANSFERT

AOÛT 2019

Université du Québec à Trois-Rivières

Service de la bibliothèque

Avertissement

L'auteur de ce mémoire ou de cette thèse a autorisé l'Université du Québec à Trois-Rivières à diffuser, à des fins non lucratives, une copie de son mémoire ou de sa thèse.

Cette diffusion n'entraîne pas une renonciation de la part de l'auteur à ses droits de propriété intellectuelle, incluant le droit d'auteur, sur ce mémoire ou cette thèse. Notamment, la reproduction ou la publication de la totalité ou d'une partie importante de ce mémoire ou de cette thèse requiert son autorisation.

UNIVERSITÉ DU QUÉBEC

THESIS PRESENTED TO
UNIVERSITÉ DU QUÉBEC À TROIS-RIVIÈRES

IN PARTIAL FULFILMENT OF THE REQUIEREMNTS
OF THE DEGREE OF DOCTOR OF PHILOSOPHY
IN ELECTRICAL ENGINEERING

BY
SIMON HISSEM

CONTRIBUTION TO THE DESIGN OF CONTROLLER FOR SYSTEMS OF BLACK
BOXES TYPE AND SYSTEMS WITH HIGH DEGREE OF TRANSFER FUNCTIONS

AUGUST 2019

UNIVERSITÉ DU QUÉBEC À TROIS-RIVIÈRES

DOCTORAT EN GÉNIE ÉLECTRIQUE (PH.D.)

Programme offert par l'Université du Québec à Trois-Rivières

CONTRIBUTION À LA CONCEPTION DE CONTRÔLEUR POUR DES SYSTÈMES
DE TYPE BOÎTES NOIRES ET DES SYSTÈMES À HAUT DEGRÉ DE FONCTIONS
DE TRANSFERT

PAR

SIMON HISSEM

Prof. Mamadou L. Doumbia, directeur de recherche Université du Québec à Trois-Rivières

Prof. Alain Goupil, président du jury Université du Québec à Trois-Rivières

Prof. Pelope Adzakpa, évaluateur Cegep de la Gaspésie et des Îles

Prof. Hicham Chaoui, évaluateur Université Carleton à Ottawa

Thèse soutenue le 15/07/19

Abstract

This research presents new reduction method for black box systems and systems with high order transfer functions. This new technique is essentially based on the nature of the three most common output responses with no overshoot, with overshoot only or with overshoot and oscillations. The approach is based on the concept of two similar systems that are not identical. This similarity is made on significant weighted elements that characterize the black box system. The controller will be designed based on the simple projected similar system and applied to the black box or higher order systems. The characteristic of this new reduction method is that every system can be reduced to a similar first order system with the same identified significant weighted elements that will be clearly defined. The merit of this new reduction technique is to avoid all mathematical equations to model the complex system and also to avoid huge mathematical equations to reduce its transfer function to an identical reduced system. The performance of the new reduction method was evaluated and compared with some reduction methods taken from the literature.

New systems called Fibonacci systems are introduced. They are derived from an original first order transfer function. Their characteristics and behaviors are quite impressive and their output signals present multiple intermediate steady states which make them irreducible to a lower order specifically second or third order. The application of reduction methods to these systems in the literature will not be possible. Their polynomial coefficients follow specific distribution with respect to the Golden ratio. The pole locations of these transfer functions follow the Fibonacci pattern and they can be created to an infinite degree following a simple recursive process. These functions have multiple resonance and anti-resonance frequencies organized in a perfect way with respect to each other. Each Fibonacci system has two well

defined Fibonacci boundary systems using Pascal's triangle. The behavior of these systems could describe coupled systems applications, transmission lines, impedance matching and other applications that can be modelled by an infinite LC ladders or infinite spring mass chain.

Keywords: High order transfer function, reduction method, black box system, Pade approximation, Integral square error (ISE), similar systems, Fibonacci irreducible systems, infinite LC ladder and infinite spring mass chain.

Avant-propos

Au terme de ce travail, je tiens à témoigner ma profonde reconnaissance à mon directeur de recherche, le professeur Mamadou Lamine Doumbia pour le rôle prépondérant qu'il a joué dans ma motivation et ma formation scientifique. L'ampleur de ses connaissances et la qualité de ses conseils m'ont permis de réaliser ce projet. Je le remercie pour la confiance qu'il a témoignée à mon égard.

Au cours de ce travail de recherche j'ai eu à apprécier le soutien moral de tous mes amis qui ont contribué de près ou de loin à l'achèvement de ce travail.

Mes remerciements vont enfin à tous les membres de ma famille et tout spécialement à ma femme et ma fille qui m'ont aidé moralement. Sans elles, je n'aurais pas été en mesure de contribuer à la recherche scientifique. J'ai une pensée très spéciale pour mes parents, que leurs âmes reposent en paix ; eux qui m'ont inculqué le sens du sérieux, le respect et le travail bien fait.

Table of Contents

Abstract.....	iv
Avant-propos	vi
Chapter 1: Introduction.....	1
1.1 Brief history on reduction methods.....	1
1.1.1 <i>Integral square error method</i>	1
1.1.2 <i>Pade approximation method</i>	1
1.1.3 <i>Other reduction methods</i>	2
1.2 Research goals	2
1.2.1 <i>Main objective</i>	2
1.2.2 <i>Contribution of this thesis</i>	2
1.2.3 <i>Thesis structure</i>	3
1.2.4 <i>Publications</i>	4
Chapter 2: Classical reduction methods.....	5
2.1 Introduction.....	5
2.2 Integral square error reduction method.....	5
2.2.1 The case of an impulse input	6
2.2.2 The case of a constant input.....	9
2.2.3 Controller design based on ISE method.....	10
2.2.4 Analysis of the ISE and its controller design.....	11
2.3 Pade approximation method	12
2.3.1 Controller design based on Padé approximation.....	14

2.3.2 Analysis of pade and its controller design.	15
2.4 Conclusion	16
Chapter 3: New proposed reduction method	17
3.1 Similar systems new approach theory.....	17
3.2 Similar systems application to black box.....	18
3.3 Application to different black box systems output	22
A. Case study 1	22
B. Case study 2	24
C. Case study 3	26
D. Case study 4	27
E. Case study 5.....	29
3.4 PI Controller design for black box systems	31
3.5 Controller design approach based on similar system.....	33
A. Case study 1	33
B. Case study 2	34
C. Case study 3	35
D. Case study 4	36
E. Case study 5.....	37
3.6 New approach and classical reduction method comparison	38
3.7 Conclusion	42
Chapter 4: New Fibonacci irreducible systems	43
4.1 Introduction.....	43

4.2 Fibonacci systems with irreducible transfer functions.....	43
4.3 Fibonacci systems characteristics.	45
4.4 Fibonacci systems analysis.	50
4.5 Fibonacci boundary systems	53
4.6 Case studies and simulations.	55
4.7 Controller Design New Approach applied to Fibonacci systems	62
4.8 Controller Design New Approach limitation.....	64
4.9 Conclusion	66
Chapter 5: Fibonacci wave functions application to LC ladder network.....	67
5.1 Introduction.....	67
5.2 RC Fibonacci electrical circuit (RC-FEC).....	67
5.3 RC-FEC and FWFs simulation (RL-FEC).....	71
5.4 RL Fibonacci electrical circuit.....	75
5.5 Simulation of FWF and its corresponding RL-FEC	78
5.6 <i>Nth</i> Order LC Ladder RC-FEC and RL-FEC general model	81
5.7 Fibonacci wave functions applied to transmission lines.....	89
5.8 Conclusion	93
Chapter 6: Fibonacci wave functions application to spring mass chain	95
6.1 Introduction.....	95
6.2 Fibonacci Spring mass chain	95
6.3 Simulation of FMSC	101
6.4 <i>Nth</i> Order Fibonacci spring mass chain general model	104

6.5 FSMC with infinite and zero kv viscous damper	112
6.6 Conclusion	115
Chapter 7: Fibonacci wave functions application to inverse LC ladder network	117
7.1 Introduction.....	117
7.2 Inverse RC Fibonacci electrical circuit (iRC-FEC)	117
7.3 Simulation of iRC-FEC AND iFWFs	121
7.4 Inverse RL Fibonacci electrical circuit (iRL-FEC).....	125
7.5 Simulation of iRL-FEC and iFWFs	129
7.6 Nth order inverse LC ladder iRC-FEC and iRL-FEC general model	131
7.8 Controller Design new Approach applied to iFWFs.....	141
7.9 Inverse Fibonacci boundary wave functions.....	143
7.10 Conclusion	149
Chapter 8: General conclusion.....	150
8.1 General conclusion	150
References.....	154
Appendix A: Résumé étendu	160
A.1 Introduction.....	160
<i>A.1.1 Problématique de recherche</i>	160
<i>A.1.2 Objectif de recherche</i>	161
<i>A.1.2.1 Contribution de recherche</i>	161
<i>A.1.2.1 Structure de la thèse</i>	162
A.2 Méthodes classiques de réduction.....	163

<i>A.2.1 Intégral de l'erreur quadratique (ISE)</i>	163
<i>A.2.2 Approximation pade</i>	164
<i>A.2.3 Autres méthodes de réductions</i>	165
A.3 Nouvelle approche de réduction	165
<i>A.3.1 Application de l'approche des systèmes similaires aux boites noires</i>	167
A.4 Systèmes irréductibles et limitations des méthodes classiques.....	168
A.5 Étude de cas et simulations	171
A.6 Nouvelle approche de conception de contrôleur appliquée aux systèmes de Fibonacci.....	172
A.7 Systèmes de Fibonacci appliqués aux Systèmes électriques et mécaniques.....	175
<i>A.7.1 Réseau récurrent LC de Fibonacci</i>	175
<i>A.7.2 Chaîne de masse-ressort de Fibonacci</i>	177
<i>A.7.3 Réseau récursif inverse LC de Fibonacci</i>	179
A.8 Conclusion	181

LIST OF FIGURES

Figure 2. 1: Open loop $G_4^{ISE}(s)$, $G_2^{ISE}(s)$ and $G_2^{PD}(s)$	10
Figure 2. 2: Closed loop $G_4^{ISE}(s)$, $G_2^{ISE}(s)$ and $G_2^{PD}(s)$	11
Figure 2. 3: Open loop $G_4^{Pade}(s)$ and $G_2^{Pade}(s)$	14
Figure 2. 4: Closed loop $G_4^{Pade}(s)$ and $G_2^{Pade}(s)$	15
Figure 3. 1: a) Two identical sets b) Two similar sets.....	17
Figure 3. 2: Two similar systems A and B.....	18
Figure 3. 3: Real system with access to its inputs values and its outputs responses.....	18
Figure 3. 4: Output response for real system with no overshoot	19
Figure 3. 5: Output response for real system with overshoot and oscillations.	19
Figure 3. 6: Output response for real system with overshoot and no oscillation.	19
Figure 3. 7: Output response of the real system in open-loop.	22
Figure 3. 8: Output response of the real and reduced open-loop system.	24
Figure 3. 9: Output response of the real open loop system with no overshoot.	24
Figure 3. 10: Real and reduced system output response in open-loop.....	25
Figure 3. 11: Output response of the real system with no overshoot with oscillations.....	26
Figure 3. 12: Output of the real and reduced system response in open loop.	27
Figure 3. 13: Output of the real system in open loop with overshoot and oscillations.....	28
Figure 3. 14: Output response of the three systems- Real, reduced in [4] and proposed similar system.	29
Figure 3. 15: Output of the real system in open loop with overshoot only.....	30
Figure 3. 16: Output response of the real, reduced system in [3] and proposed similar system.	31
Figure 3. 17: Similar closed-loop system.	31
Figure 3. 18: Real and reduced closed loop with disturbance. ($\zeta = 0.99$ and $\omega_n = 1.48$ rad/s).	33
Figure 3. 19: Real and reduced closed loop with disturbance. $\zeta = 1.2$ and $\omega_n = 1.23$ rad/s.....	34

Figure 3. 20: Real and reduced closed loop with disturbance. ($\zeta = 0.99$ and $\omega_n = 0.45$ rad/s).	34
Figure 3. 21: Real and reduced closed loop with disturbance. ($\zeta = 0.99$ and $\omega_n = 2.55$ rad/s).	35
Figure 3. 22: Real and reduced closed loop with disturbance. $\zeta = 0.7$ and $\omega_n = 3.57$ rad/s.....	35
Figure 3. 23: Real and reduced closed loop with disturbance. ($\zeta=1.5$; $\omega_n=1.28$ rad/s).....	36
Figure 3. 24: Real and reduced closed loop with disturbance. $\zeta=2$; $\omega_n=300$ rad/s	36
Figure 3. 25: Real and reduced closed loop with disturbance. ($\zeta=0.99$ $\omega_n=100$ rad/s).....	37
Figure 3. 26: Real and reduced closed loop with disturbance. ($\zeta=2$; $\omega_n=100$ rad/s).....	38
Figure 3. 27: Real and similar systems output response.	39
Figure 3. 28: Real and reduced closed loop $\zeta=1.5$; $\omega_n=1.33$ rad/s.....	40
Figure 3. 29: Real and similar systems output response.	41
Figure 3. 30: Real and reduced closed loop for $\zeta=1.5$; $\omega_n=2.66$ rad/s.	41
Figure 4. 1: FWFs recursive process	44
Figure 4. 2: Real part of $g_{40}^{(1,1)}(s)$ poles for case #1.....	50
Figure 4. 3: Real part of $g_{40}^{(1,4)}(s)$ poles for case #2.....	50
Figure 4. 4: Imaginary part of $g_{40}^{(1,1)}(s)$ poles for case #1.....	51
Figure 4. 5: Imaginary part of $g_{40}^{(1,4)}(s)$ poles for case #2.....	51
Figure 4. 6: Case #1- Odd coefficients (black). Even coefficients (Hashed) of $den_{40}^{(1,1)}(s)$	52
Figure 4. 7: Case #2- Odd coefficients (black). Even coefficients (Hashed) of $den_{40}^{(1,4)}(s)$	52
Figure 4. 8: FWF $g_n^{(1,0)}(s)$ ($n = 37, 38, 39$ and 40) outputs with unit input.	54
Figure 4. 9: FWF $g_n^{(1,0)}(s)$ ($n = 37, 38, 39$ and 40) outputs with input pulse of 30s.	54
Figure 4. 10: Bode plots of FWFs $g_1^{(1,1)}(s), \dots, g_{40}^{(1,1)}(s)$	56
Figure 4. 11: Bode plots of FWFs $g_1^{(1,1)}(s), g_{39}^{(1,1)}(s), g_{40}^{(1,1)}(s)$	57

Figure 4. 12: Poles and zeros of $g_1^{(1,1)}(s), \dots, g_{40}^{(1,1)}(s)$	57
Figure 4. 13: Output response of odd FWFs $g_1^{(1,1)}(s), g_{11}^{(1,1)}(s)$	57
Figure 4. 14: Output response of odd FWFs $g_{11}^{(1,1)}(s), g_{39}^{(1,1)}(s)$	58
Figure 4. 15: Output response of odd FWFs $g_1^{(1,1)}(s), g_{11}^{(1,1)}(s), g_{21}^{(1,1)}(s), g_{31}^{(1,1)}(s), g_{39}^{(1,1)}(s)$	58
Figure 4. 16: Output response of even FWFs $g_2^{(1,1)}(s), g_{22}^{(1,1)}(s)$	58
Figure 4. 17: Output response of even FWFs $g_2^{(1,1)}(s), g_{40}^{(1,1)}(s)$	59
Figure 4. 18: Output response of even FWFs $g_2^{(1,1)}(s), g_{12}^{(1,1)}(s), g_{22}^{(1,1)}(s), g_{32}^{(1,1)}(s), g_{40}^{(1,1)}(s)$..	59
Figure 4. 19: Output response of odd and even FWFs $g_1^{(1,1)}(s), g_{11}^{(1,1)}(s), g_{21}^{(1,1)}(s), g_{31}^{(1,1)}(s), g_{39}^{(1,1)}(s), g_2^{(1,1)}(s), g_{12}^{(1,1)}(s), g_{22}^{(1,1)}(s), g_{32}^{(1,1)}(s), g_{40}^{(1,1)}(s)$	59
Figure 4. 20: Bode plots of FWFs $g_1^{(1,4)}(s), \dots, g_{40}^{(1,4)}(s)$	60
Figure 4. 21: Bode plots of FWFs $g_1^{(1,4)}(s), g_{39}^{(1,4)}(s), g_{40}^{(1,4)}(s)$	60
Figure 4. 22: Poles and zeros of FWFs $g_1^{(1,4)}(s), \dots, g_{40}^{(1,4)}(s)$	61
Figure 4. 23: Output response of FWFs $g_1^{(1,4)}(s), g_{11}^{(1,4)}(s), g_{21}^{(1,4)}(s), g_{31}^{(1,4)}(s), g_{39}^{(1,4)}(s)$	61
Figure 4. 24: Output response of FWFs $g_2^{(1,4)}(s), g_{12}^{(1,4)}(s), g_{22}^{(1,4)}(s), g_{32}^{(1,4)}(s), g_{40}^{(1,4)}(s)$	61
Figure 4. 25: Output response of FWFs $g_1^{(1,4)}(s), g_{11}^{(1,4)}(s), g_{21}^{(1,4)}(s), g_{31}^{(1,4)}(s), g_{39}^{(1,4)}(s),$ $g_2^{(1,4)}(s), g_{12}^{(1,4)}(s), g_{22}^{(1,4)}(s), g_{32}^{(1,4)}(s), g_{40}^{(1,4)}(s)$	62
Figure 4. 26: Output response in closed loop of FWFs $g_1^{(1,1)}(s), \dots, g_1^{(1,1)}(s), g_1^{(1,4)}(s), \dots, g_{40}^{(1,4)}(s)$	64
Figure 4. 27: Output response of FWFs $g_2^{(1,0)}(s), g_{12}^{(1,0)}(s), g_{22}^{(1,0)}(s), g_{32}^{(1,0)}(s), g_{40}^{(1,0)}(s)$	64
Figure 4. 28: Output response of FWFs, $g_{11}^{(1,0)}(s), g_{21}^{(1,0)}(s), g_{31}^{(1,0)}(s), g_{39}^{(1,0)}(s)$	65
Figure 4. 29: Output response in closed loop of FWFs $g_1^{(1,0)}(s), \dots, g_{40}^{(1,0)}(s)$	65

Figure 5. 1: First order RC-FEC	68
Figure 5. 2: Second order RC-FEC	68
Figure 5. 3: Third order RC-FEC	69
Figure 5. 4: n th even order RC-FEC	70
Figure 5. 5: n th odd order RC-FEC	70
Figure 5. 6: FWF RC-FEC $(\frac{I_o}{V_i})_{40}^{(1,1)} = C * g_{40}^{(1,1)}(s)$ & Matlab-Simulink model with $I_i = 1V$	73
Figure 5. 7: FWF RC-FEC $(\frac{V_o}{I_i})_{39}^{(1,1)} = L * g_{39}^{(1,1)}(s)$ & Matlab-Simulink model with $I_i = 1A$	74
Figure 5. 8: First order RL-FEC	75
Figure 5. 9: Second order RL-FEC	75
Figure 5. 10: First order RL-FEC	76
Figure 5. 11: n th even order RL-FEC	77
Figure 5. 12: n th odd order RL-FEC	77
Figure 5. 13: FWF RL-FEC $(\frac{V_o}{I_i})_{40}^{(1,1)} = L g_{40}^{(1,1)}(s)$ & Matlab-Simulink model with $I_i = 1A$	79
Figure 5. 14: FWF RL-FEC $(\frac{I_o}{V_i})_{39}^{(1,1)} = C g_{39}^{(1,1)}(s)$ & Matlab-Simulink model with $V_i = 1V$	80
Figure 5. 15: RL-FEC and RC-FEC order 40 ; $((\frac{V_o}{I_i})_{40}^{(1,1)} = L g_{40}^{(1,1)}(s), I_i = 1A)) ((\frac{I_o}{V_i})_{40}^{(1,1)} = C * g_{40}^{(1,1)}(s), V_i = 1V))$	81
Figure 5. 16: n th even order RC-FEC	82
Figure 5. 17: n th even order RC-FEC Model using FWFs for each current and voltage branch.	82
Figure 5. 18: n th even order RC-FEC Model using FWFs for each flux and charge branch.	82
Figure 5. 19: n th even order RL-FEC	83
Figure 5. 20: n th even order RL-FEC Model using FWFs for each current and voltage branch.	83
Figure 5. 21: n th even order RL-FEC Model using FWFs for each flux and charge branch.	83
Figure 5. 22: Matlab-Simulink RC-FEC circuit and proposed FWF general model for $I_{40}^{(1,4)}$ with input $V_i = 1V$	84

Figure 5. 23: Matlab-Simulink RC-FEC circuit and proposed FWF general model for $V_{37}^{(1,4)}$ with input $V_i = 1V$	84
Figure 5. 24: Matlab-Simulink RC-FEC and FWF general model $(V_1^{(1,4)}, V_3^{(1,4)}, \dots, V_{39}^{(1,4)})$	85
Figure 5. 25: Matlab-Simulink RC-FEC and FWF general model $(I_2^{(1,4)}, I_4^{(1,4)}, \dots, I_{40}^{(1,4)})$	85
Figure 5. 26: Matlab-Simulink RC-FEC and FWF general model $(I_{40}^{(1,1)}, V_i = 1V, R = \sqrt{\frac{L}{C}})$	86
Figure 5. 27: Matlab-Simulink RC-FEC and FWF general model $(V_{11}^{(1,1)}, V_i = 1V, R = \sqrt{\frac{L}{C}})$	87
Figure 5. 28: Matlab-Simulink RC-FEC and FWF general model $(V_1^{(1,1)}, V_3^{(1,1)}, \dots, V_{39}^{(1,1)}, R = \sqrt{\frac{L}{C}})$	87
Figure 5. 29: Matlab-Simulink RC-FEC and FWF general model $(I_2^{(1,1)}, I_4^{(1,1)}, \dots, I_{40}^{(1,1)}, R = \sqrt{\frac{L}{C}})$	88
Figure 5. 30: nth even order RC-FEC general model using energy wave between branches.	88
Figure 5. 31: Matlab-Simulink RL-FEC and FWF general model $(V_{40}^{(1,0)}, I_i = 1A, R = 0\Omega)$	92
Figure 5. 32: Matlab-Simulink RL-FEC and FWF general model $(I_{21}^{(1,0)}, I_i = 1A, R = 0\Omega)$	92
Figure 5. 33: Matlab-Simulink RC-FEC and FWF general model $(V_{21}^{(1,0)}, V_i = 1V \text{ 35s pulse}, R = \infty\Omega)$	92
Figure 5. 34: Matlab-Simulink RC-FEC and FWF general model $(I_{40}^{(1,0)}, V_i = 1V \text{ 35s pulse}, R = \infty\Omega)$	93
Figure 6. 1: First order of FSMC	96
Figure 6. 2: Second order of FSMC	96
Figure 6. 3: Third order of FSMC	97
Figure 6. 4: Forth order of FSMC	97

Figure 6. 5: Fifth order of FSMC.....	98
Figure 6. 6: n th even order of FSMC.....	98
Figure 6. 7: n th odd order of FSMC	99
Figure 6. 8: FMSC ($F_{40}^{(k,x_m)} = m * g_{40}^{(k,x_m)}(s)$, $v_i = 1m/s$)	103
Figure 6. 9: FSMC ($v_{39}^{(k,x_m)} = \frac{1}{k_s} * g_{39}^{(k,x_m)}(s)$, $F_i = 1N$)	104
Figure 6. 10: n th even order FSMC Model using FWFs for each section for $(v_j^{(k,x_m)}, F_j^{(k,x_m)})$ variables.....	105
Figure 6. 11: n th even order FSMC Model using FWFs for each section for $(\mu_j^{(k,x_m)}, x_j^{(k,x_m)})$..	105
Figure 6. 12: FSMC general model for $F_{40}^{(1,4)}$ with input $v_i = 1m/s$	106
Figure 6. 13: FSMC general model for $v_{17}^{(1,4)}$ with input $v_i = 1m/s$	106
Figure 6. 14: FSMC general model for $(F_2^{(1,4)}, F_4^{(1,4)}, \dots, F_{40}^{(1,4)})$.with $v_i = 1m/s$	107
Figure 6. 15: FSMC general model for $(v_1^{(1,4)}, v_4^{(1,4)}, \dots, v_{39}^{(1,4)})$.for $v_i = 1m/s$	108
Figure 6. 16: FSMC general model for $F_{40}^{(1,1)}$ with input $v_i = 1, k_v = \sqrt{mk_s}$)	109
Figure 6. 17: FSMC general model for $v_9^{(1,1)}$ with input $v_i = 1, k_v = \sqrt{mk_s}$)	109
Figure 6. 18: FSMC general model for $F_2^{(1,1)}, F_4^{(1,1)}, \dots, F_{40}^{(1,1)}, k_v = \sqrt{mk_s}$).....	110
Figure 6. 19: FSMC general model $(v_1^{(1,1)}, v_3^{(1,1)}, \dots, v_{39}^{(1,1)}, k_v = \sqrt{mk_s})$	111
Figure 6. 20: n th even F-Spring-Mass Model using FWFs for energy transfer between sections.	112
Figure 6. 21: FSMC general model $(F_{40}^{(1,0)}, v_i = 1m/s, k_v = 0)$	114
Figure 6. 22: FSMC general model $(F_{40}^{(1,0)}, v_i = 1m/s$ (pulse of 20s), $k_v = 0)$	114
Figure 6. 23: FSMC general model $(v_2^{(1,0)}, v_i = 1m/s, k_v = 0)$	114
Figure 6. 24: FSMC general model $(v_{21}^{(1,0)}, v_i = 1ms$ (pulse of 20s), $k_v = 0)$	115

Figure 7. 1: First order iRC-FEC	118
Figure 7. 2: Second order iRC-FEC.....	118
Figure 7. 3: Third order iRC-FEC	119
Figure 7. 4: n th even order iRC-FEC.....	119
Figure 7. 5: n th odd order iRC-FEC	120
Figure 7. 6: iRC-FEC $((\frac{V_o}{I_i})_{-40}^{(1,1)} = \frac{1}{C} * g_{-40}^{(1,1)}(s)$ with $I_i = 1A$).....	124
Figure 7. 7: RC-FEC $((\frac{I_o}{V_i})_{-39}^{(1,1)} = \frac{1}{L} * g_{-39}^{(1,1)}(s)$ with $V_i = 1V$	125
Figure 7. 8: First order iRL-FEC	125
Figure 7. 9: Second order iRL-FEC	126
Figure 7. 10: Third order iRL-FEC.....	126
Figure 7. 11: n th even order iRL-FEC.....	127
Figure 7. 12: n th odd order iRL-FEC	128
Figure 7. 13: iRL-FEC $((\frac{I_o}{V_i})_{-40}^{(1,1)} = \frac{1}{L} * g_{-40}^{(1,1)}(s)$, $V_i = 1V$	129
Figure 7. 14: iRL-FEC $((\frac{V_o}{I_i})_{-39}^{(1,1)} = \frac{1}{C} * g_{-39}^{(1,1)}(s)$ with $I_i = 1A$)	130
Figure 7. 15: iRL-FEC and iRC-FEC order 40 ; $((\frac{I_o}{V_i})_{-40}^{(1,1)} = \frac{1}{L} * g_{-40}^{(1,1)}(s)$, $V_i = 1V$) $((\frac{V_o}{I_i})_{-39}^{(1,1)} = \frac{1}{C} * g_{-39}^{(1,1)}(s)$, $I_i = 1A$))......	131
Figure 7. 16: n th even order iRC-FEC.....	132
Figure 7. 17: n th even order iRC-FEC Model using iFWFs for each current and voltage branch.	132
Figure 7. 18: n th even order iRL-FEC.....	132
Figure 7. 19: n th even order iRL-FEC Model using IFWFs for each current and voltage branch.	133
Figure 7. 20: iRC-FEC circuit and general model for $V_{-40}^{(1,4)}$ with input $I_i = 1A$	134
Figure 7. 21: iRC-FEC circuit and general model for $I_{-40}^{(1,4)}$ as integral of $V_{-40}^{(1,4)}$ with input $I_i = 1A$	134

Figure 7. 22: iRC-FEC circuit and general model for $I_{-39}^{(1,4)}$ with input $I_i = 1A$	134
Figure 7. 23: iRC-FEC circuit and general model for $V_{-39}^{(1,4)}$ as integral of $I_{-39}^{(1,4)}$ with input $I_i = 1A$	135
Figure 7. 24: Matlab-Simulink iRC-FEC and general model $(V_{-2}^{(1,4)}, V_{-4}^{(1,4)}, \dots, V_{-40}^{(1,4)})$ across inductors	135
Figure 7. 25: Matlab-Simulink iRC-FEC and general model $(I_{-1}^{(1,4)}, I_{-3}^{(1,4)}, \dots, I_{-39}^{(1,4)})$ across capacitors	136
Figure 7. 26: Matlab-Simulink iRC-FEC and general model $(V_{-40}^{(1,1)}, I_i = 1A, R = \sqrt{\frac{L}{C}})$	137
Figure 7. 27: Matlab-Simulink iRC-FEC and general model $(I_{-40}^{(1,1)}, I_i = 1A, R = \sqrt{\frac{L}{C}})$ as integral of $V_{40}(1,1)$	137
Figure 7. 28: Matlab-Simulink iRC-FEC and general model $(I_{-39}^{(1,1)}, I_i = 1A, R = \sqrt{\frac{L}{C}})$	138
Figure 7. 29: Matlab-Simulink iRC-FEC and general model $(V_{-39}^{(1,1)}, I_i = 1A, R = \sqrt{\frac{L}{C}})$ as integral of $I_{-39}^{(1,1)}$	138
Figure 7. 30: Matlab-Simulink iRC-FEC and general model $(V_{-30}^{(1,1)}, I_i = 1A, R = \sqrt{\frac{L}{C}})$	139
Figure 7. 31: Matlab-Simulink iRC-FEC and general model $(I_{-30}^{(1,1)}, I_i = 1A, R = \sqrt{\frac{L}{C}})$ as integral of $V_{-30}^{(1,1)}$	140
Figure 7. 32: Matlab-Simulink iRC-FEC and general model $(V_{-2}^{(1,1)}, V_{-4}^{(1,1)}, \dots, V_{-40}^{(1,1)}, R = \sqrt{\frac{L}{C}})$ across inductors	140
Figure 7. 33: Matlab-Simulink iRC-FEC and general model $(I_{-1}^{(1,1)}, I_{-3}^{(1,1)}, \dots, I_{-39}^{(1,1)}, R = \sqrt{\frac{L}{C}})$ across capacitors	141

Figure 7. 34: Output response in closed loop of FWFs

$g_{-1}^{(1,1)}(s), \dots, g_{-40}^{(1,1)}(s), g_{-1}^{(1,4)}(s), \dots, g_{-40}^{(1,4)}(s)$ 143

Figure 7. 35: iRL-FEC and general model ($V_{-33}^{(1,0)}, V_i = 1V, R = \infty\Omega$) 146

Figure 7. 36: iRL-FEC and general model ($I_{-33}^{(1,0)}, V_i = 1V, R = \infty\Omega$) as integral of $V_{-33}^{(1,0)}$ 147

Figure 7. 37: iRL-FEC and general model ($I_{-32}^{(1,0)}, V_i = 1V, R = \infty\Omega$) 147

Figure 7. 38: iRL-FEC and general model ($V_{-32}^{(1,0)}, V_i = 1V, R = \infty\Omega$) as integral of $I_{-32}^{(1,0)}$ 147

Figure 7. 39: iRC-FEC and general model ($V_{-40}^{(1,0)}, I_i = 1A, R = 0\Omega$) 148

Figure 7. 40: iRC-FEC and general model ($I_{-40}^{(1,0)}, I_i = 1A, R = 0\Omega$) as integral of $V_{-40}^{(1,0)}$ 148

Figure 7. 41: iRC-FEC and general model ($I_{-29}^{(1,0)}, I_i = 1A, R = 0\Omega$) 148

Figure 7. 42: iRC-FEC and general model ($V_{-29}^{(1,0)}, I_i = 1A, R = 0\Omega$) as integral of $I_{-29}^{(1,0)}$ 149

Figure A. 1: a) Ensembles identiques b) Ensembles similaires 165

Figure A. 2: Deux systèmes similaires A et B 166

Figure A. 3: Réponse de sortie du système réel sans dépassement 167

Figure A. 4: Réponse de sortie du système réel avec dépassement et oscillations. 167

Figure A. 5: Réponse de sortie du système réel avec dépassement et sans oscillations. 168

Figure A. 6: FWFs processus récursif 169

Figure A. 7: Réponses de sortie en boucle ouverte des FWFs $g_1^{(1,1)}(s), g_{11}^{(1,1)}(s), g_{21}^{(1,1)}(s),$

$g_{31}^{(1,1)}(s), g_{39}^{(1,1)}(s), g_2^{(1,1)}(s), g_{12}^{(1,1)}(s), g_{22}^{(1,1)}(s), g_{32}^{(1,1)}(s), g_{40}^{(1,1)}(s)$ 171

Figure A. 8: Réponses de sortie en boucle ouverte des FWFs $g_2^{(1,4)}(s),$

$g_{22}^{(1,4)}(s), g_{32}^{(1,4)}(s), g_{40}^{(1,4)}(s)$ 172

Figure A. 9: Réponses de sortie en boucle ouverte des FWFs $g_1^{(1,4)}(s), g_{11}^{(1,4)}(s), g_{21}^{(1,4)}(s),$

$g_{31}^{(1,4)}(s), g_{39}^{(1,4)}(s), g_2^{(1,4)}(s), g_{12}^{(1,4)}(s), g_{22}^{(1,4)}(s), g_{32}^{(1,4)}(s), g_{40}^{(1,4)}(s)$ 172

Figure A. 10: Réponses de sortie en boucle fermée des FWFs $g_1^{(1,1)}(s), \dots, g_{40}^{(1,1)}(s), g_1^{(1,4)}(s), \dots, g_{40}^{(1,4)}(s)$	174
Figure A. 11: n^{ieme} ordre pair RC-FEC	175
Figure A. 12: n^{ieme} ordre impair RC-FEC	176
Figure A. 13: n^{ieme} ordre pair de FSMC.....	177
Figure A. 14: n^{ieme} ordre impair de FSMC	178
Figure A. 15: n^{ieme} ordre pair de iRC-FEC	179
Figure A. 16: n^{ieme} ordre impair de iRC-FEC	180

LIST OF TABLES

Table 4. 1: Fibonacci transfer functions FWFs.....	44
Table 4. 2: Fibonacci transfer functions for $K, x = (1,1)$	45
Table 4. 3: Pascal's triangle rearrangement coefficients of all $den_n^{(1,1)}(s)$ of Fibonacci transfer functions.	46
Table 4. 4: Denominator coefficients of FWFs with (K, x) . [red numbers are for the case $(K, x) = (1,1)$]	47
Table 4. 5: Pascal's triangle for Fibonacci transfer functions for all $den_n^{(k,x)}(s)$	48
Table 4. 6: Pascal's triangle for Fibonacci boundary systems.....	53
Table 5. 1: RC-FEC Fibonacci wave functions	71
Table 5. 2: Pascal's triangle general form with multiplication coefficients (K, x_c)	72
Table 5. 3: RL-FEC Fibonacci wave functions.....	78
Table 6. 1: F-Spring-Mass Chain Fibonacci wave functions FWFs.....	99
Table 6. 2: Pascal's triangle general form with coefficients of multiplication (k, x_m)	100
Table 6. 3: Pascal's triangle for Fibonacci FMSC boundary systems $(k, 0)$ & (k, ∞)	113
Table 7. 1: iRC-FEC Fibonacci wave functions	120
Table 7. 2: Pascal's triangle general form with multiplication coefficients (K, x_c)	122
Table 7. 3: Pascal's triangle general form Inverse with multiplication coefficients (K, x_c)	123
Table 7. 4: iRL-FEC Fibonacci wave functions	128
Table 7. 5: Pascal's triangle general form Inverse for boundary iFWF with $(k, 0)$ & (k, ∞)	146

Table A. 1: Les coefficients des dénominateurs des FWFs avec (K, x)	169
Table A. 2: Triangle de Pascal pour les $den_n^{(k,x)}$ des fonctions de transfert de Fibonacci.	170
Table A. 3: Fonctions d'onde de Fibonacci RC-FEC	176
Table A. 4: Fonctions d'onde de Fibonacci de la chaîne FSMC	178
Table A. 5: Fonctions d'onde de Fibonacci du iRC-FEC	180

LIST OF SYMBOLS

ψ_i	: Weighted element i of the system
A	: Steady state value
D	: Delay time
K	: Constant gain
K_i	: Derivative coefficient
K_p	: Proportional coefficient
K_i	: Integral coefficient
ω_n	: Natural frequency
ξ	: Damping factor
c_i	: Numerator coefficient of transfer function order i
d_i	: Denominator coefficient of transfer function order i
ρ_i	: Poles of the transfer function
(b, c)	: Real poles of $G_R(s)$
a	: Numerator coefficient of second order $G_R(s)$
$G_R(s)$: Second order transfer function with real poles
$G_C(s)$: Second order transfer function with real poles
α	: Numerator coefficient of second order $G_C(s)$
β	: Real part pole of second order $G_C(s)$
γ	: Imaginary part pole of second order $G_C(s)$
$P_N(x)$: Polynomial order N
$Q_M(x)$: Polynomial order M

$R_{N,M}(x)$: Polynomial ratio $\frac{P_N(x)}{Q_M(x)}$
p_i	: Polynomial coefficient order i of $P_N(x)$
q_i	: Polynomial coefficient order i of $Q_M(x)$
$g_n^{(K,x)}(s)$: Fibonacci transfer function order n with parameters K and x
$den_n^{(K,x)}(s)$: Denominator of $g_n^{(K,x)}(s)$
$num_n^{(K,x)}(s)$: Numerator of $g_n^{(K,x)}(s)$
ξ_f	: Fibonacci damping factor
ω_f	: Fibonacci natural frequency
L	: Inductor value in [H]
C	: Capacitor value in [F]
R	: Resistor value in [Ω]
ϕ	: Golden ratio 1.618034
x_c	: Initial slope (Time constant) $\frac{1}{RC}$ or RC
x_L	: Initial slope (Time constant) $\frac{R}{L}$ or $\frac{L}{R}$
$a_i^{(k,x)}$: Coefficient of $den_n^{(K,x)}(s)$ order i
$b_i^{(k,x)}$: Coefficient of $den_{n-1}^{(K,x)}(s)$ order i
ξ_{cf}	: Fibonacci damping factor for RC-FEC
ξ_{Lf}	: Fibonacci damping factor for RL-FEC
ξ_{mf}	: Fibonacci damping factor for spring-mass
n_c	: Number of capacitors in the circuit
n_L	: Number of inductors in the circuit

V_o	: Output voltage
I_o	: Output current
V_i	: Input voltage
I_i	: Input current
$Q_j^{(k,x)}$: Charge in the capacitor of section j of LC ladder
$\phi_j^{(k,x)}$: Flux in the inductor of section j of LC ladder
$I_j^{(k,x)}$: Current in the inductor of section j of LC ladder
$V_j^{(k,x)}$: Voltage in the capacitor of section j of LC ladder
x_m	: Mechanical time constant $\frac{k_v}{m}$
k_v	: Viscous damper coefficient
k_s	: Spring coefficient
m	: Mass
n_s	: Number of springs in the chain
n_m	: Number of masses in the chain
v_o	: Output speed
F_o	: Output force
v_i	: Input speed
F_i	: Input force
$v_j^{(k,x)}$: Speed of section j in the mass-spring chain
$F_j^{(k,x)}$: Force of section j in the mass-spring chain
$\mu_j^{(k,x)}$: Momentum of section j in the mass-spring chain

- $x_j^{(k,x)}$: Displacement of section j in the mass-spring chain
- $(e_m)_j^{(k,x)}$: Energy of mass m in section j in the mass-spring chain
- $(e_s)_j^{(k,x)}$: Energy of spring in section j in the mass-spring chain
- $(e_L)_j^{(k,x)}$: Energy of inductor in section j in LC ladder chain
- $(e_c)_j^{(k,x)}$: Energy of capacitor in section j in the LC ladder chain

Chapter 1: Introduction

1.1 Brief history on reduction methods

The majority of reduction techniques in the literature [1], [2], [3], [8], [10], [13] are based mainly on the knowledge of the transfer function of the system that should be reduced. These reduced methods involve a lot of mathematical equations manipulations to find an identical reduced system. In most cases, this reduced system is a second order system. Once the transfer function is reduced, a controller is developed based on the reduced function, and then applied to the real system.

1.1.1 Integral square error method

Minimization of integral square error (ISE) [1], [13] is based on minimizing the squared error area between a known real system transfer function output and unknown reduced second order transfer function output. This technique involves a lot of mathematical equations and computer analysis to find the unknown coefficients of the second order system that makes the squared error area as close as possible to zero. The reduced system is then achieved.

1.1.2 Pade approximation method

Pade approximation and its improvements [2], [3], [8], [10] is another reduction method based on Taylor-McLaurin series. The real system transfer function should be known prior to using this technique to find a reduced second order transfer function identical to the real system. This method also uses a lot of mathematical equations using McLaurin series to find the numerator and the denominator coefficients of the reduced system.

1.1.3 Other reduction methods

Dominant pole retention method [1], pole clustering [3], Big Bang big Crunch reduction method [11] and many other methods [5], [14-18] have the same objective, finding an identical reduced system with known original transfer function but with different mathematical approaches. The objective of all these reduction methods is not to find a reduced identical system only, but to design a controller in closed loop that controls the real system perfectly in the same way as the approximated model.

1.2 Research goals

1.2.1 Main objective

The main objective of this research is to design a controller for a high order complex system with no need of its transfer function and to avoid heavy differential equations to find an identical approximated system. This new proposed reduction method is based on a similar system concept. This similarity is achieved by using weighted elements that characterize the real system. Those elements are determined from the output response only. The complex system transfer function is not needed to find a reduced similar system.

1.2.2 Contribution of this thesis

The main contribution of this thesis is to develop a new approach based on a new concept called “similarity”. This new method uses only the output response of the real system. Output response data can be obtained either by experimentation or by simulation. Based on this notion of similarity, the real system output is reduced to a first order system output that is similar in its weighted elements. These elements must be clearly and carefully defined. The controller design is based on this reduced similar first order system and will be applied to the black box

or higher order system. Simulation is conducted to highlight the performance of this proposed new method compared to existing classical reduction methods.

The second contribution of this research is to introduce new irreducible high order transfer functions systems that classical reduction methods cited above are unable to reduce to a lower order especially second order systems. This will highlight the limits of the classical reduction methods. In the meantime, the application of the new approach based on first order original or similar system should be still valid to design a controller for such high order irreducible systems.

The last contribution of this research is to find some applications to these theoretical irreducible systems. New electrical circuit as an application of Fibonacci wave functions (FWFs) called Fibonacci electrical circuits (FECs), are introduced for the first time to model perfectly the recursive LC ladder network. These FECs can be used to model transmission cables [21], [22], [25], the neural dynamic in biology [24] and the behavior and interaction of the infinitely small particles using the infinite LC networks [23] in quantum mechanics. These Fibonacci systems have irreducible transfer function and cannot be reduced to an equivalent second order system.

Spring mass chain as another application of these irreducible Fibonacci wave functions is also introduced in this research. This Fibonacci spring mass chain (FSMC) is also used in many applications to model the behavior and interaction of particles from mechanical view, especially in fluid mechanics and quantum mechanics.

1.2.3 Thesis structure

This thesis is structured into eight chapters. The first chapter is an introduction highlighting the research in the literature related to classical reduction methods and their requirements to

reduce any specific high order transfer function. Chapter two assesses two well-known reduction methods, integral square error (ISE) and the pade approximation as well as their approaches to design controllers. Chapter three is dedicated to the new approach based on similar systems to design controllers for black box systems. Performance comparison with the two conventional methods of chapter two is also highlighted. Chapter four is dedicated to new systems called Fibonacci systems with specific transfer functions that classical methods cannot reduce. Chapter five is an application of Fibonacci systems to recursive LC ladders as irreducible systems. Chapter six is another application of Fibonacci systems, the mechanical mass-spring chain which has irreducible transfer functions. Chapter seven is dedicated to another recursive electrical circuit as an application of Fibonacci systems called inverse LC ladder. Finally, the general conclusion of this thesis will be presented in chapter eight.

1.2.4 Publications

- [1] S. Hissem, M. L. Doumbia, M. Keddar “Novel Controller Design Based on Black Box Systems Approach”, *IEEE Conference, Annual American Control Conference (ACC)*, June 27-29, 2018, pp 6427-6432.
- [2] S. Hissem, M. L. Doumbia “Novel Controller Design for High Order Transfer Functions Based on Similar Systems Approach”, *IEEE Conference on Advanced Research in Engineering Science (ARES)*, June 2018.
- [3] S. Hissem, M. L. Doumbia “New Fibonacci Recurrent Systems Applied to Transmission Lines Input Impedance and Admittance”, *IEEE Conference on Advances Science and Engineering Technology (ASET)*, March 2019.
- [4] S. Hissem, M. L. Doumbia “Infinite Spring-Mass Chain Model Using Fibonacci Wave Functions”, *IEEE Conference on Advances Science and Engineering Technology (ASET)*, March 2019.
- [5] S. Hissem, M. L. Doumbia “Signal Propagation in N^{th} LC Ladder Network Using Fibonacci Wave Functions”, *IEEE Antennas and Propagation Magazine (APM)*, Submitted

Chapter 2: Classical reduction methods

2.1 Introduction

This chapter is dedicated to a bibliographical research on existing approximation methods in the literature for systems with high order transfer functions and their controller design. A study and analysis of these methods will be made theoretically and by simulation to be able to do a comparison analysis.

A new reduction method to design controllers for such systems as black boxes will also be introduced in chapter 3 and compared it to those existing methods.

This chapter will be organised in various parts; each part will be dedicated to one classical reduction method with a theoretical study and a simulation of an example taken from the literature.

2.2 Integral square error reduction method

The method based on the integral square error (ISE) presented in [3] and detailed in [4] is one of known reduction methods in the literature that minimizes the integral square error between the actual system transfer function response and the unknown reduced model transfer function whose coefficients are to be determined using the ISE theory.

Define a high and stable n order system transfer function of order n of the form

$$F(s) = \frac{c_o + c_1s + \dots + c_{n-1}s^{n-1}}{d_o + d_1s + \dots + d_ns^n} \quad (2.1)$$

For simplicity, we set $c_o = d_o$ the system gain is equal to 1.

Suppose that $F(s)$ has poles $\rho_1, \rho_2, \dots, \rho_n$ which may be real or complex. Reduction model is chosen to be a second-order transfer function, either with real or complex poles (2.2).

$$G_R(s) = \frac{as + bc}{(s + b)(s + c)} \quad (2.2)$$

$$G_C(s) = \frac{\alpha s + \beta^2 + \gamma^2}{s^2 + 2\beta s + \beta^2 + \gamma^2} = \frac{\alpha s + \beta^2 + \gamma^2}{(s + \beta + j\gamma)(s + \beta - j\gamma)}$$

For these two reduction models $G_R(s)$ and $G_C(s)$, the parameters $a, b, c, \alpha, \beta, \gamma$ that are unknown will be determined by ISE technique. The index of performance depends on the type of entry (impulse or constant entry).

2.2.1 The case of an impulse input

The output response will be:

$$f(t) = \sum_{i=1}^n a_i e^{\rho_i t} \quad (2.3)$$

$$a_i = \lim_{s \rightarrow \rho_i} (s - \rho_i) F(s)$$

For $G_R(s)$;

$$g_R(t) = \frac{b(a - c)}{b - c} e^{-bt} + \frac{c(b - a)}{b - c} e^{-ct} \quad (2.4)$$

For $G_C(s)$;

$$g_C(t) = e^{-\beta t} (\alpha \cos(\gamma t) + \delta \sin(\gamma t)) \quad (2.5)$$

$$\delta = \frac{\beta^2 + \gamma^2 - \alpha\beta}{\gamma}$$

The integral square error method is defined as

$$I_R = \int_0^\infty (g_R(t) - f(t))^2 dt = \int_0^\infty (g_R(t)^2 - 2g_R(t)f(t) + f(t)^2) dt \quad (2.6)$$

There are three terms in (2.6), the first term is:

$$\int_0^{\infty} g_R(t)^2 dt = \int_0^{\infty} \left\{ \frac{b^2(a-c)^2 e^{-2bt} + 2bc(a-c)(b-a)e^{-(b+a)t} + c^2(b-a)^2 e^{-2ct}}{(b-c)^2} \right\} dt \quad (2.7)$$

$$\int_0^{\infty} g_R(t)^2 dt = \frac{b(a-c)^2}{2(b-c)^2} + \frac{2bc}{(b+c)} \frac{(a-c)(b-a)}{(b-c)^2} + \frac{c(b-a)^2}{2(b-c)^2} \quad (2.8)$$

The second term is:

$$\begin{aligned} \int_0^{\infty} -2g_R(t)f(t)dt &= -2 \int_0^{\infty} \sum_1^n \frac{a_i}{(b-c)} \{b(a-c)e^{-(b-\rho_i)t} + c(b-a)e^{-(c-\rho_i)t}\} dt \\ &= -2 \sum_1^n \frac{a_i}{(b-c)} \left\{ \frac{b(a-c)}{b-\rho_i} + \frac{c(b-a)}{c-\rho_i} \right\} \end{aligned} \quad (2.9)$$

The index of performance I_R becomes

$$\begin{aligned} I_R &= \frac{b(a-c)^2}{2(b-c)^2} + \frac{2bc}{(b+c)} \frac{(a-c)(b-a)}{(b-c)^2} + \frac{c(b-a)^2}{2(b-c)^2} \\ &\quad - 2 \sum_1^n \frac{a_i}{(b-c)} \left\{ \frac{b(a-c)}{b-\rho_i} + \frac{c(b-a)}{c-\rho_i} \right\} + K_I \end{aligned} \quad (2.10)$$

$K_I = \int_0^{\infty} f(t)^2 dt$ is constant and independent of the unknown coefficients.

The parameters a, b, c will be determined to minimize the index of performance I_R and the second order reduction model will be found.

To determine the parameters α, β, γ , the index of performance I_c should be at its minimum.

I_c is defined as follows in (2.11).

$$I_c = \int_0^{\infty} (g_c(t) - f(t))^2 dt = \int_0^{\infty} (g_c(t)^2 - 2g_c(t)f(t) + f(t)^2) dt \quad (2.11)$$

In the same way, I_C has three terms.

The first term:

$$\begin{aligned} \int_0^\infty g_C(t)^2 dt &= \int_0^\infty e^{-2\beta t} (\alpha^2 \cos^2(\gamma t) + 2\alpha\delta \cos(\gamma t) \sin(\gamma t) \\ &\quad + \delta^2 \sin^2(\gamma t)) dt \end{aligned} \quad (2.12)$$

$$\int_0^\infty g_C(t)^2 dt = \frac{\alpha^2 + \delta^2}{4\beta} + \frac{\beta(\alpha^2 - \delta^2)}{4(\beta^2 + \gamma^2)} + \frac{\alpha\delta\gamma}{2(\beta^2 + \gamma^2)}$$

The second term:

$$\begin{aligned} \int_0^\infty -2g_C(t)f(t)dt \\ = -2 \int_0^\infty \sum_1^n a_i e^{-(\beta-\rho_i)t} (\alpha \cos(\gamma t) + \delta \sin(\gamma t)) dt \end{aligned} \quad (2.13)$$

$$\int_0^\infty -2g_C(t)f(t)dt = -2 \sum_1^n a_i \left\{ \frac{\beta^2 + \gamma^2 - \alpha\rho_i}{(\beta - \rho_i)^2 + \gamma^2} \right\}$$

The index of performance I_C will be

$$\begin{aligned} I_C &= \frac{\alpha^2 + \delta^2}{4\beta} + \frac{\beta(\alpha^2 - \delta^2)}{4(\beta^2 + \gamma^2)} + \frac{\alpha\delta\gamma}{2(\beta^2 + \gamma^2)} \\ &\quad - 2 \sum_1^n a_i \left\{ \frac{\beta^2 + \gamma^2 - \alpha\rho_i}{(\beta - \rho_i)^2 + \gamma^2} \right\} + K_I \end{aligned} \quad (2.14)$$

Where $K_I = \int_0^\infty f(t)^2 dt = \text{constant}$ is independent of the unknown coefficients.

The parameters α , β , γ will be determined to minimize the index of performance I_C , the reduction second order model parameters will be found.

2.2.2 The case of a constant input

The output response will be

$$y(t) = \sum_{i=1}^n b_i e^{\rho_i t} \quad (2.15)$$

$$\text{where } b_i = \lim_{s \rightarrow \rho_i} (s - \rho_i) \frac{F(s)}{s}$$

For $y_R(s)$;

$$y_R(t) = 1 + \frac{(c-a)}{b-c} e^{-bt} + \frac{(a-b)}{b-c} e^{-ct} \quad (2.16)$$

For $y_C(s)$;

$$y_C(t) = 1 - e^{-\beta t} (\cos(\gamma t) + \mu \sin(\gamma t)); \quad \text{where } \mu = \frac{\beta - \alpha}{\gamma} \quad (2.17)$$

The performance index will be calculated in the same way as for real poles reduction model.

$$\begin{aligned} S_R &= \int_0^\infty (y_R(t) - y(t))^2 dt = \int_0^\infty (y_R(t)^2 - 2y_R(t)y(t) + y(t)^2) dt \\ S_R &= \frac{(c-a)^2}{2b(b-c)^2} + \frac{2}{(b+c)} \frac{(c-a)(a-b)}{(b-c)^2} + \frac{(a-b)^2}{2c(b-c)^2} \\ &\quad - 2 \sum_1^n \frac{b_i}{(b-c)} \left\{ \frac{(c-a)}{b-\rho_i} + \frac{(a-b)}{c-\rho_i} \right\} + K_S \end{aligned} \quad (2.18)$$

Where $K_S = \int_0^\infty y(t)^2 dt = \text{constant}$ is independent of the unknown coefficients

Performance index will be calculated also in the same way for the complex poles reduction model.

$$\begin{aligned} S_C &= \int_0^\infty (y_C(t) - y(t))^2 dt = \int_0^\infty (y_C(t)^2 - 2y_C(t)y(t) + y(t)^2) dt \\ S_C &= \frac{\mu^2 + 1}{4\beta} + \frac{\beta(1-\mu^2)}{4(\beta^2 + \gamma^2)} + \frac{\beta - \alpha}{2(\beta^2 + \gamma^2)} + 2 \sum_1^n b_i \left\{ \frac{2\beta - \alpha - \rho_i}{(\beta - \rho_i)^2 + \gamma^2} \right\} + K_S \end{aligned} \quad (2.19)$$

The example that is presented in [3] is the following fourth-order transfer function

$$G_4^{ISE}(s) = \frac{18.439s^3 + 14.446s^2 + 11.454s + 1.3765}{35.83s^4 + 40.388s^3 + 32.541s^2 + 13.94s + 1} \quad (2.20)$$

Using the ISE technique, the model obtained is:

$$G_2^{ISE}(s) = \frac{0.5683s + 0.06965}{s^2 + 0.70038s + 0.506} \quad (2.21)$$

And by dominant poles method, according to [3]

$$G_2^{PD}(s) = \frac{0.5683s + 0.06965}{s^2 + 0.70038s + 0.506} \quad (2.22)$$

The three systems open loop output response with unit input is presented in figure 2.1 are almost identical.

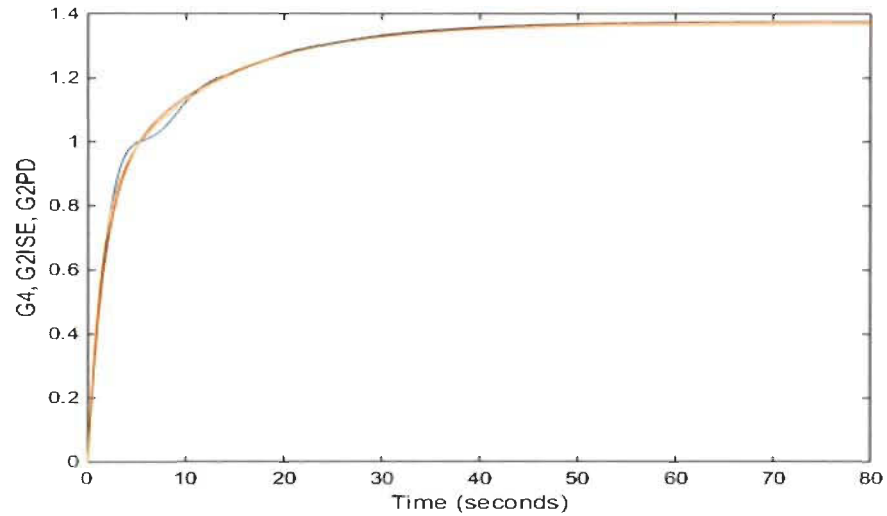


Figure 2. 1: Open loop $G_4^{ISE}(s)$, $G_2^{ISE}(s)$ and $G_2^{PD}(s)$

2.2.3 Controller design based on ISE method

The design of the controller in [1] has been developed using the reduction model based on ISE. This same controller will be applied to the real system. The design of the controller is based on the following second order reference function.

$$G_{ref}(s) = \frac{2.25}{s^2 + 2.1s + 2.25} \quad (2.23)$$

For natural frequency $\omega = 1.5$ rad/s and damping factor $\xi = 0.7$, the design of the controller is as follows:

$$C_{reduit}(s) = \frac{G_{ref}(s)}{G_{reduit}(s)[1 - G_{ref}(s)]} \quad (2.24)$$

$$C_{reduit}(s) = \frac{2.25s^2 + 2.02579s + 0.16085}{0.69611s^3 + 1.56023s^2 + 0.20664s}$$

Simulation was made in closed loop with the controller applied to the real system as well as to the reduced system; the results are shown in figure 2.2.

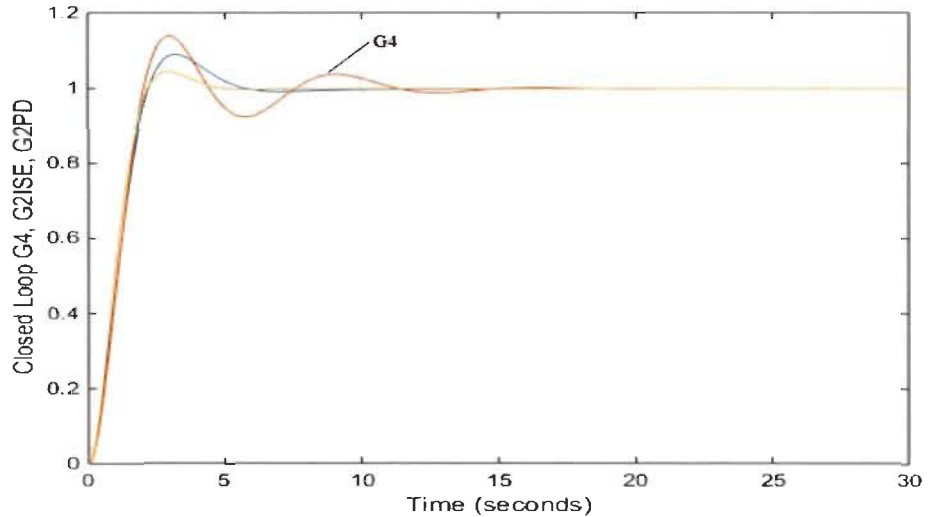


Figure 2. 2: Three systems in closed loop : $G_4^{ISE}(s)$, $G_2^{ISE}(s)$ and $G_2^{PD}(s)$

2.2.4 Analysis of the ISE and its controller design.

The integral square error ISE technique is based on the knowledge of the real system transfer function, which means finding the real system transfer function is necessary prior to applying ISE to reduce it. This implies a lot of mathematical operation to model the actual system. The

technique itself is also based on a lot of mathematical equations to reduce the actual transfer function to a second-order transfer function.

Simulation results of these reduced systems in open loop are almost identical when compared to the real system output response. However, the method of designing the controller gives less satisfactory results when applied to the real system; simulation results illustrate this difference between the reduced models and the real system in closed loop (figure 2.2).

2.3 Pade approximation method

The pade approximation technique is another reduction method of high order transfer functions to lower degree, preferably second order in order to be able to design controllers that will be applied to real systems.

The pade approximation technique is mainly based on the reduction of any function $f(x)$ to a ratio of two polynomials $P_N(x)$ and $Q_M(x)$ with respective degree N and M , $R_{N,M}(x)$ will be defined as the ratio of these two polynomials.

$$R_{N,M}(x) = \frac{P_N(x)}{Q_M(x)} \quad \text{for } a \leq x \leq b \quad (2.25)$$

The goal is to minimize the error between the original function $f(x)$ and $R_{N,M}(x)$. Let's define the two polynomials as follow

$$\begin{aligned} P_N(x) &= p_0 + p_1x + p_2x^2 + \dots + p_Nx^N \\ Q_M(x) &= q_0 + q_1x + q_2x^2 + \dots + q_Mx^M \quad q_0 = 1 \end{aligned} \quad (2.26)$$

They are built so that the functions $f(x)$ and $R_{N,M}(x)$ and their derivatives coincide at all points from origin $x=0$ to $N+M$.

In the case $Q_M(x) = 1$, the approximation is simply the Maclaurin series of $f(x)$.

Assume the function $f(x)$ is continuous, analytical and its derivatives are continuous at the point $x = 0$ so that we can write it in the form of Taylor-Maclaurin series:

$$f(x) = a_0 + a_1x + a_2x^2 + \dots + a_kx^k + \dots$$

$$f(x)Q_M(x) - P_N(x) = Z(x) \quad (2.27)$$

$$\left(\sum_{j=0}^{\infty} a_j x^j\right) \left(\sum_{j=0}^M q_j x^j\right) - \sum_{j=0}^N p_j x^j = \sum_{j=M+N+1}^{\infty} c_j x^j$$

In this equation, the summation of the right side starts from $M + N + 1$. This value is the number of unknown coefficients between the polynomial $P_N(x)$ and $Q_M(x)$ knowing that $q_0 = 1$

This equation can be written in linear form as follows:

$$\begin{aligned} a_0 - p_0 &= 0 \\ q_1 a_0 + a_1 - p_1 &= 0 \\ q_2 a_0 + q_1 a_1 + a_2 - p_2 &= 0 \\ q_3 a_0 + q_2 a_1 + q_1 a_2 + a_3 - p_3 &= 0 \\ q_M a_{N-M} + q_{M-1} a_{N-M+1} + \dots + a_N - p_N &= 0 \\ q_M a_{N-M+1} + q_{M-1} a_{N-M+2} + \dots + q_1 a_N + a_{N+1} &= 0 \\ q_M a_{N-M+2} + q_{M-1} a_{N-M+3} + \dots + q_1 a_{N+1} + a_{N+2} &= 0 \\ &\dots \\ q_M a_N + q_{M-1} a_{N+1} + \dots + q_1 a_{N+M-1} + a_{N+M} &= 0 \end{aligned} \quad (2.28)$$

It should be noted that, from these equations we can determine q_1, q_2, \dots, q_M coefficients first which will be used in other equations to find the coefficients p_1, p_2, \dots, p_N .

As a result; the two polynomials $P_N(x)$ and $Q_M(x)$ will be determined. Their ratio will be the best approximation of the function $f(x)$ until $N + M$ degree.

Example of illustration in (2.29) taken from [2] as a direct application of pade approximation to find a second order reduced model and its controller design.

$$G_4^{Pade}(s) = \frac{28s^3 + 496s^2 + 1800s + 2400}{2s^4 + 36s^3 + 204s^2 + 360s + 240} \quad (2.29)$$

Applying pade approximation method, the transfer function is reduced to:

$$G_2^{Pade}(s) = \frac{11.98s + 12.53}{s^2 + 2.138s + 1.253} \quad (2.30)$$

Simulation is made to compare the real and reduced system in open loop. The results are shown in figure 2.3. Both systems are almost identical.

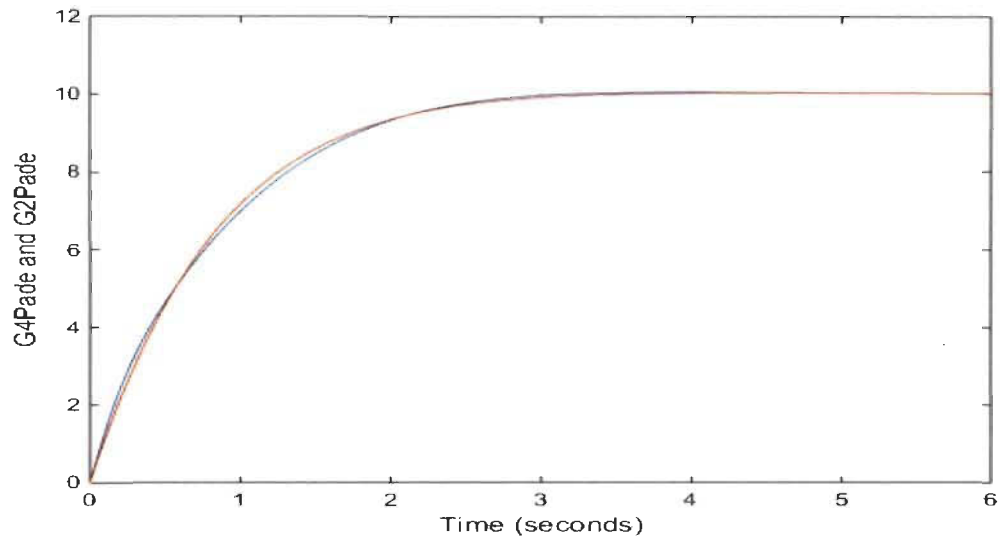


Figure 2. 3: Open loop $G_4^{Pade}(s)$ and $G_2^{Pade}(s)$

2.3.1 Controller design based on Pade approximation

From [2], the design of the controller will be made with the method of zeros and poles cancellation applies to the reduced system in (2.30), the controller is a PID, the coefficients of the controller obtained with this method are $K_p = 2.1224$; $K_i = 1.257$; $K_d = 1$

Another optimization step of these PID parameters is done by computer. The final PID parameters according to [2] are.

$$K_p = 50; \quad K_i = 2; \quad K_d = 0.001$$

It must be noted that this step is necessary to obtain the desired results in closed loop.

Simulation in closed loop with the designed controller applied to the real and reduced model are illustrated in figure 2.4.

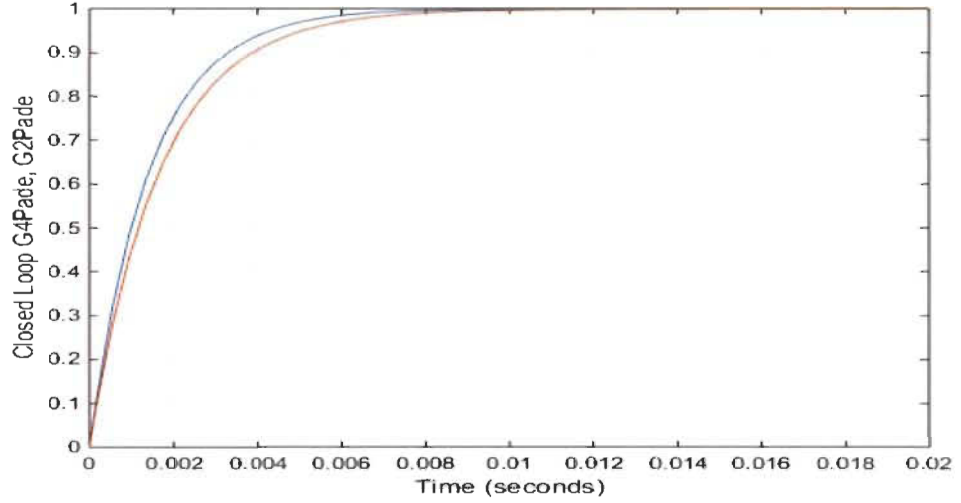


Figure 2. 4: Closed loop $G_4^{Pade}(s)$ and $G_2^{Pade}(s)$

2.3.2 Analysis of pade and its controller design.

The pade technique is based on the knowledge of the transfer function of the real system in the same way as ISE, which means that real system transfer function is necessary prior to finding its second order reduced model, that involves a lot of mathematical operation before even applying this technique. The Pade technique itself is also based on heavy mathematical equations to reduce the actual transfer function in a reduced second-order transfer function. Simulation results in the open-loop are illustrated in figure 2.3. The reduced model with pade is identical to the real system output response. However, the method of designing the controller based on the reduced model gives good results but this design is done in two steps. The first step is based on the cancellation of the zeros and poles and the second step is based on computer simulation for a final desired output in closed loop.

2.4 Conclusion

Pade approximation method is a reduction technique of systems with high order transfer function, the knowledge of the transfer function of these systems is necessary before starting to use the method. The technique itself has a lot of heavy mathematical operations based on Taylor-Maclaurin series. The controller considered in [1] is a PID, which is designed in two steps, the first is the elimination of poles and zeros of the reduced model, and the second step uses computer algorithms for a final optimization of K_p , K_i , K_d to meet the desired closed loop output response.

Chapter 3: New proposed reduction method

3.1 Similar systems new approach theory

In mathematics, it is well known that two sets A and B are identical if and only if:

$$(\forall x \in A, x \in B \Rightarrow x \in A) \text{ and } (\forall x \in B, x \in A \Rightarrow x \in B)$$

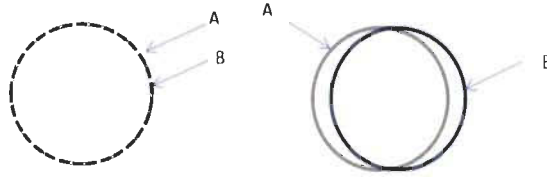


Figure 3. 1: a) Two identical sets b) Two similar sets

Two similar sets are presented in figure 3.1(b). In this case, any element belonging to the intersection of A and B must first be a weighted element of the two sets A and B. The low weighted elements may or may not belong to this intersection.

$$\left(\begin{array}{l} \forall x; x \text{ is a weighted element;} \\ x \in A \cap B \end{array} \right) \Rightarrow A \text{ and } B \text{ are similar}$$

In each set or system, the weighted elements are to be defined first in order to conclude on the similarity of the two systems.

Real systems which can be mechanical, electrical, etc., will be defined by their significant weighted elements that characterize them. In our case, systems are characterized in the first place by the number of input-output (Multi Input Multi Output, Single Input Single Output, Single Input Multi Output, Multi Input Single Output). In the case of a stable system, the weighted elements will be defined as:

ψ_1 : Input value applied to the system

ψ_2 : Steady state value of the system

ψ_3 : Projected rising time of the output response

ψ_4 : Output response in transient regime

ψ_5 : System gain

ψ_6 : Initial delay time of the output response.

Two systems are similar if all their respective weighted elements ψ_i of both systems are identical (figure 3.2).

$$\left(\begin{array}{l} \forall x; x \text{ is a weighted element} \\ x \in A \cap B \end{array} \right) \Rightarrow A \text{ and } B \text{ are similar}$$

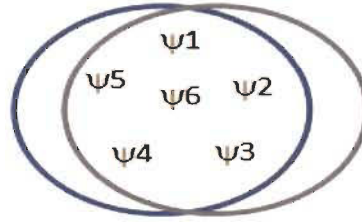


Figure 3. 2: Two similar systems A and B.

3.2 Similar systems application to black box

The presented “**similar systems**” notion is applied to approximate the real system taken as a black box and based only on its input value and output response.

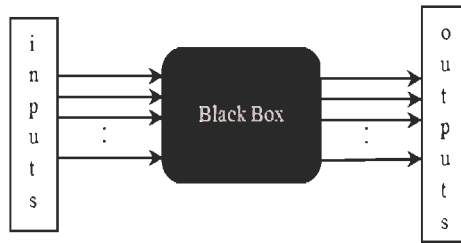


Figure 3. 3: Real system with access to its inputs values and its outputs responses.

For a unit input value applied to the system, the output response will be recorded as shown in the figures 3.4, 3.5, 3.6.

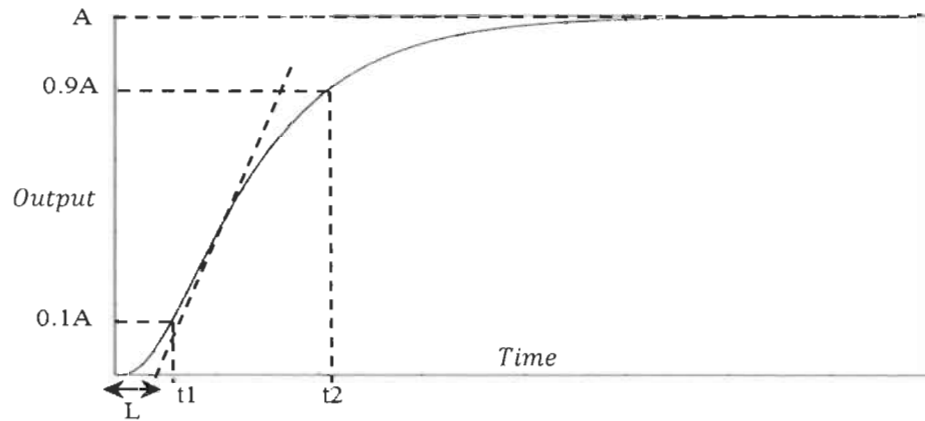


Figure 3. 4: Output response for real system with no overshoot

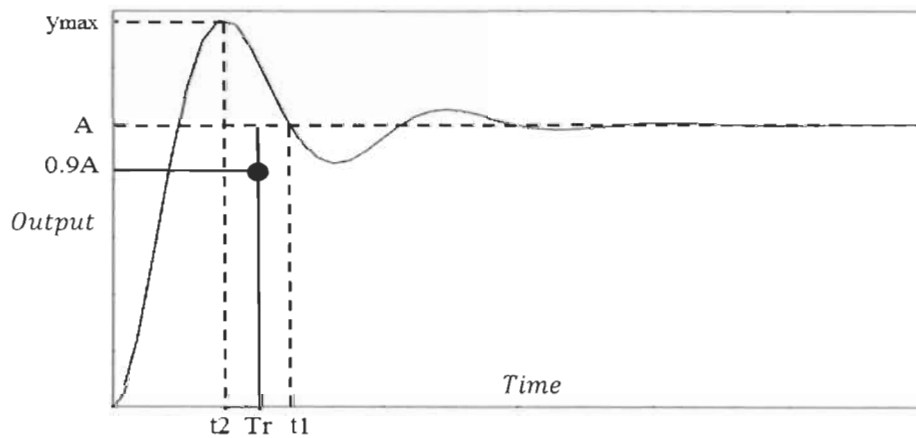


Figure 3. 5: Output response for real system with overshoot and oscillations.

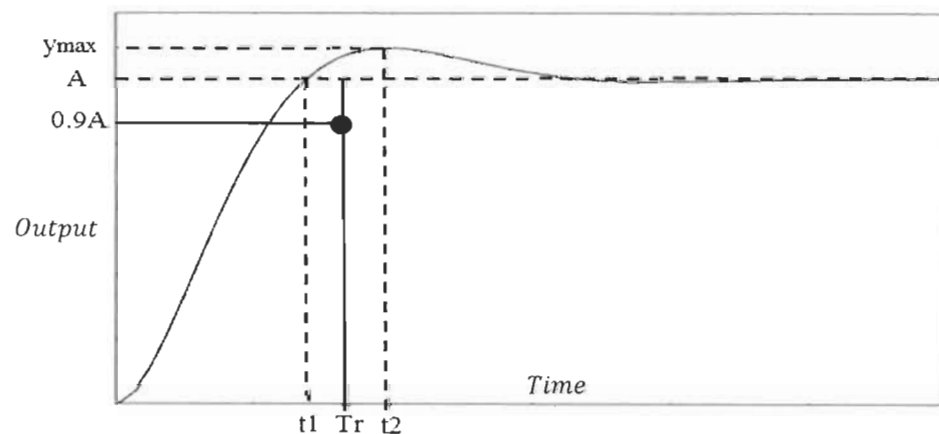


Figure 3. 6: Output response for real system with overshoot and no oscillation.

After recording the input value and the output response, the weighted elements of the black box system can be determined.

For simplicity, the first weighted element ψ_1 is 1 (unit input).

$$\psi_1 = 1 \quad (3.1)$$

The weighted element ψ_2 is determined directly from figure 3.4, 3.5, 3.6.

$$\psi_2 = A \quad (3.2)$$

The weighted element system gain ψ_5 is also directly determined from ψ_1 and ψ_2 .

$$\psi_5 = \frac{\psi_2}{\psi_1} = \frac{A}{1} \quad (3.3)$$

The weighted element ψ_3 , the projected rise time will be also determined from the output response figure 3.4 if the output response presents no overshoot.

$$\begin{aligned} \psi_3 &= t_2 - t_1 = T_r \\ t_2 &= \text{time at } 0.9A \\ t_1 &= \text{time at } 0.1A \end{aligned} \quad (3.4)$$

And in figure 3.5 and 3.6, the first step is to draw the 0.9A value. The projected rising time T_r will be defined as the average time between t_1 and t_2

$$\begin{aligned} \psi_3 &= \frac{(t_2 + t_1)}{2} = T_r \\ t_2 &= \text{time correspondant to } y_{max} \\ t_1 &= \text{time correspondant to } y(t) \text{ at } y = A \end{aligned} \quad (3.5)$$

The weighted element ψ_6 which is the initial delay is also determined from the output response curve (figure 3.4, 3.5, 3.6):

$$\psi_6 = D \quad (3.6)$$

After finding the weighted elements ψ_1 , ψ_2 , ψ_3 , ψ_5 and ψ_6 , an approximation of a first order system with the same weighted elements will be determined. The weighted element ψ_4 is the last element to be determined to find the final tuned first order transfer function.

The approximate system will have the following transfer function type

$$G_{NA}(s) = \frac{K}{s + x} e^{-sD} \quad (3.7)$$

The weighted element ψ_1 is applied to this first order system.

$$\begin{aligned} \psi_1 &= 1; \quad \psi_2 = \frac{K}{x} \\ \psi_5 &= \frac{\psi_2}{\psi_1} = \frac{K}{x} \end{aligned} \quad (3.8)$$

From these three weighted elements.

$$\frac{K}{x} = A \quad (3.9)$$

Knowing that the rising time of a first-order transfer function is:

$$\psi_3 = \frac{2.2}{x} \quad (3.10)$$

This weighted element should coincide with that of the real system (black box).

$$\frac{2.2}{x} = T_r \quad (3.11)$$

We can then determine the constants K and x as follows:

$$x = \frac{2.2}{T_r} \quad ; \quad K = \frac{2.2}{T_r} A \quad (3.12)$$

Now, real and approximated systems have the same weighted elements $\psi_1, \psi_2, \psi_3, \psi_5, \psi_6$. The approximated system of first-order transfer function will be.

$$G(s) = \frac{K}{s + x} e^{-sD} \quad (3.13)$$

$$x = \frac{2.2}{T_r} \quad ; \quad K = \frac{2.2}{T_r} A$$

The last weighted element ψ_4 will be validated once the output of first-order is compared to the real system output. In this case we say that both systems are similar.

3.3 Application to different black box systems output

A. Case study 1

$$G_1(s) = \frac{s + 1}{s^3 + 5s^2 + 17s + 13} \quad (3.14)$$

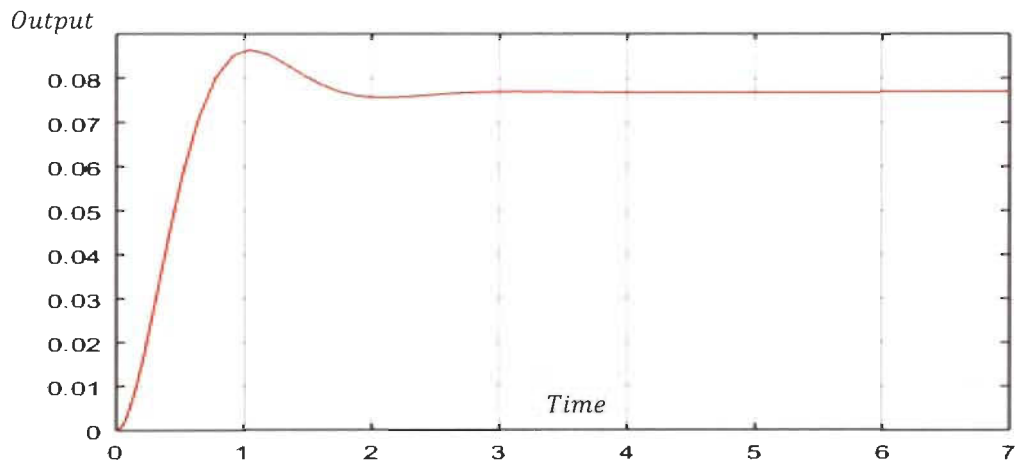


Figure 3. 7: Output response of the real system in open-loop.

This output response will be used to find the approximated transfer function using the six weighted elements.

A unit input is applied to the real system. The steady-state of the output response is $A = 0.07691$ and the three weighted elements are:

$$\psi_1 = 1 ; \quad \psi_2 = \frac{K}{x} = 0.07691$$

$$\psi_5 = \frac{\psi_2}{\psi_1} = \frac{K}{x} = 0.07691$$

The weighted element ψ_3 related to the rising time will be determined as shown in figure 3.5.

Then, the weighted element ψ_4 can be optimized at the same time.

$$\psi_3 = \frac{2.2}{x} = T_r = \frac{t_1 + t_2}{2} = 0.7615$$

From these equations, we can easily determine the parameters K and x .

$$x = \frac{2.2}{T_r} = 2.889 \quad ; \quad K = \frac{2.2}{T_r} A = 0.2222$$

The weighted element ψ_6 which is the initial delay will be determined directly from the output response figure 3.5.

$$\psi_6 = D = 0.07$$

The first-order transfer function will be.

$$G_1^{NA}(s) = \frac{K}{s + x} e^{-sD} = \frac{0.2222}{s + 2.889} e^{-s0.07} \quad (3.15)$$

Simulation for comparison between the real and reduced open loop system is made (Figure 3.8).

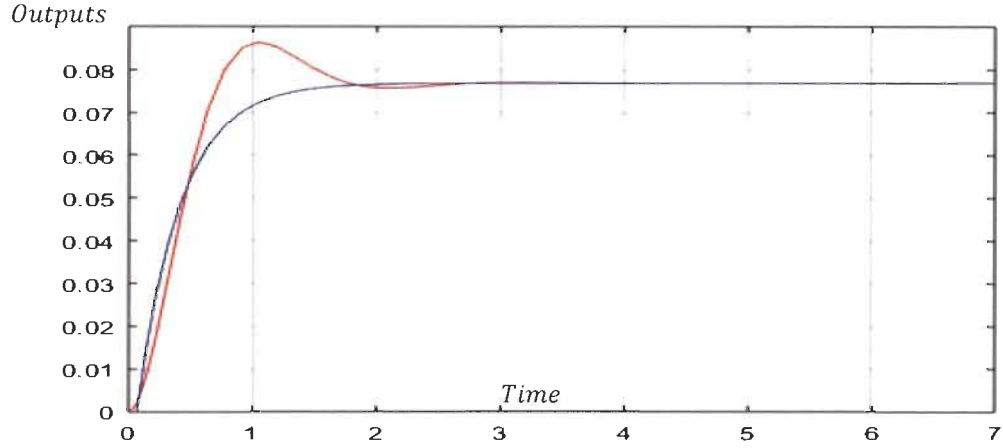


Figure 3. 8: Output response of the real and reduced open-loop system.

One can see that both outputs coincide on all elements $\psi_1, \psi_2, \psi_3, \psi_4, \psi_5$ and ψ_6 . However, the two curves do not absolutely coincide on the overshoot of the real system output, but this element is a low weighted element and will not influence the design of the closed loop controller.

B. Case study 2

$$G_2(s) = \frac{0.5s + 20}{s^4 + 10s^3 + 35s^2 + 50s + 24} \quad (3.16)$$

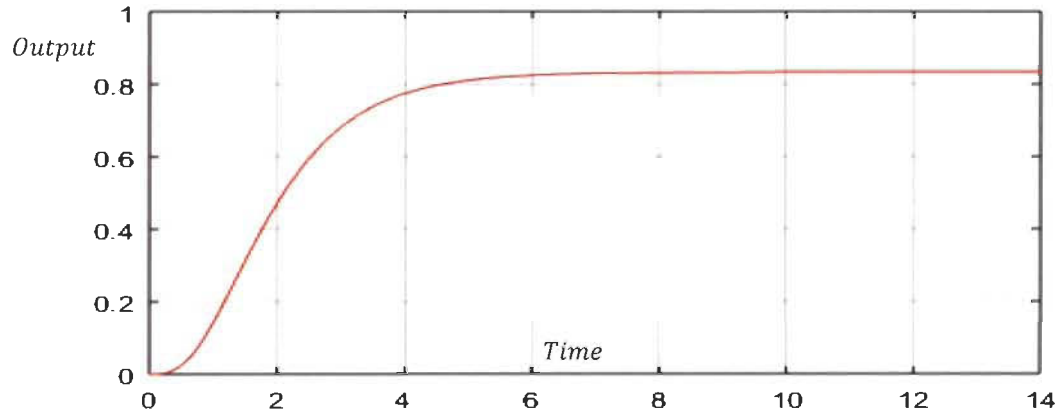


Figure 3. 9: Output response of the real open loop system with no overshoot.

A unit entry is applied to the real system, the steady-state of the output response is $A=0.8333$. Then the three weighted elements are found as:

$$\psi_1 = 1 \quad ; \quad \psi_2 = \frac{\kappa}{x} = 0.8333$$

$$\psi_5 = \frac{\psi_2}{\psi_1} = \frac{K}{x} = 0.8333$$

The fact that the real system output does not have an overshoot, the element ψ_3 is determined using figure 3.4.

$$\psi_3 = \frac{2.2}{x} = T_r = 2.79$$

$$x = \frac{2.2}{T_r} = 0.786 ; K = \frac{2.2}{T_r} A = 0.655$$

The element ψ_6 which is the initial delay will be determined at the same time that ψ_4 is validated due to the nature of the output response (no overshoot).

$$\psi_6 = D = 0.7$$

The first-order transfer function will be.

$$G_2^{NA}(s) = \frac{0.655}{s + 0.786} e^{-s0.7} \quad (3.17)$$

Simulation for comparison between the real and reduced open loop system is illustrated on figure 3.10.

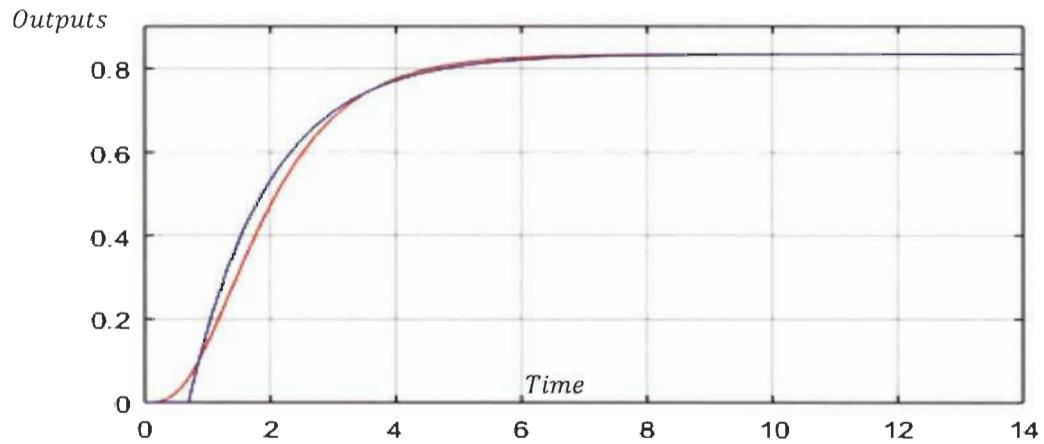


Figure 3. 10: Real and reduced system output response in open-loop.

C. Case study 3

$$G_3(s) = \frac{0.5s + 20}{s^3 + 8s^2 + 420s + 1616} \quad (3.18)$$

This real system is a third order with an output response presenting oscillations with decreasing amplitude until its steady state regime as shown in figure 3.11. The approximate similar system will be the average first order using the weighted elements, especially ψ_3 the projected rising time.

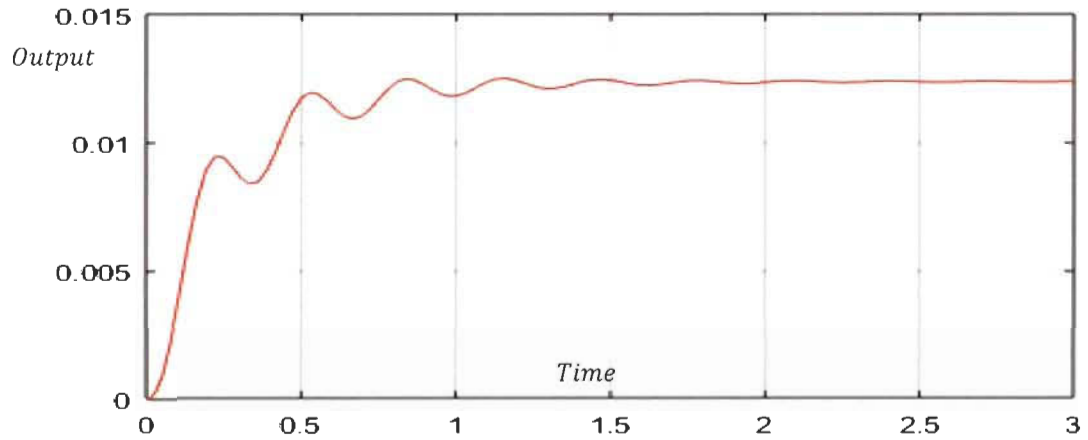


Figure 3. 11: Output response of the real system with no overshoot with oscillations.

A unit input is applied to the real system, the steady-state of the output response is $A = 0.01238$ then the three weighted elements are also found:

$$\psi_1 = 1 \quad ; \quad \psi_2 = \frac{\kappa}{x} = 0.01238$$

$$\psi_5 = \frac{\psi_2}{\psi_1} = \frac{K}{x} = 0.01238$$

The element ψ_3 , the rising time is then determined. The real system output response presents small oscillations, so the element ψ_3 will be determined using figure 3.4.

$$\psi_3 = \frac{2.2}{x} = T_r = 0.44$$

From the previous equations, the parameters K and x can be easily determined.

$$x = \frac{2.2}{T_r} = 5 ; K = \frac{2.2}{T_r} A = 0.0619$$

The weighted element ψ_6 which is the initial delay is determined directly from the output response with a validation of the element ψ_4 .

$$\psi_6 = D = 0.05$$

Finally, the first order transfer function approximation is.

$$G_3^{NA}(s) = \frac{0.0619}{s + 5} e^{-s0.05} \quad (3.19)$$

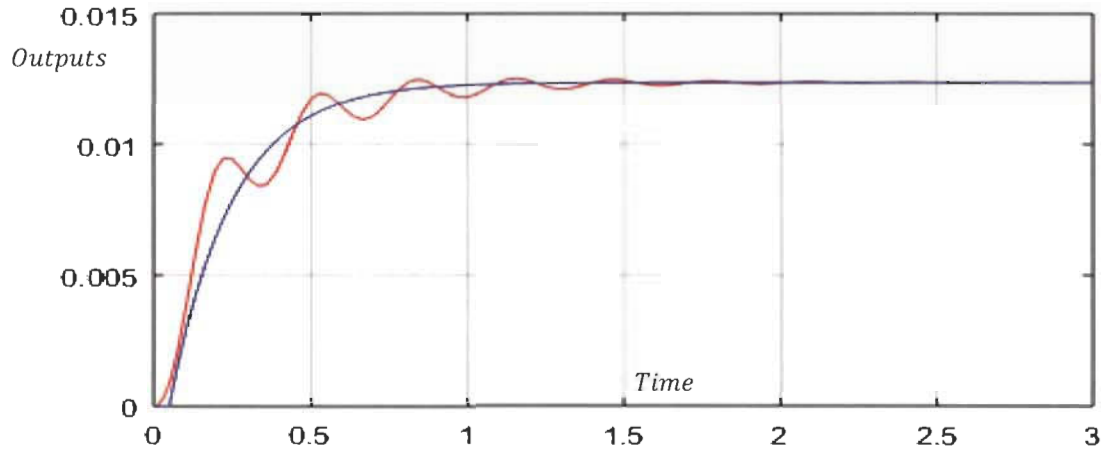


Figure 3. 12: Output of the real and reduced system response in open loop.

D. Case study 4

This system is taken from [4] for the purpose of comparison and analysis with its reduced model using improved pole clustering and PSO reduction method.

$$G_4(s) = \frac{35s^7 + 1086s^6 + 13285s^5 + 82402s^4 + 278376s^3 + 511812s^2 + 482964s + 194480}{s^8 + 21s^7 + 220s^6 + 1558s^5 + 7669s^4 + 24469s^3 + 46350s^2 + 45952s + 17760} \quad (3.20)$$

$$G_{Red[4]}(s) = \frac{38.777313s + 405.710876}{s^2 + 12.0490936s + 37.0496961}$$

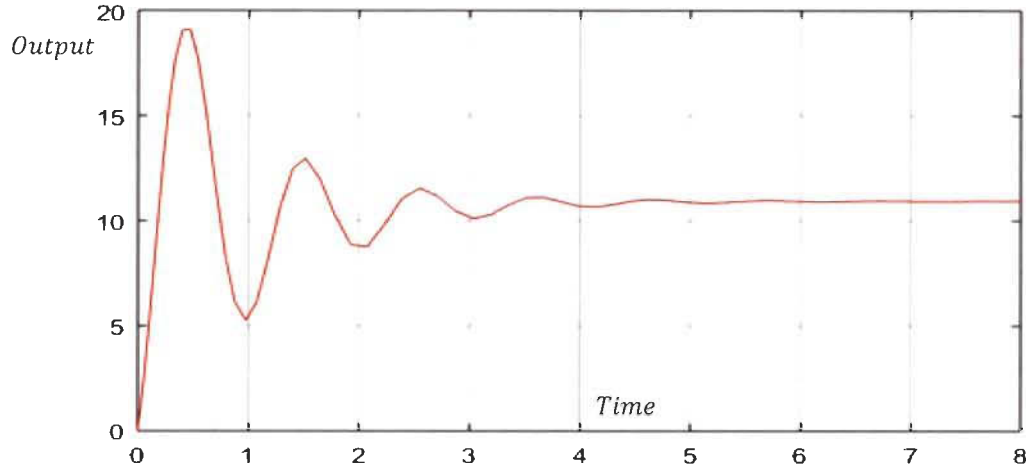


Figure 3. 13: Output of the real system in open loop with overshoot and oscillations.

A unit input is applied to the real system, the steady-state of the output response is $A=10.9474$, then the three weighted elements are found:

$$\psi_1 = 1 ; \quad \psi_2 = \frac{K}{x} = 10.9474$$

$$\psi_5 = \frac{\psi_2}{\psi_1} = \frac{K}{x} = 10.9474$$

The rising time ψ_3 will be determined as shown in figure 3.5 because the output response of the real system presents overshoot plus oscillations.

$$\psi_3 = \frac{2.2}{x} = T_r = \frac{t_2 + t_1}{2} = 0.5813$$

From these equations, one can easily determine the parameters K , x .

$$x = \frac{2.2}{T_r} = 0.37846 ; \quad K = \frac{2.2}{T_r} A = 41.4315$$

$$\psi_6 = D = 0$$

The element ψ_6 which is the initial delay will be determined directly from the output response.

The first-order transfer function will be.

$$G_4^{NA}(s) = \frac{41.4315}{s + 3.7846} \quad (3.21)$$

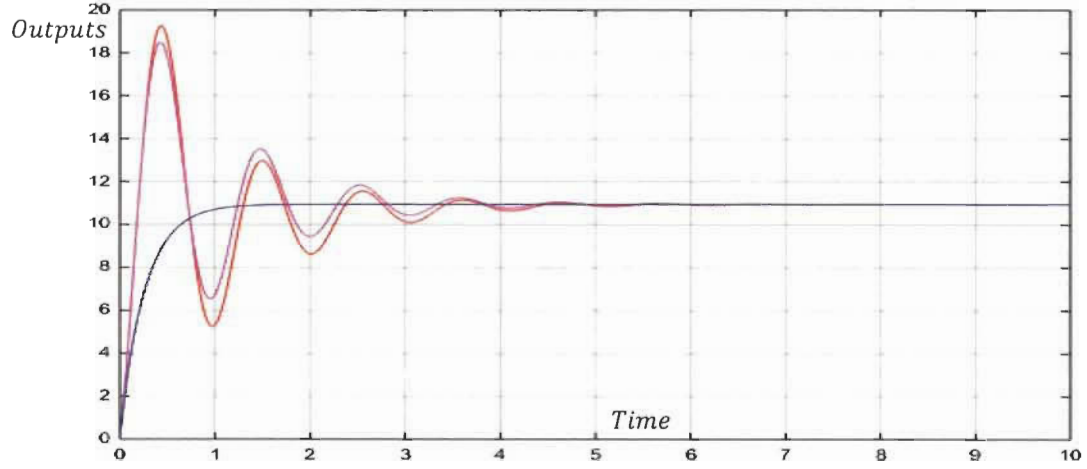


Figure 3. 14: Output response of the three systems- Real, reduced in [4] and proposed similar system.

In figure 3.14, the two systems taken from [4] are almost identical using the pole clustering and PSO reduction method that uses a lot of mathematical equations to find this identical reduced model. The similar reduced system is not identical to the real system but similar based on their common weighted elements $\psi_1, \psi_2, \psi_3, \psi_4, \psi_5$ and ψ_6 .

E. Case study 5

This system is taken from [3] for purpose of comparison and analysis and its reduced model using modified pole clustering and pade approximation.

$$G_5(s) = \frac{18s^7 + 514s^6 + 5982s^5 + 36380s^4 + 122664s^3 + 222088s^2 + 185760s + 40320}{s^8 + 36s^7 + 546s^6 + 4536s^5 + 22449s^4 + 67284s^3 + 8118124s^2 + 109584s + 40320} \quad (3.22)$$

$$G_{Red[5]}(s) = \frac{16.51145s + 5.45971}{s^2 + 6.19642s + 5.45971}$$

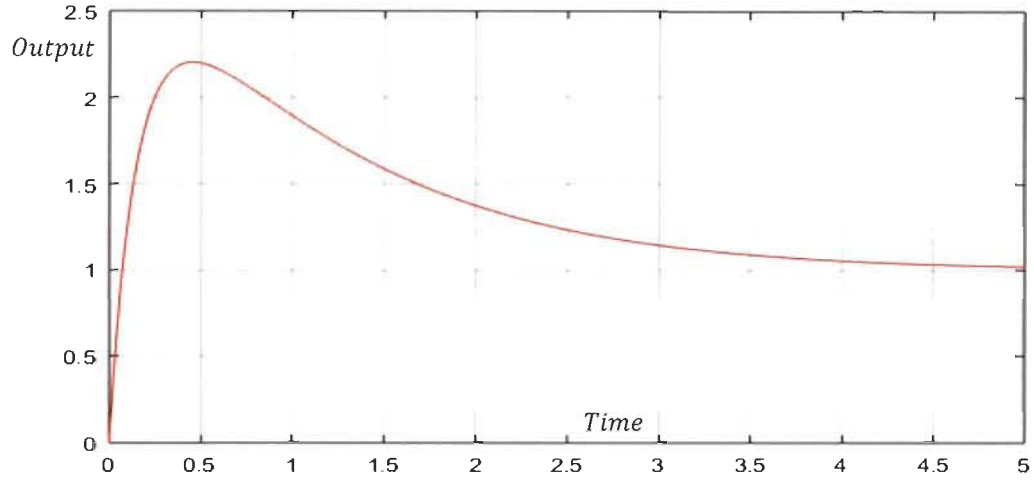


Figure 3. 15: Output of the real system in open loop with overshoot only.

A unit input is applied to the real system; the steady-state of the output response is 1 then:

$$\psi_1 = 1 \quad ; \quad \psi_2 = \frac{K}{x} = 1 \quad ; \quad \psi_5 = \frac{P_2}{P_1} = \frac{K}{x} = 1$$

The rising time ψ_3 will be determined as shown in figure 3.6 because the output response of the real system presents overshoot without oscillations.

$$\psi_3 = \frac{2.2}{x} = T_r = \frac{t_1+t_2}{2} = 0.244 \quad ; \quad \psi_6 = D = 0$$

From these equations, one can easily determine the parameters K and x.

$$x = \frac{2.2}{T_r} = 9 \quad ; \quad K = \frac{2.2}{T_r} A = 9 \quad (3.23)$$

$$G_5^{NA}(s) = \frac{9}{s+9}$$

The simulation in open-loop is shown in figure 3.16.

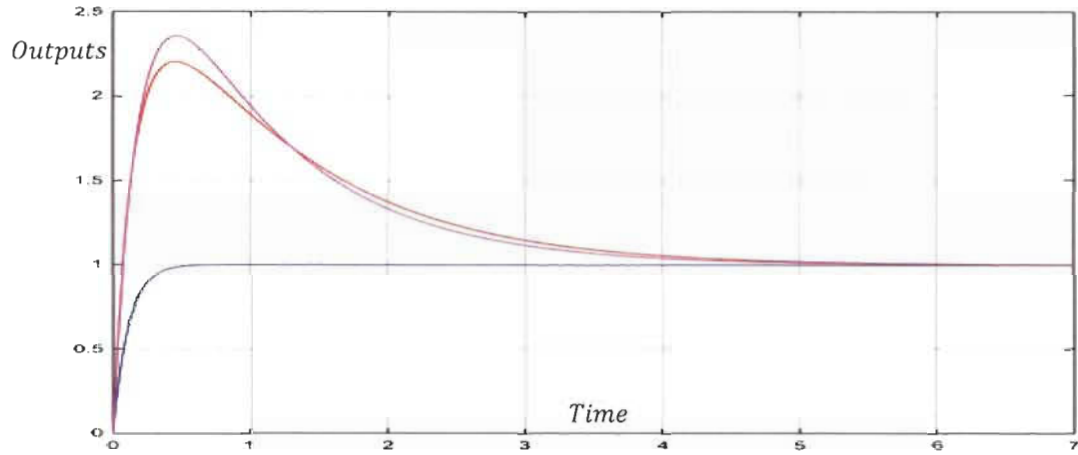


Figure 3. 16: Output response of the real, reduced system in [3] and proposed similar system.

In figure 3.16, the real and reduced systems taken from [3] are identical using pade approximation and modified pole clustering. This mixed method uses more mathematical equations to find the approximate identical low order transfer function. At the same time, the proposed reduced system based on the common weighted elements ψ_1 , ψ_2 , ψ_3 , ψ_4 , ψ_5 and ψ_6 is similar and found with simple equations based only on output response. It is sufficient to design a controller based on this similar system to perfectly control the real system.

3.4 PI Controller design for black box systems

Our system is a black box and can be approximated by a first order transfer function. For simplicity the PI controller design using the first order similar system will be without delay. Once the controller is designed, the delay will be added to the closed loop.

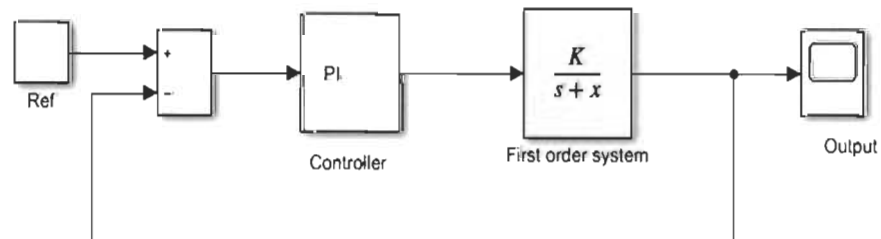


Figure 3. 17: Similar closed-loop system.

The PI controller transfer function is.

$$C(s) = K_p + \frac{K_I}{s} = \frac{sK_p + K_I}{s}$$

Closed loop transfer function of the blocks diagram (figure 3.17) will be.

$$G_{CL}^{NA}(s) = \frac{sKK_p + KK_I}{s^2 + s(x + KK_p) + KK_I} \quad (3.24)$$

Depending on the design criteria required as a closed loop output response, the damping factor ζ and the natural frequency ω_n will be defined. In this case the reference closed loop transfer function of second order will be determined:

$$G_{CL}^{ref}(s) = \frac{\omega_n^2}{s^2 + 2\xi\omega_n s + \omega_n^2} \quad (3.25)$$

The design of the controller will be:

$$\begin{aligned} K_I K &= \omega_n^2 \quad ; \quad K_I = \frac{\omega_n^2}{K} \\ x + K_p K &= 2\xi\omega_n \quad ; \quad K_p = \frac{2\xi\omega_n - x}{K} \end{aligned} \quad (3.26)$$

For design reasons, the proportionality coefficient of the controller must be positive. The choice of the damping factor ξ is very important to control the overshoot percentage. Once the controller design is finalized for the similar first order system, the controller will be applied to the black box system.

$$\begin{aligned} K_p &= \frac{2\xi\omega_n - x}{K} > 0 \\ \omega_n &> \frac{x}{2\xi} \end{aligned} \quad (3.27)$$

3.5 Controller design approach based on similar systems

A. Case study 1

$$G_1(s) = \frac{s + 1}{s^3 + 5s^2 + 17s + 13}$$

$$G_1^{NA}(s) = \frac{0.2222}{s + 2.889} e^{-s0.07}$$

Using equation (3.27), the values of K_I and K_p are obtained for $\zeta = 0.99$ and $\omega_n = 1.48 \text{ rad/s}$

$$K_I = \frac{\omega_n^2}{K} = 9.8578 \quad ; \quad K_p = \frac{2\zeta\omega_n - x}{K} = 0.1863$$

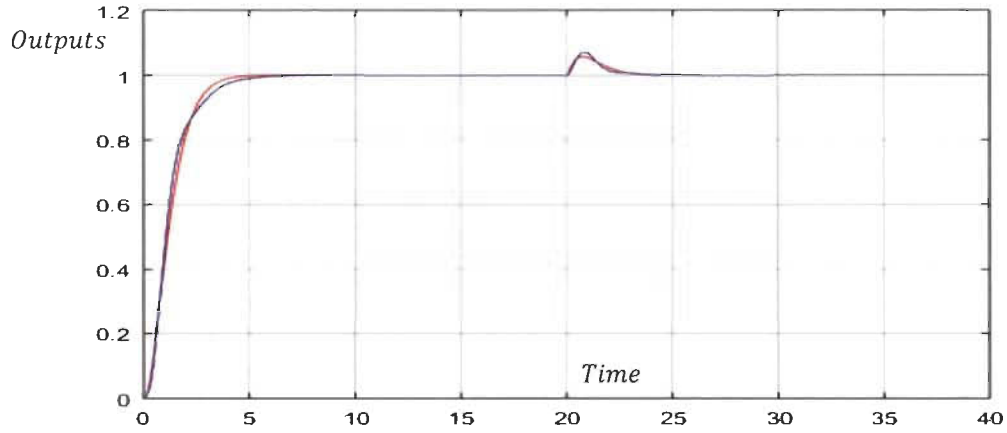


Figure 3. 18: Real and reduced closed loop with disturbance. ($\zeta = 0.99$ and $\omega_n = 1.48 \text{ rad/s}$).

From equation (3.27), for $\zeta = 1.2$; ω is 1.23 rad/s and from equation (3.26)

$$K_I = \frac{\omega_n^2}{K} = 6.8087 \quad ; \quad K_p = \frac{2\zeta\omega_n - x}{K} = 0.2835$$

The controller is applied to both the real and the similar systems. Figures 3.18 and 3.19 show improved settling time outputs simulation. Both systems are identical in closed loop without necessarily being identical in open loop; but they are similar in their significant weighted elements.

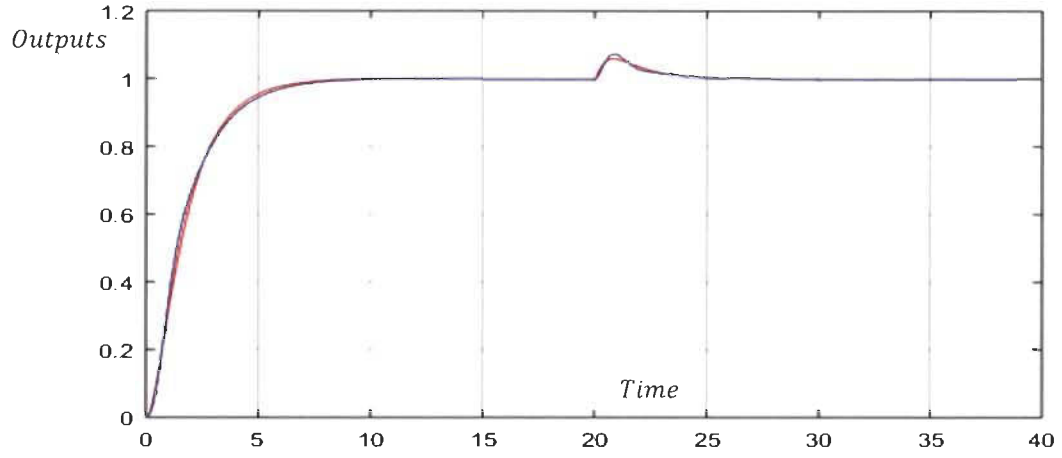


Figure 3. 19: Real and reduced closed loop with disturbance. $\zeta = 1.2$ and $\omega_n = 1.23$ rad/s.

B. Case study 2

$$G_2(s) = \frac{0.5s + 20}{s^4 + 10s^3 + 35s^2 + 50s + 24}$$

$$G_2^{NA}(s) = \frac{0.655}{s + 0.786} e^{-s0.7}$$

Applying the new approach for PI controller design (3.26) and (3.27) for

$$\zeta = 0.99 ; \omega_n = 0.45 \text{ rad/s} \quad \omega_n > \frac{x}{2\xi} = 0.4 \text{ rad/s}.$$

$$K_I = \frac{\omega_n^2}{K} = 0.309 \quad K_p = \frac{2\xi\omega_n - x}{K} = 0.16$$

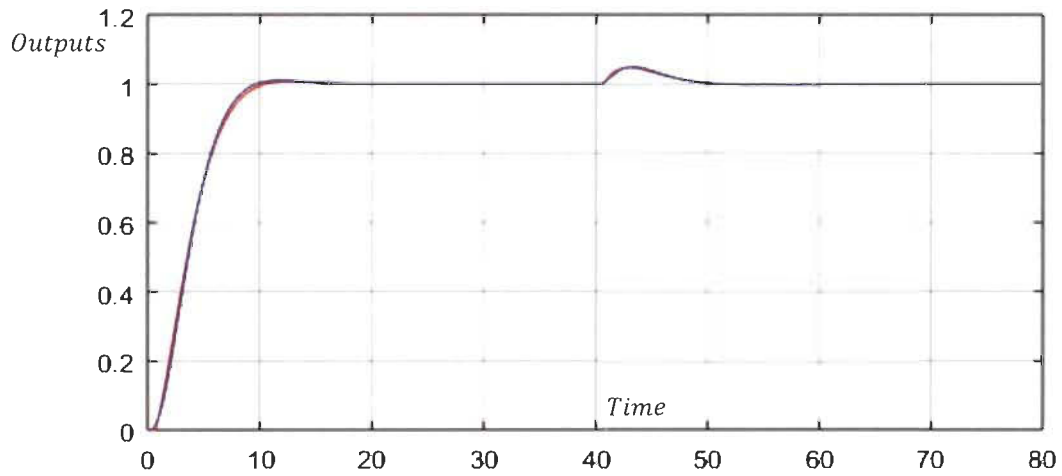


Figure 3. 20: Real and reduced closed loop with disturbance. ($\zeta = 0.99$ and $\omega_n = 0.45$ rad/s).

C. Case study 3

The design of PI controller will be made on the transfer function of the first order in equation 3.19 which is our reduced system. Applying the new approach design concept with $\zeta = 0.99$; $\omega_n = 2.55\text{rad/s}$; $\omega_n > \frac{x}{2\zeta} = 0.52\text{rad/s}$, the PI coefficients are determined.

$$K_I = \frac{\omega_n^2}{K} = 105.048 \ ; \ K_p = \frac{2\zeta\omega_n - x}{K} = 0.7915$$

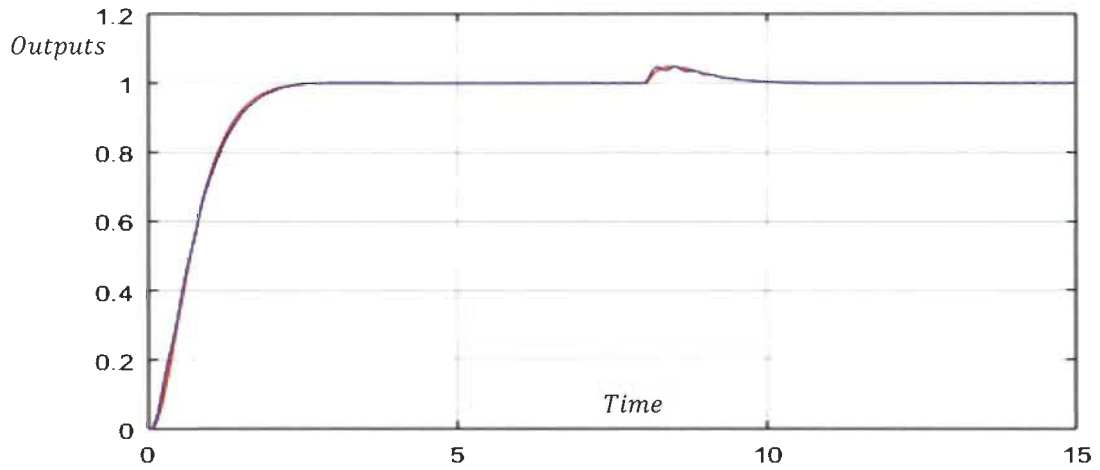


Figure 3. 21: Real and reduced closed loop with disturbance. ($\zeta = 0.99$ and $\omega_n = 2.55$ rad/s).

For $\zeta = 0.7$ and $\omega_n = 3.6\text{rad/s}$ $\omega_n > \frac{x}{2\zeta} = 3.57\text{rad/s}$

$$K_I = \frac{\omega_n^2}{K} = 209.3699 \quad K_p = \frac{2\zeta\omega_n - x}{K} = 0.6462$$

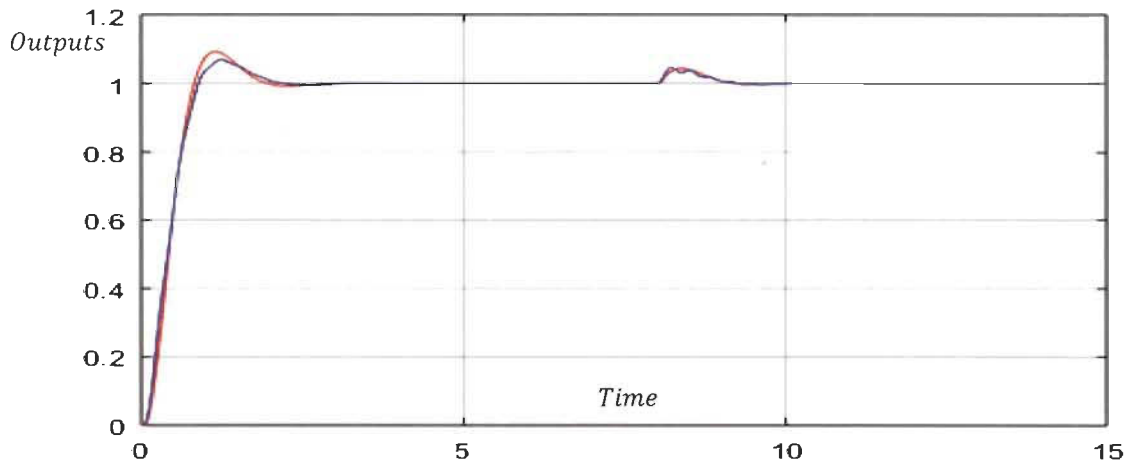


Figure 3. 22: Real and reduced closed loop with disturbance. $\zeta = 0.7$ and $\omega_n = 3.57$ rad/s.

D. Case study 4

The design of PI controller will be made on the first order highlighted in equation 21 and will be applied to the real system, reduced system in [4] and the first order similar system for low and high natural frequencies (figure 3.23 and 3.24).

For damping factor $\zeta = 1.5$ and $\omega_n > \frac{x}{2\xi} = 1.26\text{rad/s}$, chosen $\omega_n = 1.28\text{rad/s}$, the PI controller are found.

$$K_I = \frac{\omega_n^2}{K} = 0.001337 \quad K_p = \frac{2\xi\omega_n - x}{K} = 0.03954$$

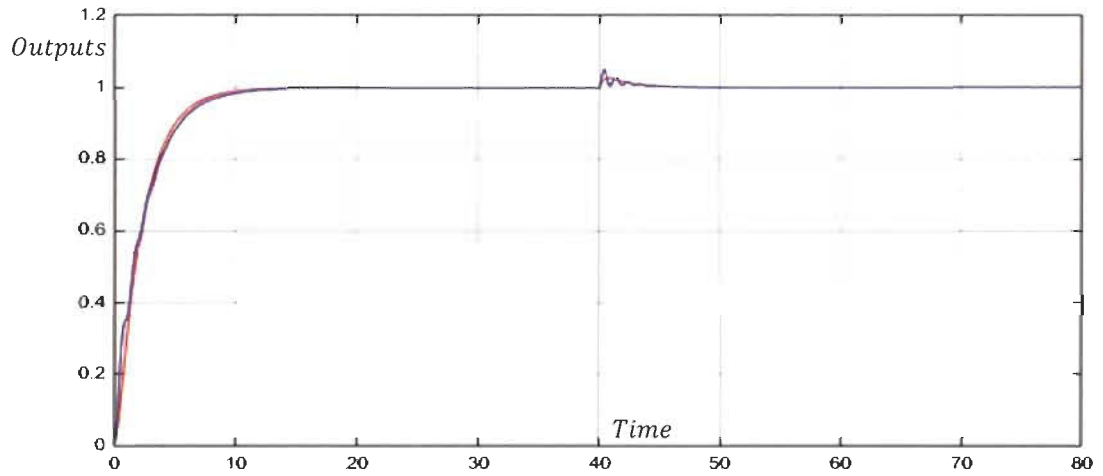


Figure 3. 23: Real and reduced closed loop with disturbance. ($\zeta=1.5$; $\omega_n=1.28\text{rad/s}$)

For high natural frequency $\omega = 300\text{rad/s}$ damping factor $\zeta = 2$

$$K_I = \frac{\omega_n^2}{K} = 2172.26 \quad K_p = \frac{2\xi\omega_n - x}{K} = 28.8721$$

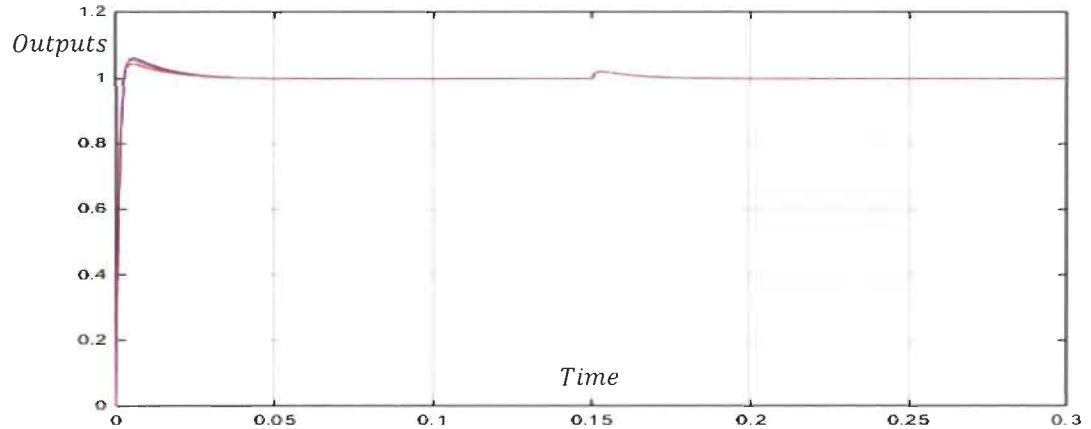


Figure 3. 24: Real and reduced closed loop with disturbance. $\zeta=2$; $\omega_n=300\text{rad/s}$

Simulations were done with the same PI controller designed based on the proposed similar system with disturbance at $t = 40\text{s}$ in figure 3.23 and $t = 0.15\text{s}$ in figure 3.24. The results show that all three systems are controlled perfectly and almost identically.

E. Case study 5

The design of PI controller will be made on the first order system highlighted in equation 23 and will be applied to the real system, reduced system in [3] and the first order similar system. For damping factor $\zeta = 0.99$ and $\omega = 100\text{rad/s}$; The controller PI coefficients are:

$$K_I = \frac{\omega_n^2}{K} = 1111.111 ; \quad K_p = \frac{2\zeta\omega_n - x}{K} = 21$$

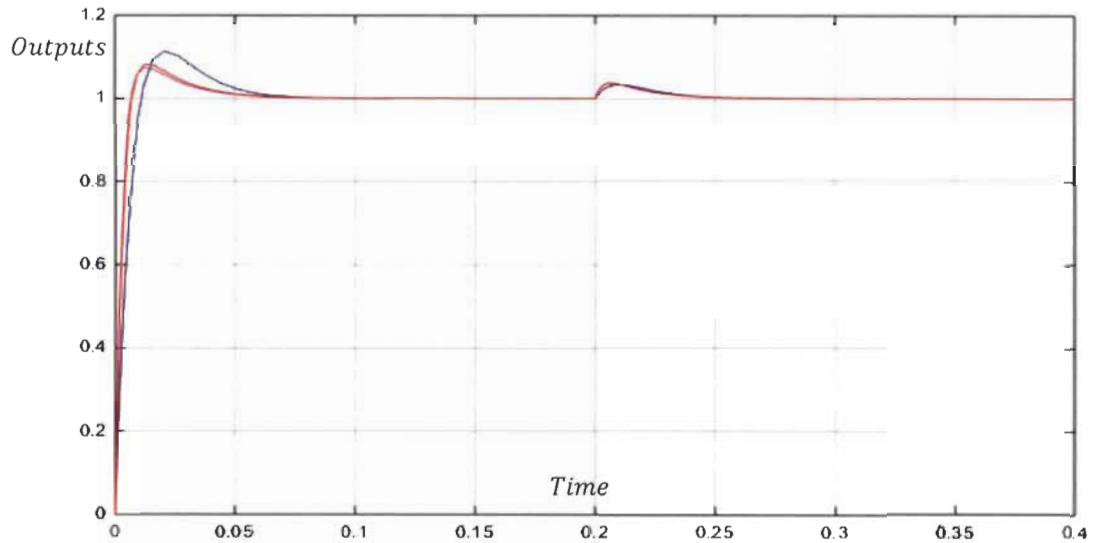


Figure 3. 25: Real and reduced closed loop with disturbance. ($\zeta=0.99$ $\omega_n=100\text{rad/s}$).

Another controller is designed with $\zeta = 2$ and $\omega_n = 100\text{rad/s}$.

$$K_I = \frac{\omega_n^2}{K} = 1111.11 ; \quad K_p = \frac{2\zeta\omega_n - x}{K} = 43.44$$

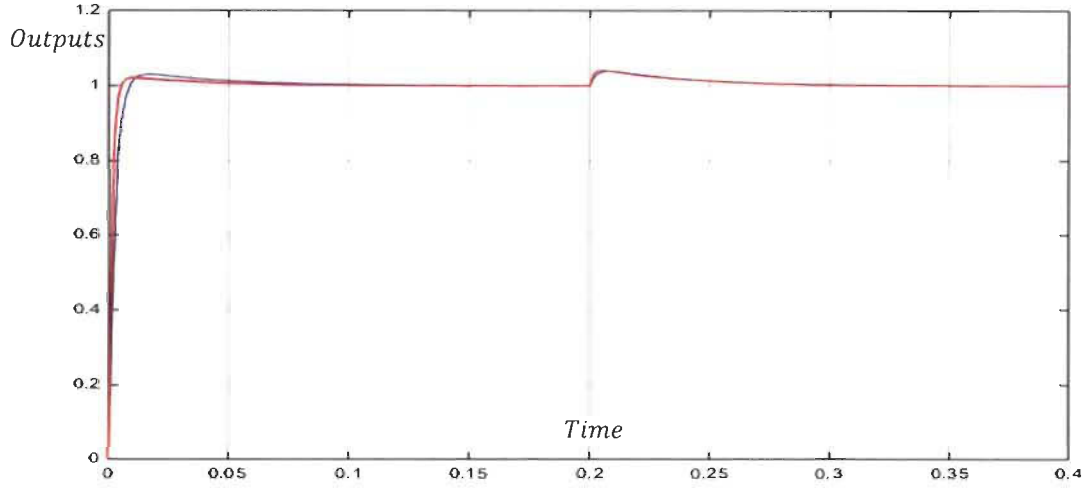


Figure 3. 26: Real and reduced closed loop with disturbance. ($\zeta=2$; $\omega_n=100\text{rad/s}$).

Simulations were done with the same PI controller design based on the proposed similar system with disturbance at $t = 0.2\text{s}$ and results (figure 3.25 and 3.26) show that all three systems are controlled perfectly and almost identically.

3.6 New approach and classical reduction method comparison

In chapter 2, two reduction methods were studied to highlight the complexity of most of reduction methods found in the literature. In this section the same systems that are shown in chapter 2 with ISE and pade approximation methods application will be controlled using the new approach reduction method.

The first reduced system controlled by ISE reduction method in chapter 2 in (2.20) is taken from [1].

$$G_4^{ISE}(s) = \frac{18.439s^3 + 14.446s^2 + 11.454s + 1.3765}{35.83s^4 + 40.388s^3 + 32.541s^2 + 13.94s + 1}$$

This system can be reduced to a first order similar system based on the output response in figure 2.1

Using the weighted elements that characterize the real system $G_4^{ISE}(s)$.

$$\psi_5 = 1.3765 = \frac{K}{x}$$

$$\psi_3 = T_r = \frac{2.2}{x} = 16.296s$$

Using these two equations the coefficients K and x are easily determined.

$$K = 0.1858 \text{ and } x = 0.135$$

$$G_{NA}^{ISE}(s) = \frac{0.1858}{s + 0.135} \quad (3.28)$$

Figure 3.27 shows both real and similar systems output responses in open loop.

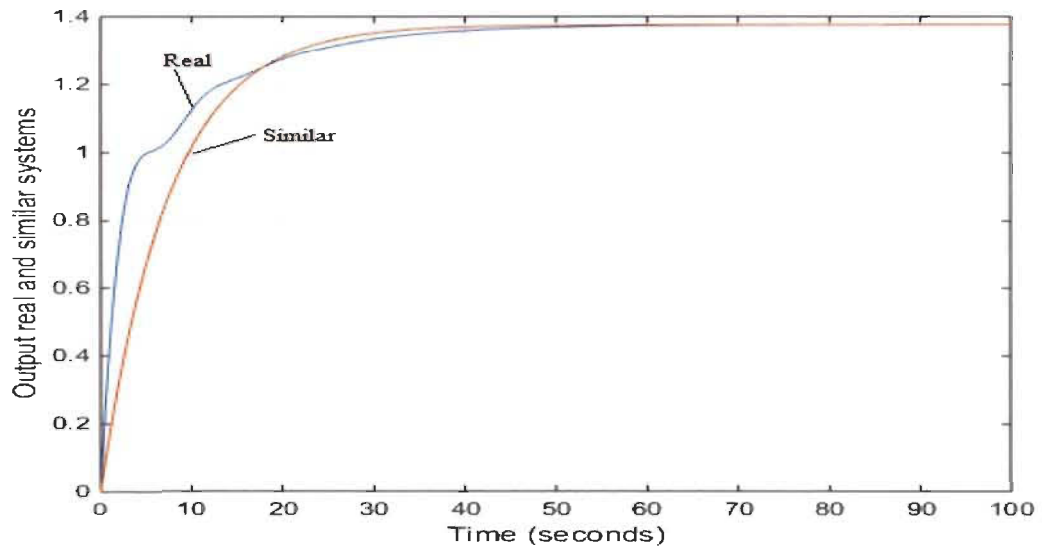


Figure 3. 27: Real and similar systems output response.

The controller will be designed based on section 3.4 and using the first order similar system in (3.28).

For damping factor $\zeta = 1.5$ and settling time $T_s = 2s$; $\omega_n = 1.33\text{rad/s}$.

$$K_I = \frac{\omega_n^2}{K} = 9.563 ; \quad K_p = \frac{2\zeta\omega_n - x}{K} = 20.79$$

Figure 3.28 shows both systems in closed loop with the same controller.

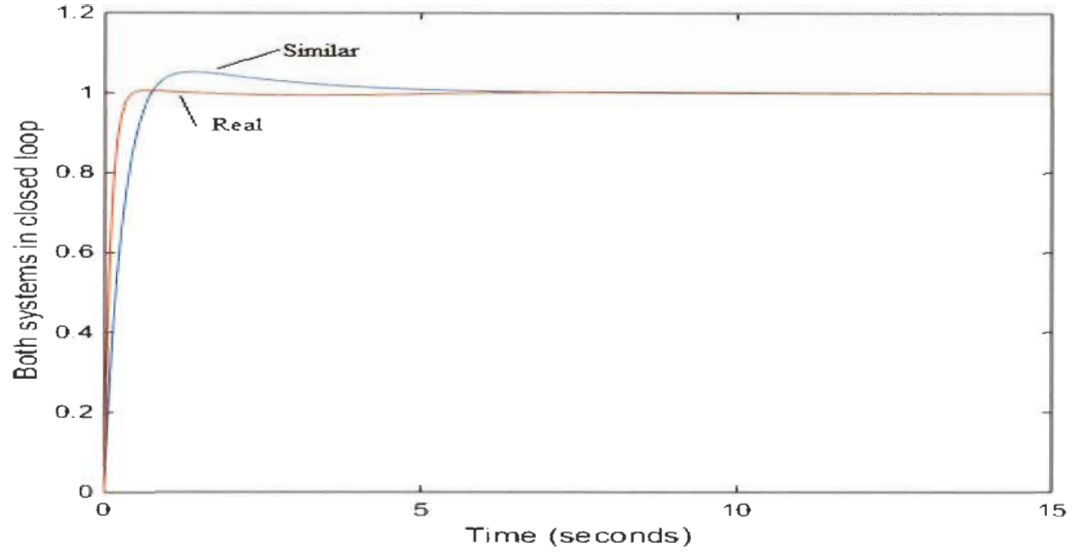


Figure 3. 28: Real and reduced closed loop $\zeta=1.5$; $\omega_n=1.33\text{rad/s}$.

The second system controlled using Pade approximation reduction method in chapter 2 in (2.29) is taken from [2]:

$$G_4^{Pade}(s) = \frac{28s^3 + 496s^2 + 1800s + 2400}{2s^4 + 36s^3 + 204s^2 + 360s + 240}$$

This system can be reduced to a first order similar system based on the output response in figure 2.3

Using the weighted elements that characterize the real system $G_4^{ISE}(s)$.

$$\psi_5 = 10 = \frac{K}{x}$$

$$\psi_3 = T_r = \frac{2.2}{x} = 1.7s$$

Using these two equations the coefficients K and a are easily determined.

$$K = 12.956 \text{ and } x = 1.2956$$

$$G_{NA}^{Pade}(s) = \frac{12.956}{s + 1.2956} \quad (3.29)$$

Figure 3.29 shows both real and similar systems output responses in open loop.

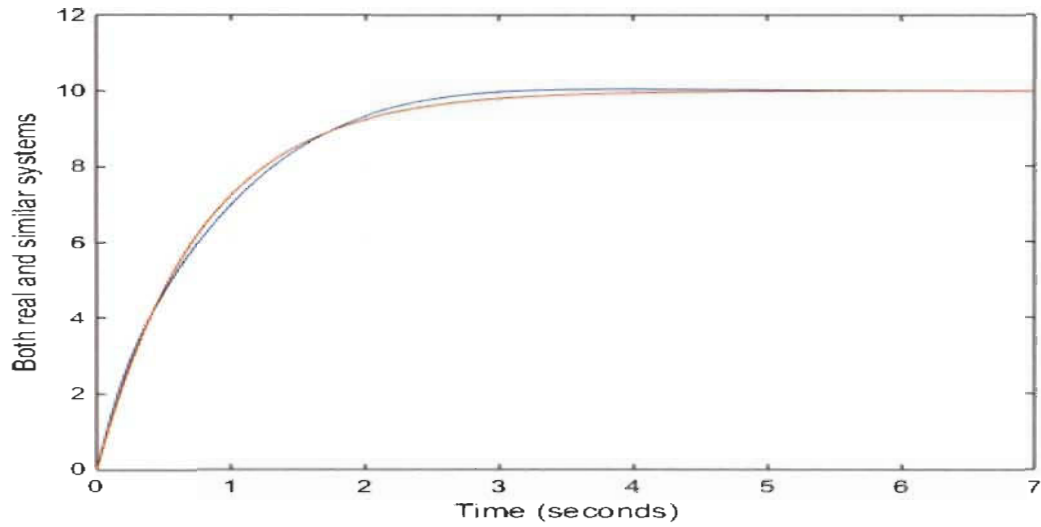


Figure 3. 29: Real and similar systems output response.

The controller will be designed based on section 3.4 and using the first order similar system in (3.29).

For damping factor $\zeta = 1.5$ and settling time $T_s = 0.01s$; $\omega_n = 266\text{rad/s}$.

$$K_I = \frac{\omega_n^2}{K} = 5461; \quad K_p = \frac{2\zeta\omega_n - x}{K} = 61.49$$

Figure 3.28 shows both systems in closed loop with the same controller.

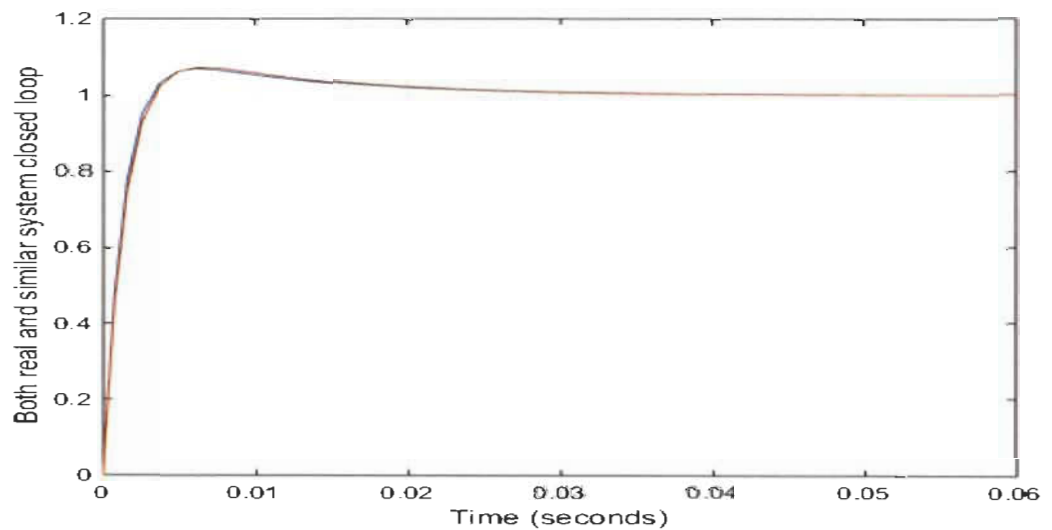


Figure 3. 30: Real and reduced closed loop for $\zeta=1.5$; $\omega_n=2.66\text{rad/s}$.

3.7 Conclusion

In this chapter, a new approximation method was presented to reduce high order systems and to design their controllers based on similar system approach. Therefore, transfer functions are not needed, and the design is based only on the output response of these systems. The technique uses weighted elements that characterize the complex system to approximate its transfer function. Based on this first order reduced similar transfer function, a PI controller is developed and applied to the real system. The performance of this new approach was investigated and was compared with case studies taken from the literature. The obtained results show the performance of this new proposed method.

Chapter 4: New Fibonacci irreducible systems

4.1 Introduction

New systems called Fibonacci systems are introduced. The transfer functions of these systems are irreducible, i.e. they cannot be approximated or reduced to a lower order model. Their Fibonacci transfer functions called Fibonacci wave functions (FWFs) have many extraordinary behaviors and show the limitation of classical reduction methods. Their pole locations follow certain Fibonacci patterns and their frequency responses present multiple resonance and anti-resonance frequencies in a perfect harmony. Moreover, their polynomial coefficients are exactly those of Pascal triangle or Golden triangle and follow specific distribution with respect to Golden ratio $\phi=1.618034$ and their output responses present multiple steady states with final steady states presenting continuous oscillations with low amplitudes. These FWFs are created from a recursive process of a first order system source that generates infinite Fibonacci systems. Each group of FWFs has two boundary transfer function systems.

Pade approximation [8], [10], Integral Square error (ISE) [10], and many others [11], [12], [13] cannot reduce such FWFs systems to a second or third order approximate transfer function because of their intermediate steady states and continuous oscillations at their final steady states. These characteristics make these FWFs irreducible systems.

4.2 Fibonacci systems with irreducible transfer functions

Fibonacci systems transfer functions are built from first-order initial transfer function as shown in figure 4.1.

$$g_1^{(k,x)}(s) = \frac{K}{s + x} \quad (4.1)$$

Where x is the variable, and K is constant.

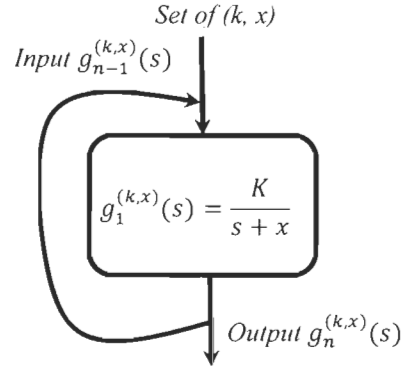


Figure 4. 1: FWFs recursive process

The obtained transfer functions are presented in Table 4.1.

Table 4. 1: Fibonacci wave functions FWFs

$g_1^{(k,x)}(s) = \frac{K}{s+x}$	$g_1^{(k,x)}(s) = \frac{K}{s+x}$
$g_2^{(k,x)}(s) = \frac{K}{s + \frac{K}{s+x}}$	$g_2^{(k,x)}(s) = \frac{Ks + Kx}{s^2 + xs + K}$
$g_3^{(k,x)}(s) = \frac{K}{s + \frac{K}{s + \frac{K}{s+x}}}$	$g_3^{(k,x)}(s) = \frac{Ks^2 + Ksx + K^2}{s^3 + xs^2 + 2Ks + Kx}$
$g_4^{(k,x)}(s) = \frac{K}{s + \frac{K}{s + \frac{K}{s + \frac{K}{s+x}}}}$	$g_4^{(k,x)}(s) = \frac{Ks^3 + Kxs^2 + 2K^2s + K^2x}{s^4 + xs^3 + 3Ks^2 + 2Kxs + K^2}$
$g_n^{(k,x)}(s) = \frac{K}{s + g_{n-1}^{(k,x)}(s)}$	$g_n^{(k,x)}(s) = \frac{Kden_{n-1}^{(k,x)}(s)}{sden_{n-1}^{(k,x)}(s) + num_{n-1}^{(k,x)}(s)}$
$num_n^{(k,x)}(s) = Kden_{n-1}^{(k,x)}(s)$	$den_n^{(k,x)}(s) = sden_{n-1}^{(k,x)}(s) + num_{n-1}^{(k,x)}(s)$

The first-order transfer function is always included in the n^{th} order transfer function as shown in the left column in Table 4.1.

4.3 Fibonacci systems characteristics.

This section presents study and analysis of the calculated transfer functions with different values of K and x .

Case #1: $(K, x) = (1, 1)$. The transfer functions are indicated in Table 4.2.

Table 4. 2: Fibonacci wave functions for $(K, x) = (1, 1)$.

$g_1^{(1,1)}(s) = \frac{1}{s+1}$	$g_1^{(1,1)}(s) = \frac{1}{s+1}$
$g_2^{(1,1)}(s) = \frac{1}{s + \frac{1}{s+1}}$	$g_2^{(1,1)}(s) = \frac{s+1}{s^2 + s + 1}$
$g_3^{(1,1)}(s) = \frac{1}{s + \frac{1}{s + \frac{1}{s+1}}}$	$g_3^{(1,1)}(s) = \frac{s^2 + s + 1}{s^3 + s^2 + 2s + 1}$
$g_4^{(1,1)}(s) = \frac{1}{s + \frac{1}{s + \frac{1}{s + \frac{1}{s+1}}}}$	$g_4^{(1,1)}(s) = \frac{s^3 + s^2 + 2s + 1}{s^4 + s^3 + 3s^2 + 2s + 1}$
$g_n^{(k,x)}(s) = \frac{K}{s + g_{n-1}^{(1,1)}(s)}$	$g_n^{(1,1)}(s) = \frac{den_{n-1}^{(1,1)}(s)}{sden_{n-1}^{(1,1)}(s) + num_{n-1}^{(1,1)}(s)}$
$num_n^{(1,1)}(s) = den_{n-1}^{(1,1)}(s)$	$den_n^{(1,1)}(s) = sden_{n-1}^{(1,1)}(s) + num_{n-1}^{(1,1)}(s)$

Arranging all denominators coefficients of all Fibonacci wave functions in a table, it is clear that the table 4.3 is exactly Pascal triangle that can be found easily in the literature.

Table 4. 3: Pascal's triangle rearrangement coefficients of all $den_n^{(1,1)}$ of Fibonacci wave functions.

den 1	1																
den 2	1	1															
den 3	1	1	2														
den 4	1	1	3	3													
den 5	1	1	4	6	4												
den 6	1	1	5	10	10	5											
den 7	1	1	6	15	20	15	6										
den 8	1	1	7	21	35	35	21	7									
den 9	1	1	8	28	56	70	56	28	8								
den 10	1	1	9	36	84	126	126	84	36	9							
den 11	1	1	10	45	120	210	252	210	120	45	10						
den 12	1	1	11	55	165	330	462	462	330	165	55	11					
den 13	1	1	12	66	220	495	792	792	495	220	66	12					
den 14	1	1	13	78	286	715											
den 15	1	1	14	91	364												
den 16	1	1	15	105													
den 17	1	1	16														
den 18	1																

As an example, denominators $den_{13}^{(1,1)}(s)$ and $den_{14}^{(1,1)}(s)$ of $g_{14}^{(1,1)}(s)$ using Pascal's triangle

Table 4.3 is shown above.

$$\begin{aligned}
 den_{14}^{(1,1)}(s) &= 1s^{14} + 1s^{13} + 13s^{12} + 12s^{11} + 66s^{10} + 55s^9 + 165s^8 + 120s^7 \\
 &\quad + 210s^6 + 126s^5 + 126s^4 + 56s^3 + 28s^2 + 7s + 1 \\
 den_{13}^{(1,1)}(s) &= 1s^{13} + 1s^{12} + 12s^{11} + 11s^{10} + 55s^9 + 45s^8 + 120s^7 + 84s^6 \\
 &\quad + 126s^5 + 70s^4 + 56s^3 + 21s^2 + 7s + 1 \\
 g_{14}^{(1,1)}(s) &= K \frac{den_{13}^{(1,1)}(s)}{den_{14}^{(1,1)}(s)}
 \end{aligned} \tag{4.2}$$

From Table 4.3, we observe that all coefficients of the denominator will be determined for any transfer function of degree n. The characteristics of this table is the Pascal's triangle that can be found in the literature. In addition, the sum of the diagonals is exactly the Fibonacci numbers with the Golden ratio $\phi=1.618$.

Remarks:

- Knowing the first-order wave function, any resulting Fibonacci wave function can be determined from the coefficients of the golden triangle for any degree.
- Knowing an n^{th} order Fibonacci wave function, the first-order wave function source can be determined.

Case #2: $(K, x) \neq (1, 1)$ and $K > 0$; $x > 0$

Table 4. 4: Denominator coefficients of FWFs with (K, x) . [red numbers are for the case $(K, x) = (1, 1)$]

$g_1^{(k,x)}(s) = \frac{K}{s+x}$	$g_1^{(k,x)}(s) = \frac{K}{\mathbf{1}s + \mathbf{1}x}$
$g_2^{(k,x)}(s) = \frac{K}{s + \frac{K}{s+x}}$	$g_2^{(k,x)}(s) = \frac{1Ks + 1Kx}{\mathbf{1}s^2 + \mathbf{1}xs + \mathbf{1}K}$
$g_3^{(k,x)}(s) = \frac{K}{s + \frac{K}{s + \frac{K}{s+x}}}$	$g_3^{(k,x)}(s) = \frac{1Ks^2 + 1Ksx + 1K^2}{\mathbf{1}s^3 + \mathbf{1}xs^2 + \mathbf{2}Ks + \mathbf{1}Kx}$
$g_4^{(k,x)}(s) = \frac{K}{s + \frac{K}{s + \frac{K}{s + \frac{K}{s+K}}}}$	$g_4^{(k,x)}(s) = \frac{1Ks^3 + 1Kxs^2 + 2K^2s + 1K^2x}{\mathbf{1}s^4 + \mathbf{1}xs^3 + \mathbf{3}Ks^2 + \mathbf{2}Kxs + \mathbf{1}K^2}$
$g_n^{(k,x)}(s) = \frac{K}{s + g_{n-1}^{(k,x)}(s)}$	$g_n^{(k,x)}(s) = \frac{Kden_{n-1}^{(k,x)}(s)}{sden_{n-1}^{(k,x)}(s) + num_{n-1}^{(k,x)}(s)}$

In Table 4.4 numbers highlighted in red are exactly the coefficients of the denominators of the first case $(K, x) = (1, 1)$ multiplied by coefficients

$$x; K; xK; K^2; xK^2; K^3; xK^3; K^4; xK^4; \text{etc}$$

The final steady-states for these transfer functions can be determined as follow:

$$\begin{aligned} den_{14}^{(K,x)}(s) = & \mathbf{1}s^{14} + \mathbf{1}xs^{13} + \mathbf{13}Ks^{12} + \mathbf{12}Kxs^{11} + \mathbf{66}K^2s^{10} + \mathbf{55}K^2xs^9 + \mathbf{165}K^3s^8 \\ & + \mathbf{120}K^3xs^7 + \mathbf{210}K^4s^6 + \mathbf{126}K^4xs^5 + \mathbf{126}K^5s^4 + \mathbf{56}K^5xs^3 + \mathbf{28}K^6s^2 \\ & + \mathbf{7}K^6xs + \mathbf{1}K^7 \end{aligned}$$

From Table 4.5, all coefficients of the denominator can be determined for any wave function of degree n for any positive value of K and x .

Note that the second order Fibonacci wave function is:

$$g_2^{(k,x)}(s) = \frac{Ks + Kx}{s^2 + xs + K} \quad (4.4)$$

With a Fibonacci natural frequency ω_f and Fibonacci damping factor ξ_f . We can highlight the relationship between (K, x) and (ω_f, ξ_f) of the second order transfer function.

$$K = \omega_f^2 \quad \text{and} \quad x = 2 \xi_f \omega_f \quad (4.5)$$

The multiplication coefficients will be.

$$2 \xi_f \omega_f; \omega_f^2; 2 \xi_f \omega_f^3; \omega_f^4; 2 \xi_f \omega_f^5; \omega_f^6; 2 \xi_f \omega_f^7; \omega_f^8; 2 \xi_f \omega_f^9, etc$$

For the case $\xi_f = 0.5$ $x = \omega_f$ the multiplication coefficients will be:

$$\omega_f; \omega_f^2; \omega_f^3; \omega_f^4; \omega_f^5; \omega_f^6; \omega_f^7; \omega_f^8; \omega_f^9; etc$$

The two conditions mentioned above can be generalized for any positive value of (K, x) or (ξ_f, ω_f) .

- Knowing the first order wave function $g_1^{(k,x)}(s)$, any Fibonacci wave function FWF resulting is perfectly determined from the coefficients of the golden triangle with the multiplying coefficients cited above for any degree.
- Knowing a Fibonacci wave function $g_n^{(k,x)}(s)$, the first-order wave function source and other related FWFs are perfectly determined.

4.4 Fibonacci systems analysis.

In both groups $K = x^2$ and $K \neq x^2$, the sum of all the real parts of the poles of an FWF $g_n^{(K,x)}(s)$ is always equal to the pole p of the first-order original transfer function $g_1^{(K,x)}(s)$

$$\sum_{i=1}^n \text{Re}(p_i) = p = -x \quad (4.6)$$

p : pole of $g_1^{(K,x)}(s)$

$p_1, p_2, \dots, p_i \dots p_n$: poles of $g_n^{(K,x)}(s)$

The real part of the poles of an FWF presents specific distribution as shown in the figure 4.2 for $\text{abs}(\text{real}(\text{pole}(g_{40}^{(1,1)}(s))))$ of case #1. In case #2, all real part of poles of high order FWFs follow a specific distribution for $\text{abs}(\text{real}(\text{pole}(g_{40}^{(1,4)}(s))))$ figure 4.3.

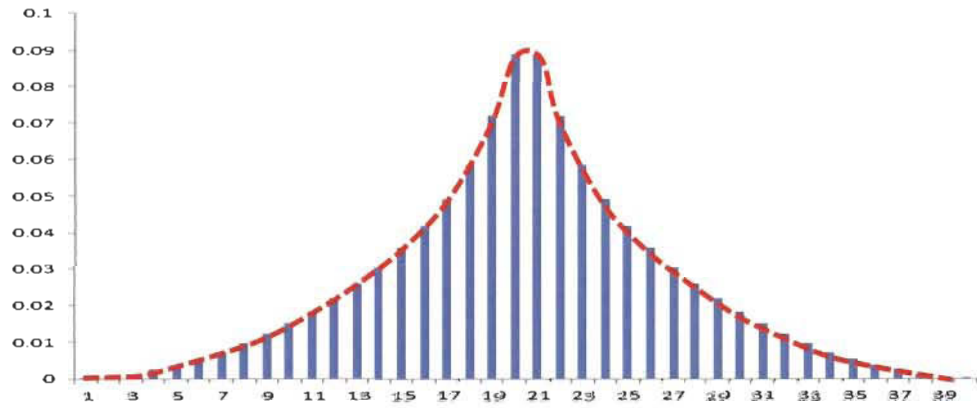


Figure 4. 2: Real part of $g_{40}^{(1,1)}(s)$ poles for case #1.

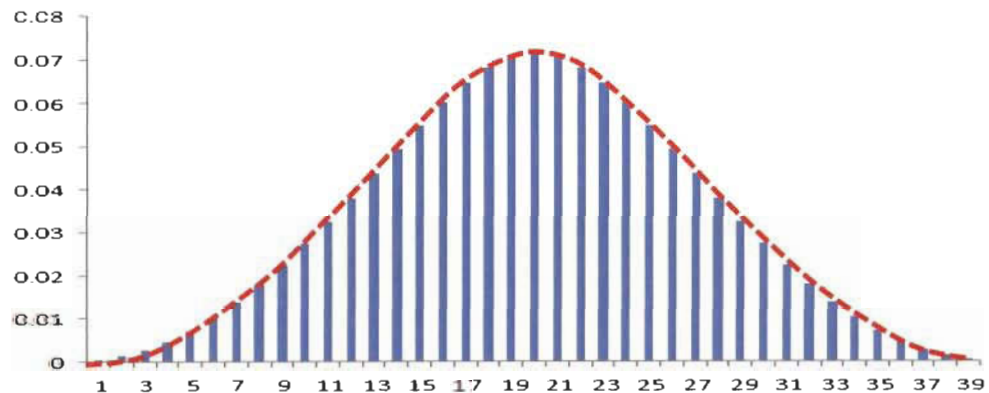


Figure 4. 3: Real part of $g_{40}^{(1,4)}(s)$ poles for case #2

On the other hand all imaginary parts of poles of high order FWF follow another specific distribution as shown in the figure 4.4 for $abs(imag(pole(g_{40}^{(1,1)}(s))))$. Case #2, all imaginary poles for $abs(imag(pole(g_{40}^{(1,4)}(s))))$ follow same specific distribution shown in the figure 4.5.

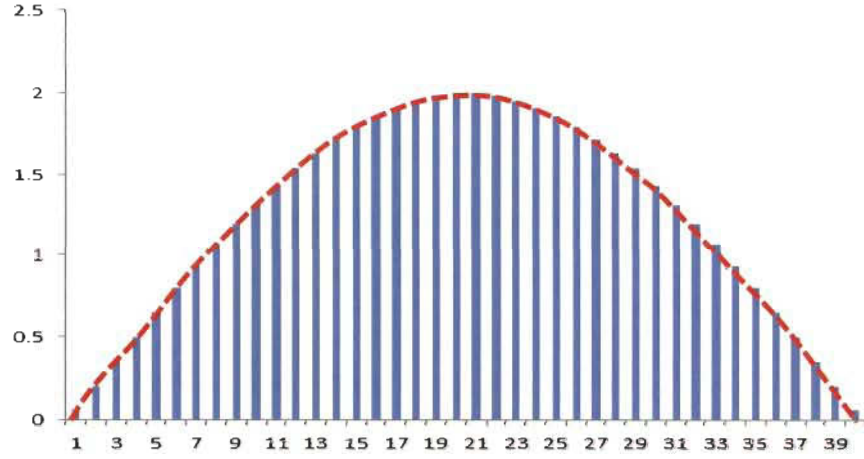


Figure 4. 4: Imaginary part of $g_{40}^{(1,1)}(s)$ poles for case #1.

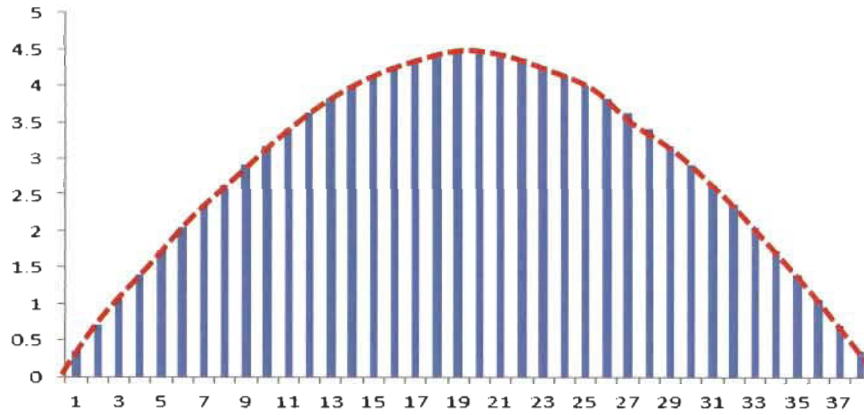


Figure 4. 5: Imaginary part of $g_{40}^{(1,4)}(s)$ poles for case #2

- ✓ The polynomial coefficients of $den_n^{(k,x)}(s)$ follow two different distributions. Figure 4.6 shows $g_{40}^{(1,1)}(s)$ as an example for case #1 and figure 4.7 shows $g_{40}^{(1,4)}(s)$ for case #2.

Distribution 1 for all coefficients $a_i^{(k,x)}$ related to s^i for an odd i

Distribution 2 for all coefficients $a_i^{(k,x)}$ related to s^i for an even i

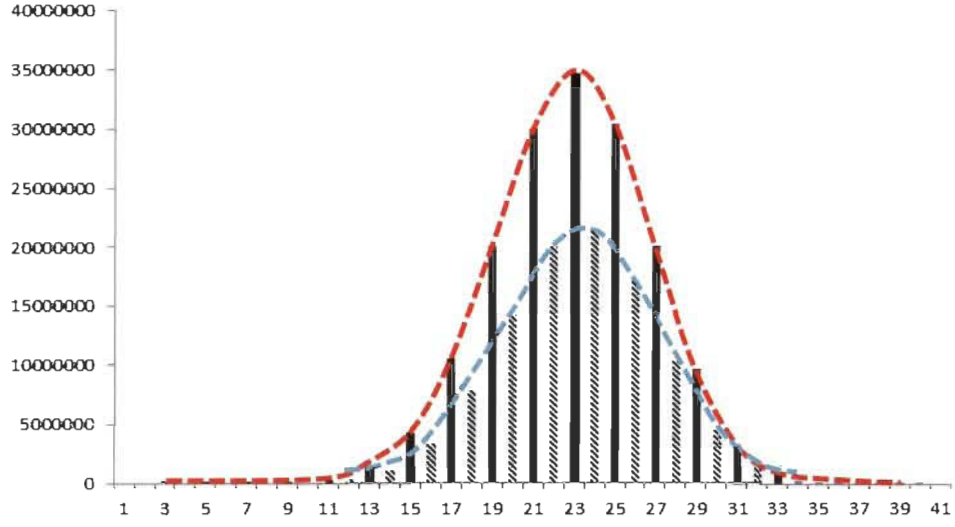


Figure 4. 6: Case #1- Odd coefficients (black). Even coefficients (Hashed) of $den_{40}^{(1,1)}(s)$

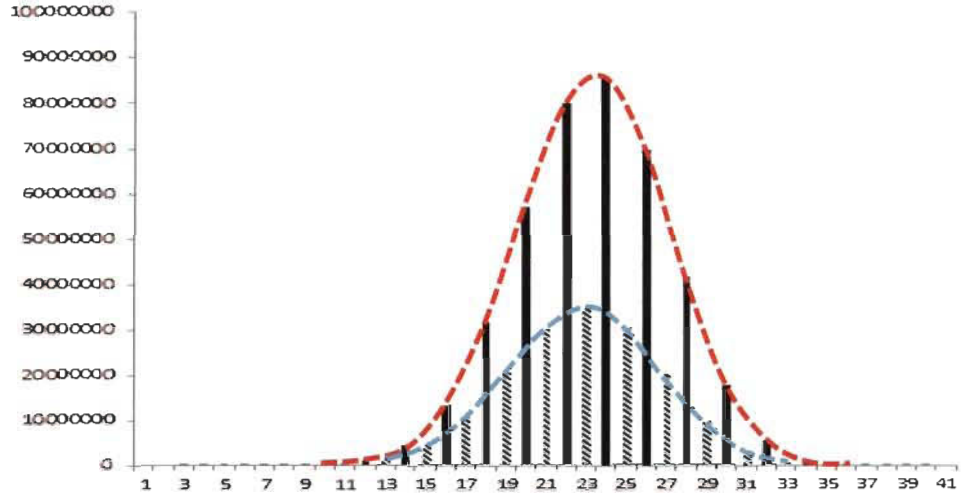


Figure 4. 7: Case #2- Odd coefficients (black). Even coefficients (Hashed) of $den_{40}^{(1,4)}(s)$

✓ The ratio of the sum of all odd coefficients to the sum of all even coefficients of FWF

$g_n^{(1,x)}(s)$ denominator is equal to the Golden ratio $\frac{\phi}{x}$.

$$\frac{\sum_{i=0}^{n/2} a_{2i}^{(1,x)}}{\sum_{i=1}^{n/2} a_{2i-1}^{(1,x)}} = \frac{\phi}{x}; \quad n \text{ even} \quad (4.7)$$

$$\frac{\sum_{i=1}^{(n+1)/2} a_{2i-1}^{(1,x)}}{\sum_{i=0}^{(n-1)/2} a_{2i}^{(1,x)}} = \frac{\phi}{x}; \quad n \text{ odd}$$

- ✓ The ratio of the sum of all $den_n^{(1,x)}(s)$ coefficients of FWFs $g_n^{(1,x)}(s)$ over the sum of all $den_{n-1}^{(1,x)}(s)$ coefficients of FWF $g_{n-1}^{(1,x)}(s)$ is equal to the Golden ratio $\phi = 1.618034$.

$$\frac{\sum_{i=0}^n a_i^{(1,x)}}{\sum_{i=0}^{n-1} b_i^{(1,x)}} = \phi = 1.618034 \quad (4.8)$$

$a_i^{(1,x)}$ The denominator coefficients for $den_n^{(1,x)}(s)$

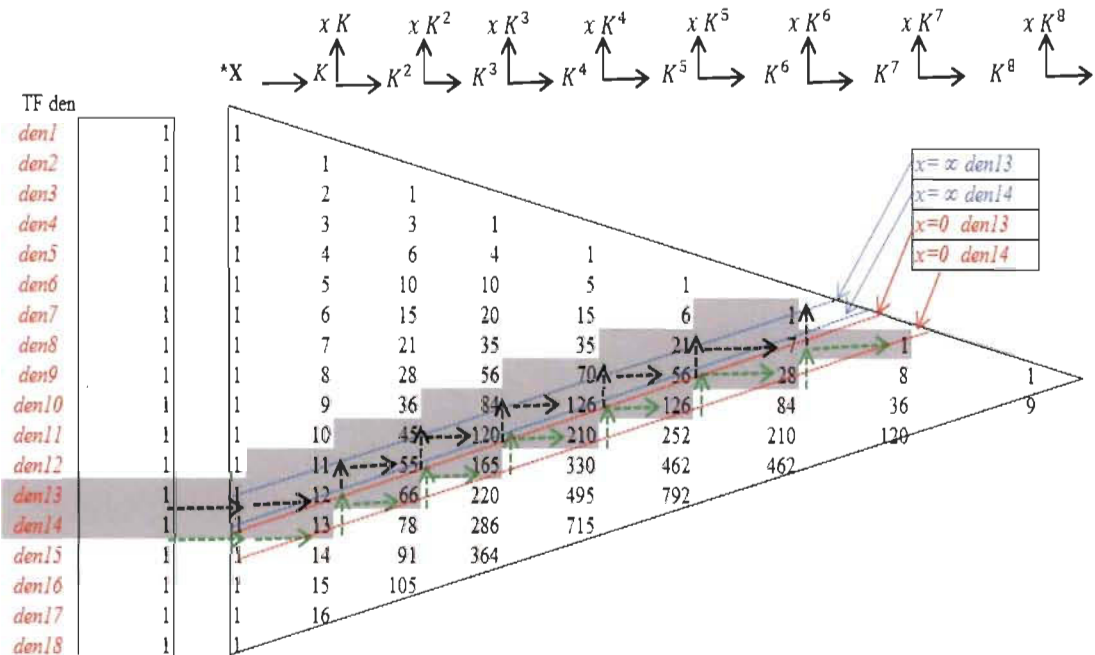
$b_i^{(1,x)}$ The denominator coefficients for $den_{n-1}^{(1,x)}(s)$

4.5 Fibonacci boundary systems

Fibonacci systems are dependent on the variable x as shown in table 4.4. Fibonacci boundary systems $g_n^{(k,0)}(s)$ and $g_n^{(k,\infty)}(s)$ can be easily determined by finding the limit when $x \rightarrow 0$ and $x \rightarrow \infty$ using Pascal's triangle general form shown in Table 4.6 below or using (4.2).

The FWF boundary systems $g_{14}^{(1,0)}(s)$ and $g_{14}^{(1,\infty)}(s)$ are determined as an example.

Table 4. 6: Pascal's triangle for Fibonacci boundary systems



$$\lim_{x \rightarrow 0} g_{14}^{(K,x)}(s) = g_{14}^{(K,0)}(s) = K * \frac{1s^{13} + 12Ks^{11} + 55K^2s^9 + 120K^3s^7 + 126K^4s^5 + 56K^5s^3 + 7K^6s}{1s^{14} + 13Ks^{12} + 66K^2s^{10} + 165K^3s^8 + 210K^4s^6 + 126K^5s^4 + 28K^6s^2 + 1K^7} \quad (4.9)$$

$$\lim_{x \rightarrow \infty} g_{14}^{(K,x)}(s) = g_{14}^{(K,\infty)}(s) = K * \frac{1s^{12} + 11Ks^{10} + 45K^2s^8 + 84K^3s^6 + 70K^4s^4 + 21K^5s^2 + 1K^6}{1s^{13} + 12Ks^{11} + 55K^2s^9 + 120K^3s^7 + 126K^4s^5 + 56K^5s^3 + 7K^6s}$$

Simulation in figures 4.8 and 4.9 below show the Fibonacci boundary systems $g_{40}^{(1,0)}(s)$ and $g_{39}^{(1,0)}(s)$ and $g_{38}^{(1,0)}(s)$ and $g_{37}^{(1,0)}(s)$ with unit constant input and with input pulse of $t = 30s$.

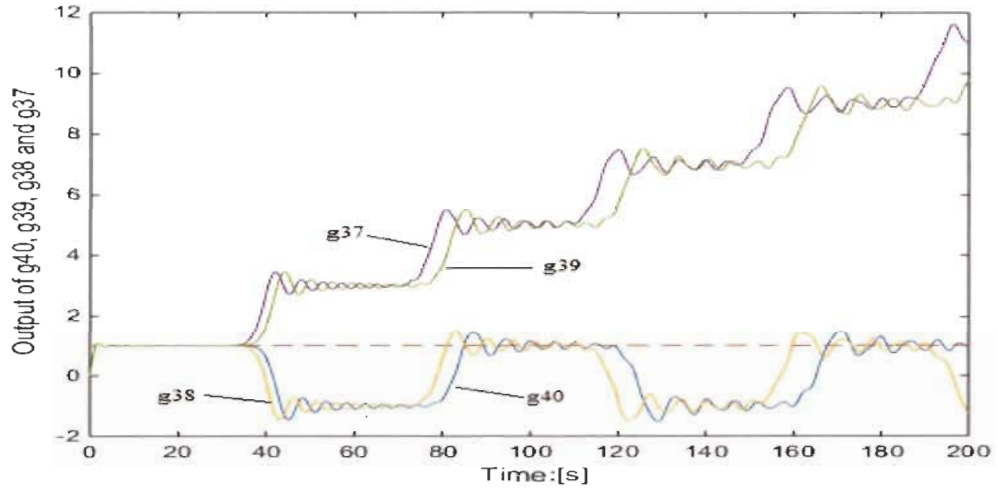


Figure 4. 8: FWF $g_n^{(1,0)}(s)$ ($n = 37, 38, 39$ and 40) outputs with unit input.

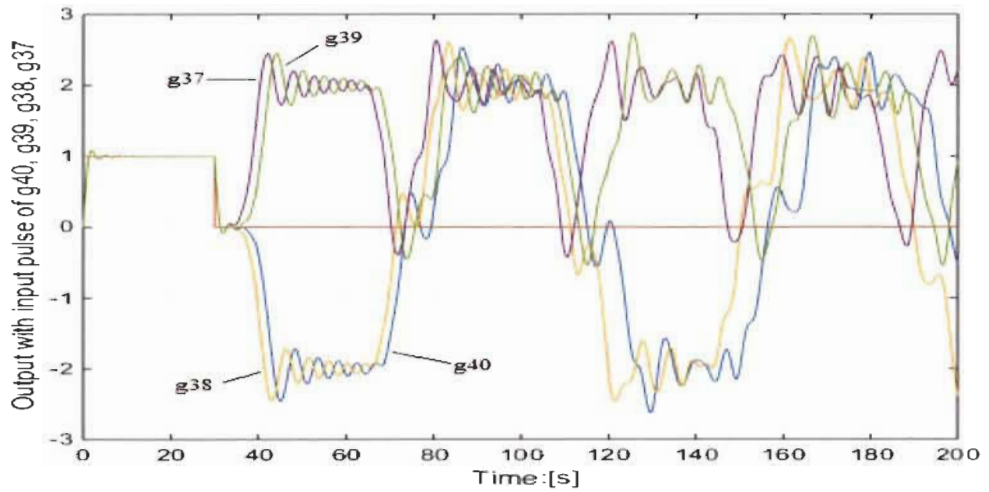


Figure 4. 9: FWF $g_n^{(1,0)}(s)$ ($n = 37, 38, 39$ and 40) outputs with input pulse of $30s$.

Figure 4.9 shows an amazing behavior of the FWFs $g_n^{(1,0)}(s)$ with an input pulse. After 30 seconds, the input is set to zero, but their outputs are none zero with amplitude between (2,-2).

4.6 Case studies and simulations.

Analysis and simulations in open loop of all FWFs are presented for two cases. Fibonacci transfer functions are determined based on Pascal's triangle for case #1 and case #2.

Case study #1: $K = x^2$; $\xi_f = 0.5$; $K = \omega_f^2$; $x = \omega_f$. One final steady state $x = \omega_f$.

Case #2: $K \neq x^2$; $\xi_f \neq 0.5$; $K = \omega_f^2$; $x = 2 \xi_f \omega_f$. Two final steady states $\frac{K}{x} = \frac{\omega_f}{2 \xi_f}$ and $x = 2 \xi_f \omega_f$.

A. Case #1: $(K, x) = (1, 1)$; $\xi_f = 0.5$; $K = \omega_f^2 = 1$; $x = \omega_f = 1$

The transfer functions are shown in Table 4.2. Simulation and analysis of Bode, poles and zeros locations as well as output response for all FWFs in each case will be conducted to highlight their extraordinary behavior. These FWFs are calculated until $g_{40}^{(1,1)}(s)$ using Matlab software.

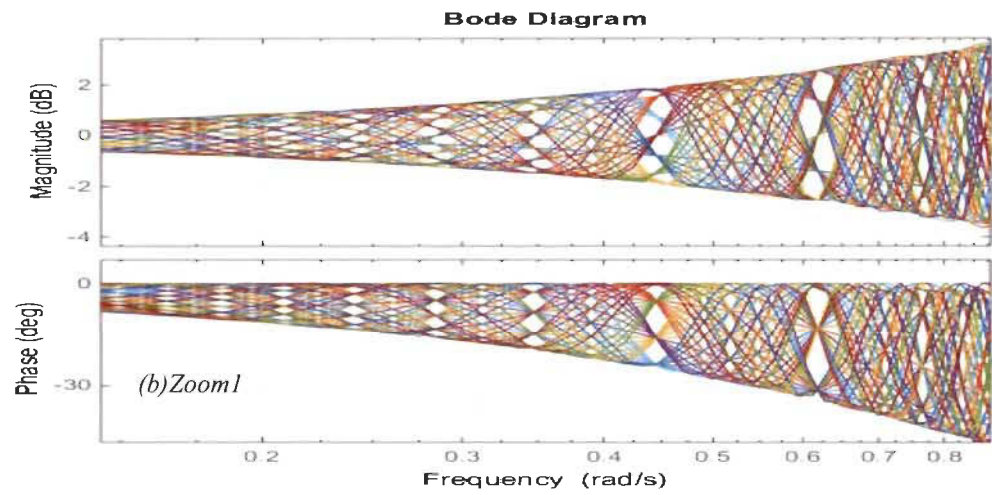
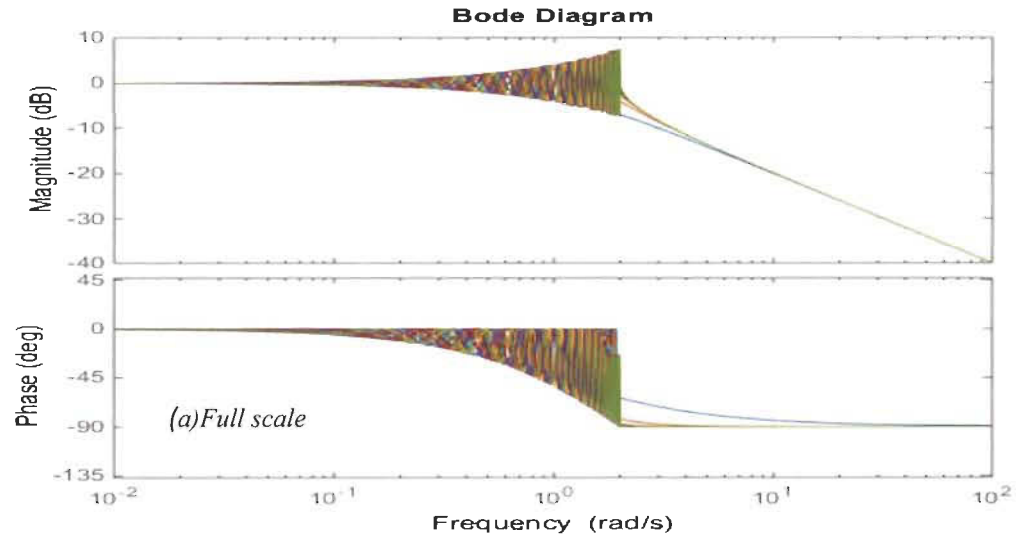
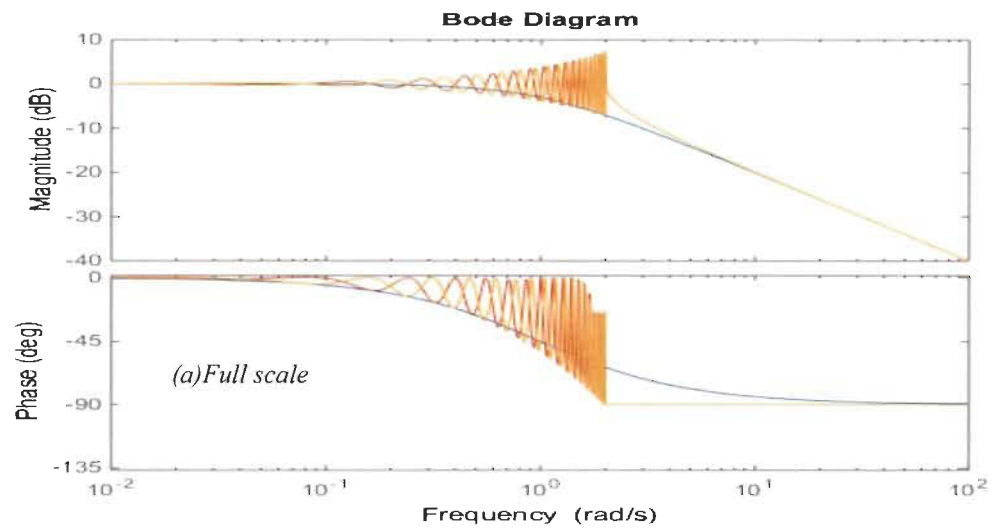


Figure 4. 10: Bode plots of FWFs $g_1^{(1,1)}(s), \dots, g_{40}^{(1,1)}(s)$



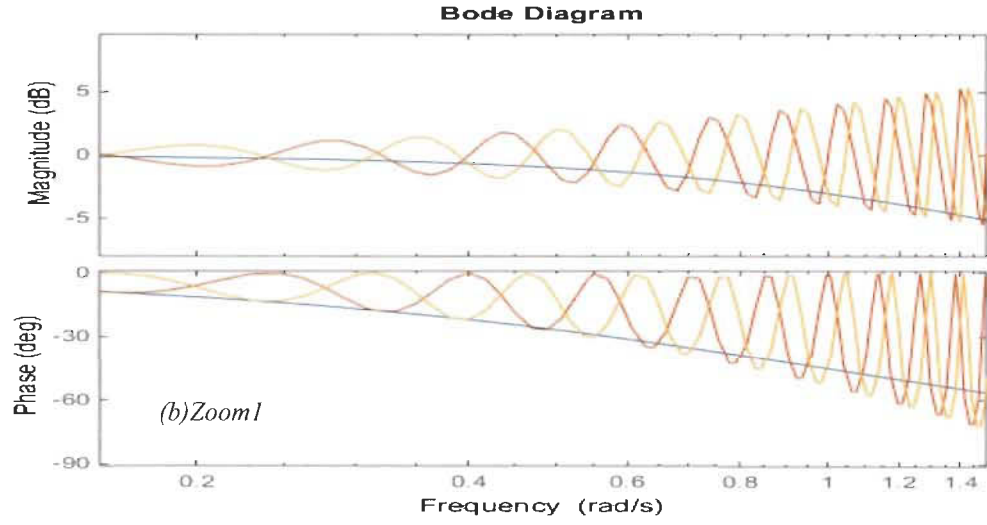


Figure 4. 11: Bode plots of FWFs $g_1^{(1,1)}(s)$, $g_{39}^{(1,1)}(s)$, $g_{40}^{(1,1)}(s)$

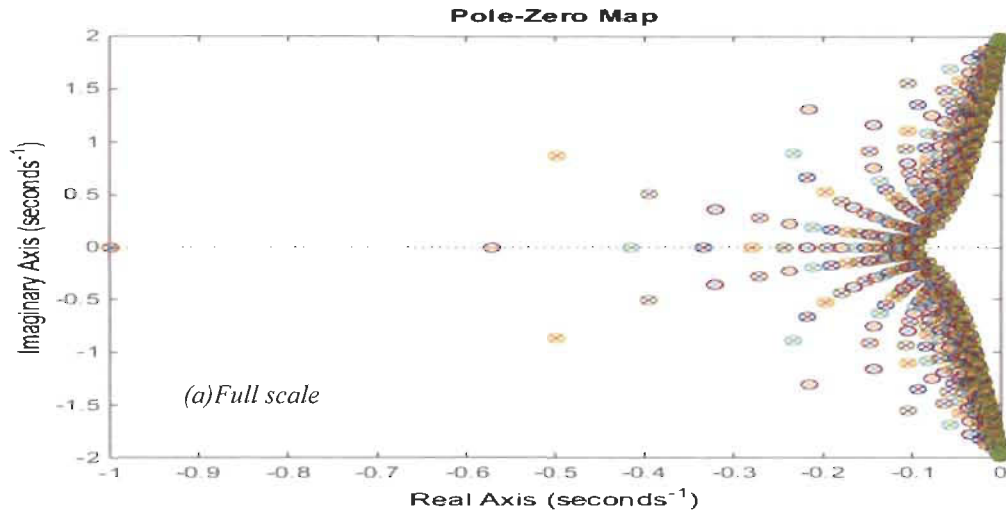


Figure 4. 12: Poles and zeros of $g_1^{(1,1)}(s)$, ..., $g_{40}^{(1,1)}(s)$

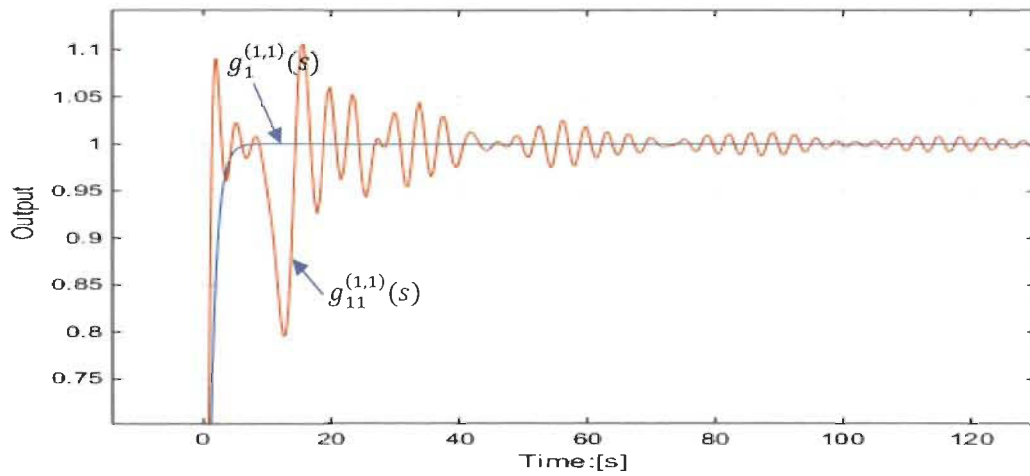


Figure 4. 13: Output response of odd FWFs $g_1^{(1,1)}(s)$, $g_{11}^{(1,1)}(s)$.

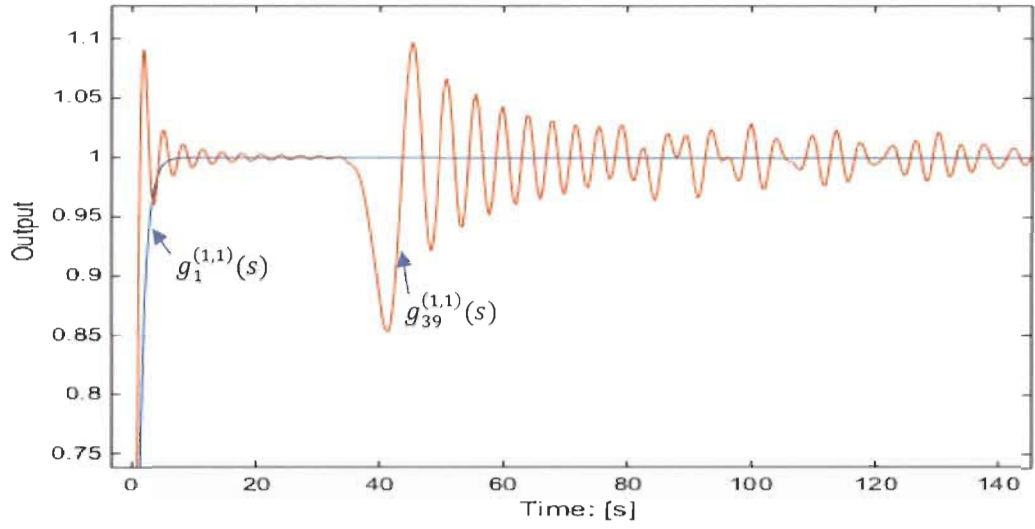


Figure 4. 14: Output response of odd FWFs $g_1^{(1,1)}(s)$, $g_{39}^{(1,1)}(s)$.

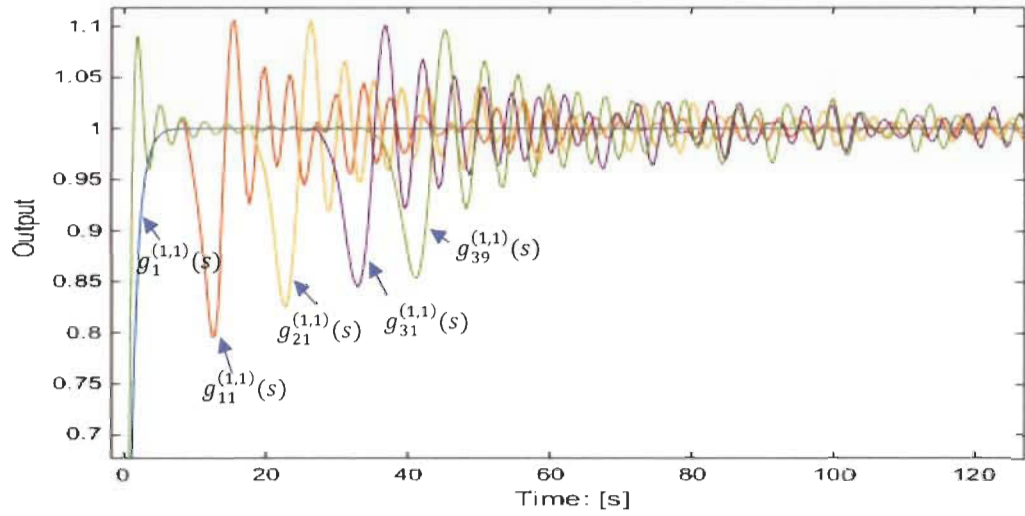


Figure 4. 15: Output response of odd FWFs $g_1^{(1,1)}(s)$, $g_{11}^{(1,1)}(s)$, $g_{21}^{(1,1)}(s)$, $g_{31}^{(1,1)}(s)$, $g_{39}^{(1,1)}(s)$.

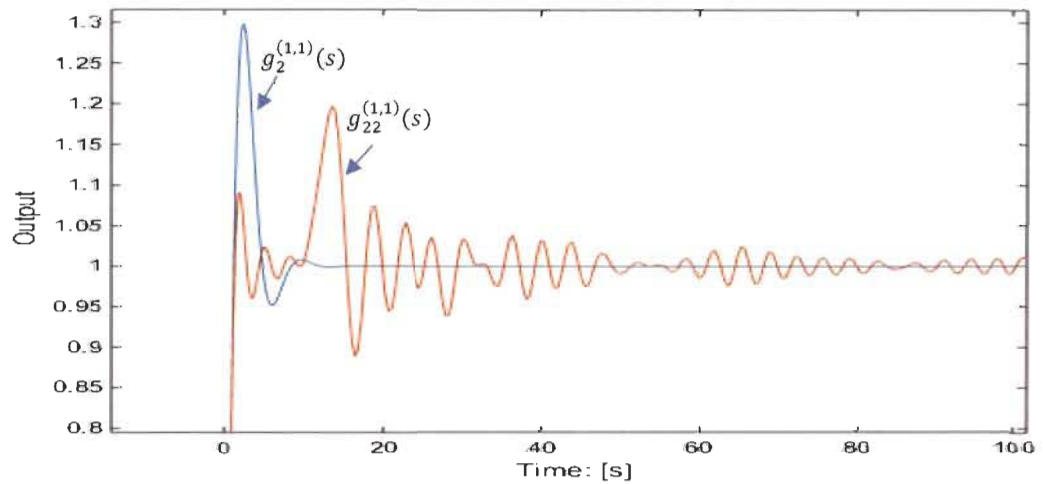


Figure 4. 16: Output response of even FWFs $g_2^{(1,1)}(s)$, $g_{22}^{(1,1)}(s)$

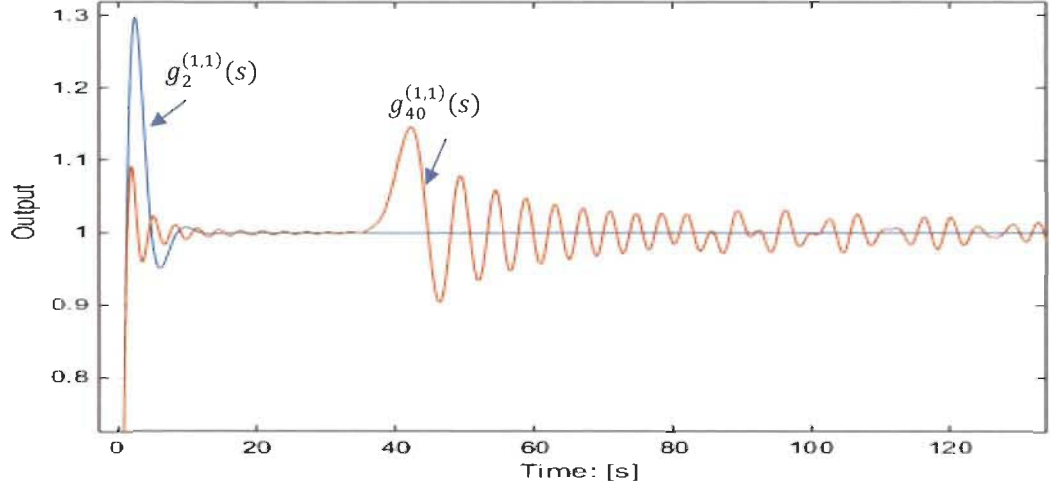


Figure 4.17: Output response of even FWFs $g_2^{(1,1)}(s)$, $g_{40}^{(1,1)}(s)$.

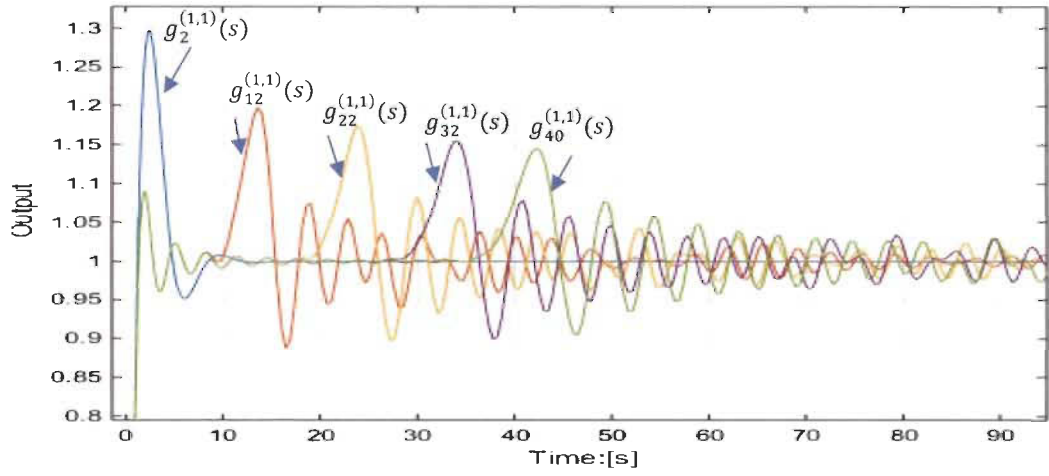


Figure 4.18: Output response of even FWFs $g_2^{(1,1)}(s)$, $g_{12}^{(1,1)}(s)$, $g_{22}^{(1,1)}(s)$, $g_{32}^{(1,1)}(s)$, $g_{40}^{(1,1)}(s)$

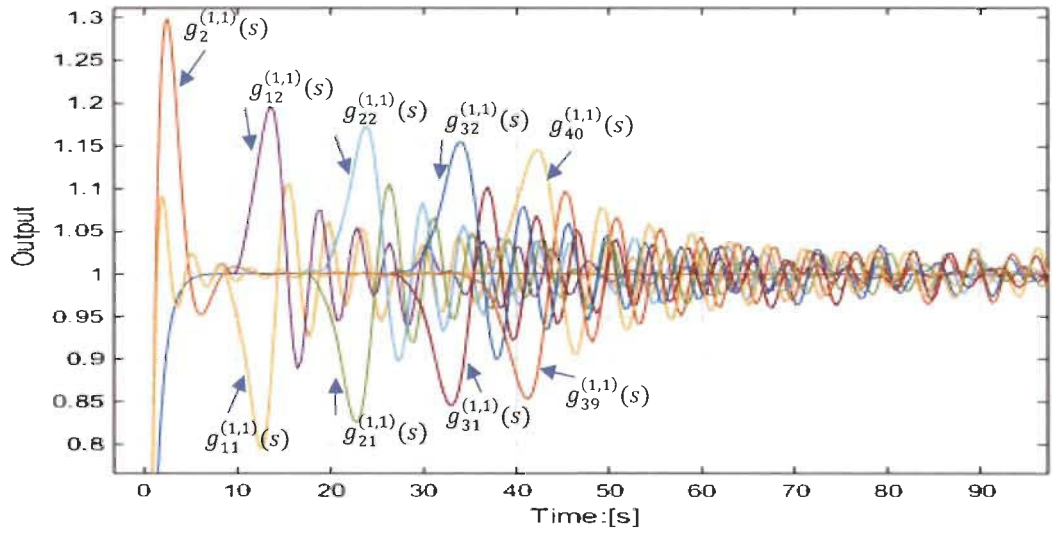


Figure 4.19: Output response of odd and even FWFs $g_1^{(1,1)}(s)$, $g_{11}^{(1,1)}(s)$, $g_{21}^{(1,1)}(s)$, $g_{31}^{(1,1)}(s)$, $g_{39}^{(1,1)}(s)$, $g_2^{(1,1)}(s)$, $g_{12}^{(1,1)}(s)$, $g_{22}^{(1,1)}(s)$, $g_{32}^{(1,1)}(s)$, $g_{40}^{(1,1)}(s)$.

B. Case #2: $(K, x) = (1, 4)$; $(\omega_f, \xi_f) = (1, 2)$;

with two final steady states: $\frac{K}{x} = \frac{\omega_f}{2\xi_f} = 0.25$ and $x = 2\xi_f\omega_f = 4$

In this case the FWFs are arranged in two groups.

- ✓ Group 1: All FWFs with even order of their transfer functions have x as steady state.
- ✓ Group 2: All FWFs with odd order of their transfer functions have $\frac{K}{x}$ steady state.

Simulations were conducted for all FWFs where $(K, x) = (1, 4)$ in Table 4.3 up to order 40

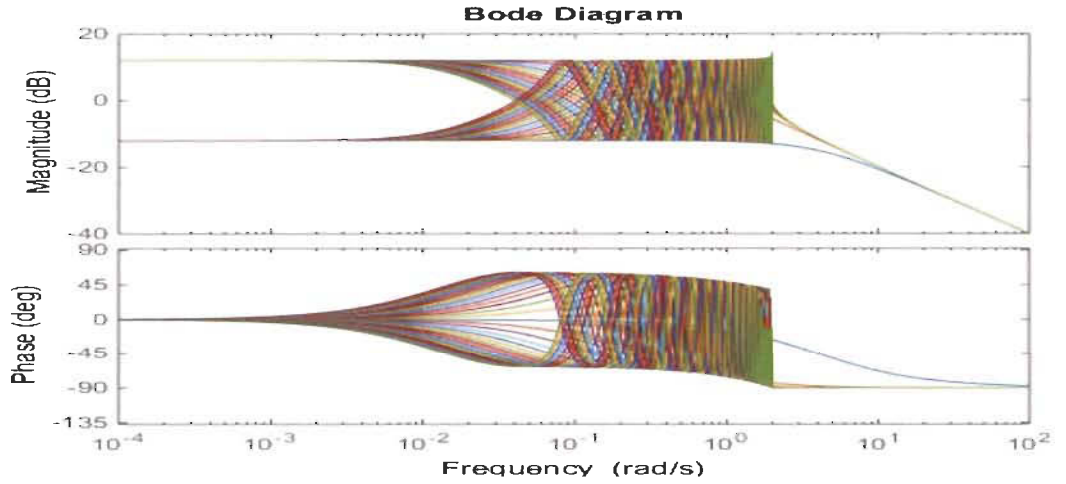


Figure 4. 20: Bode plots of FWFs $g_1^{(1,4)}(s), \dots, g_{40}^{(1,4)}(s)$.

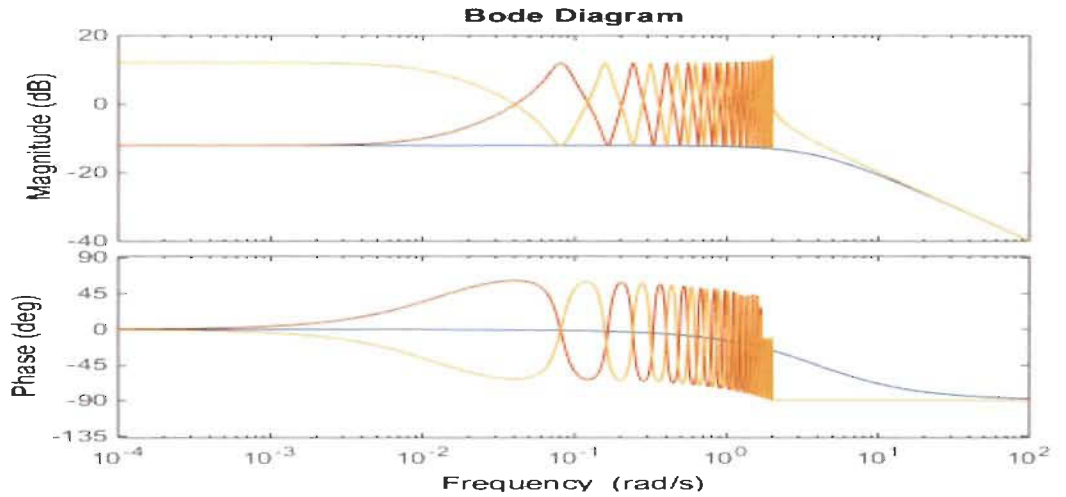


Figure 4. 21: Bode plots of FWFs $g_1^{(1,4)}(s), g_{39}^{(1,4)}(s), g_{40}^{(1,4)}(s)$.

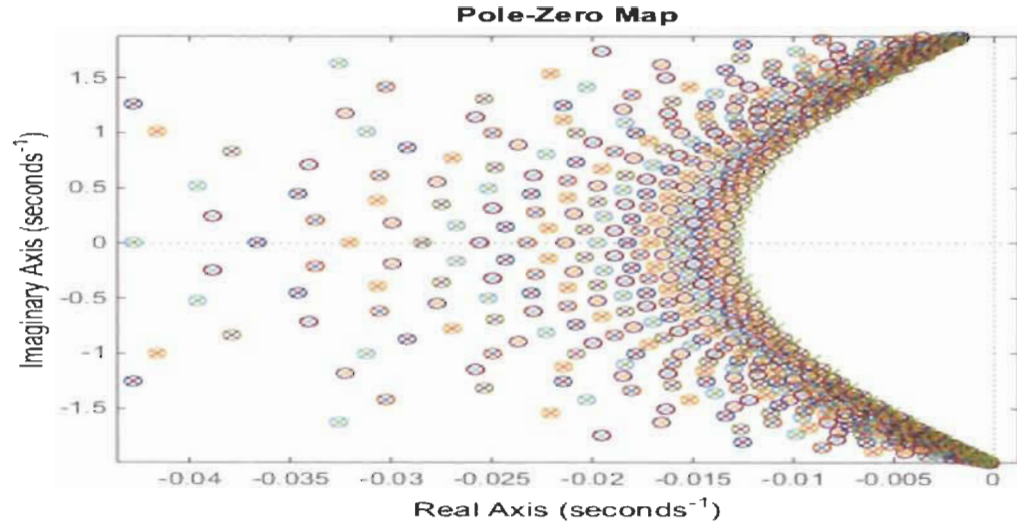


Figure 4. 22: Poles and zeros of FWFs $g_1^{(1,4)}(s), \dots, g_{40}^{(1,4)}(s)$.

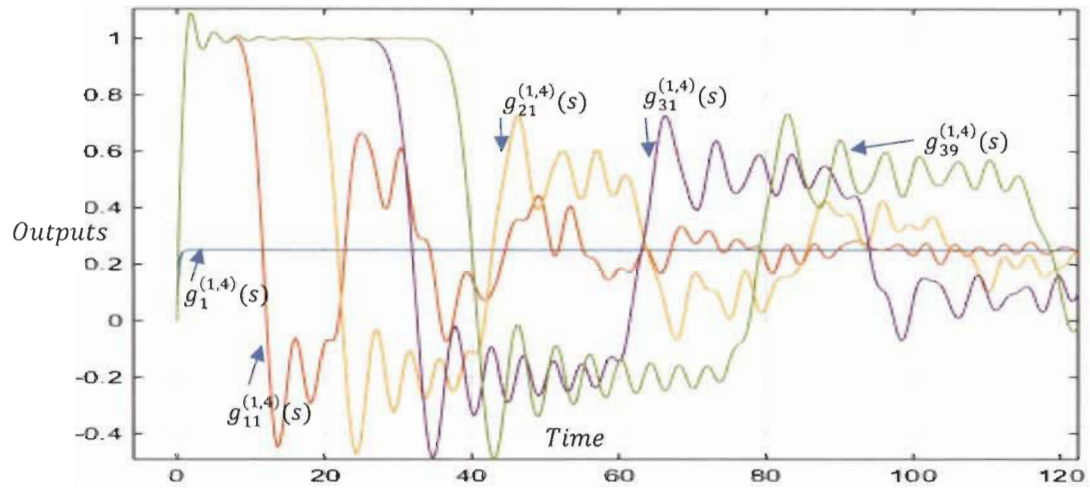


Figure 4. 23: Output response of FWFs $g_1^{(1,4)}(s), g_{11}^{(1,4)}(s), g_{21}^{(1,4)}(s), g_{31}^{(1,4)}(s), g_{39}^{(1,4)}(s)$.

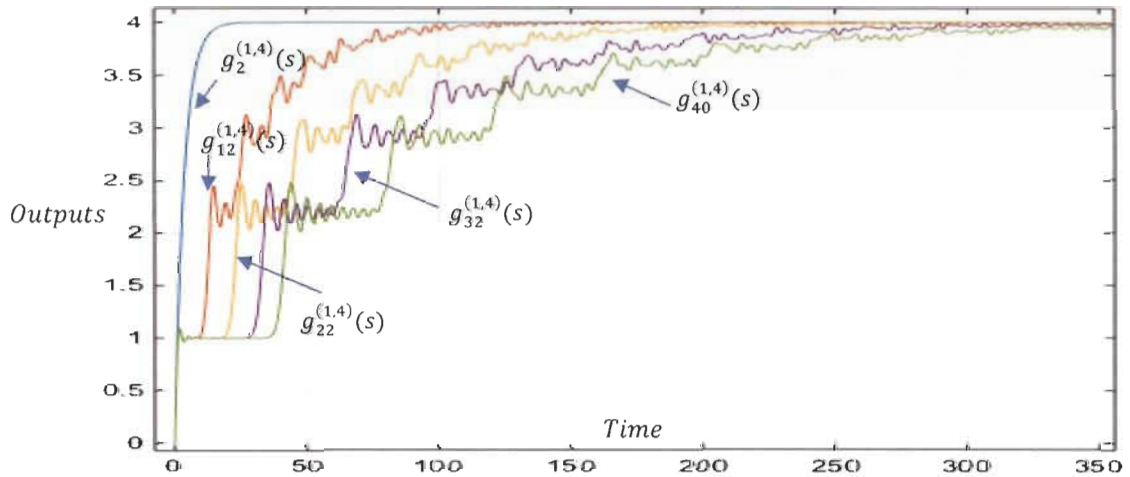


Figure 4. 24: Output response of FWFs $g_2^{(1,4)}(s), g_{12}^{(1,4)}(s), g_{22}^{(1,4)}(s), g_{32}^{(1,4)}(s), g_{40}^{(1,4)}(s)$.

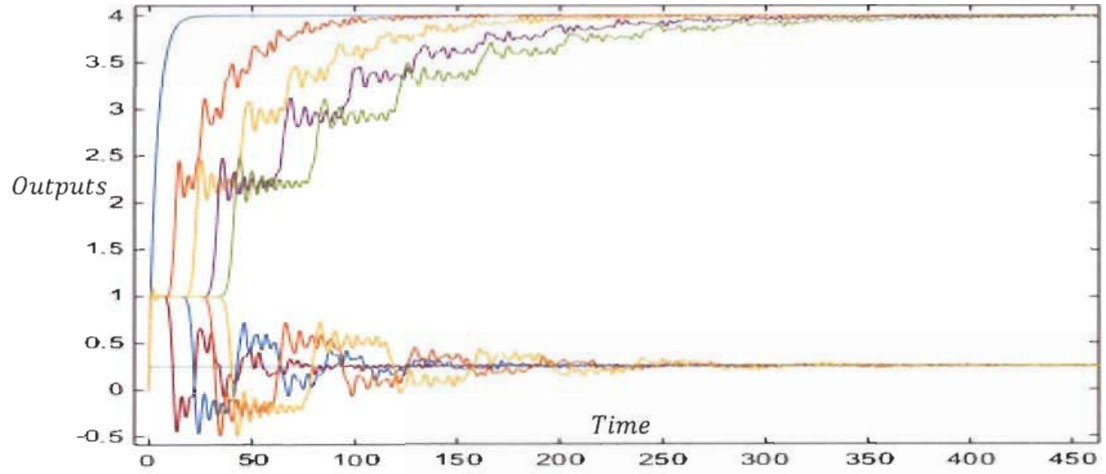


Figure 4. 25: Output response of FWFs $g_1^{(1,4)}(s)$, $g_{11}^{(1,4)}(s)$, $g_{21}^{(1,4)}(s)$, $g_{31}^{(1,4)}(s)$, $g_{39}^{(1,4)}(s)$, $g_2^{(1,4)}(s)$, $g_{12}^{(1,4)}(s)$, $g_{22}^{(1,4)}(s)$, $g_{32}^{(1,4)}(s)$, $g_{40}^{(1,4)}(s)$.

Each FWF defined for a specific (K, x) has two boundary systems $(K, 0)$ and (K, ∞) well defined from Pascal's triangle. Poles and zeros are perfectly organized. Those FWF present multiple resonance and anti-resonance frequencies with respect to each other.

4.7 Controller Design New Approach applied to Fibonacci systems

We have developed a new approach to design a controller for black box systems or high order transfer functions systems. This new approach will be applied to these FWF systems. Their source is a first-order transfer function. The PI controller will be designed based on this simple system and will be applied to all FWF systems.

Knowing the first-order transfer function, one can directly determine the coefficients K_p and K_i of the PI controller for a specific damping ratio ξ natural frequency ω_n (4.10).

$$\begin{aligned} K_p &= \frac{2\xi\omega_n - x}{K} & ; & \quad K_i = \frac{\omega_n^2}{K} ; \\ K_p &= \frac{2\xi\omega_n - 2\xi_f\omega_f}{\omega_f^2} & ; & \quad K_i = \frac{\omega_n^2}{\omega_f^2} \end{aligned} \quad (4.10)$$

We Apply the new approach to design a controller for all FWFs systems for both cases.

A. Case #1: $(K, x) = (1, 1)$.

From bode figure 4.10, the choice of ω_n should be outside the resonance and anti-resonance frequencies. The chosen ω_n is 80 rad/s . For $\xi = 2$, the coefficients of the controller using (3.29) are :

$$K_p = 319 \quad ; \quad K_i = 6400 \quad (4.11)$$

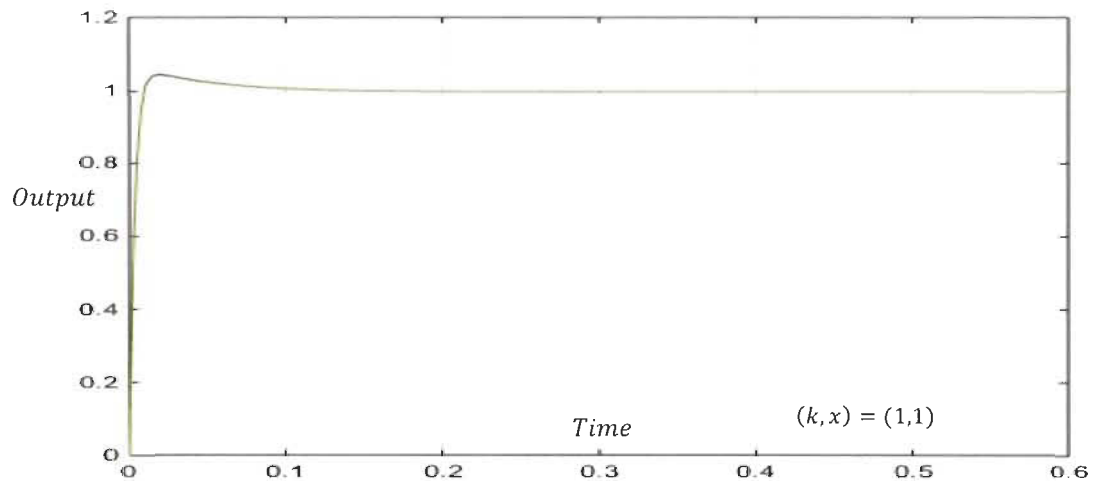
Simulation was conducted in closed loop for all FWFs systems $g_1^{(1,1)}(s), \dots, g_{40}^{(1,1)}(s)$, the outputs are exactly the same, figure 4.26.

B. Case #2: $(K, x) = (1, 4)$.

From bode figure 4.20, the choice of ω_n should be outside the frequencies of resonance and anti-resonances. The choice of ω_n is 500 rad/s and $\xi = 2$, the coefficients of the controller using (4.10) are :

$$K_p = 395 \quad ; \quad K_i = 10000 \quad (4.12)$$

Simulation was made in closed loop for all FWFs systems $g_1^{(1,4)}(s), \dots, g_{40}^{(1,4)}(s)$, the outputs are exactly the same figure 4.26.



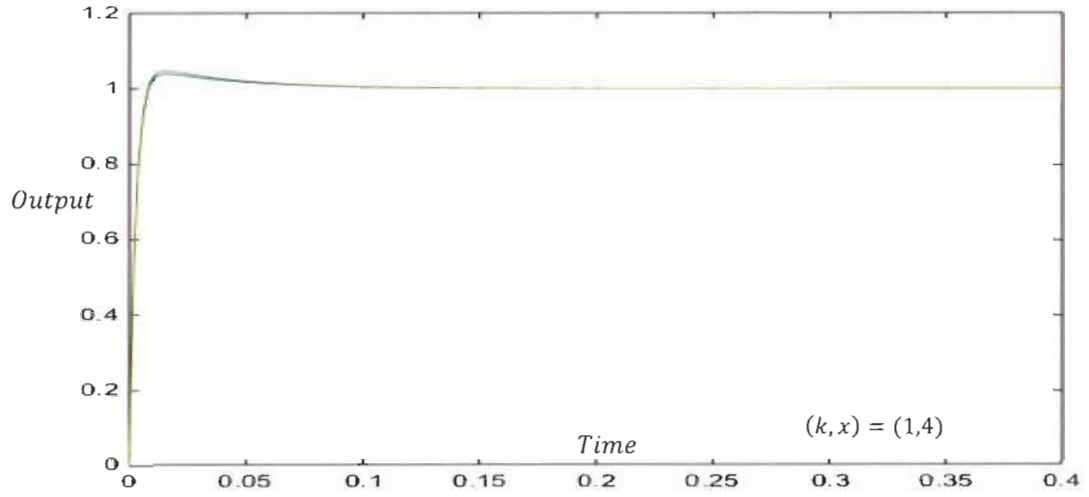


Figure 4. 26: Output response in closed loop for FWFs $g_1^{(1,1)}(s), \dots, g_{40}^{(1,1)}(s), g_1^{(1,4)}(s), \dots, g_{40}^{(1,4)}(s)$.

4.8 Controller Design New Approach limitation

In paragraph 4.7, the new approach was applied to stable systems called Fibonacci systems with known first order system source. The controller was designed based on this first order system and was applied to all subsequent high order Fibonacci systems.

In this paragraph, the new approach will be applied to Fibonacci boundary systems that are marginally stable and unstable as shown in figure 4.27 and 4.28. A controller will be design based on the first order integrator transfer function source with $(K, x) = (1, 0)$.

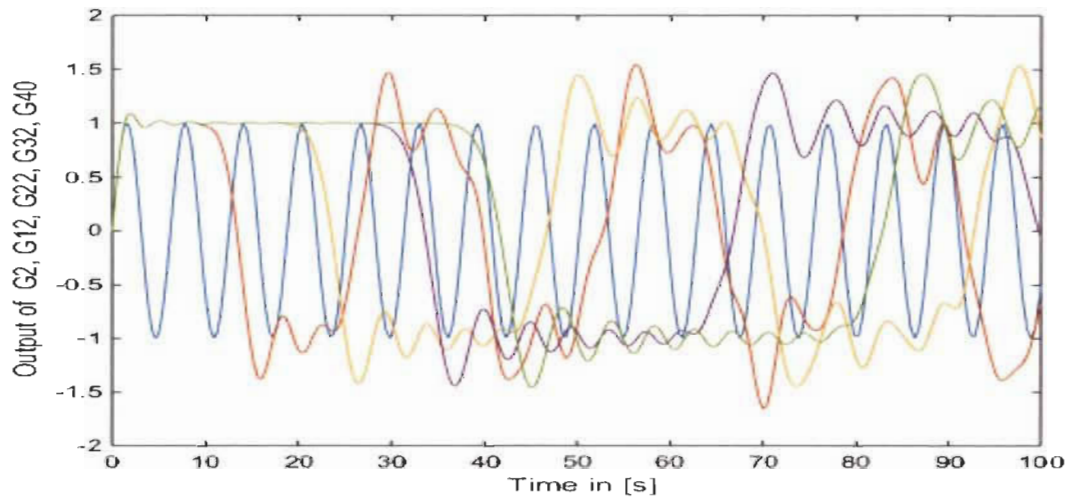


Figure 4. 27: Output response for FWFs $g_2^{(1,0)}(s), g_{12}^{(1,0)}(s), g_{22}^{(1,0)}(s), g_{32}^{(1,0)}(s), g_{40}^{(1,0)}(s)$.

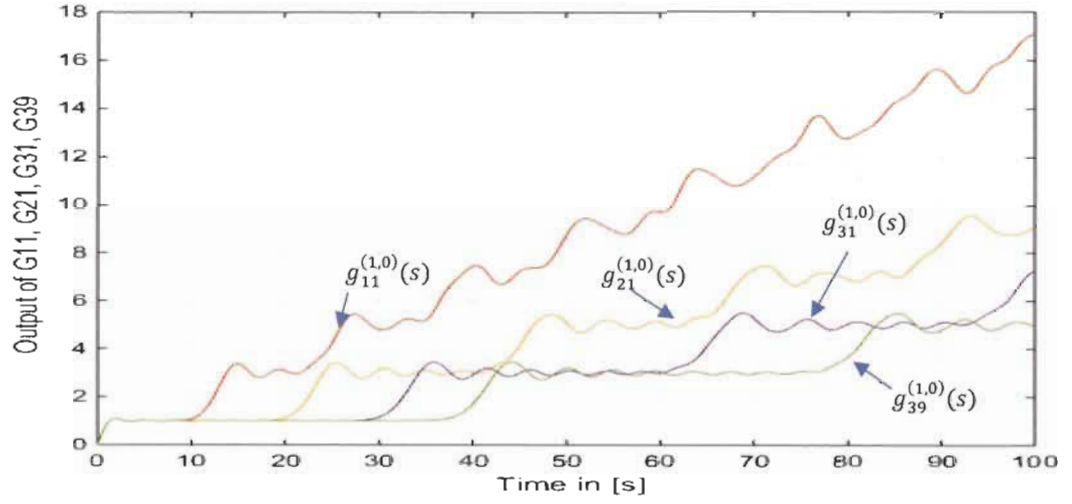


Figure 4. 28: Output response of FWFs, $g_{11}^{(1,0)}(s)$, $g_{21}^{(1,0)}(s)$, $g_{31}^{(1,0)}(s)$, $g_{39}^{(1,0)}(s)$.

Since the first order source is

$$g_1^{(1,0)}(s) = \frac{1}{s} \quad (4.13)$$

The controller will be designed based on $(K, x) = (1, 0)$ and equation (4.10). For a damping factor $\xi = 2$ and $\omega_n = 200 \text{ rad/s}$, the Controller coefficients are :

$$K_p = 800 \quad ; \quad K_i = 40000 \quad (4.14)$$

Simulation was performed for all Fibonacci boundary systems with the same controller in closed loop and shown in figure 4.29.

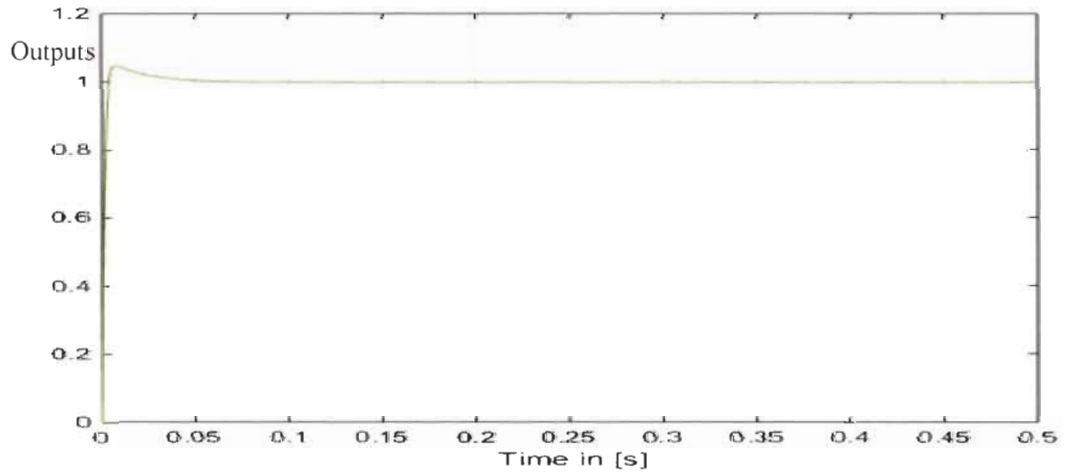


Figure 4. 29: Output response in closed loop of FWFs $g_1^{(1,0)}(s)$, ..., $g_{40}^{(1,0)}(s)$.

All Fibonacci boundary systems are stable in closed loop and well controlled with the same controller designed based on similar systems new approach. In general, applying this new approach to unstable systems may not be possible even if it was successful to all Fibonacci boundary systems that are marginally stable or unstable, the reason is that the initial first order will not be possible to determine.

4.9 Conclusion

In this chapter, specific systems called Fibonacci systems FWFs with transfer functions of high degree have been highlighted from a source of first order transfer function. These FWFs have particular behaviors. The coefficients of their denominators perfectly follow the Pascal's triangle and they also respect the Golden ratio $\phi = 1.618034$. Their poles are located in harmony with each other following certain Fibonacci pattern and specific distribution for their real and imaginary parts. Frequency spectrum of these FWFs present resonance and anti-resonance frequencies perfectly ordered with each other. Their output responses present multiple intermediate steady-states. Their final steady-states have continuous oscillations with low amplitudes. These FWFs systems are irreducible. It is impossible to reduce their transfer functions to a second or third order degree. Each FWF system $g_n^{(K,x)}(s)$ has two Fibonacci boundaries $g_n^{(K,0)}(s)$ and $g_n^{(K,\infty)}(s)$ that can be determined from Pascal's triangle.

For future research, it will be very interesting to compare this new approach to design a controller based on black box systems with artificial neural network (ANN) and fuzzy logic (FL) controllers applied to the same Fibonacci systems. This comparison is necessary since ANN and FL are well known in engineering research community because of their performance and robustness.

Chapter 5: Fibonacci wave functions application to LC ladder network

5.1 Introduction

In this chapter, we present a new general model for an infinite LC ladder network using Fibonacci wave functions introduced in chapter 4. As a practical application for the recursive Fibonacci systems that are derived from a first order system wave function, a simple RC or RL circuit will be a first order circuit source. As an application, LC ladder network will be modelled by these FWFs and it will be used to model and analyze lossless transmission lines for input impedance or admittance, matching impedance and short or open load. The n^{th} order Fibonacci wave function of an LC ladder denominator and numerator coefficients are easily determined from Pascal's triangle new general form introduced in chapter 4. The coefficients follow specific distribution with respect to the golden ratio. Their pole locations follow an ordered Fibonacci pattern. The LC ladder network model can be created to any order for each inductor current or flux and for each capacitor voltage or charge. Based on this new proposed FWF general model, many applications in the literature using lossless LC ladder model like particles interaction behavior in quantum mechanics, sound propagation model in the ear and many other applications can carry the analysis and research to an upper level.

5.2 RC Fibonacci electrical circuit (RC-FEC)

The original Fibonacci wave function has the following as described in chapter 4.

$$g_1^{(k, x_c)}(s) = \frac{K}{s + x_c} \quad (5.1)$$

With

$$K = \omega_f^2 \quad \text{and} \quad x_c = 2 \xi_{cf} \omega_f$$

The first order electrical circuit RC-FEC is presented in figure 5.1.

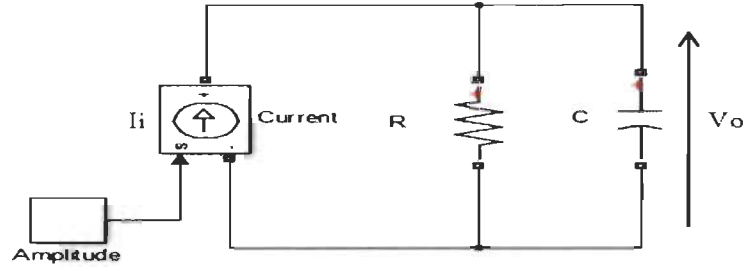


Figure 5. 1: First order RC-FEC

$$\frac{V_o}{I_i} = \frac{\frac{1}{C}}{s + \frac{1}{RC}} = L \frac{\frac{1}{LC}}{s + \frac{1}{RC}} = L \frac{K}{s + x_c} = L g_1^{(K, x_c)}(s)$$

$$\left(\frac{V_o}{L I_i}\right)_1^{(K, x_c)} = \frac{K}{s + x_c} = g_1^{(K, x_c)}(s) \quad (5.2)$$

$$K = \frac{1}{LC} \quad \text{and} \quad x_c = 2 \xi_{cf} \omega_f = \frac{1}{RC}$$

The second order RC-FEC circuit diagram is shown in figure 5.2 and its wave function in (3).

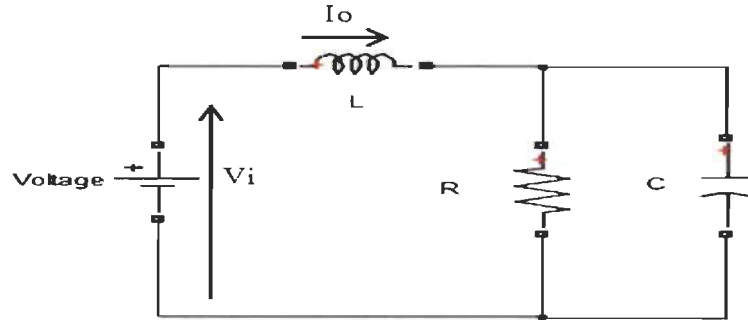


Figure 5. 2: Second order RC-FEC

$$V_i = \left(L g_1^{(K, x_c)}(s) + sL \right) I_o = \frac{LC \left(s + g_1^{(K, x_c)}(s) \right) I_o}{C}$$

$$\left(\frac{I_o}{CV_i}\right)_2^{(K,x_c)} = \frac{K}{s + \frac{K}{s + x_c}} = g_2^{(K,x_c)}(s) \quad (5.3)$$

The wave function of the third order RC-FEC (5.4) is derived from circuit diagram presented in figure 5.3

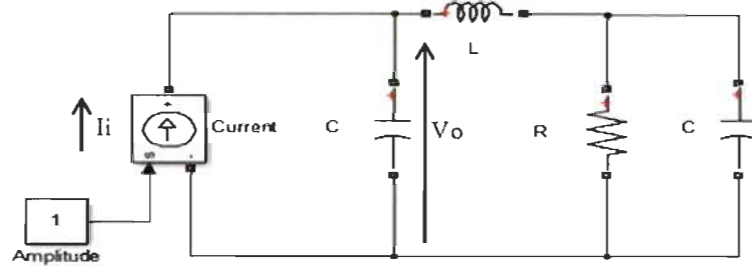


Figure 5. 3: Third order RC-FEC

$$I_i = \left(C g_2^{(K,x_c)}(s) + sC\right) V_o = \frac{LC \left(s + g_2^{(K,x_c)}(s)\right) V_o}{L}$$

$$\left(\frac{V_o}{LI_i}\right)_3^{(K,x_c)} = \frac{K}{s + \frac{K}{s + \frac{K}{s + x_c}}} = g_3^{(K,x_c)}(s) \quad (5.4)$$

One can see that an even n^{th} order RC-FEC (figure 5.4) will have voltage as input and current as output.

$$n = n_c + n_L \quad (5.5)$$

n_c is the total number of capacitors in the circuit.

n_L is the total number of inductance in the circuit.

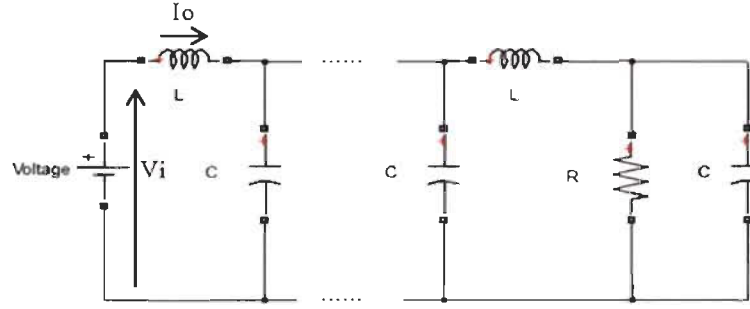


Figure 5. 4: n^{th} even order RC-FEC

The FWF of this circuit is.

$$\left(\frac{I_o}{CV_i}\right)_n^{(K,x_c)} = \frac{K}{s + g_{n-1}^{(K,x_c)}(s)} = g_n^{(K,x_c)}(s) \quad (5.6)$$

For n^{th} odd order, the wave function is.

$$\left(\frac{V_o}{LI_i}\right)_n^{(K,x_c)} = \frac{K}{s + g_{n-1}^{(K,x_c)}(s)} = g_n^{(K,x_c)}(s) \quad (5.7)$$

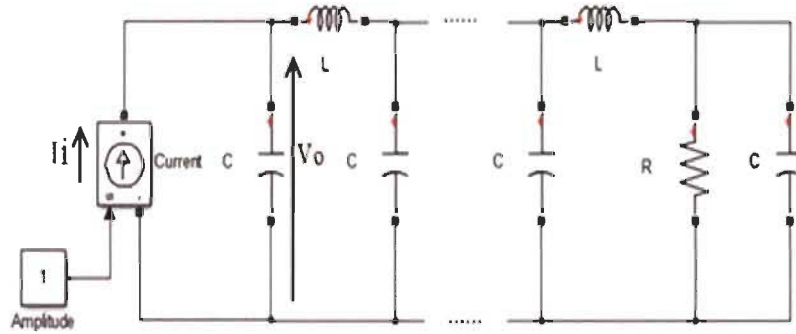


Figure 5. 5: n^{th} odd order RC-FEC

In general, n^{th} even order RC-FEC with voltage as input and current as output has a final steady-state value $C * x_c$.

An n^{th} odd order RC-FEC with current as input and voltage as output has a final steady-state value $L * \frac{K}{x_c}$.

Table 5.1 summarizes all FWFs for RC-FECs

Table 5. 1: RC-FEC Fibonacci wave functions

$(\frac{V_o}{LI_i})_1^{(K,x_c)} = g_1^{(K,x_c)} = \frac{K}{s + x_c}$	$(\frac{V_o}{LI_i})_1^{(K,x_c)} = g_1^{(K,x_c)} = \frac{K}{1s + 1x_c}$
$(\frac{I_o}{CV_i})_2^{(K,x_c)} = g_2^{(K,x_c)} = \frac{K}{s + \frac{K}{s + x_c}}$	$(\frac{I_o}{CV_i})_2^{(K,x_c)} = g_2^{(K,x_c)} = \frac{Ks + Kx_c}{1s^2 + 1x_cs + 1K}$
$(\frac{V_o}{LI_i})_3^{(K,x_c)} = g_3^{(K,x_c)} = \frac{K}{s + \frac{K}{s + \frac{K}{s + x_c}}}$	$(\frac{V_o}{LI_i})_3^{(K,x_c)} = g_3^{(K,x_c)} = \frac{Ks^2 + Ksx_c + K^2}{1s^3 + 1x_cs^2 + 2Ks + 1Kx_c}$
$(\frac{I_o}{CV_i})_4^{(K,x_c)} = g_4^{(K,x_c)} = \frac{K}{s + \frac{K}{s + \frac{K}{s + \frac{K}{s + x_c}}}}$	$(\frac{I_o}{CV_i})_4^{(K,x_c)} = g_4^{(K,x_c)} = \frac{Ks^3 + Kx_cs^2 + 2K^2s + K^2x_c}{1s^4 + 1x_cs^3 + 3Ks^2 + 2Kx_cs + 1K^2}$
$(\frac{I_o}{CV_i})_n^{(K,x_c)} = g_n^{(K,x_c)} = \frac{K}{s + g_{n-1}^{(K,x_c)}(s)}$ <i>n even</i> $(\frac{V_o}{LI_i})_n^{(K,x_c)} = g_n^{(K,x_c)} = \frac{K}{s + g_{n-1}^{(K,x_c)}(s)}$ <i>n odd</i>	$g_n^{(K,x_c)}(s) = \frac{Kden_{n-1}^{(K,x_c)}(s)}{sden_{n-1}^{(K,x_c)}(s) + num_{n-1}^{(K,x_c)}(s)}$ $g_n^{(K,x_c)}(s) = \frac{Kden_{n-1}^{(K,x_c)}(s)}{den_n^{(K,x_c)}(s)}$

5.3 RC-FEC and FWFs simulation (RL-FEC)

Simulation studies were conducted to compare the previous electrical circuits with Fibonacci wave functions and Matlab-Simulink electrical circuit model. The studies confirm that these circuits follow the logic of a recursive Fibonacci sequence and can be modelled by FWFs.

A. Case #1: $R=1\Omega$; $L=1H$; $C=1F$; $(K, x_c) = (1,1)$

In this case $(K, x_c) = (1,1)$. Pascal's Triangle in Table 5.2 will be used to determine all FWFs.

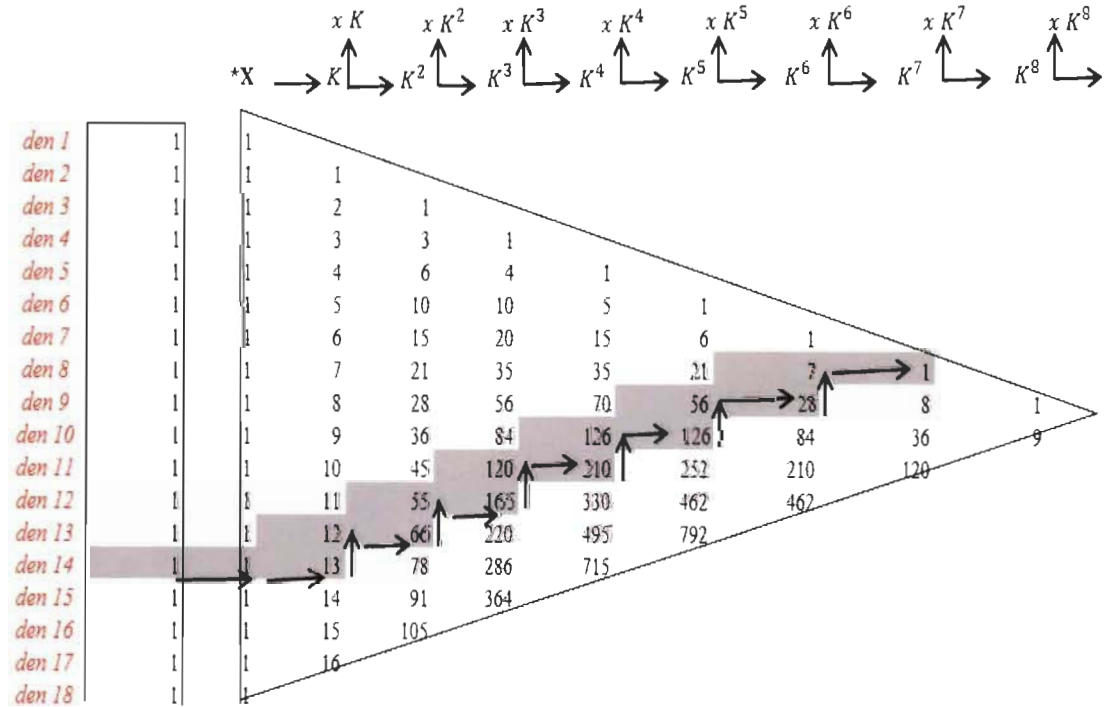
Order 14 FWF taken as example is an even function, using its numerator and denominator coefficients are expressed in (5.8) using Table 5.2.

$$\left(\frac{I_o}{CV_i}\right)_{14}^{(K, x_c)} = g_{14}^{(K, x_c)}(s) = \frac{K \text{den}_{13}^{(K, x_c)}(s)}{\text{den}_{14}^{(K, x_c)}(s)} \quad (5.8)$$

$$\text{den}_{13}^{(K, x_c)}(s) = 1s^{13} + 1x_c s^{12} + 12Ks^{11} + 11Kx_c s^{10} + 55K^2 s^9 + 45K^2 x_c s^8 + 120K^3 s^7 + 84K^3 x_c s^6 + 126K^4 s^5 + 70K^4 x_c s^4 + 56K^5 s^3 + 21K^5 x_c s^2 + 7K^6 s + 1K^6 x_c$$

$$\text{den}_{14}^{(K, x_c)}(s) = 1s^{14} + 1x_c s^{13} + 13Ks^{12} + 12Kx_c s^{11} + 66K^2 s^{10} + 55K^2 x_c s^9 + 165K^3 s^8 + 120K^3 x_c s^7 + 210K^4 s^6 + 126K^4 x_c s^5 + 126K^5 s^4 + 56K^5 x_c s^3 + 28K^6 s^2 + 7K^6 x_c s + 1K^7$$

Table 5. 2: Pascal's triangle general form with multiplication coefficients (K, x_c) .



Simulations of $(\frac{I_o}{V_i})_{40}^{(1,1)} = C * g_{40}^{(1,1)}(s)$ FWF model and Matlab-Simulink RC-FEC electrical circuit model order 40 are illustrated in figure 5.6. The final steady-state is $C * \frac{k}{x_c} = 1$ with unit input voltage.

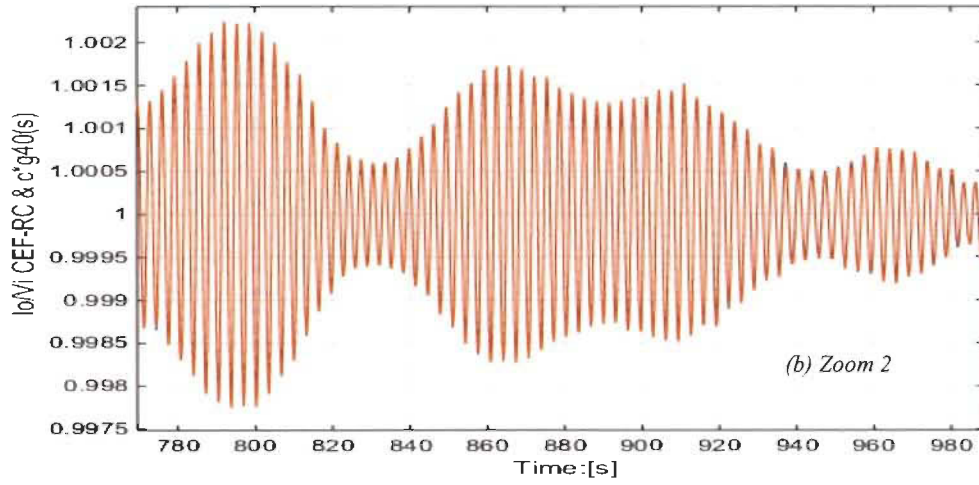
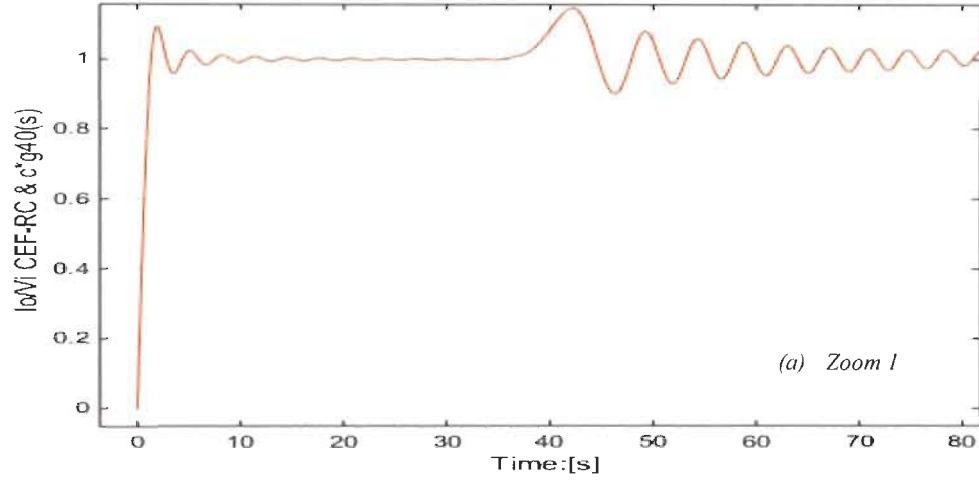


Figure 5. 6: FWF RC-FEC $(\frac{I_o}{V_i})_{40}^{(1,1)} = C * g_{40}^{(1,1)}(s)$ & Matlab-Simulink model with $V_i = 1V$

The $(\frac{V_o}{I_i})_{39}^{(K,x_c)} = L * g_{39}^{(K,x_c)}(s)$, which is odd order, will be determined using Pascal's triangle table 5.2.

Simulation results of FWF $(\frac{V_o}{I_i})_{39}^{(1,1)} = L * g_{39}^{(1,1)}(s)$ and Matlab-Simulink RC-FEC electrical circuit of order 39 model are identical as illustrated in figure 5.7. The final steady-state is $L * x_c = 1$ with unit input current.

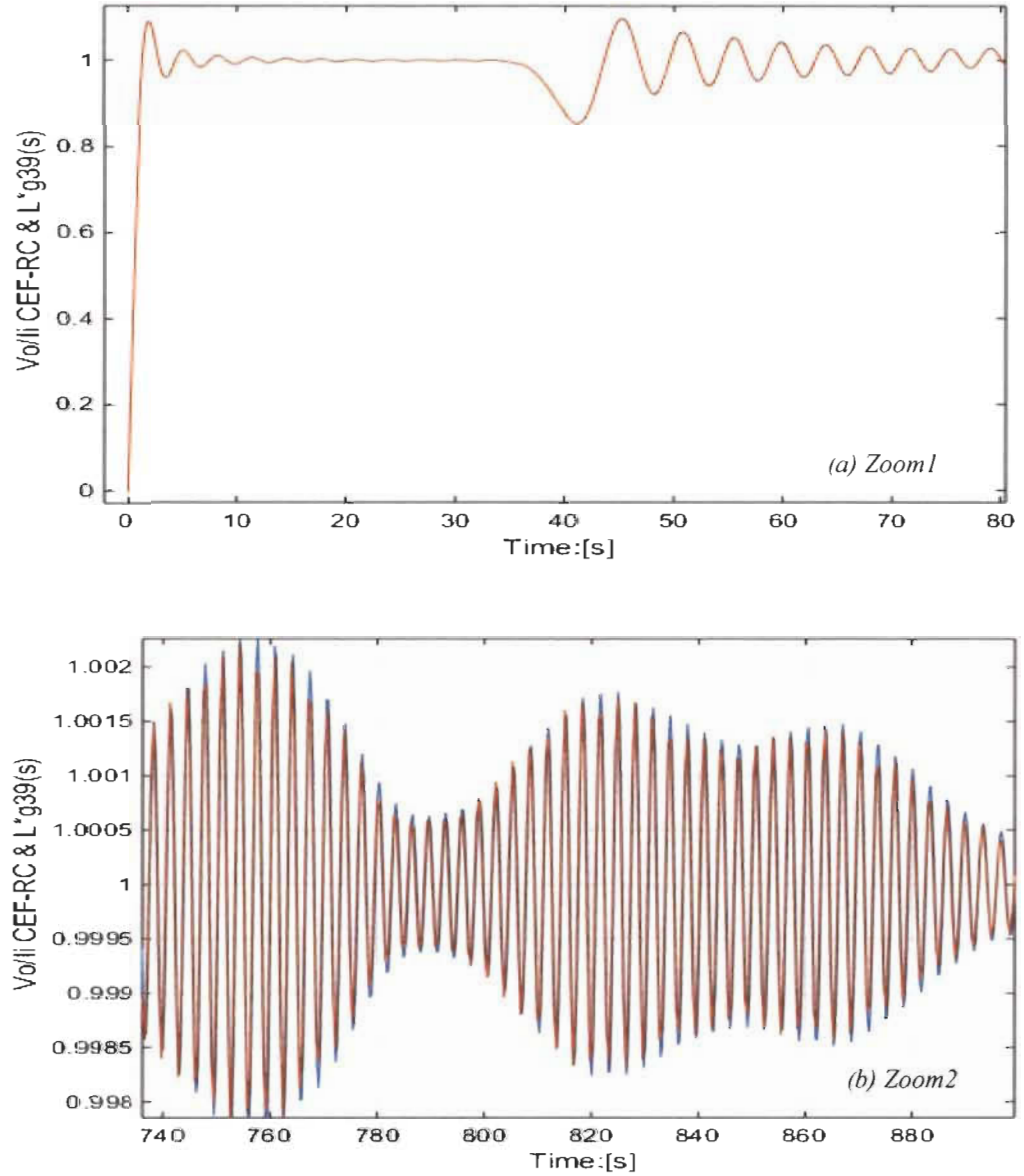


Figure 5. 7: FWF RC-FEC $(\frac{V_o}{I_i})_{39}^{(1,1)} = L * g_{39}^{(1,1)}(s)$ & Matlab-Simulink model with $I_i = 1A$

5.4 RL Fibonacci electrical circuit

RL-FEC is determined in the same way as RC-FEC. The first order circuit in figure 5.8 and its FWF is presented in (5.9).

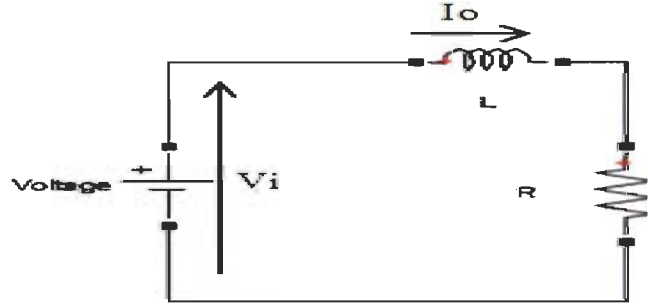


Figure 5. 8: First order RL-FEC

$$\begin{aligned} \frac{I_o}{V_i} &= \frac{\frac{1}{L}}{s + \frac{R}{L}} = C \frac{\frac{1}{LC}}{s + \frac{R}{L}} = C \frac{K}{s + x_L} = C g_1^{(K, x_L)}(s) \\ \left(\frac{I_o}{CV_i}\right)_1^{(K, x_L)} &= \frac{K}{s + x_L} = g_1^{(K, x_L)}(s) \\ K &= \frac{1}{LC} \quad \text{and} \quad x_L = 2 \xi_{Lf} \omega_f = \frac{R}{L} \\ K &= \frac{1}{LC} = x_c x_L = 4 \xi_{cf} \xi_{Lf} \omega_f^2 \quad \text{and} \quad \xi_{cf} \xi_{Lf} = \frac{1}{4} \end{aligned} \tag{5.9}$$

The second order RL-FEC will be defined with current input and voltage output (figure 5.9) and its FWF expressed in (5.10).

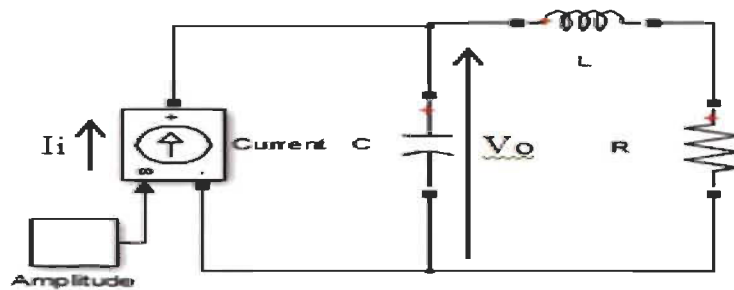


Figure 5. 9: Second order RL-FEC

$$I_i = \left(C g_1^{(K, x_L)}(s) + sC \right) V_o = \frac{LC \left(s + g_1^{(K, x_L)}(s) \right) V_o}{L} \quad (5.10)$$

$$\left(\frac{V_o}{LI_i} \right)_2^{(K, x_L)} = \frac{K}{s + \frac{K}{s + x_L}} = g_2^{(K, x_L)}(s)$$

The third order RL-FEC will be defined with an input voltage and output current (Figure 5.10) and its FWF in (5.11).

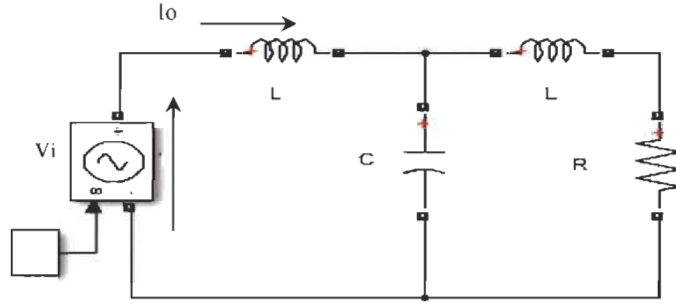


Figure 5. 10: First order RL-FEC

$$V_i = \left(L g_2^{(K, x_L)}(s) + sL \right) I_o = \frac{LC \left(s + g_2^{(K, x_L)}(s) \right) I_o}{C} \quad (5.11)$$

$$\left(\frac{I_o}{CV_i} \right)_3^{(K, x_L)} = \frac{K}{s + \frac{K}{s + \frac{K}{s + x_L}}} = g_3^{(K, x_L)}(s)$$

In general, RL-FEC with an even n^{th} order in figure 5.11 has current as input and voltage as output.

$$n = n_c + n_L \quad (5.12)$$

n_c is the total number of capacitors in the circuit.

n_L is the total number of inductance in the circuit.

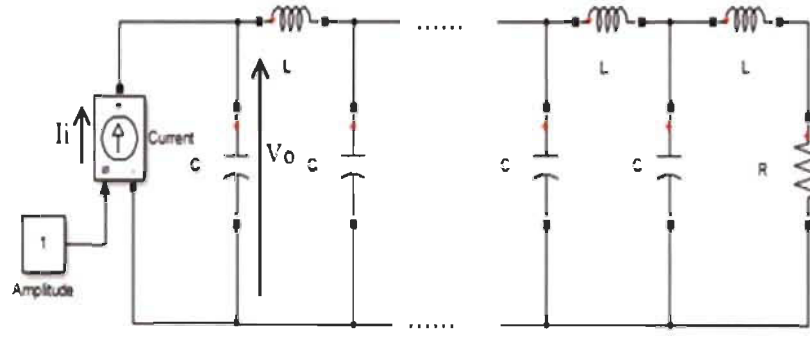


Figure 5. 11: n^{th} even order RL-FEC

The Wave function is as follow.

$$\left(\frac{V_o}{LI_i}\right)_n^{(K,x_L)} = \frac{K}{s + g_{n-1}^{(K,x_L)}(s)} = g_n^{(K,x_L)}(s) \quad (5.13)$$

An RL-FEC with n^{th} odd order (Figure 5.12) has voltage as input and current as output and its wave function expressed in (5.14).

$$\left(\frac{I_o}{CV_i}\right)_n^{(K,x_L)} = \frac{K}{s + g_{n-1}^{(K,x_L)}(s)} = g_n^{(K,x_L)}(s) \quad (5.14)$$

In general, n^{th} even order RL-FEC has a current input and voltage output with a final steady-state value of $L * x_L$.

n^{th} odd order RL-FEC with voltage as input and current as output has a final steady-state value of $C * \frac{K}{x_L}$.

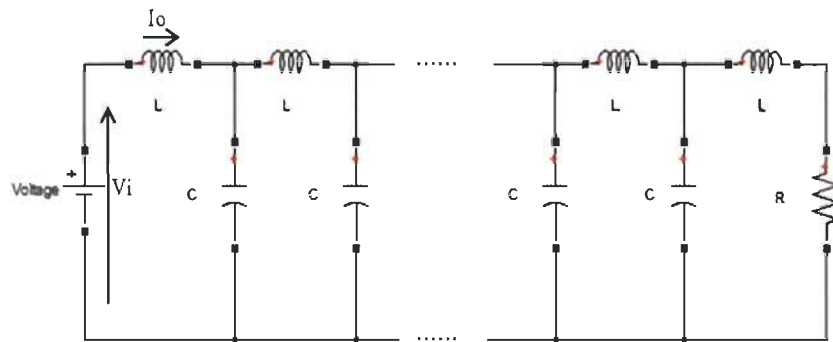


Figure 5. 12: n^{th} odd order RL-FEC

Table 5.3 summarize all FWFs for RL-FECs

Table 5. 3: RL-FEC Fibonacci wave functions

$(\frac{I_o}{LV_i})_1^{(K,x_L)} = g_1^{(K,x_L)} = \frac{K}{s + x_L}$	$(\frac{I_o}{LV_i})_1^{(K,x_L)} = g_1^{(K,x_L)} = \frac{K}{1s + 1x_L}$
$(\frac{V_o}{LI_i})_2^{(K,x_L)} = g_2^{(K,x_L)} = \frac{K}{s + \frac{K}{s + x_L}}$	$(\frac{V_o}{LI_i})_2^{(K,x_L)} = g_2^{(K,x_L)} = \frac{Ks + Kx_L}{1s^2 + 1x_Ls + 1K}$
$(\frac{I_o}{LV_i})_3^{(K,x_L)} = g_3^{(K,x_L)} = \frac{K}{s + \frac{K}{s + \frac{K}{s + x_L}}}$	$(\frac{I_o}{LV_i})_3^{(K,x_L)} = g_3^{(K,x_L)} = \frac{Ks^2 + Ksx_L + K^2}{1s^3 + 1x_Ls^2 + 2Ks + 1Kx_L}$
$(\frac{V_o}{LI_i})_4^{(K,x_L)} = g_4^{(K,x_L)} = \frac{K}{s + \frac{K}{s + \frac{K}{s + \frac{K}{s + x_L}}}}$	$(\frac{V_o}{LI_i})_4^{(K,x_L)} = g_4^{(K,x_L)}$ $= \frac{Ks^3 + Kx_Ls^2 + 2K^2s + K^2x_L}{1s^4 + 1x_Ls^3 + 3Ks^2 + 2Kx_Ls + 1K^2}$
$(\frac{V_o}{LI_i})_n^{(K,x_L)} = g_n^{(K,x_L)} = \frac{K}{s + g_{(n-1)L}(s)}$ <i>n even</i> $(\frac{I_o}{LV_i})_n^{(K,x_L)} = g_n^{(K,x_L)} = \frac{K}{s + g_{(n-1)L}(s)}$ <i>n odd</i>	$g_n^{(K,x_L)}(s) = \frac{Kden_{n-1}^{(K,x_L)}(s)}{sden_{n-1}^{(K,x_L)}(s) + num_{n-1}^{(K,x_L)}(s)}$ $g_n^{(K,x_L)}(s) = \frac{Kden_{n-1}^{(K,x_L)}(s)}{den_n^{(K,x_L)}(s)}$

5.5 Simulation of FWF and its corresponding RL-FEC

Simulations will be made with the same values as RC-FEC.

A. Case #1: $R=1\Omega$; $L=1H$; $C=1F$; $(K, x_L) = (1,1)$.

$$x_L = \frac{R}{L} = 1; \quad K = \frac{1}{LC} = 1$$

Simulations of the FWF $\left(\frac{v_o}{I_i}\right)_{40}^{(1,1)} = Lg_{40}^{(1,1)}(s)$ and Matlab-Simulink RL-FEC electrical circuit model order 40 are shown in the figure 5.13 below. It is clear that the final and the only steady-state is $\frac{K}{x_L} = x_c = x_L = 1$.

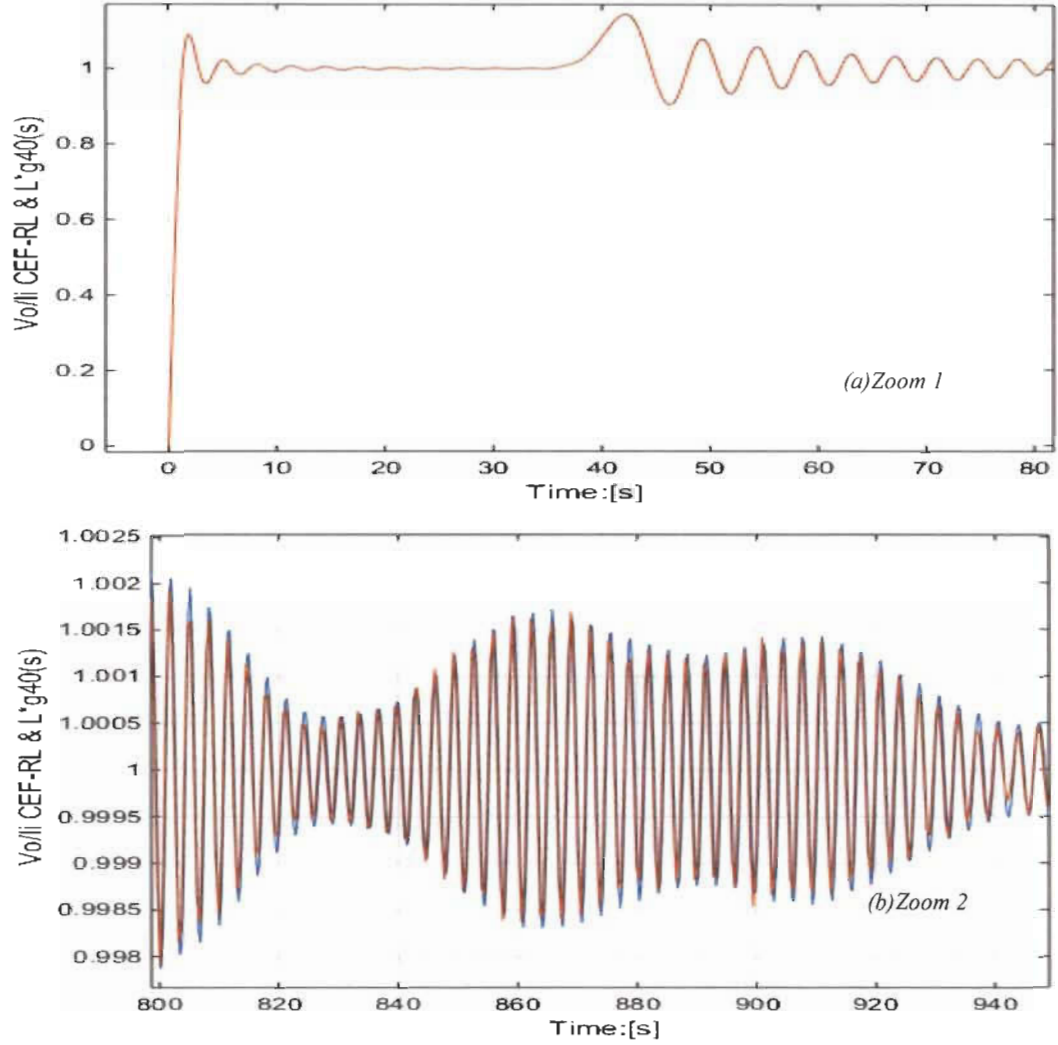


Figure 5. 13: FWF RL-FEC $\left(\frac{v_o}{I_i}\right)_{40}^{(1,1)} = Lg_{40}^{(1,1)}(s)$ & Matlab-Simulink model with $I_i = 1A$

The wave function $\left(\frac{I_o}{V_i}\right)_{39}^{(1,1)} = Cg_{39}^{(1,1)}(s)$, is shown in figure 5.14 with its equivalent Matlab-Simulink electrical circuit RL-FEC model order 39, and both are exactly identical.

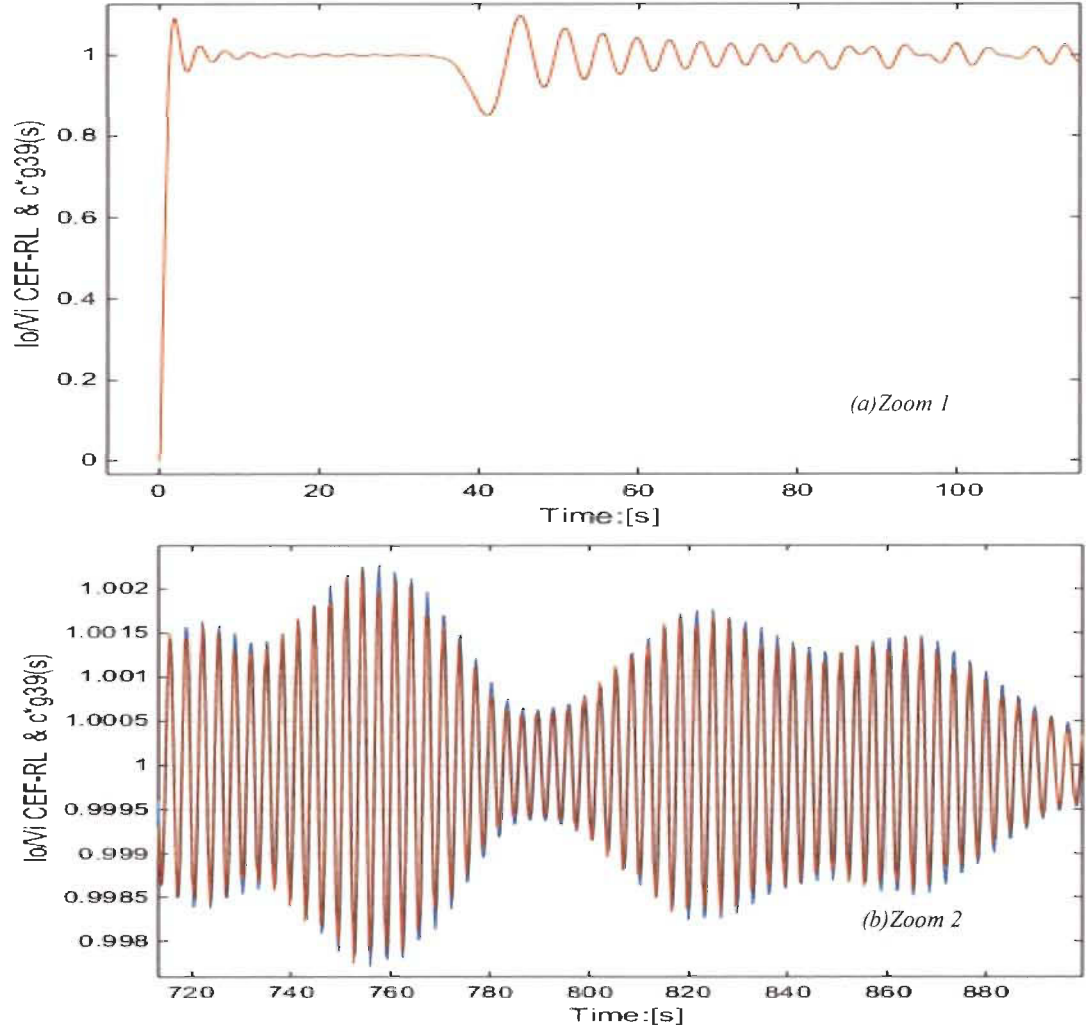


Figure 5. 14: FWF RL-FEC $\left(\frac{I_o}{V_i}\right)_{39}^{(1,1)} = \mathcal{C}g_{39}^{(1,1)}(s)$ & Matlab-Simulink model with $V_i = 1V$

An n^{th} order RL-FEC and its FWF behaves exactly the same way as an n^{th} order RC-FEC and its FWF only if $x_L = x_c$.

$$\left(\frac{V_o}{LI_i}\right)_n^{(K,x_L)} = g_n^{(K,x_L)} = \left(\frac{I_o}{CV_i}\right)_n^{(K,x_c)} = g_n^{(K,x_c)} \text{ with } x_L = x_c$$

$$R = \sqrt{\frac{L}{C}}; \quad K = \omega_f^2; \quad x_L = x_c = \omega_f = \frac{1}{\sqrt{LC}} \quad (5.15)$$

$$x_L = x_c = \frac{R}{L} = \frac{1}{RC}$$

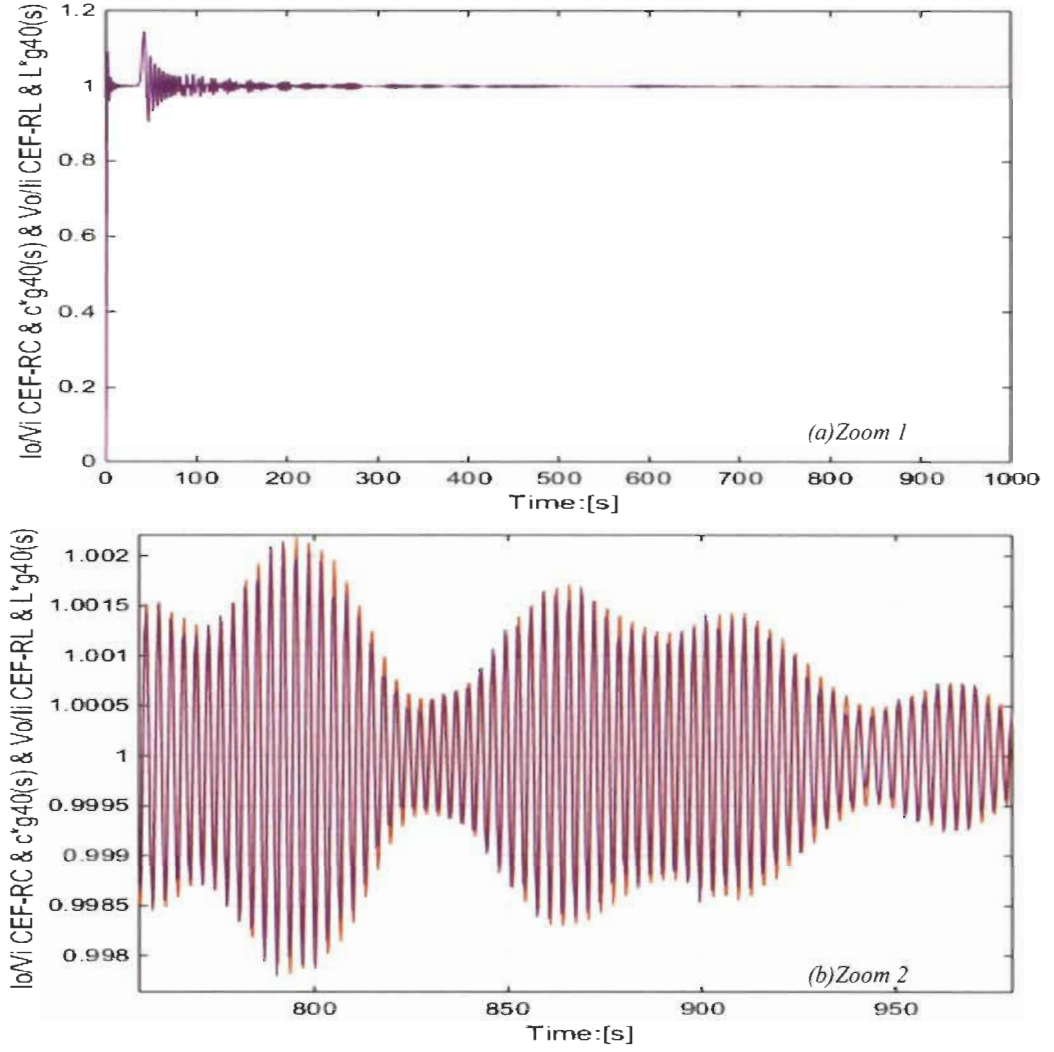


Figure 5. 15: RL-FEC and RC-FEC order 40 ; $\left(\left(\frac{V_o}{I_i}\right)_{40}^{(1,1)} = L g_{40}^{(1,1)}(s), I_i = 1A\right)$; $\left(\left(\frac{I_o}{V_i}\right)_{40}^{(1,1)} = C * g_{40}^{(1,1)}(s), V_i = 1V\right)$

5.6 N^{th} Order LC Ladder RC-FEC and RL-FEC general model

The n^{th} order RC-FEC and RL-FEC are perfectly modeled. All currents through each inductor and voltages through each capacitor are perfectly determined by Fibonacci wave functions. The model is shown in figure 5.17 for $n = 40$ and can be extended to an infinite order knowing that each FWF can be determined using Pascal's triangle general form in table 5.2.

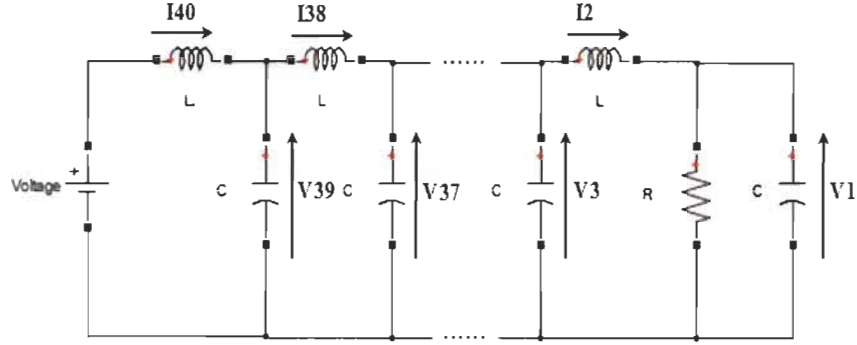


Figure 5.16: n^{th} even order RC-FEC

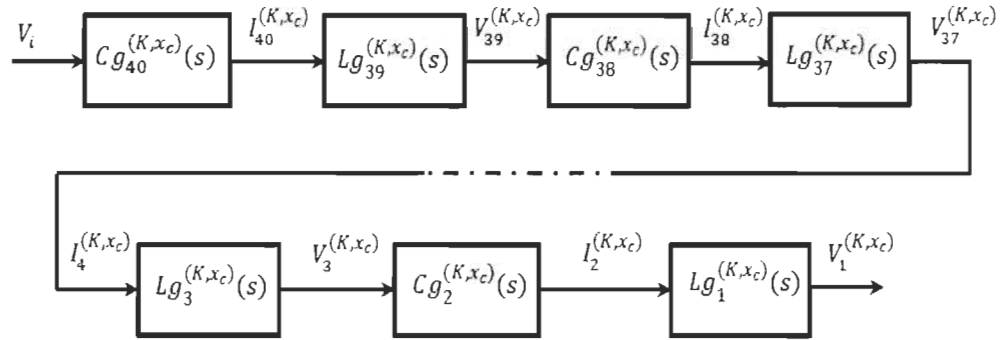


Figure 5.17: n^{th} even order RC-FEC Model using FWFs for each current and voltage branch.

This model can be presented with the variable charge $Q_j^{(K,x_c)} = CV_j^{(K,x_c)}$ in each capacitor and the electromagnetic flux $\phi_j^{(K,x_c)} = LI_j^{(K,x_c)}$ in each inductor as shown in figure 5.18.

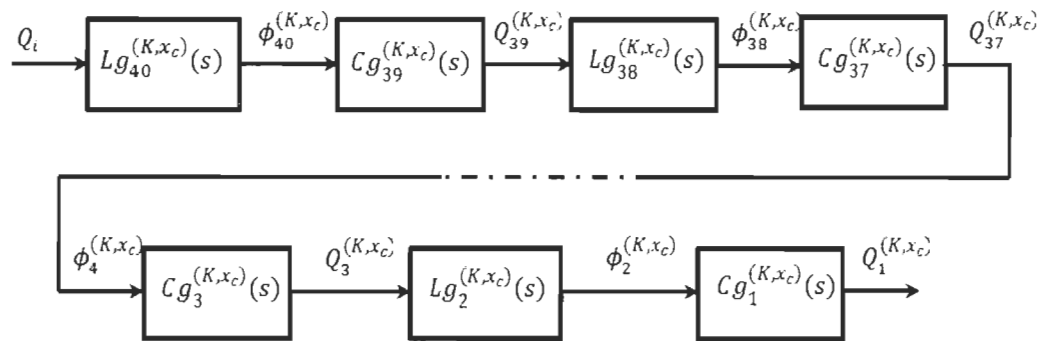


Figure 5.18: n^{th} even order RC-FEC Model using FWFs for each flux and charge branch.

In the same way, the RL-FEC general model is illustrated in figure 5.20 below for $n = 40$.

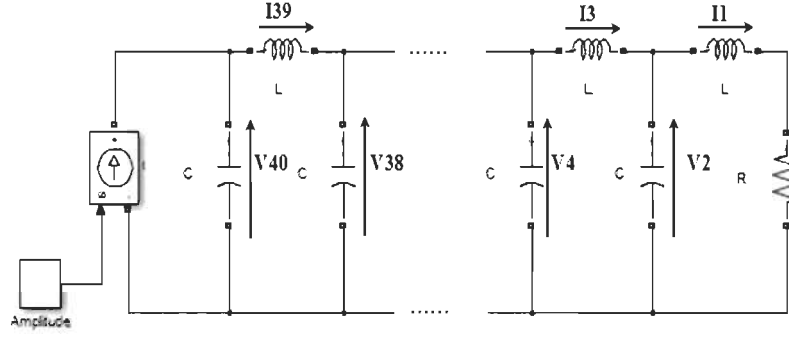


Figure 5.19: n^{th} even order RL-FEC

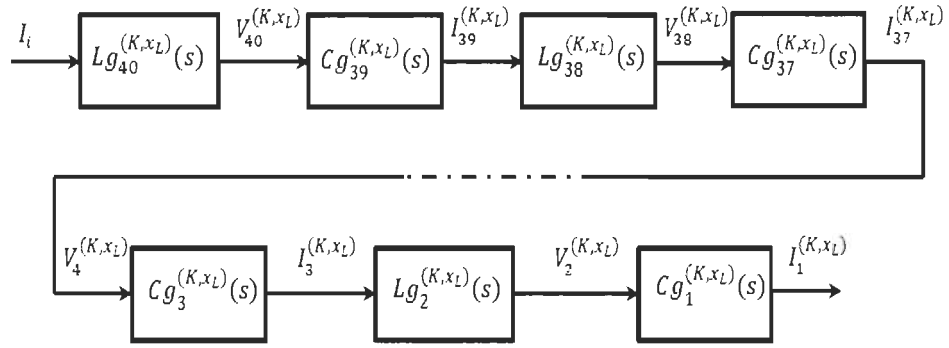


Figure 5.20: n^{th} even order RL-FEC Model using FWFs for each current and voltage branch.

This model can be also presented with the variable charge $Q_j^{(K,x_L)} = CV_j^{(K,x_L)}$ in each capacitor and the electromagnetic flux $\phi_j^{(K,x_L)} = LI_j^{(K,x_L)}$ in each inductor as shown in figure 5.21.

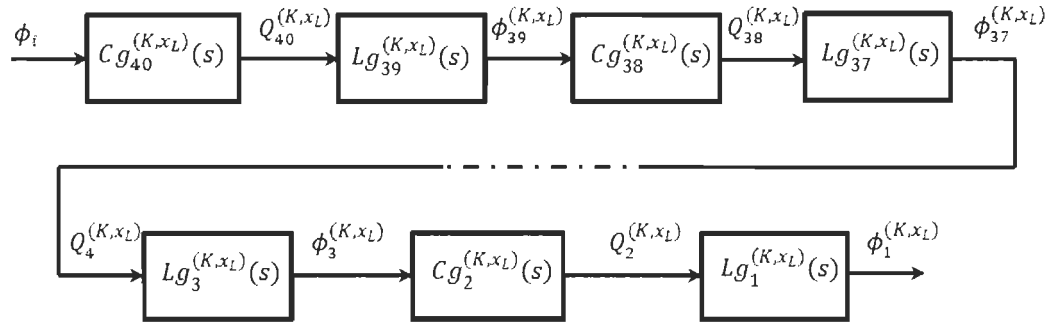


Figure 5.21: n^{th} even order RL-FEC Model using FWFs for each flux and charge branch.

Simulation was conducted for RC-FEC using Matlab-Simulink electrical circuit and the corresponding FWF model for $n = 40$ to confirm the accuracy of the proposed model for all

currents and voltages. Note that this model is applicable to any order n of the RC-FEC and any order n of RL-FEC.

The figures 5.22 and 5.23 show simulation for both RC-FEC models for voltage V_{37} and current I_{40} for the case $(K, x_c) = (1, 4)$.

A. Case #2: $(K, x_c) = (1, 4)$; $R=10\Omega$.

$$K = \frac{1}{LC} = \omega_f^2 = x_L x_c ; C = \frac{1}{R x_c} = 0.025F ; L = \frac{1}{K C} = 40H ; x_L = \frac{R}{L} = 0.25 \quad (5.16)$$

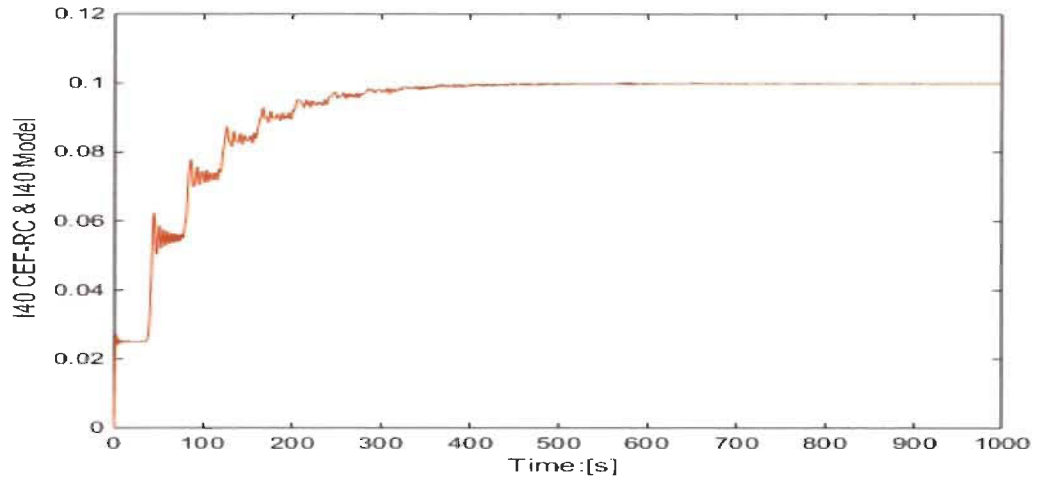


Figure 5. 22: Matlab-Simulink RC-FEC circuit and proposed FWF general model for $I_{40}^{(1,4)}$ with input $V_i = 1V$

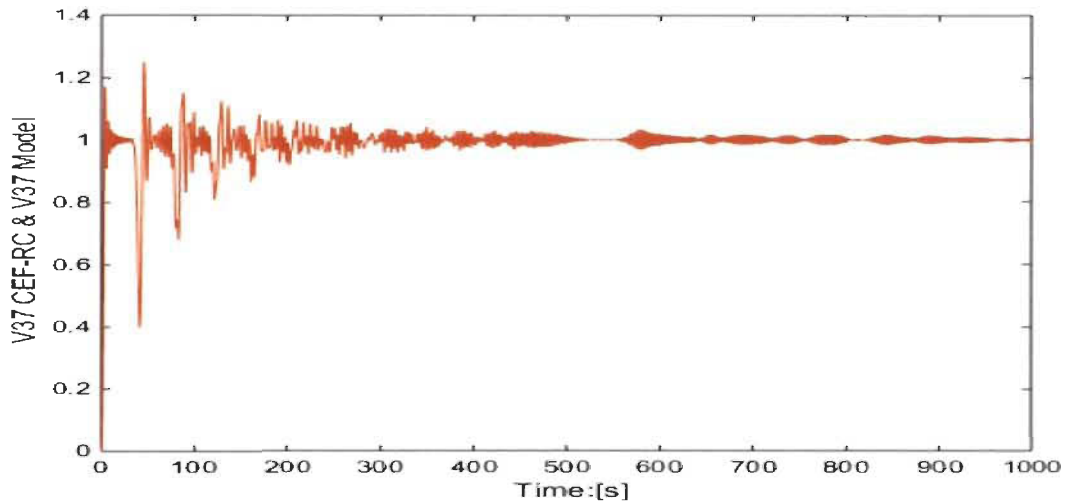


Figure 5. 23: Matlab-Simulink RC-FEC circuit and proposed FWF general model for $V_{37}^{(1,4)}$ with input $V_i = 1V$

FWFs model presented in figures 5.17 and 5.20 are exactly the same as Matlab-Simulink RC-FEC and RL-FEC circuits of all inductors currents and all capacitors voltages. Thus the RC-FEC and RL-FEC can be shaped for any order due to the fact that every order is well defined with its Fibonacci wave function precisely determined from Pascal's triangle. Figures 5.24 and 5.25 show the behavior of all voltages for each capacitor (odd FWFs) and all currents in each inductor (even FWFs). Simulation results also show the delay of each branch based on its position from the input source.

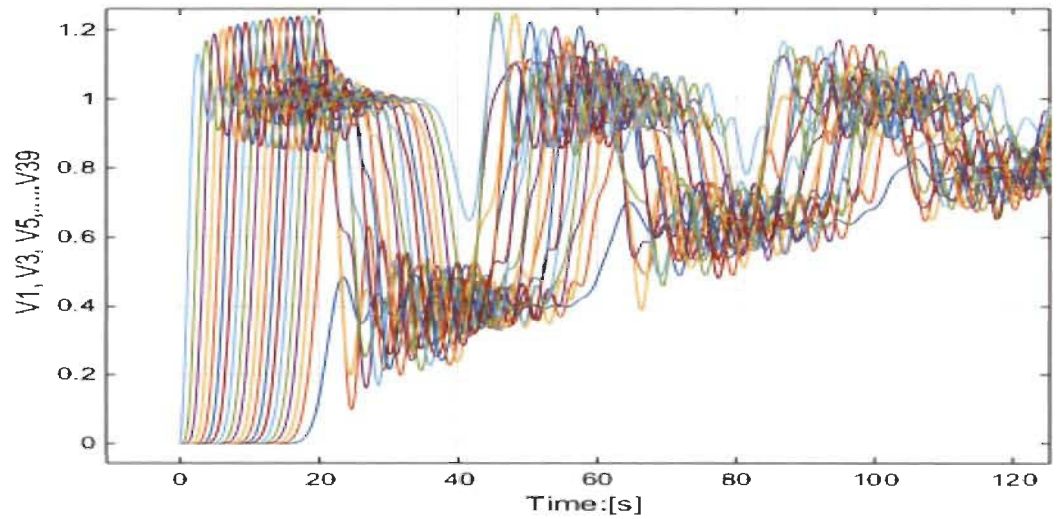


Figure 5. 24: Matlab-Simulink RC-FEC and FWF general model ($V_1^{(1,4)}, V_3^{(1,4)}, \dots, V_{39}^{(1,4)}$)

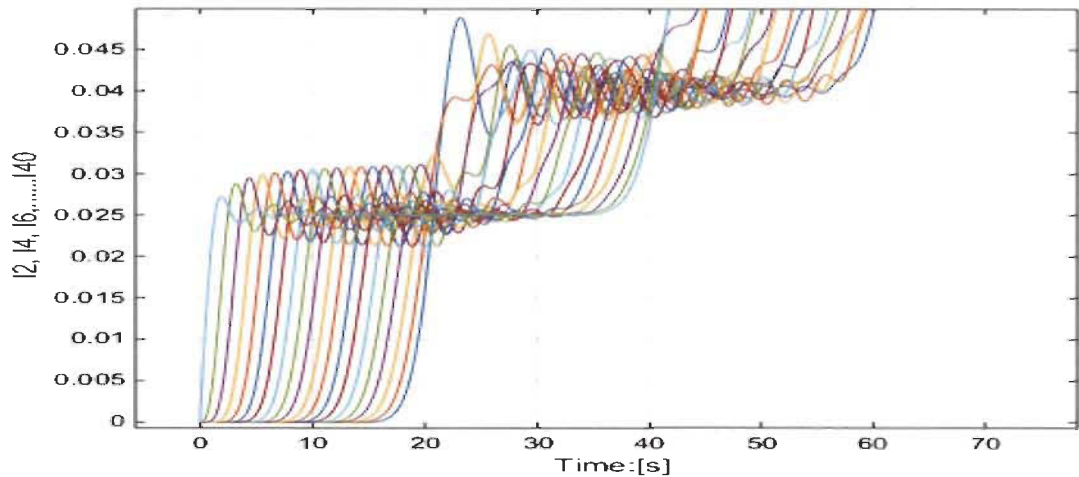


Figure 5. 25: Matlab-Simulink RC-FEC and FWF general model ($I_2^{(1,4)}, I_4^{(1,4)}, \dots, I_{40}^{(1,4)}$)

For the case where both RC-FEC and RL-FEC have the same time constant $x_c = x_L$; simulation was conducted to confirm the accuracy of the FWF general model proposed in figure 5.17 and 5.20 and Matlab-Simulink circuit model.

B. Case #1: $R=1\Omega$; $L=1H$; $C=1F$; $(K, x_c) = (1,1)$;

$$C = \frac{1}{R \cdot x_c} = 1F; \quad L = \frac{1}{K \cdot C} = 1H; \quad R = \sqrt{\frac{L}{C}} = 1$$

$$x_L = \frac{R}{L} = x_c = \frac{1}{R \cdot C} = 1 \quad (5.17)$$

$$K = \frac{1}{LC} = \omega_f^2 = x_L x_c = x_L^2 = x_c^2$$

Simulation in figure 5.26 and 5.27 for Matlab-Simulink RC-FEC and its FWF model for order 40 for $I_{40}^{(1,1)}$, $V_{11}^{(1,1)}$ with input voltage $V_i = 1V$ and load $R = \sqrt{\frac{L}{C}}$, shows no intermediate steady states and this due to the fact that

$$K = \frac{1}{LC} = \omega_f^2 = x_L x_c = x_L^2 = x_c^2$$

$$x_c = 2\xi_{cf}\omega_f = x_L = 2\xi_{Lf}\omega_f \quad \text{and} \quad \xi_{Lf} = \xi_{cf} = \frac{1}{2}$$

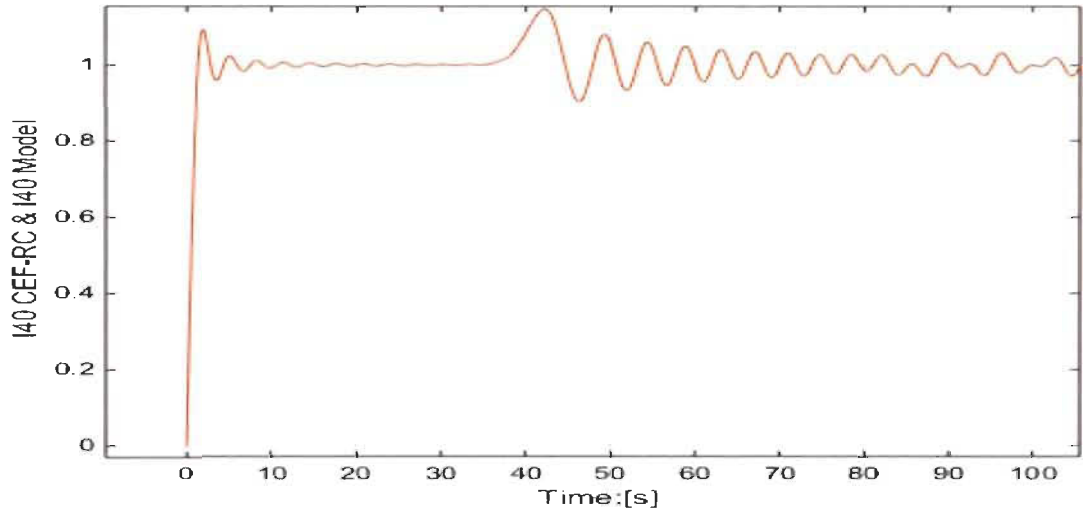


Figure 5. 26: Matlab-Simulink RC-FEC and FWF general model ($I_{40}^{(1,1)}$, $V_i = 1V$, $R = \sqrt{\frac{L}{C}}$)

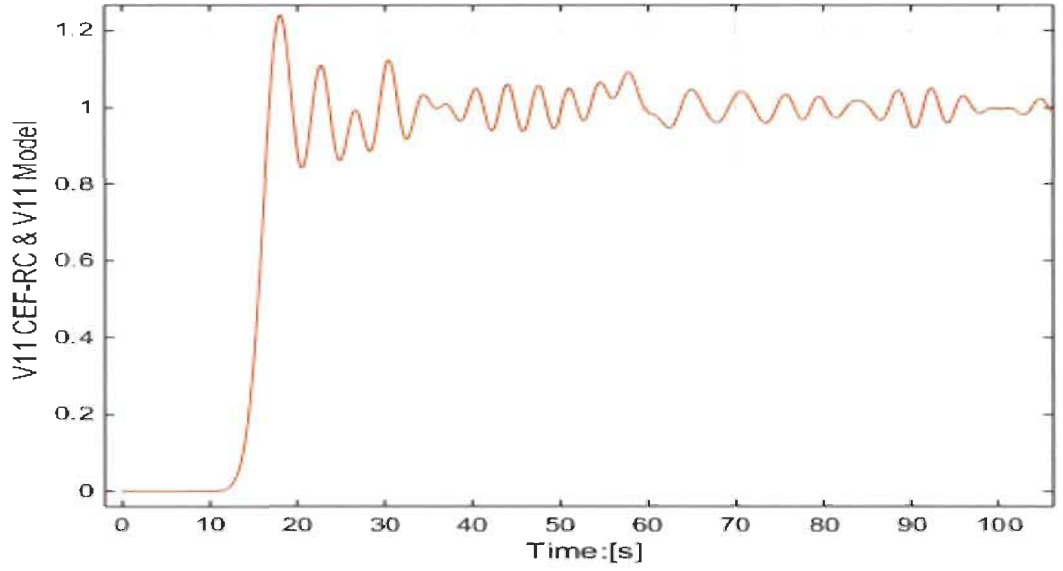


Figure 5. 27: Matlab-Simulink RC-FEC and FWF general model ($V_{11}^{(1,1)}$, $V_i = 1V$, $R = \sqrt{\frac{L}{C}}$)

The figures 5.28 and 5.29 show the behavior of all voltages in each capacitor (odd order) and all currents of each inductor (even order) using FWF general model of figure 5.17 and compared with Matlab-Simulink RC-FEC circuit (figure 5.16).

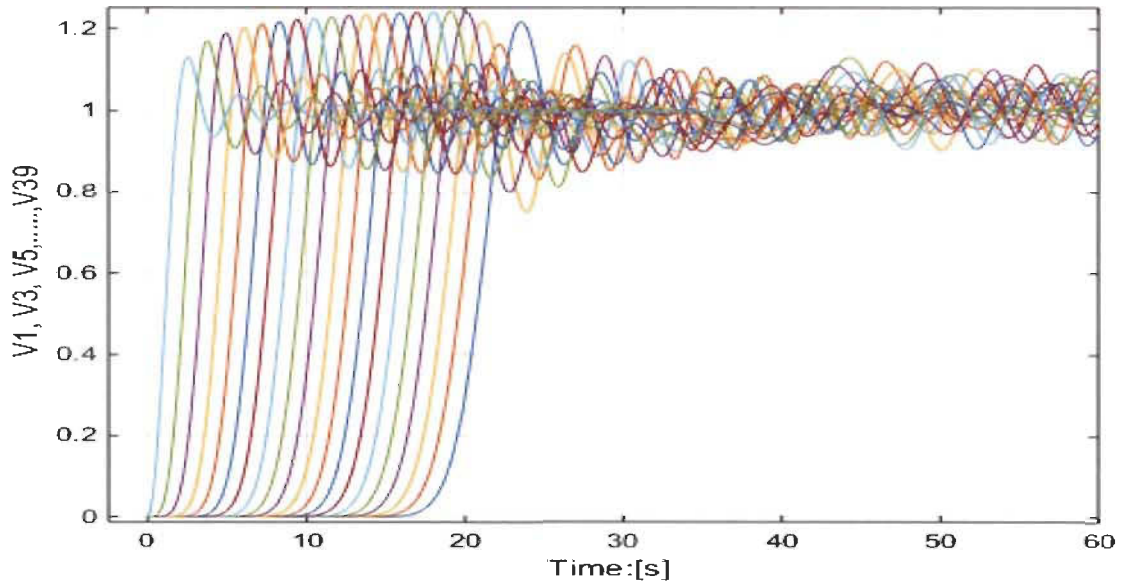


Figure 5. 28: Matlab-Simulink RC-FEC and FWF general model ($V_1^{(1,1)}$, $V_3^{(1,1)}$, ..., $V_{39}^{(1,1)}$, $R = \sqrt{\frac{L}{C}}$)

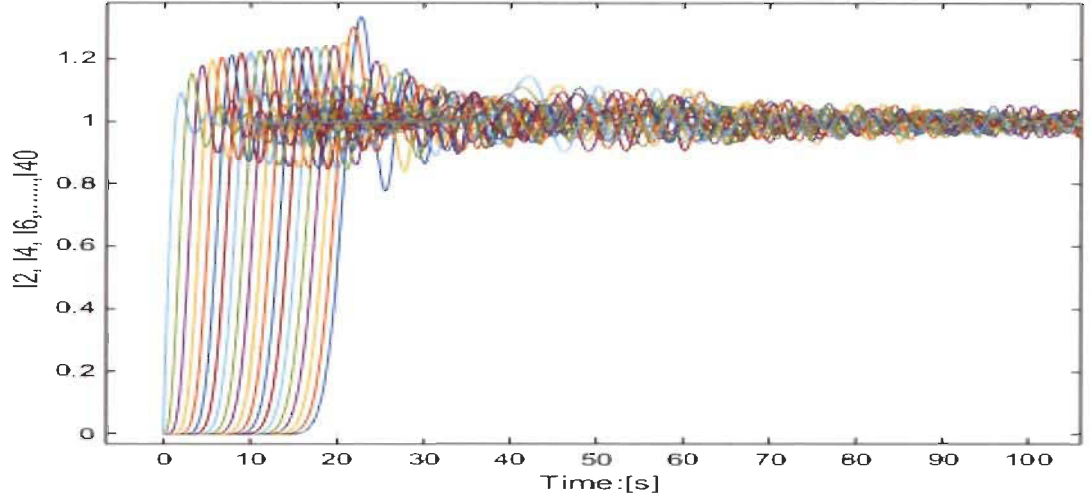


Figure 5.29: Matlab-Simulink RC-FEC and FWF general model $(I_2^{(1,1)}, I_4^{(1,1)}, \dots, I_{40}^{(1,1)}, R = \sqrt{\frac{L}{C}})$

RC-FEC and RL-FEC general model can be also derived based on the energy for each capacitor and inductor.

For RC-FEC energy general model for $n = 40$ is presented.

$$\begin{aligned}
 (e_c)_{2j+1}^{(K,x_c)} &= \frac{1}{2} C (V_{2j+1}^{(K,x_c)})^2 \\
 (e_L)_{2j}^{(K,x_c)} &= \frac{1}{2} L (I_{2j}^{(K,x_c)})^2 \\
 \frac{(e_L)_{2j}^{(K,x_c)}}{(e_c)_{2j+1}^{(K,x_c)}} &= \frac{(g_{2j}^{(K,x_c)}(s))^2}{\omega_f^2} \\
 \frac{(e_c)_{2j+1}^{(K,x_c)}}{(e_L)_{2j}^{(K,x_c)}} &= \frac{(g_{2j+1}^{(K,x_c)}(s))^2}{\omega_f^2}
 \end{aligned} \tag{5.18}$$

Below is the energy general model for RC-FEC $n = 40$ with input energy e_i^m .

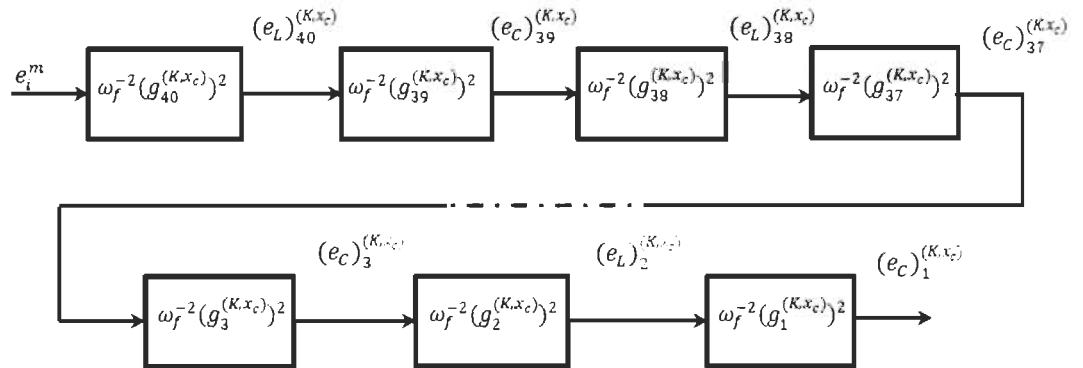


Figure 5.30: n^{th} even order RC-FEC general model using energy wave between branches.

5.7 Fibonacci wave functions applied to transmission lines

In the literature, several papers have studied and modeled the transmission cables [2] with a variety of analytical methods but very few have noticed that Fibonacci numbers and especially Pascal's triangle can be used [2], [3].

It is well known that transmission cables can be modeled with a recursive LC depending on the length of the cable. There have been studies to analyze the input impedance as well as the load impedance to better understand the reflection phenomena when the input impedance is different from the load. In [2], it was shown that in a transmission cable with a short-circuit ($R=0\Omega$), the input impedance or admittance can be found using Pascal's triangle for the case $L=1H$ and $C=1F$. This is a particular case of Pascal's triangle general form detailed in Table 5.2 with $K=1$ and $x_c = \infty$.

Table 4.6 is the Pascal triangle general form for boundary systems with the multiplication coefficients based only on parameter K .

Below is an example of $g_{14}(s)$ using Pascal's triangle for Fibonacci boundary systems

$$\begin{aligned}
 den_{14}^{(k,x)} &= 1s^{14} + 1xs^{13} + 13Ks^{12} + 12Kxs^{11} + 66K^2s^{10} + 55K^2xs^9 \\
 &\quad + 165K^3s^8 + 120K^3xs^7 + 210K^4s^6 + 126K^4xs^5 + 126K^5s^4 \\
 &\quad + 56K^5xs^3 + 28K^6s^2 + 7K^6xs + 1K^7 \\
 den_{13}^{(k,x)} &= 1s^{13} + 1xs^{12} + 12Ks^{11} + 11Kxs^{10} + 55K^2s^9 + 45K^2xs^8 \\
 &\quad + 120K^3s^7 + 84K^3xs^6 + 126K^4s^5 + 70K^4xs^4 + 56K^5s^3 \\
 &\quad + 21K^5xs^2 + 7K^6s + 1K^6x \\
 den_{12}^{(k,x)} &= 1s^{12} + 1xs^{11} + 11Ks^{10} + 10Kxs^9 + 45K^2s^8 + 36K^2xs^7 \\
 &\quad + 84K^3s^6 + 56K^3xs^5 + 70K^4s^4 + 35K^4xs^3 + 21K^5s^2 \\
 &\quad + 6K^5xs + 1K^6
 \end{aligned} \tag{5.19}$$

For RL-FEC circuit in figure 5.19 for order 13 and 14

$$\begin{aligned}
\left(\frac{I_o}{CV_i}\right)_{13}^{(K,x_L)} &= g_{13}^{(K,x_L)}(s) = \frac{K \text{den}_{12}^{(K,x_L)}(s)}{\text{den}_{13}^{(K,x_L)}(s)} \\
\left(\frac{V_o}{LI_i}\right)_{14}^{(K,x_L)} &= g_{14}^{(K,x_L)}(s) = \frac{K \text{den}_{13}^{(K,x_L)}(s)}{\text{den}_{14}^{(K,x_L)}(s)} \\
x &= x_L = \frac{R}{L}
\end{aligned} \tag{5.20}$$

For RC-FEC circuit in figure 5.16 for order 13 and 14.

$$\begin{aligned}
\left(\frac{I_o}{CV_i}\right)_{14}^{(K,x_c)} &= g_{14}^{(K,x_c)}(s) = \frac{K \text{den}_{13}^{(K,x_L)}(s)}{\text{den}_{14}^{(K,x_c)}(s)} \\
\left(\frac{V_o}{LI_i}\right)_{13}^{(K,x_L)} &= g_{13}^{(K,x_c)}(s) = \frac{K \text{den}_{12}^{(K,x_c)}(s)}{\text{den}_{13}^{(K,x_c)}(s)} \\
x &= x_c = \frac{1}{RC}
\end{aligned} \tag{5.21}$$

Note that depending on the Fibonacci circuit, either RC-FEC or RL-FEC, one can easily determine the input impedance or input admittance for any order n and for both short-circuit and open-circuit using only general Pascal's triangle table 4.6 or (5.19), (5.20) and (5.21).

For the purpose of comparison with [2] for a short-circuit case ($R = 0\Omega$), $x_c = \infty$ using RC-FEC and $x_L = 0$ using RL-FEC, equations (5.19), (5.20) and (5.21) become:

$$\begin{aligned}
\left(\frac{V_o}{LI_i}\right)_{14L}^{(k,0)} &= g_{14L}^{(K,0)}(s) = K * \frac{1s^{13} + 12Ks^{11} + 55K^2s^9 + 120K^3s^7 + 126K^4s^5 + 56K^5s^3 + 7K^6s}{1s^{14} + 13Ks^{12} + 66K^2s^{10} + 165K^3s^8 + 210K^4s^6 + 126K^5s^4 + 28K^6s^2 + 1K^7} \\
\left(\frac{I_o}{CV_i}\right)_{13L}^{(k,0)} &= g_{13L}^{(K,0)}(s) = K * \frac{1s^{12} + 11Ks^{10} + 45K^2s^8 + 84K^3s^6 + 70K^4s^4 + 21K^5s^2 + 1K^6}{1s^{13} + 12Ks^{11} + 55K^2s^9 + 120K^3s^7 + 126K^4s^5 + 56K^5s^3 + 7K^6s} \\
\left(\frac{I_o}{CV_i}\right)_{14c}^{(K,\infty)} &= g_{14c}^{(K,\infty)}(s) = K * \frac{1s^{12} + 11Ks^{10} + 45K^2s^8 + 84K^3s^6 + 70K^4s^4 + 21K^5s^2 + 1K^6}{1s^{13} + 12Ks^{11} + 55K^2s^9 + 120K^3s^7 + 126K^4s^5 + 56K^5s^3 + 7K^6s} \\
\left(\frac{V_o}{LI_i}\right)_{13c}^{(K,\infty)} &= g_{13c}^{(K,\infty)}(s) = K * \frac{1s^{11} + 10Ks^9 + 36K^2s^7 + 56K^3s^5 + 35K^4s^3 + 6K^5s^1}{1s^{12} + 11Ks^{10} + 45K^2s^8 + 84K^3s^6 + 70K^4s^4 + 21K^5s^2 + 1K^6}
\end{aligned} \tag{5.22}$$

For an open-circuit ($R = \infty \Omega$), $x_c = 0$ using RC-FEC and for RL-FEC $x_L = \infty$. Equations (5.19), (5.20) and (5.21) become:

$$\begin{aligned}
 \left(\frac{I_o}{CV_i}\right)_{14c}^{(K,0)} &= g_{14c}^{(K,0)}(s) = K * \frac{1s^{13} + 12Ks^{11} + 55K^2s^9 + 120K^3s^7 + 126K^4s^5 + 56K^5s^3 + 7K^6s}{1s^{14} + 13Ks^{12} + 66K^2s^{10} + 165K^3s^8 + 210K^4s^6 + 126K^5s^4 + 28K^6s^2 + 1K^7} \\
 \left(\frac{V_o}{LI_i}\right)_{13c}^{(K,0)} &= g_{13c}^{(K,0)}(s) = K * \frac{1s^{12} + 11Ks^{10} + 45K^2s^8 + 84K^3s^6 + 70K^4s^4 + 21K^5s^2 + 1K^6}{1s^{13} + 12Ks^{11} + 55K^2s^9 + 120K^3s^7 + 126K^4s^5 + 56K^5s^3 + 7K^6s} \quad (5.23) \\
 \left(\frac{V_o}{LI_i}\right)_{14L}^{(k,\infty)} &= g_{14L}^{(K,\infty)}(s) = K * \frac{1s^{12} + 11Ks^{10} + 45K^2s^8 + 84K^3s^6 + 70K^4s^4 + 21K^5s^2 + 1K^6}{1s^{13} + 12Ks^{11} + 55K^2s^9 + 120K^3s^7 + 126K^4s^5 + 56K^5s^3 + 7K^6s} \\
 \left(\frac{I_o}{CV_i}\right)_{13L}^{(k,\infty)} &= g_{13L}^{(K,\infty)}(s) = K * \frac{1s^{11} + 10Ks^9 + 36K^2s^7 + 56K^3s^5 + 35K^4s^3 + 6K^5s^1}{1s^{12} + 11Ks^{10} + 45K^2s^8 + 84K^3s^6 + 70K^4s^4 + 21K^5s^2 + 1K^6}
 \end{aligned}$$

Simulation for short and open circuit were conducted using FWF general model and Matlab-Simulink RC-FEC and RL-FEC for $n = 40$. $V_{40}^{(1,x_L=0)}$, $I_{21}^{(1,x_L=0)}$, $I_{40}^{(1,x_c=0)}$, $V_{21}^{(1,x_c=0)}$ are shown in figure 5.31, 5.32, 5.33 and 5.34.

With open-circuit ($R = \infty \Omega$) or short-circuit ($R = 0 \Omega$) RL-FEC and RC-FEC, their respective FWF general model show continuous oscillations for constant unit and for pulse unit input and are exactly identical with Matlab-Simulink circuit model. These behaviors can be used in reflection wave analysis related to transmission lines with load in matching impedance, and with short load or without load.

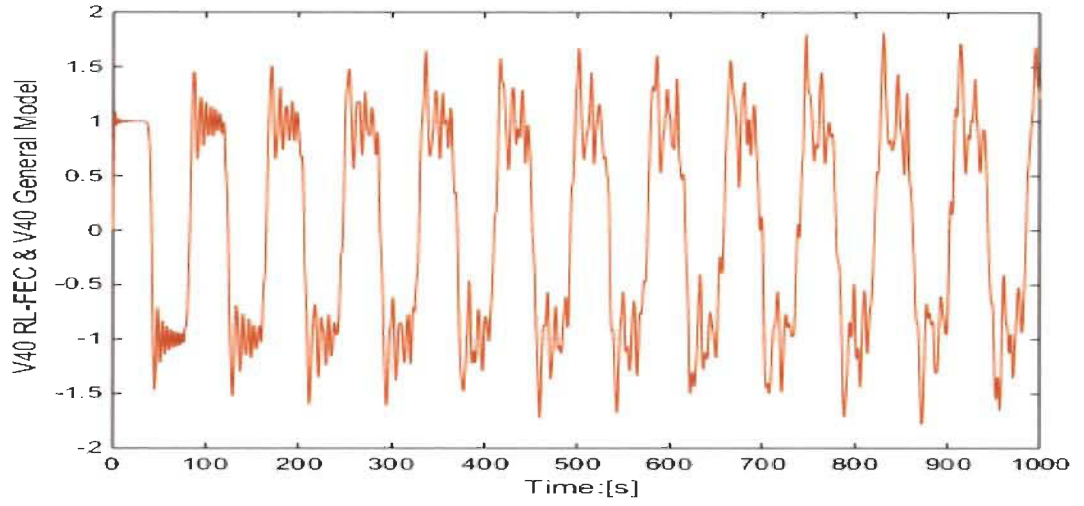


Figure 5. 31: Matlab-Simulink RL-FEC and FWF general model ($V_{40}^{(1,0)}$, $I_i = 1A$, $R = 0\Omega$)

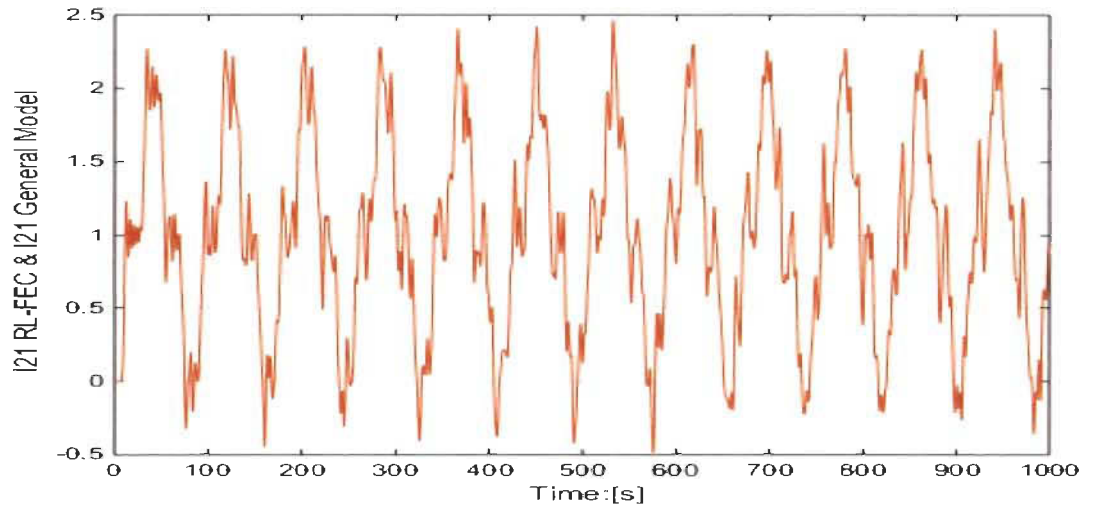


Figure 5. 32: Matlab-Simulink RL-FEC and FWF general model ($I_{21}^{(1,0)}$, $I_i = 1A$, $R = 0\Omega$)

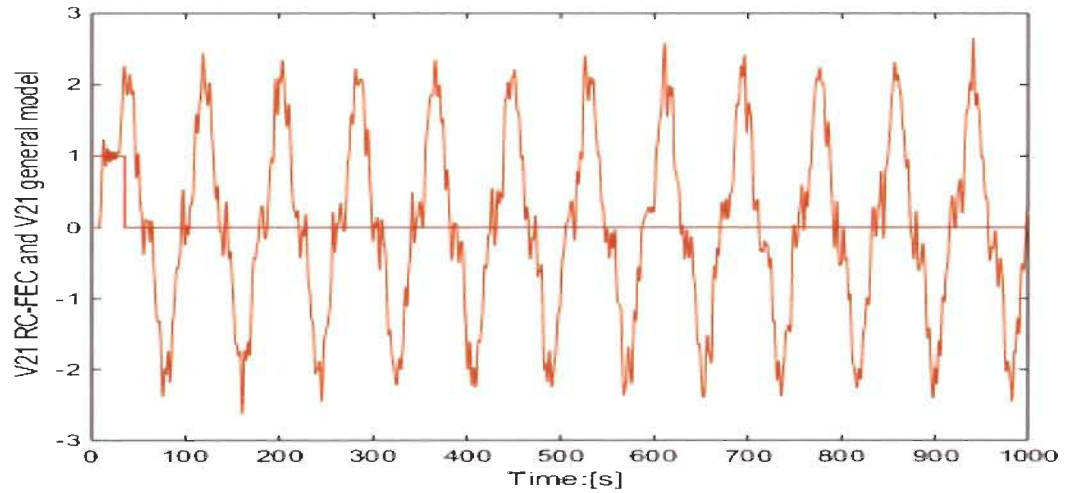


Figure 5. 33: Matlab-Simulink RC-FEC and FWF general model ($V_{21}^{(1,0)}$, $V_i = 1V$ 35s pulse, $R = \infty\Omega$)

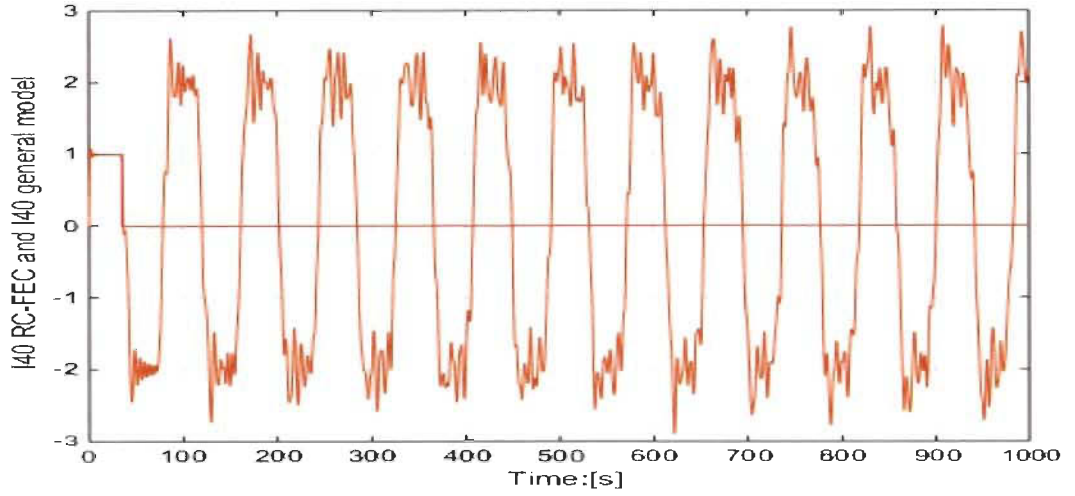


Figure 5. 34: Matlab-Simulink RC-FEC and FWF general model ($I_{40}^{(1,0)}$, $V_i = 1V$ 35s pulse, $R = \infty\Omega$)

5.8 Conclusion

In this chapter, a complete LC ladder general model is highlighted as an application of Fibonacci wave functions FWFs that was introduced in chapter 4. The importance for LC ladder comes from its application that can be found in the literature like lossless transmission lines model, the sound propagation model in the ear and in quantum mechanics in the understanding of the interaction between particles. The detailed model that is proposed for each LC ladder branch with precise Fibonacci wave functions shows that the FWF general model and its corresponding Matlab-Simulink circuit_model are perfectly identical for each inductor current and capacitor voltage with load, without load ($R = 0\Omega$) or with infinite load ($R = \infty\Omega$). The FWF general model using the charge in the capacitor and the flux in the inductor for each branch is also presented for all charge and flux LC ladder branches.

The LC ladder input impedance and admittance can be derived using Pascal's triangle general form presented in section VII with defined coefficients K , x_L and x_C .

Transmission lines, short-circuit and open-circuit were studied and simulated for both Fibonacci model and Fibonacci electrical circuit to show that these are particular cases of the

general model and their Fibonacci wave functions are easy to determine based on Pascal's triangle for short load ($x_c = \infty$ and $x_L = 0$) and for open load ($x_L = \infty$ and $x_c = 0$).

The LC ladder general model for energy transfer between L and C in each section could be used for many other applications that use lossless LC recursive circuit as model for more research and analysis especially, in quantum mechanics, biology and communication.

Chapter 6: Fibonacci wave functions application to spring mass chain

6.1 Introduction

In chapter 4, we introduced Fibonacci wave functions (FWFs). These functions have the particularity of being irreducible, presenting multiple intermediate stationary regimes before reaching the final steady-state. These steady states present oscillations with low amplitudes. These FWFs have been created theoretically from a first-order transfer function source.

In this chapter, the Fibonacci spring-mass chain (FSMC) is introduced as another application is presented. It has exactly the same FWFs than those mentioned in chapter 3 as mathematical model. The Fibonacci spring-mass chain (FSMCs) can be used to model the interaction of small particles in quantum mechanics and in fluid mechanics using this new FSMC general model. This chapter will be divided into three major parts. Part one, will be dedicated to FSMC theory. Part two will be dedicated to two case studies with one and two final steady states. Finally, the last part will treat the FSMC general model and its simulation to highlight the interaction between each mass based on its position in the chain.

6.2 Fibonacci Spring mass chain

Let's recall that Fibonacci wave function source has the following form.

$$g_1^{(k,x_m)}(s) = \frac{K}{s + x_m} \quad (6.1)$$

$$K = \omega_f^2 \quad \text{and} \quad x_m = 2 \xi_{mf} \omega_f$$

The first order spring-mass is shown in figure 6.1:

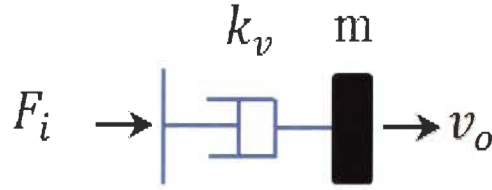


Figure 6. 1: First order of FSMC

$$\begin{aligned} \frac{v_o}{F_i} &= \frac{1}{ms + k_v} = \frac{1}{k_s} \frac{\frac{k_s}{m}}{s + \frac{k_v}{m}} = \frac{1}{k_s} \frac{K}{s + x_m} = \frac{1}{k_s} g_1^{(k, x_m)}(s) \\ \left(\frac{k_s v_o}{F_i}\right)_1^{(k, x_m)} &= \frac{K}{s + x_m} = g_1^{(k, x_m)}(s) \\ K &= \frac{k_s}{m} = \omega_f^2 \quad \text{and} \quad x_m = 2 \xi_{mf} \omega_f = \frac{k_v}{m} \end{aligned} \quad (6.2)$$

Where ω_f is the Fibonacci natural frequency.

ξ_{mf} is the Fibonacci damping ratio.

The transfer function of the second order FSMC shown below will be.

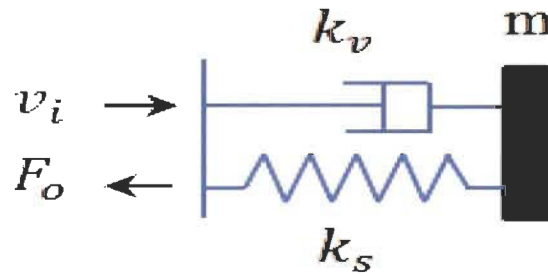


Figure 6. 2: Second order of FSMC

$$\begin{aligned} v_i &= \left(\frac{1}{k_s} g_1^{(k, x_m)}(s) + \frac{s}{k_s} \right) F_o = \frac{m \left(s + g_1^{(k, x_m)}(s) \right) F_o}{k_s m} \\ \left(\frac{F_o}{m v_i}\right)_2^{(k, x_m)} &= \frac{K}{s + \frac{K}{s + x_m}} = g_2^{(k, x_m)}(s) \end{aligned} \quad (6.3)$$

This transfer function is exactly that of Fibonacci determined in chapter 4. The transfer function of third order FSMC is

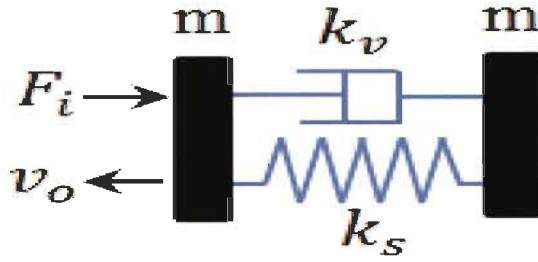


Figure 6. 3: Third order of FSMC

$$F_i = \left(m g_2^{(k, x_m)}(s) + ms \right) v_o = \frac{k_s m \left(s + g_2^{(k, x_m)}(s) \right) v_o}{k_s}$$

$$\left(\frac{k_s v_o}{F_i} \right)_3^{(k, x_m)} = \frac{K}{s + \frac{K}{s + \frac{K}{s + x_m}}} = g_3^{(k, x_m)}(s) \quad (6.4)$$

The 4th order for FSMC transfer function.

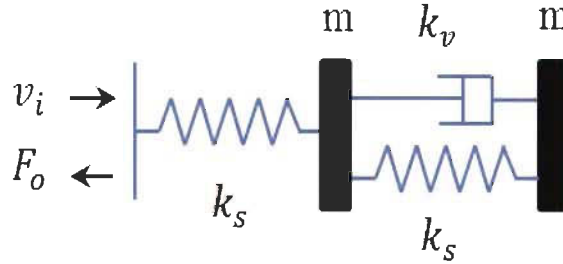


Figure 6. 4: Forth order of FSMC

$$v_i = \left(\frac{1}{k_s} g_3^{(k, x_m)}(s) + \frac{s}{k_s} \right) F_o = \frac{m \left(s + g_3^{(k, x_m)}(s) \right) F_o}{k_s m}$$

$$\left(\frac{F_o}{m v_i} \right)_4^{(k, x_m)} = \frac{K}{s + \frac{K}{s + \frac{K}{s + \frac{K}{s + x_m}}}} = g_4^{(k, x_m)}(s)$$

The 5th order for the FSMC transfer function.

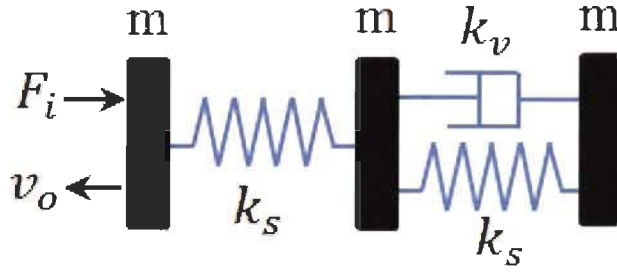


Figure 6. 5: Fifth order of FSMC

$$F_i = \left(m g_4^{(k, x_m)}(s) + m s \right) v_o = \frac{k_s m \left(s + g_4^{(k, x_m)}(s) \right) v_o}{k_s}$$

$$\left(\frac{k_s v_o}{F_i} \right)_5^{(k, x_m)} = \frac{K}{s + \frac{K}{s + \frac{K}{s + \frac{K}{s + \frac{K}{s + x_m}}}}} = g_5^{(k, x_m)}(s)$$

One can see that an n^{th} order F-Spring-Mass with n even will have speed as input and force as output.

$$n = n_s + n_m$$

n_s is the total number of springs in the chain.

n_m is the total number of masses in the chain.

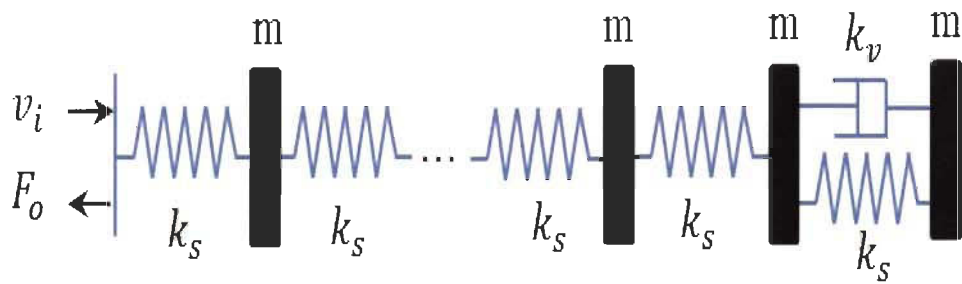


Figure 6. 6: n^{th} even order of FSMC

The FWF will be.

$$\left(\frac{F_o}{mv_i}\right)_n^{(k,x_m)} = \frac{K}{s + g_{(n-1)}(s)} = g_n^{(k,x_m)}(s) \quad (6.5)$$

In the case where the circuit is of odd order n , the transfer function will be.

$$\left(\frac{k_s v_o}{F_i}\right)_n^{(k,x_m)} = \frac{K}{s + g_{(n-1)}(s)} = g_n^{(k,x_m)}(s) \quad (6.6)$$

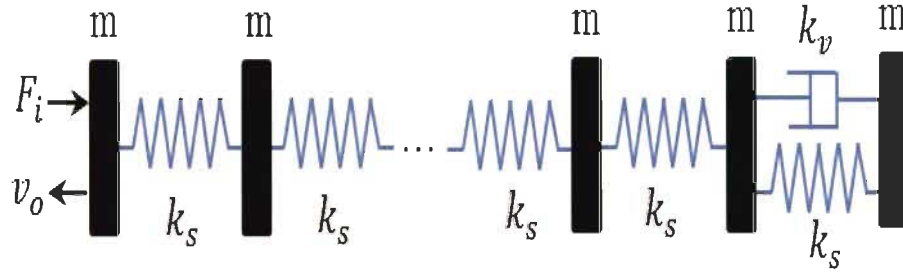


Figure 6. 7: n^{th} odd order of FSMC

In general, F-Spring-Mass chain with even order n has speed as input and force as output; it has a final steady-state value $m * x_m$ of unit input speed.

For F-Spring- Mass chain with n odd order with force as input and speed as output has a final steady-state value $\frac{K}{k_s x_m}$.

The table below shows all FSMC FWFs.

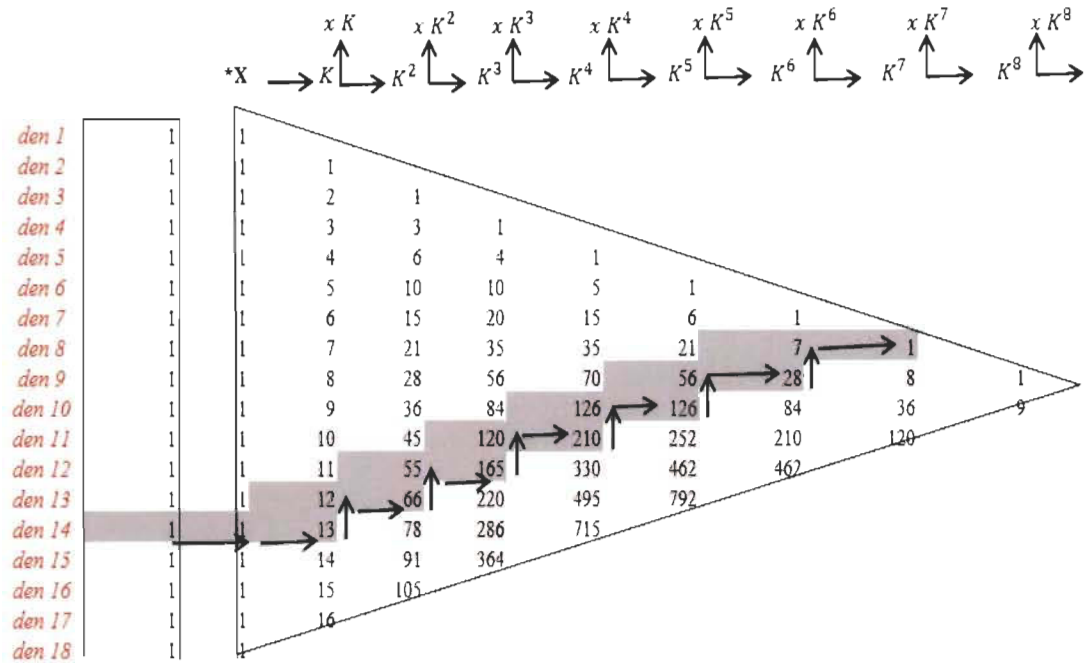
Table 6. 1: F-Spring-Mass Chain Fibonacci wave functions FWFs

$\left(\frac{k_s v_o}{F_i}\right)_1^{(k,x_m)} = g_1^{(k,x_m)}(s) = \frac{K}{s + x_c}$	$\left(\frac{k_s v_o}{F_i}\right)_1^{(k,x_m)} = g_1^{(k,x_m)}(s) = \frac{K}{1s + 1x_m}$
$\left(\frac{F_o}{mv_i}\right)_2^{(k,x_m)} = g_2^{(k,x_m)}(s) = \frac{K}{s + \frac{K}{s + x_m}}$	$\left(\frac{F_o}{mv_i}\right)_2^{(k,x_m)} = \frac{Ks + Kx_m}{1s^2 + 1x_ms + 1K}$

$\left(\frac{k_s v_o}{F_i}\right)_3^{(k, x_m)} = g_3^{(k, x_m)}(s) = \frac{K}{s + \frac{K}{s + \frac{K}{s + x_m}}}$	$\begin{aligned} \left(\frac{k_s v_o}{F_i}\right)_3^{(k, x_m)} &= g_3^{(k, x_m)}(s) \\ &= \frac{Ks^2 + Ksx_m + K^2}{1s^3 + 1x_ms^2 + 2Ks + 1Kx_m} \end{aligned}$
$\left(\frac{F_o}{mv_i}\right)_4^{(k, x_m)} = g_4^{(k, x_m)}(s) = \frac{K}{s + \frac{K}{s + \frac{K}{s + \frac{K}{s + x_m}}}}$	$\begin{aligned} \left(\frac{F_o}{mv_i}\right)_4^{(k, x_m)} &= g_4^{(k, x_m)}(s) \\ &= \frac{Ks^3 + Kx_ms^2 + 2K^2s + K^2x_m}{1s^4 + 1x_ms^3 + 3Ks^2 + 2Kx_ms + 1K^2} \end{aligned}$
$\left(\frac{F_o}{mv_i}\right)_n^{(k, x_m)} = g_n^{(k, x_m)}(s) = \frac{K}{s + g_{n-1}^{(k, x_m)}(s)}$ <i>n even</i> $\left(\frac{k_s v_o}{F_i}\right)_n^{(k, x_m)} = g_n^{(k, x_m)}(s) = \frac{K}{s + g_{n-1}^{(k, x_m)}(s)}$ <i>n odd</i>	$g_n^{(k, x_m)}(s) = \frac{Kden_{n-1}^{(k, x_m)}(s)}{sden_{n-1}^{(k, x_m)}(s) + num_{n-1}^{(k, x_m)}(s)}$ $g_n^{(k, x_m)}(s) = \frac{Kden_{n-1}^{(k, x_m)}(s)}{den_n^{(k, x_m)}(s)}$

From table 6.1, Pascal triangle general form in table 6.2 is used to determine each Fibonacci wave function for any FSMC order.

Table 6. 2: Pascal's triangle general form with coefficients of multiplication (k, x_m).



Below is an example of $g_{14}^{(k,x_m)}(s)$ and $g_{13}^{(k,x_m)}(s)$ using Pascal's triangle Table 2.

$$\begin{aligned}
den_{14}^{(k,x_m)}(s) &= 1s^{14} + 1x_ms^{13} + 13Ks^{12} + 12Kx_ms^{11} + 66K^2s^{10} + 55K^2x_ms^9 \\
&\quad + 165K^3s^8 + 120K^3x_ms^7 + 210K^4s^6 + 126K^4x_ms^5 + 126K^5s^4 \\
&\quad + 56K^5x_ms^3 + 28K^6s^2 + 7K^6x_ms + 1K^7 \\
den_{13}^{(k,x_m)}(s) &= 1s^{13} + 1x_ms^{12} + 12Ks^{11} + 11Kx_ms^{10} + 55K^2s^9 + 45K^2x_ms^8 \\
&\quad + 120K^3s^7 + 84K^3x_ms^6 + 126K^4s^5 + 70K^4x_ms^4 + 56K^5s^3 \\
&\quad + 21K^5x_ms^2 + 7K^6s + 1K^6x_m \\
den_{12}^{(k,x_m)}(s) &= 1s^{12} + 1x_ms^{11} + 11Ks^{10} + 10Kx_ms^9 + 45K^2s^8 + 36K^2x_ms^7 \\
&\quad + 84K^3s^6 + 56K^3x_ms^5 + 70K^4s^4 + 35K^4x_ms^3 + 21K^5s^2 \\
&\quad + 6K^5x_ms + 1K^6
\end{aligned} \tag{6.7}$$

$$\left(\frac{F_o}{mv_i}\right)_{14}^{(k,x_m)} = g_{14}^{(k,x_m)}(s) = K \frac{den_{13}^{(k,x_m)}(s)}{den_{14}^{(k,x_m)}(s)}$$

$$\left(\frac{k_s v_o}{F_i}\right)_{13}^{(k,x_m)} = g_{13}^{(k,x_m)}(s) = K \frac{den_{12}^{(k,x_m)}(s)}{den_{13}^{(k,x_m)}(s)}$$

$$x_m = \frac{k_v}{m} = 2 \xi_f \omega_f$$

6.3 Simulation of FMSC

Simulations were conducted for all Fibonacci wave function up to order 40 for FSMC to confirm that these coupled spring mass chain follow the logic of a recursive Fibonacci sequence detailed in chapter 4.

A. Case #1: $k_v = 1Ns/m$; $m = 1kg$; $k_s = 1N/m$; $(K, x_m) = (1,1)$;

In this case we can easily calculate the parameters K and x_m or ω_f and ξ_{mf} to determine the Fibonacci wave functions from the table using Pascal's Triangle.

$$x_m = 1; \quad K = 1.$$

$$\omega_f = 1; \quad \xi_{mf} = 0.5$$

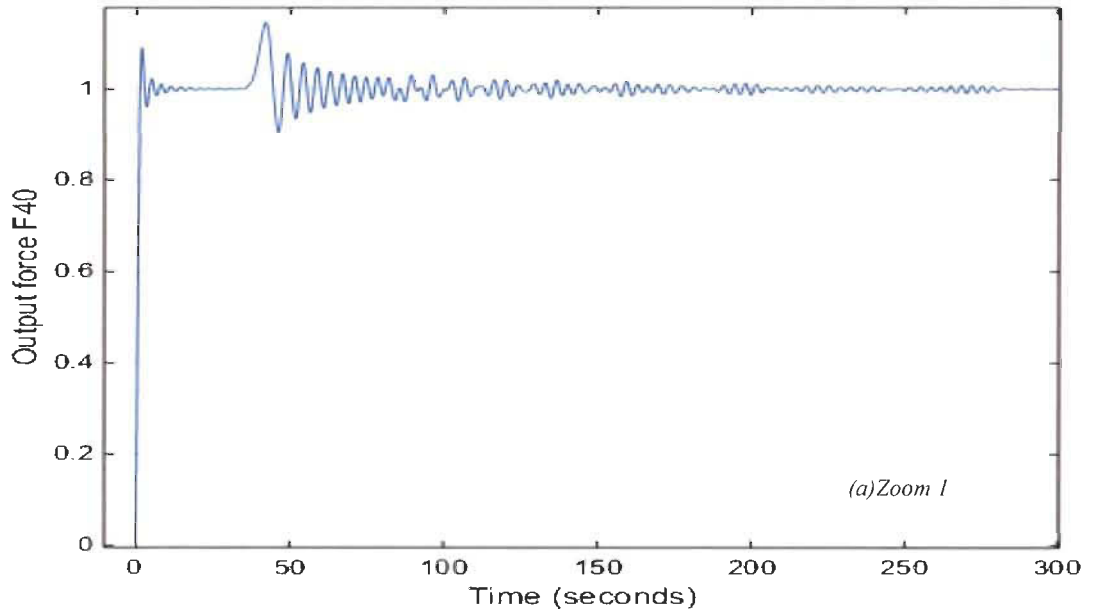
Order 40 FWF taken as example is an even function, using Pascal's triangle to determine its numerator and denominator coefficients as detailed in chapter 4 gives.

$$\left(\frac{F_o}{mv_i}\right)_{40}^{(k,x_m)} = g_{40}^{(k,x_m)}(s) = \frac{K}{s + g_{39}^{(k,x_m)}(s)}$$

$$\left(\frac{F_o}{mv_i}\right)_{40}^{(k,x_m)} = g_{40}^{(k,x_m)}(s) = \frac{Kden_{39}^{(k,x_m)}(s)}{sden_{39}^{(k,x_m)}(s) + num_{39}^{(k,x_m)}(s)}$$

$$\left(\frac{F_o}{mv_i}\right)_{40}^{(k,x_m)} = g_{40}^{(k,x_m)}(s) = \frac{Kden_{39}^{(k,x_m)}(s)}{den_{40}^{(k,x_m)}(s)}$$

Simulations of $m * g_{40}^{(k,x_m)}(s)$ model is illustrated in figure 6.8 below. The final steady-state is $m * x_m = 1$.



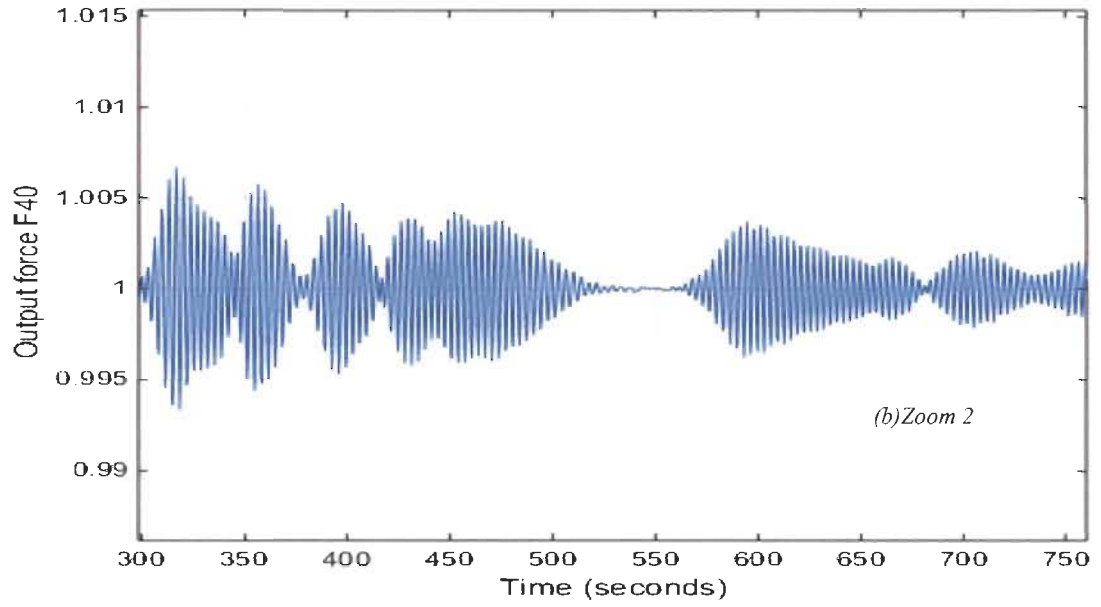


Figure 6. 8: FMSC ($F_{40}^{(1,1)} = m * g_{40}^{(1,1)}(s)$, $v_i = 1m/s$)

In the same way the FWF $g_{39}^{(k,x_m)}(s)$ which is odd, is determined using Pascal's triangle.

$$\left(\frac{k_s v_o}{F_i}\right)_{39}^{(k,x_m)} = g_{39}^{(k,x_m)}(s) = \frac{K}{s + g_{38}^{(k,x_m)}(s)}$$

$$\left(\frac{k_s v_o}{F_i}\right)_{39}^{(k,x_m)} = g_{39}^{(k,x_m)}(s) = \frac{K den_{38}^{(k,x_m)}(s)}{s den_{38}^{(k,x_m)}(s) + num_{38}^{(k,x_m)}(s)}$$

$$\left(\frac{k_s v_o}{F_i}\right)_{39}^{(k,x_m)} = g_{39}^{(k,x_m)}(s) = \frac{K den_{38}^{(k,x_m)}(s)}{den_{39}^{(k,x_m)}(s)}$$

Simulations of order 39 FSMC $\left(\frac{v_o}{F_i}\right)_{39}^{(k,x_m)} = \frac{1}{k_s} * g_{39}^{(k,x_m)}(s)$ is illustrated in figure 6.9. It is

clear that the final steady-state is $\frac{K}{k_s * x_m} = 1$.

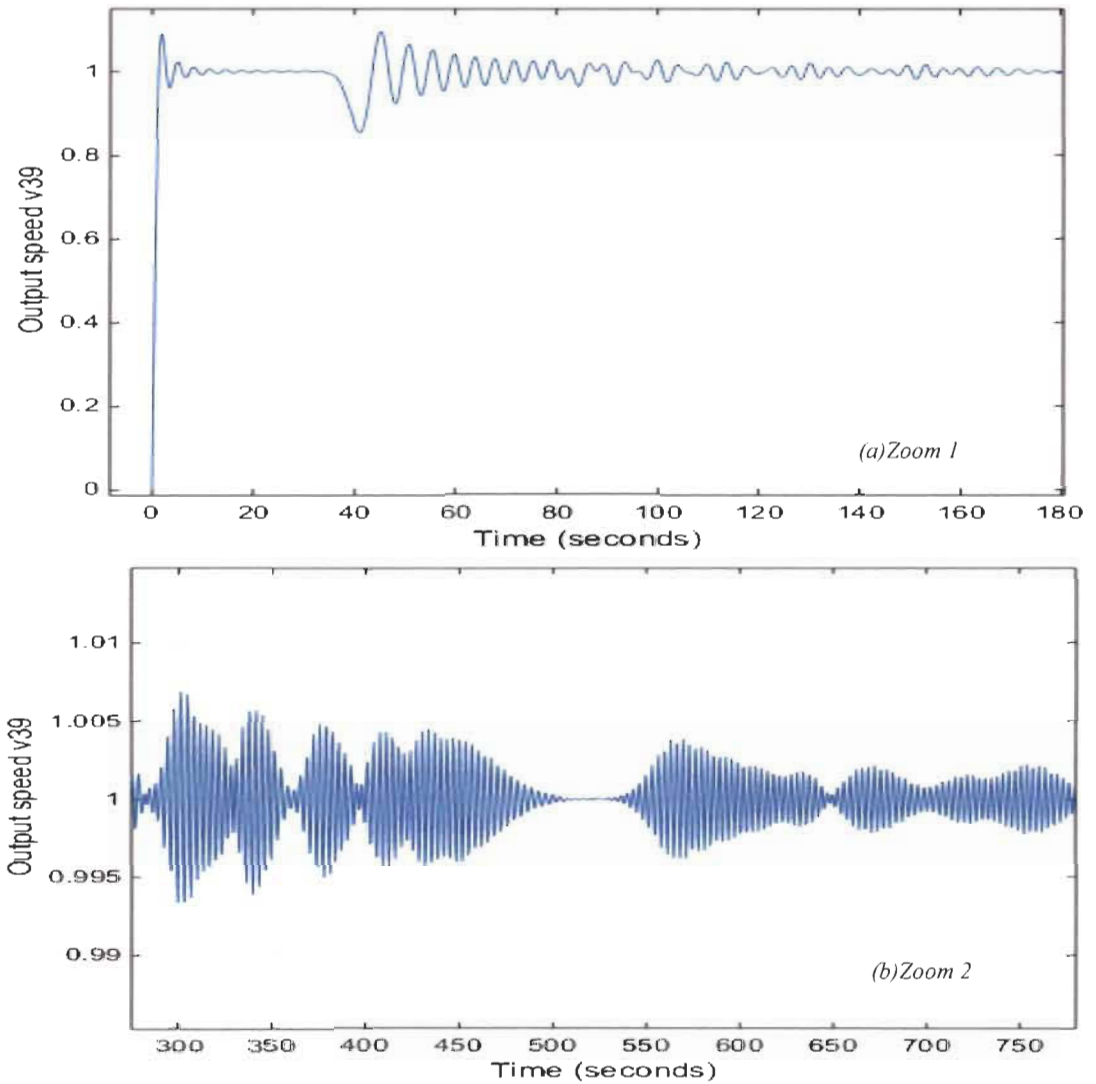


Figure 6. 9: FSMC ($v_{39}^{(1,1)} = \frac{1}{k_s} * g_{39}^{(1,1)}(s)$, $F_i = 1N$)

6.4 N^{th} Order Fibonacci spring mass chain general model

The N^{th} order F-Mass-Spring is perfectly modeled. All forces and speeds are perfectly determined by the Fibonacci wave functions illustrated in section 1. The model is illustrated in the figure 6.10 for order 40 and can be extended to an infinite Spring-Mass chain knowing that each FWF can be determined using Pascal's triangle general form in table 2.

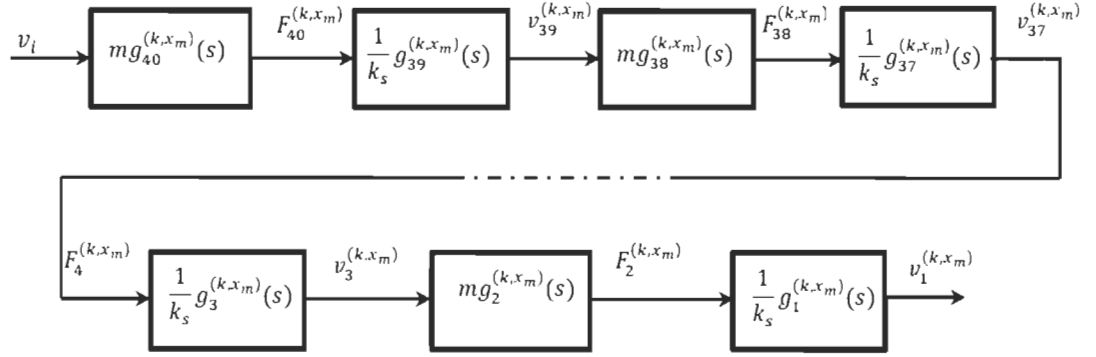


Figure 6. 10: n^{th} even order FSMC Model using FWFs for each section for $(v_j^{(k,x_m)}, F_j^{(k,x_m)})$ variables

This model can be presented with the variable momentum $\mu_j^{(k,x_m)} = m v_j^{(k,x_m)}$ for each mass

and position $x_j^{(k,x_m)} = \frac{F_j^{(k,x_m)}}{k_s}$ related to each spring as shown in figure 6.11.

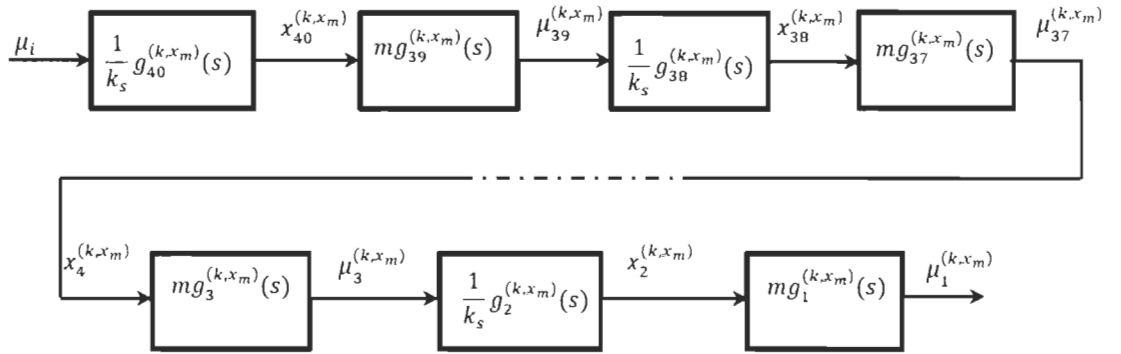


Figure 6. 11: n^{th} even order FSMC Model using FWFs for each section for $(\mu_j^{(k,x_m)}, x_j^{(k,x_m)})$

A. Case #2: $k_v=4 \text{ Ns/m}$; $k_s=1 \text{ N/m}$; $m=1 \text{ Kg}$; $(K, x_m) = (1, 4)$;

$$K = \frac{k_s}{m} = \omega_f^2 = 1; \quad x_m = \frac{k_v}{m} = 4; \quad k_v \neq \sqrt{m k_s} \quad (6.8)$$

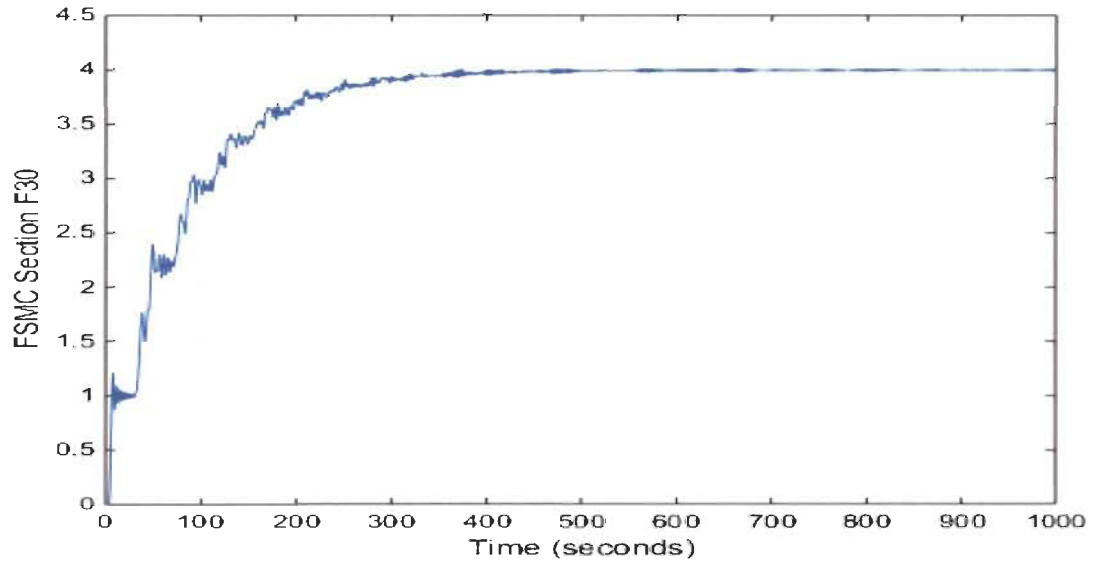


Figure 6. 12: FSMC general model for $F_{30}^{(1,4)}$ with input $v_i = 1m/s$

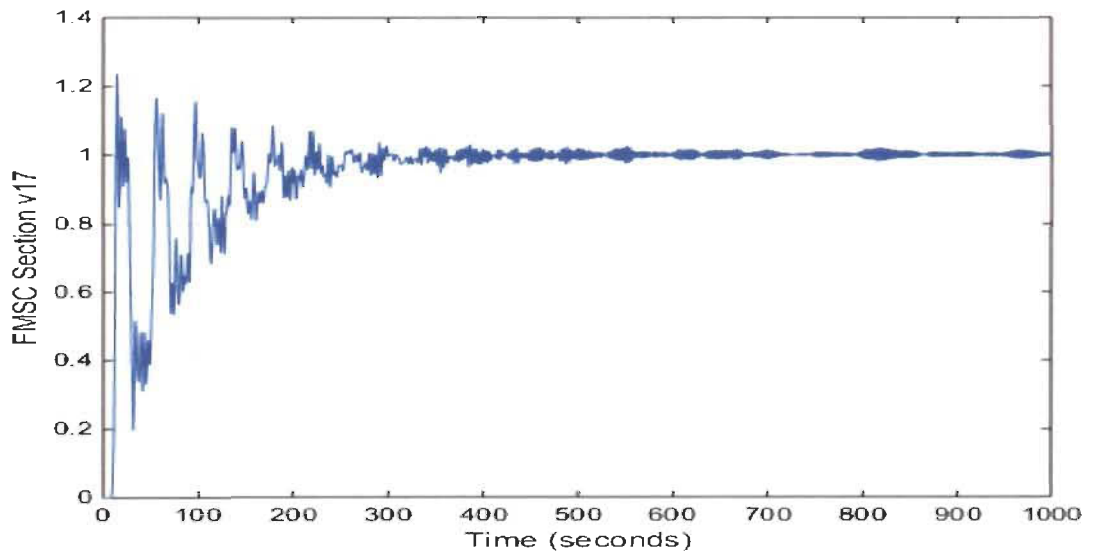


Figure 6. 13: FSMC general model for $v_{17}^{(1,4)}$ with input $v_i = 1m/s$

The figures 6.14 and 6.15 show the behavior of all speeds for each mass (odd FWFs) and all forces for each spring (even FWFs). Simulation shows also the delay of each branch based on its position from the input source.

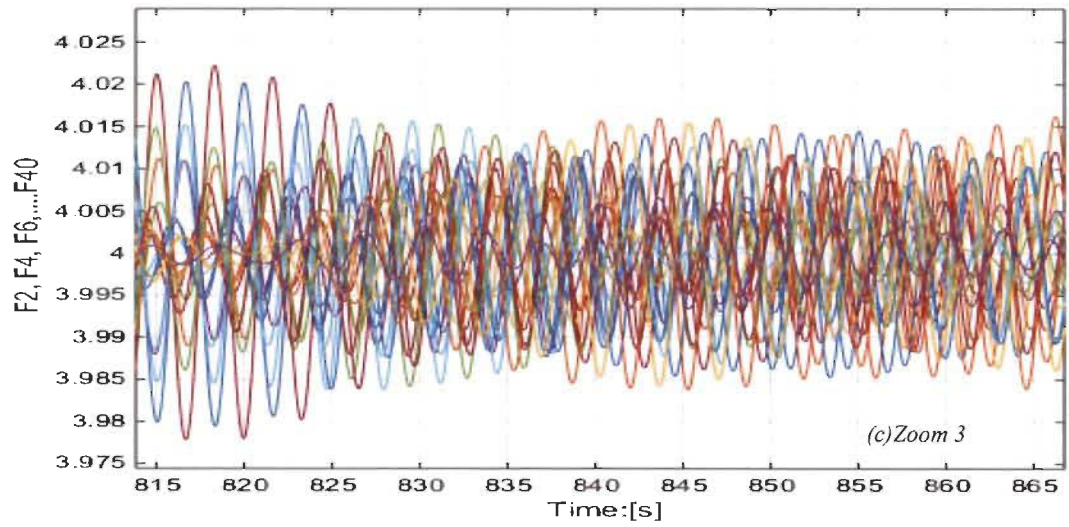
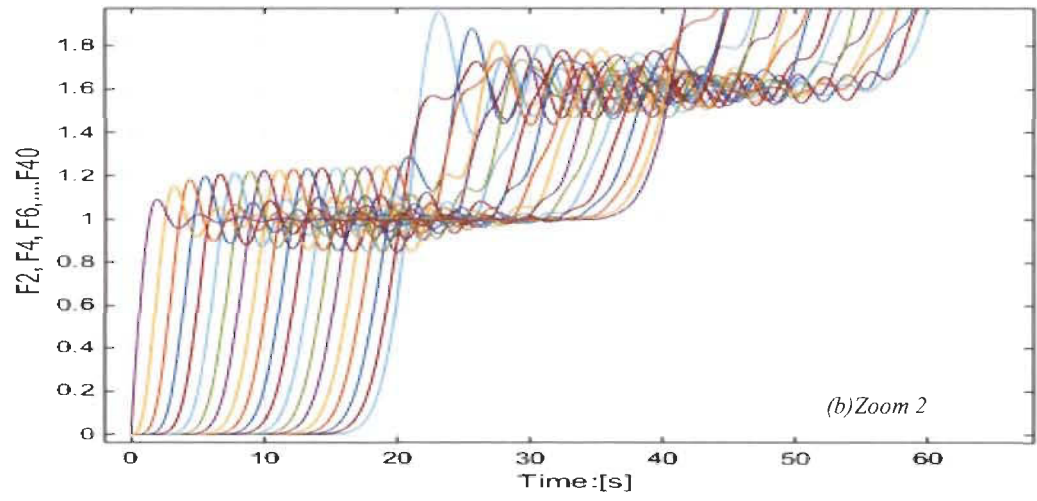
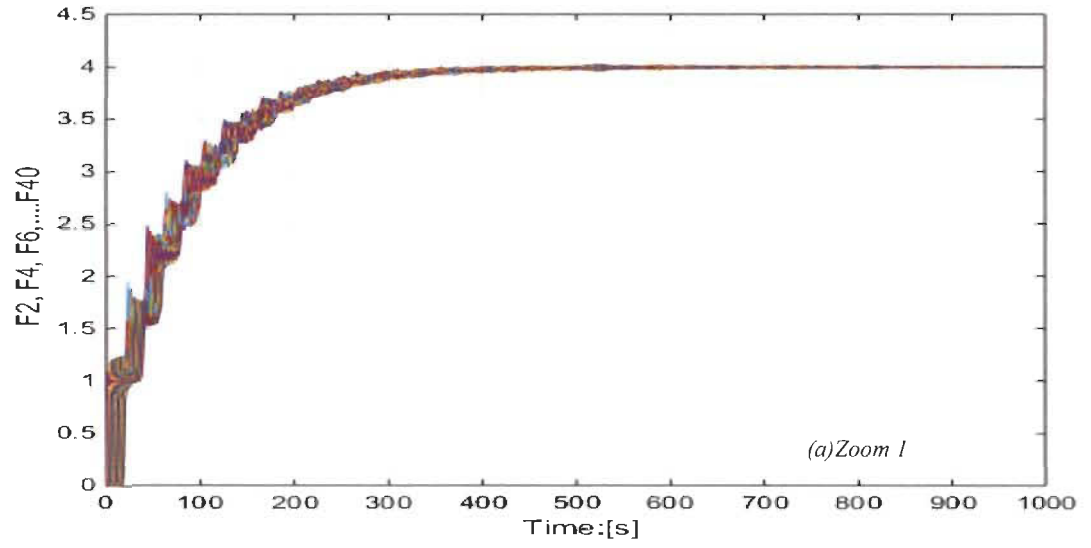


Figure 6. 14: FSMC general model for $(F_2^{(1,4)}, F_4^{(1,4)}, \dots, F_{40}^{(1,4)})$ with $v_i = 1\text{m/s}$

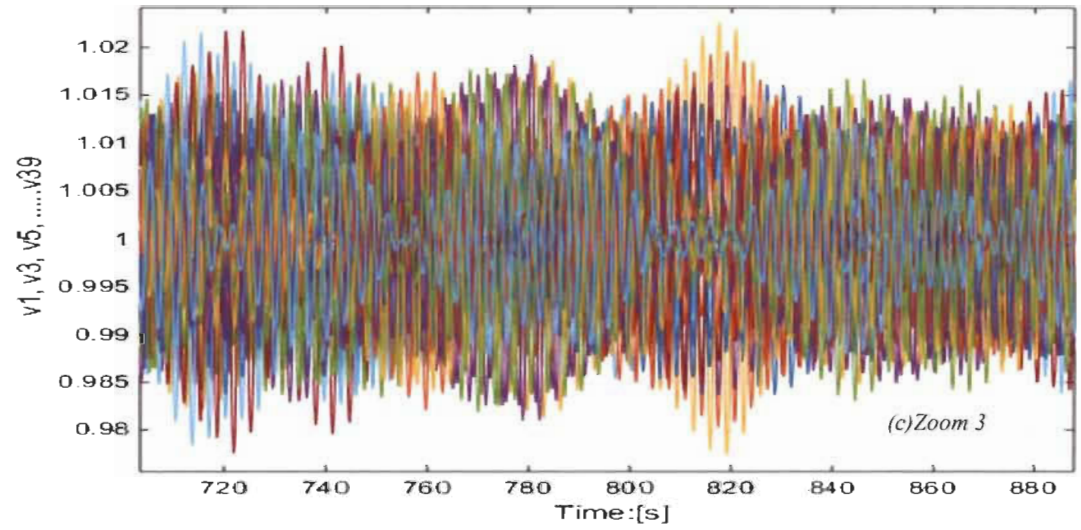
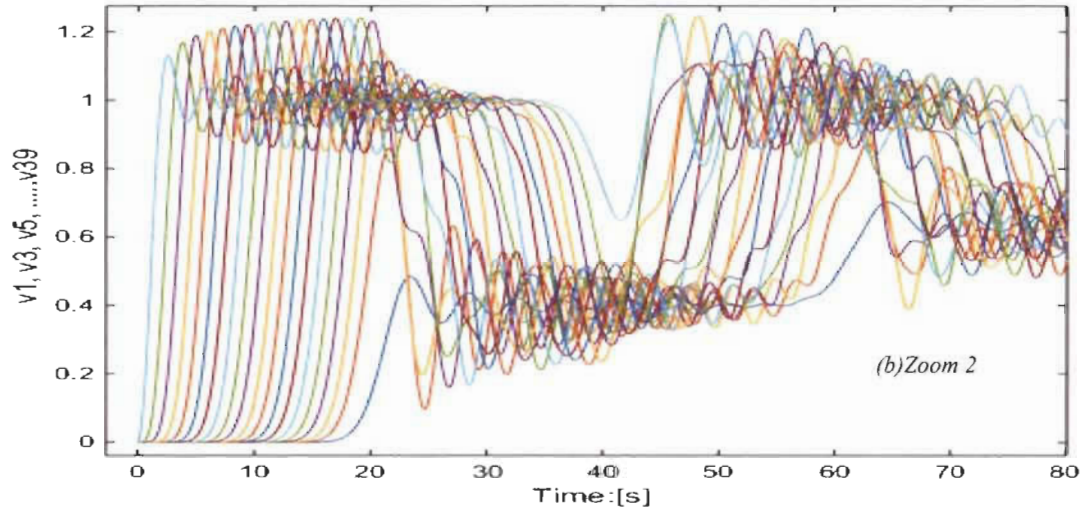
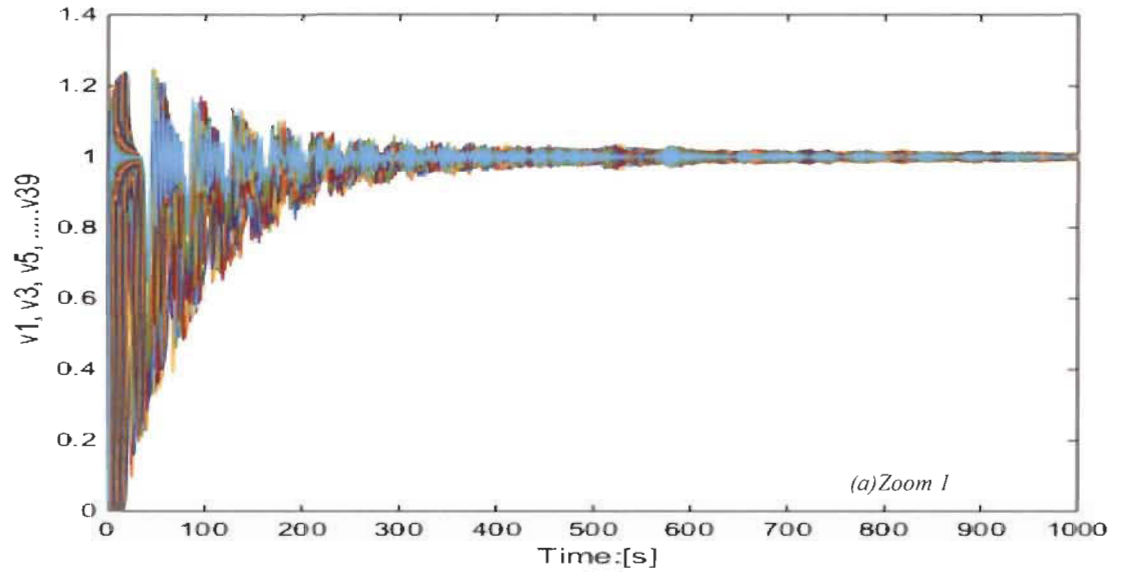


Figure 6. 15: FSMC general model for $(v_1^{(1,4)}, v_3^{(1,4)}, \dots, v_{39}^{(1,4)})$ for $v_i = 1m/s$

B. Case #1: $k_v=1 \text{ Ns/m}$; $k_s=1 \text{ N/m}$; $m=1 \text{ Kg}$; $(K, x_m) = (1,1)$;

$$K = \frac{k_s}{m} = \omega_f^2 = x_m^2; \quad x_m = \frac{k_v}{m} = 1; \quad k_v = \sqrt{mk_s} = 1$$

The simulation in figure 16 and 17 below for the FSMC model for order 40 shows no intermediate steady states and this is due to the fact that

$$K = \frac{k_s}{m} = \omega_f^2 = x_m^2; \quad x_m = 2\xi_f\omega_f; \quad \xi_f = \frac{1}{2}$$

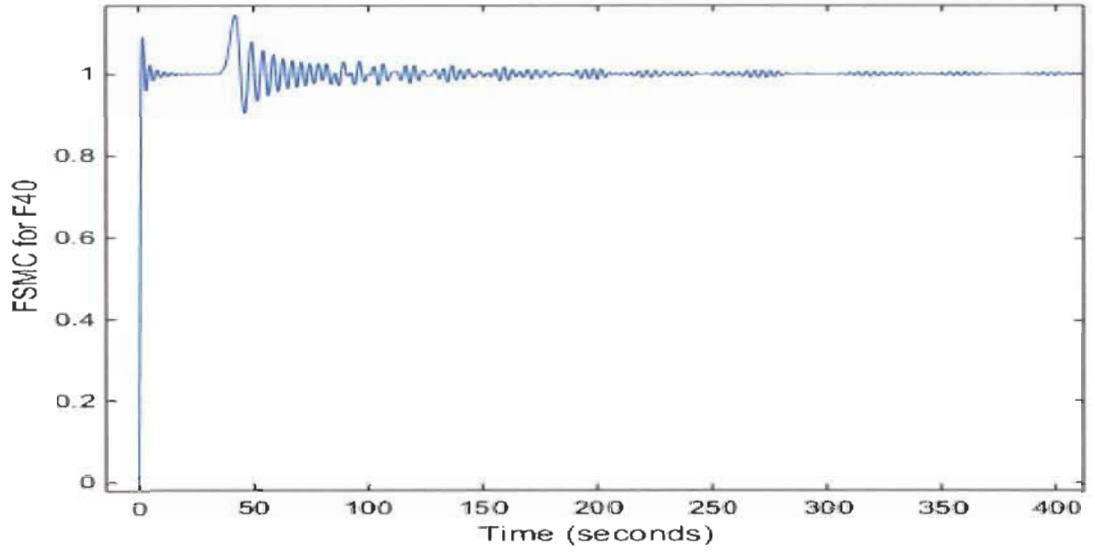


Figure 6. 16: FSMC general model for $F_{40}^{(1,1)}$ with input $v_i = 1, k_v = \sqrt{mk_s}$)

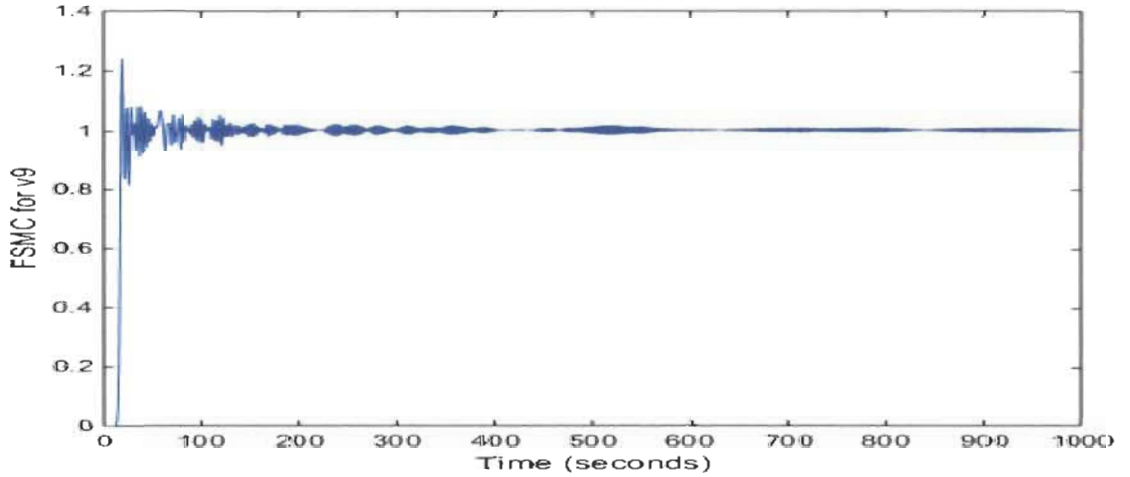


Figure 6. 17: FSMC general model for $v_9^{(1,1)}$ with input $v_i = 1, k_v = \sqrt{mk_s}$)

The figures 6.18 and 6.19 show the behavior of all speeds for each mass (odd order) and all forces for each spring (even order) using general model of figure 6.10.

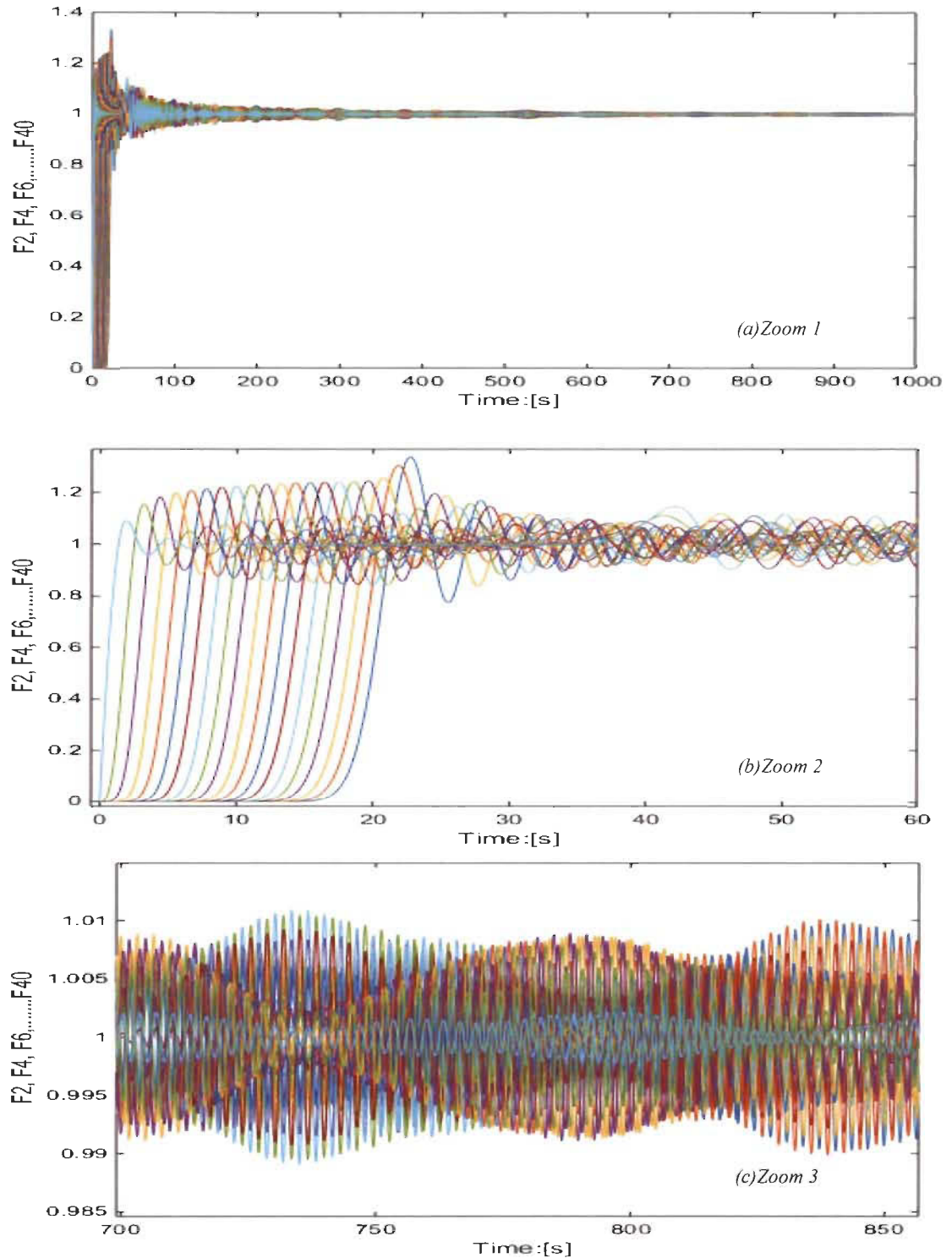


Figure 6. 18: FSMC general model for $F_2^{(1,1)}, F_4^{(1,1)}, \dots, F_{40}^{(1,1)}$ with input $v_i = 1, k_v = \sqrt{mk_s}$

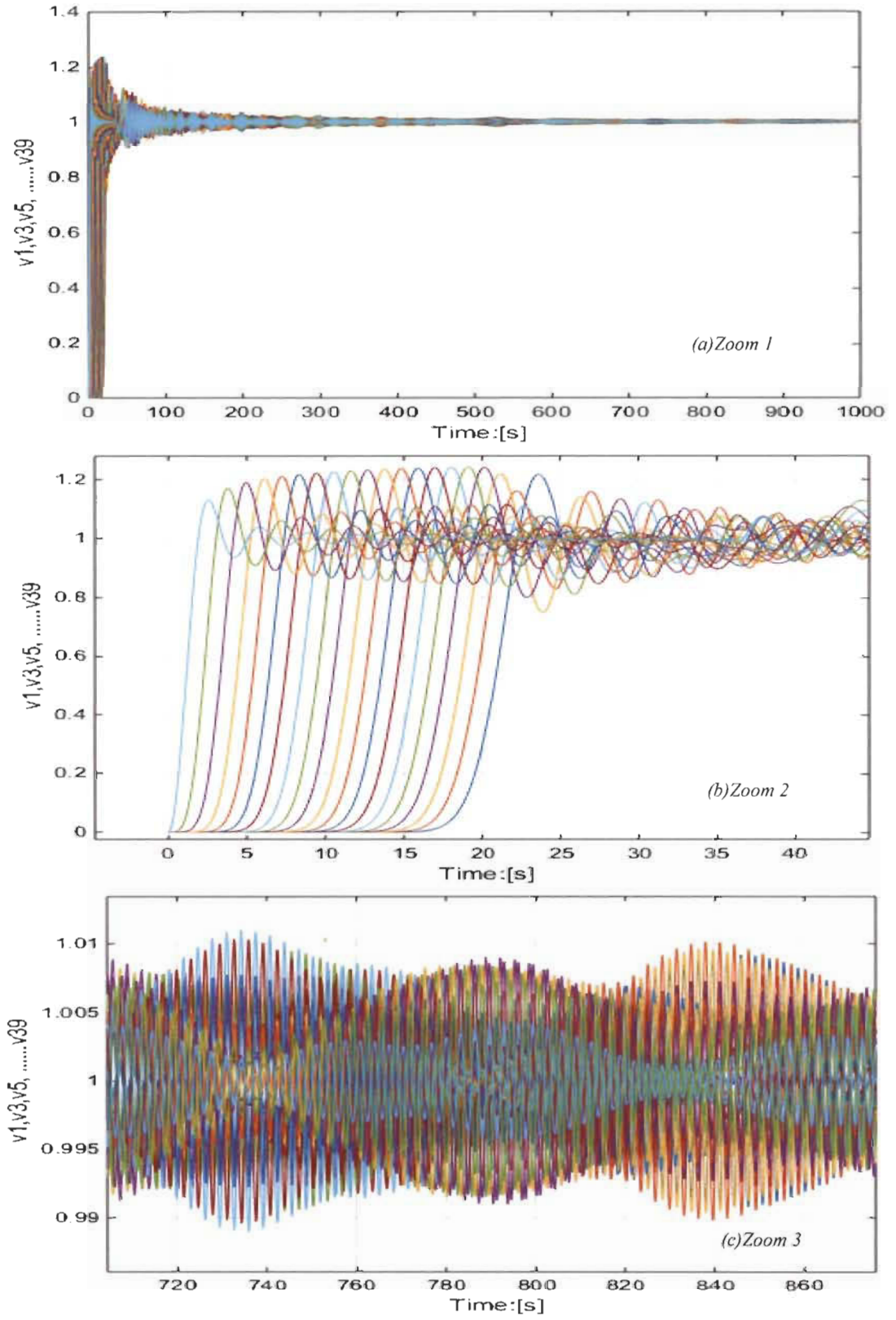


Figure 6. 19: FSMC general model ($v_1^{(1,1)}, v_3^{(1,1)}, \dots, v_{39}^{(1,1)}, k_v = \sqrt{mk_s}$)

FSMC general model can be also determined based on the energy for each capacitor and inductor. For FSMC energy general model for order 40 is presented.

$$\begin{aligned}
 (e_m)_{2j+1}^{(k,x_m)} &= \frac{1}{2} m (v_{2j+1}^{(k,x_m)})^2 \\
 (e_s)_{2j}^{(k,x_m)} &= \frac{1}{2k_s} (F_{2j}^{(k,x_m)})^2 \\
 \frac{(e_s)_{2j}^{(k,x_m)}}{(e_m)_{2j+1}^{(k,x_m)}} &= \frac{(g_{2j}^{(k,x_m)}(s))^2}{\omega_f^2} \\
 \frac{(e_m)_{2j+1}^{(k,x_m)}}{(e_s)_{2j}^{(k,x_m)}} &= \frac{(g_{2j+1}^{(k,x_m)}(s))^2}{\omega_f^2}
 \end{aligned} \tag{6.9}$$

Below is the energy general model for FSMC order 40 with input energy $(e)_i^{(k,x_m)}$

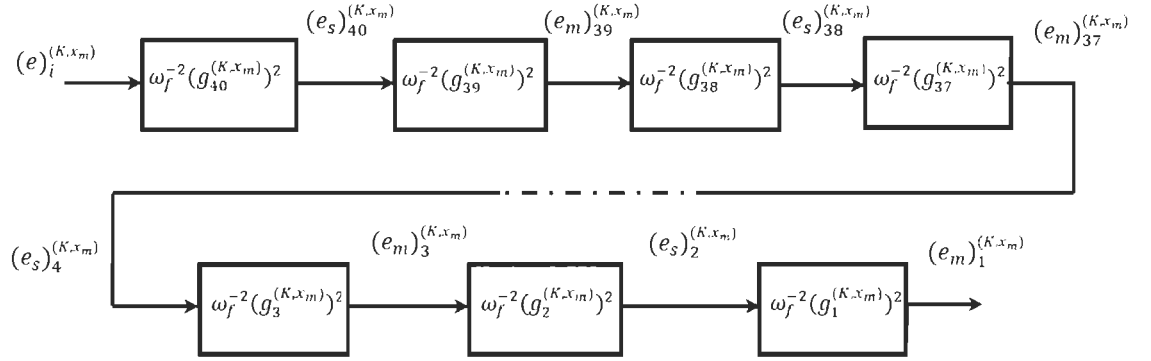


Figure 6. 20: n^{th} even F-Spring-Mass Model using FWFs for energy transfer between sections.

6.5 FSMC with infinite and zero k_v viscous damper

Note that based on FSMC in figure 6.6, one can easily determine the transfer function for any order n for infinite or zero k_v viscous damper using only Pascal's triangle general form with $x_m = 0$ or $x_m = \infty$ shown in Table 6.3.

For $x_m = \infty$; $k_v = \infty$. Viscous damper infinite resistance, Sections 14 and 13 in FSMC,

with $(g)_{14}^{(k,\infty)}(s)$, $(g)_{13}^{(k,\infty)}(s)$ are determined in (6.10).

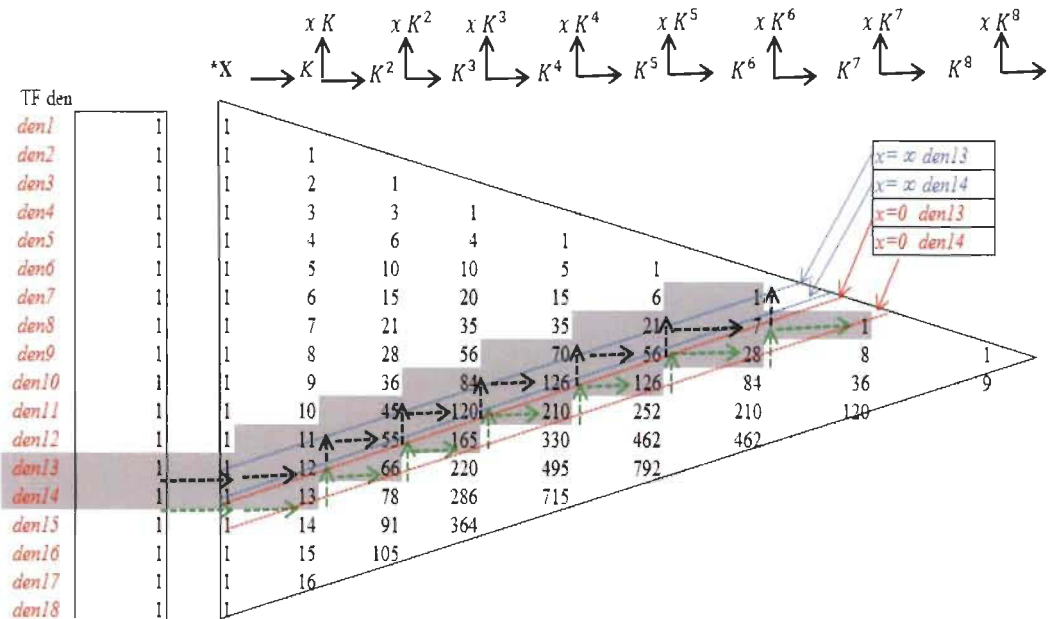
$$\begin{aligned}
\left(\frac{F_o}{mv_i}\right)_{14}^{(k,\infty)} &= (g)_{14}^{(k,\infty)}(s) = K * \frac{1s^{12} + 11Ks^{10} + 45K^2s^8 + 84K^3s^6 + 70K^4s^4 + 21K^5s^2 + 1K^6}{1s^{13} + 12Ks^{11} + 55K^2s^9 + 120K^3s^7 + 126K^4s^5 + 56K^5s^3 + 7K^6s} \\
\left(\frac{k_s v_o}{F_i}\right)_{13}^{(k,\infty)} &= (g)_{13}^{(k,\infty)}(s) = K * \frac{1s^{11} + 10Ks^9 + 36K^2s^7 + 56K^3s^5 + 35K^4s^3 + 6K^5s^1}{1s^{12} + 11Ks^{10} + 45K^2s^8 + 84K^3s^6 + 70K^4s^4 + 21K^5s^2 + 1K^6}
\end{aligned} \tag{6.10}$$

For $x_m = 0$; $k_v = 0$. Viscous damper with no resistance, sections 14 and 13 in FSMC with their FWFs $(g)_{14}^{(k,0)}(s)$, $(g)_{13}^{(k,0)}(s)$ are shown in (6.11).

$$\begin{aligned}
\left(\frac{F_o}{mv_i}\right)_{14}^{(k,0)} &= (g)_{14}^{(k,0)}(s) = K * \frac{1s^{13} + 12Ks^{11} + 55K^2s^9 + 120K^3s^7 + 126K^4s^5 + 56K^5s^3 + 7K^6s}{1s^{14} + 13Ks^{12} + 66K^2s^{10} + 165K^3s^8 + 210K^4s^6 + 126K^5s^4 + 28K^6s^2 + 1K^7} \\
\left(\frac{k_s v_o}{F_i}\right)_{13}^{(k,0)} &= (g)_{13}^{(k,0)}(s) = K * \frac{1s^{12} + 11Ks^{10} + 45K^2s^8 + 84K^3s^6 + 70K^4s^4 + 21K^5s^2 + 1K^6}{1s^{13} + 12Ks^{11} + 55K^2s^9 + 120K^3s^7 + 126K^4s^5 + 56K^5s^3 + 7K^6s}
\end{aligned} \tag{6.11}$$

Simulation of FSMC general model order 40 is shown in figure 6.21 and 6.22 for $F_{40}^{(1,0)}$, and $v_{21}^{(1,0)}$ as an example with unit and pulse input speed

Table 6. 3: Pascal's triangle for Fibonacci FMSC boundary systems $(k, 0)$ & (k, ∞)



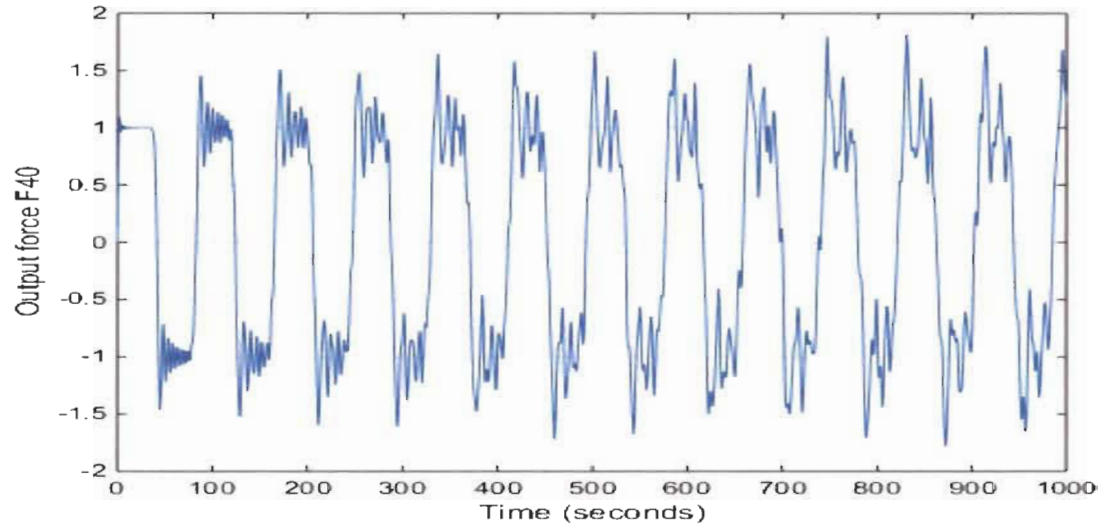


Figure 6. 21: FSMC general model ($F_{40}^{(1,0)}$, $v_i = 1\text{m/s}$, $k_v = 0$)

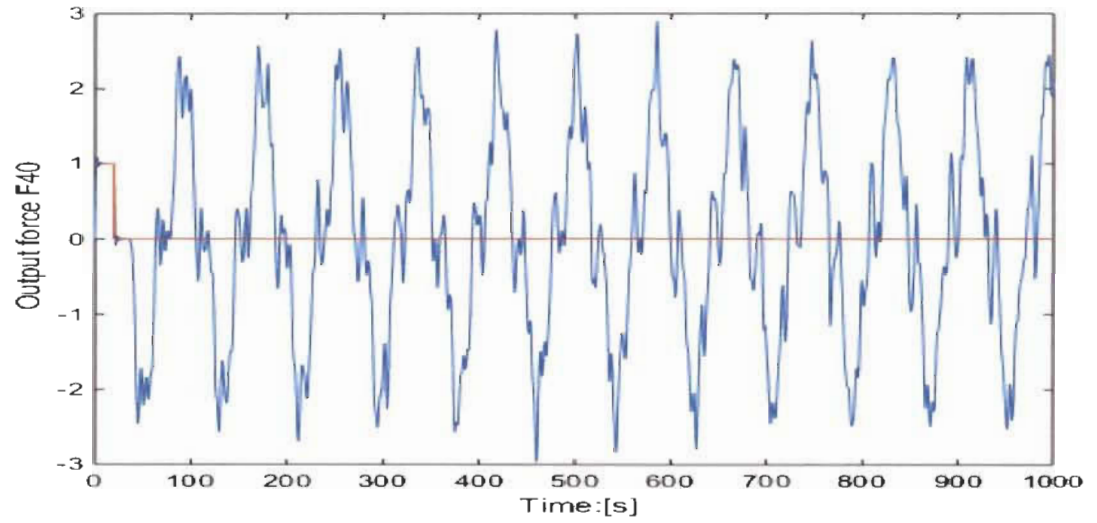


Figure 6. 22: FSMC general model ($F_{40}^{(1,0)}$, $v_i = 1\text{m/s}$ (pulse of 20s), $k_v = 0$)

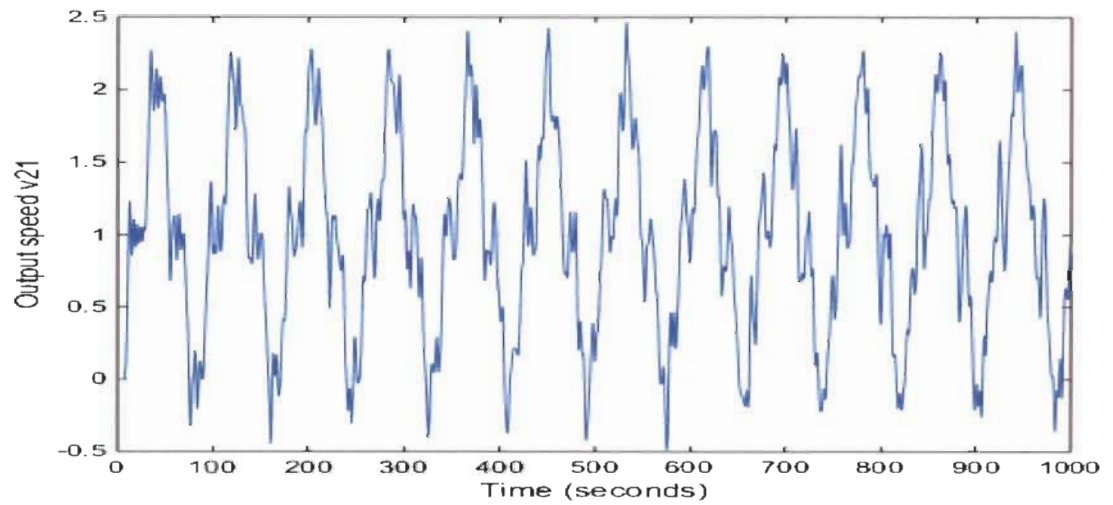


Figure 6. 23: FSMC general model ($v_{21}^{(1,0)}$, $v_i = 1\text{m/s}$, $k_v = 0$)

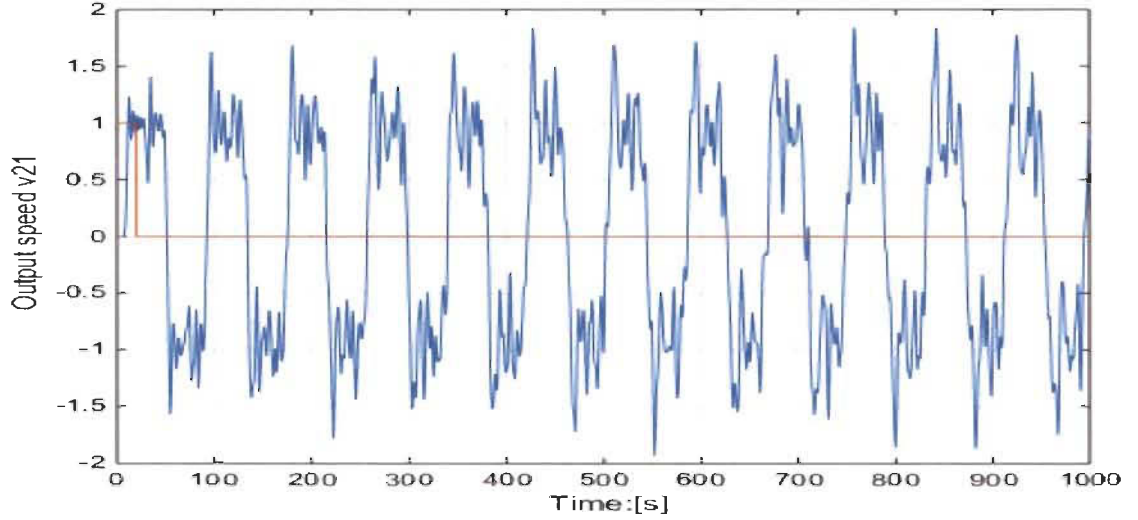


Figure 6. 24: FSMC general model ($v_{21}^{(1,0)}$, $v_i = 1\text{m/s}$ (pulse of 20s), $k_v = 0$)

6.6 Conclusion

In this chapter, we introduced a complete spring-mass chain general model using Fibonacci wave functions FWFs that was developed in chapter 3. The importance of spring-mass chain like LC ladder network comes from its application that can be found in the literature [35], [36], [37] and [38] especially in quantum mechanics or fluid mechanics to understand the interaction between the particles. The detailed model that is proposed for each spring-mass section with precise Fibonacci wave functions can help understand perfectly the behavior and the interaction between each section using the variables $(v_j^{(k,x_m)}, F_j^{(k,x_m)})$. The general model using the momentum and the position is also presented for each section in the chain $(\mu_j^{(k,x_m)}, x_j^{(k,x_m)})$.

The particular cases when the viscous damper coefficient is zero or infinite were studied and simulated. These cases are particular cases of general model and their Fibonacci wave functions are easy to determine based on Pascal's triangle with $x_m = \infty$ and $x_m = 0$.

The spring-mass chain general model using energy between each spring and mass in the chain is also presented to highlight the energy transfer from input source toward the last section in the chain.

Chapter 7: Fibonacci wave functions application to inverse LC ladder network

7.1 Introduction

The FWFs have been created theoretically from a first-order original wave function. The goal was to find transfer functions with high degree that cannot be reduced by any classical reduction methods found in the literature in order to show the limits of these methods.

In this chapter, new electrical circuit application of FWFs called inverse Fibonacci electrical circuits (iFECs) are introduced to model perfectly the recursive inverse LC ladder network. These iFECs can be used to model piezoelectric, [3], [6].

This chapter is organized as follows. Section II describes a general model of series resistive-capacitive inverse Fibonacci electrical circuit (iRC-FEC). Section III presents a comparative study of inverse Fibonacci wave functions (iFWFs) and Matlab-Simulink iRC-FEC. Section IV describes a general model of parallel resistive-inductive inverse Fibonacci electrical circuit (iRL-FEC). Section V gives a comparative study of iFWF and Matlab-Simulink circuit model iRL-FEC. The n^{th} order iRC-FEC and iRL-FEC models are presented in section VI.

7.2 Inverse RC Fibonacci electrical circuit (iRC-FEC)

The original Fibonacci wave function has the following form.

$$g_{-1}^{(k,x_c)}(s) = \frac{K}{s^{-1} + x_c} \quad (7.1)$$
$$K = \omega_f^2 \quad \text{and} \quad x_c = 2 \xi_{cf} \omega_f$$

The first order electrical circuit RC-FEC is presented in figure 7.1.

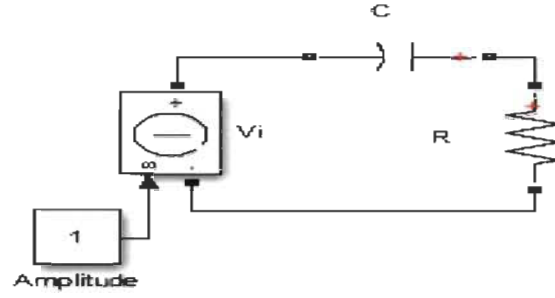


Figure 7. 1: First order iRC-FEC

$$\frac{I_o}{V_i} = \frac{Cs}{1 + RCs} = \frac{1}{L} \frac{LC}{s^{-1} + RC} = \frac{1}{L} \frac{K}{s^{-1} + x_c} = \frac{1}{L} g_{-1}^{(K, x_c)}(s)$$

$$\left(\frac{LI_o}{V_i}\right)^{(K, x_c)}_{-1} = \frac{K}{s^{-1} + x_c} = g_{-1}^{(K, x_c)}(s) \quad (7.2)$$

$$K = LC \quad \text{and} \quad x_c = 2 \xi_{cf} \omega_f = RC$$

The second order RC-FEC circuit diagram is shown in figure 7.2 and its wave function in (7.3).

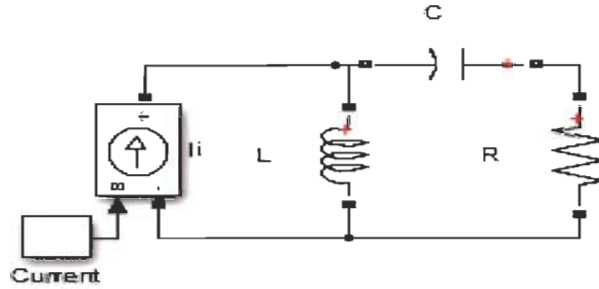


Figure 7. 2: Second order iRC-FEC

$$I_i = \frac{1}{L} \left(g_{-1}^{(K, x_c)}(s) + s^{-1} \right) V_o = \frac{C \left(s^{-1} + g_1^{(K, x_c)}(s) \right) V_o}{LC}$$

$$\left(\frac{CV_o}{I_i}\right)^{(K, x_c)}_{-2} = \frac{K}{s^{-1} + \frac{K}{s^{-1} + x_c}} = g_{-2}^{(K, x_c)}(s) \quad (7.3)$$

The wave function of the third order RC-FEC (7.4) is derived from circuit diagram presented in figure 7.3.

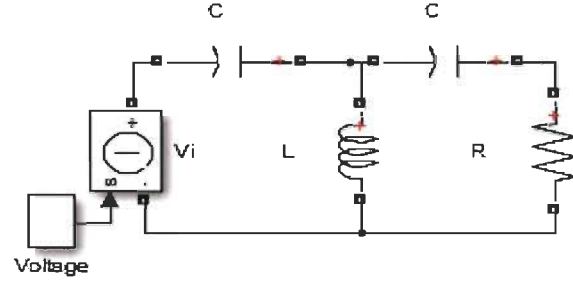


Figure 7. 3: Third order iRC-FEC

$$V_i = \left(C g_2^{(K, x_c)}(s) + sC \right) V_o = \frac{L \left(s + g_2^{(K, x_c)}(s) \right) I_o}{LC}$$

$$\left(\frac{LI_o}{V_i} \right)^{(K, x_c)}_{-3} = \frac{K}{s^{-1} + \frac{K}{s^{-1} + \frac{K}{s^{-1} + x_c}}} = g_{-3}^{(K, x_c)}(s) \quad (7.4)$$

One can see that an even n^{th} order iRC-FEC (figure 7.4) will have current as input and voltage as output.

$$n = n_c + n_L \quad (7.5)$$

n_c is the total number of capacitors in the circuit.

n_L is the total number of inductance in the circuit.

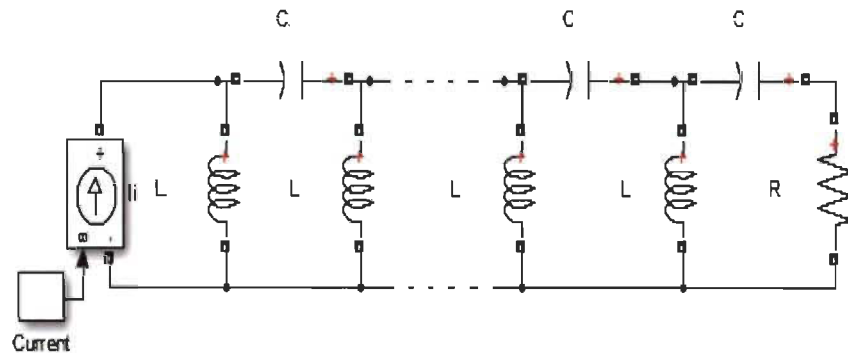


Figure 7. 4: n^{th} even order iRC-FEC

The iFWF of this circuit is.

$$\left(\frac{CV_o}{I_i}\right)_{-n}^{(K,x_c)} = \frac{K}{s^{-1} + g_{-(n-1)}^{(K,x_c)}(s)} = g_{-n}^{(K,x_c)}(s) \quad (7.6)$$

For n^{th} odd order, the wave function is.

$$\left(\frac{LI_o}{V_i}\right)_{-n}^{(K,x_c)} = \frac{K}{s^{-1} + g_{-(n-1)}^{(K,x_c)}(s)} = g_{-n}^{(K,x_c)}(s) \quad (7.7)$$

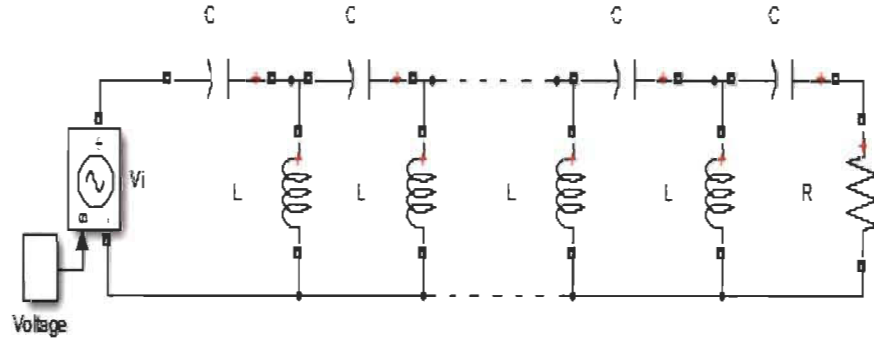


Figure 7. 5: n^{th} odd order iRC-FEC

In general, n^{th} even order iRC-FEC has current as input and voltage as output. In the same time the n^{th} odd order iRC-FEC has voltage as input and current as output.

Table 1 shows all iFWFs in RC-FEC case.

Table 7. 1: iRC-FEC Fibonacci wave functions

$\left(\frac{LI_o}{V_i}\right)_{-1}^{(K,x_c)} = g_{-1}^{(K,x_c)} = \frac{K}{s^{-1} + x_c}$	$\left(\frac{LI_o}{V_i}\right)_{-1}^{(K,x_c)} = g_{-1}^{(K,x_c)} = \frac{K}{1s^{-1} + 1x_c}$
$\left(\frac{CV_o}{I_i}\right)_{-2}^{(K,x_c)} = g_2^{(K,x_c)} = \frac{K}{s^{-1} + \frac{K}{s^{-1} + x_c}}$	$\left(\frac{CV_o}{I_i}\right)_{-2}^{(K,x_c)} = g_2^{(K,x_c)} = \frac{Ks^{-1} + Kx_c}{1s^{-2} + 1x_cs^{-1} + 1K}$
$\left(\frac{LI_o}{V_i}\right)_{-3}^{(K,x_c)} = g_3^{(K,x_c)}$ $= \frac{K}{s^{-1} + \frac{K}{s^{-1} + \frac{K}{s^{-1} + x_c}}}$	$\left(\frac{LI_o}{V_i}\right)_{-3}^{(K,x_c)} = g_3^{(K,x_c)}$ $= \frac{Ks^{-2} + Kx_cs^{-1} + K^2}{1s^{-3} + 1x_cs^{-2} + 2Ks^{-1} + 1Kx_c}$

$\left(\frac{CV_o}{I_i}\right)_{-4}^{(K,x_c)} = g_{-4}^{(K,x_c)}$ $= \frac{K}{s^{-1} + \frac{K}{s^{-1} + \frac{K}{s^{-1} + x_c}}}$	$\left(\frac{CV_o}{I_i}\right)_{-4}^{(K,x_c)} = g_{-4}^{(K,x_c)}$ $= \frac{Ks^{-3} + Kx_cs^{-2} + 2K^2s^{-1} + K^2x_c}{1s^{-4} + 1x_cs^{-3} + 3Ks^{-2} + 2Kx_cs^{-1} + 1K^2}$
$\left(\frac{CV_o}{I_i}\right)_{-n}^{(K,x_c)} = g_{-n}^{(K,x_c)} = \frac{K}{s^{-1} + g_{-(n-1)}^{(K,x_c)}(s)}$ <p><i>n even</i></p> $\left(\frac{LI_o}{V_i}\right)_{-n}^{(K,x_c)} = g_{-n}^{(K,x_c)} = \frac{K}{s^{-1} + g_{-(n-1)}^{(K,x_c)}(s)}$ <p><i>n odd</i></p>	$g_{-n}^{(K,x_c)}(s) = \frac{Kden_{-(n-1)}^{(K,x_c)}(s)}{s^{-1}den_{-(n-1)}^{(K,x_c)}(s) + num_{-(n-1)}^{(K,x_c)}(s)}$ $g_{-n}^{(K,x_c)}(s) = \frac{Kden_{-(n-1)}^{(K,x_c)}(s)}{den_{-n}^{(K,x_c)}(s)}$

7.3 Simulation of iRC-FEC AND iFWFs

Simulation studies were conducted to compare the previous electrical circuits using Matlab-Simulink model and with inverse Fibonacci wave functions. The studies confirm that these circuits follow the logic of a recursive Fibonacci sequence and can be modelled by iFWFs.

A. Case 1: $R=1\Omega$; $L=1H$; $C=1F$; $(K, x_c) = (1,1)$;

In this case $(K, x_c) = (1,1)$. Pascal's Triangle in Table 2 will be used to determine all iFWFs.

iFWF of order 14 taken as example is an even function, its numerator and denominator coefficients are expressed in (7.8) using Table 7.2 with s^{-1} as Laplace variable or Table 7.3 with s as Laplace variable.

Using Table 7.2, iFWF order 14th is:

$$\left(\frac{CV_0}{I_i}\right)_{-14}^{(K,x_c)} = g_{-14}^{(K,x_c)}(s) = \frac{K \text{den}_{-13}^{(K,x_c)}(s)}{\text{den}_{-14}^{(K,x_c)}(s)}$$

$$\begin{aligned} \text{den}_{-13}^{(K,x_c)}(s) = & 1s^{-13} + 1x_c s^{-12} + 12Ks^{-11} + 11Kx_c s^{-10} + 55K^2s^{-9} + 45K^2x_c s^{-8} \\ & + 120K^3s^{-7} + 84K^3x_c s^{-6} + 126K^4s^{-5} + 70K^4x_c s^{-4} + 56K^5s^{-3} \\ & + 21K^5x_c s^{-2} + 7K^6s^{-1} + 1K^6x_c \end{aligned} \quad (7.8)$$

$$\begin{aligned} \text{den}_{-14}^{(K,x_c)}(s) = & 1s^{-14} + 1x_c s^{-13} + 13Ks^{-12} + 12Kx_c s^{-11} + 66K^2s^{-10} + 55K^2x_c s^{-9} \\ & + 165K^3s^{-8} + 120K^3x_c s^{-7} + 210K^4s^{-6} + 126K^4x_c s^{-5} \\ & + 126K^5s^{-4} + 56K^5x_c s^{-3} + 28K^6s^{-2} + 7K^6x_c s^{-1} + 1K^7 \end{aligned}$$

Using Table 7.3, iFWF order 14th is:

$$\left(\frac{CV_0}{I_i}\right)_{14}^{(K,x_c)} = g_{14}^{(K,x_c)}(s) = \frac{K s \text{den}_{13}^{(K,x_c)}(s)}{\text{den}_{14}^{(K,x_c)}(s)}$$

$$\begin{aligned} \text{den}_{13}^{(K,x_c)}(s) = & 1 + 1x_c s^1 + 12Ks^2 + 11Kx_c s^3 + 55K^2s^4 + 45K^2x_c s^5 + 120K^3s^6 \\ & + 84K^3x_c s^7 + 126K^4s^8 + 70K^4x_c s^9 + 56K^5s^{10} + 21K^5x_c s^{11} \\ & + 7K^6s^{12} + 1K^6x_c s^{13} \end{aligned} \quad (7.9)$$

$$\begin{aligned} \text{den}_{14}^{(K,x_c)}(s) = & 1 + 1x_c s^1 + 13Ks^2 + 12Kx_c s^3 + 66K^2s^4 + 55K^2x_c s^5 + 165K^3s^6 \\ & + 120K^3x_c s^7 + 210K^4s^8 + 126K^4x_c s^9 + 126K^5s^{10} + 56K^5x_c s^{11} \\ & + 28K^6s^{12} + 7K^6x_c s^{13} + 1K^7s^{14} \end{aligned}$$

Table 7. 2: Pascal's triangle general form with multiplication coefficients (K, x_c) .

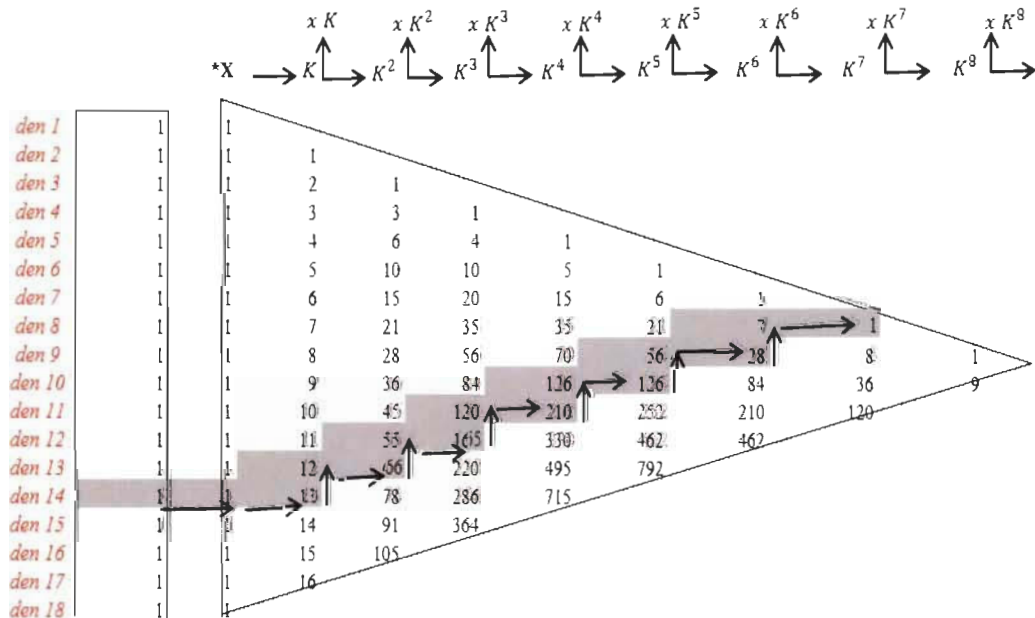
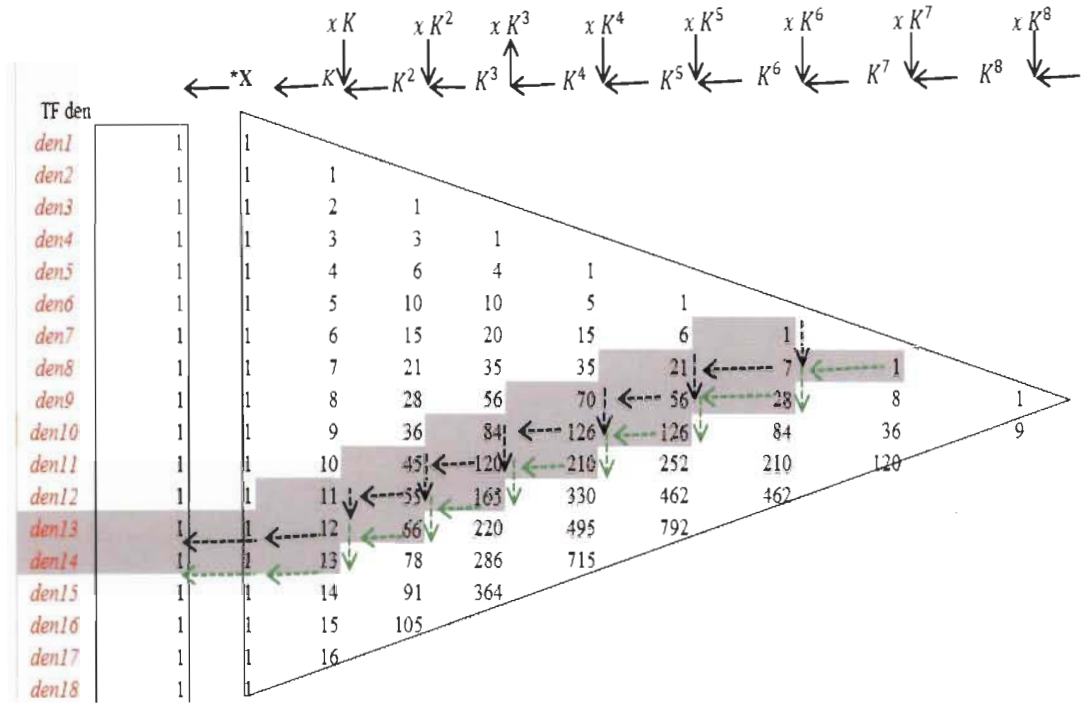
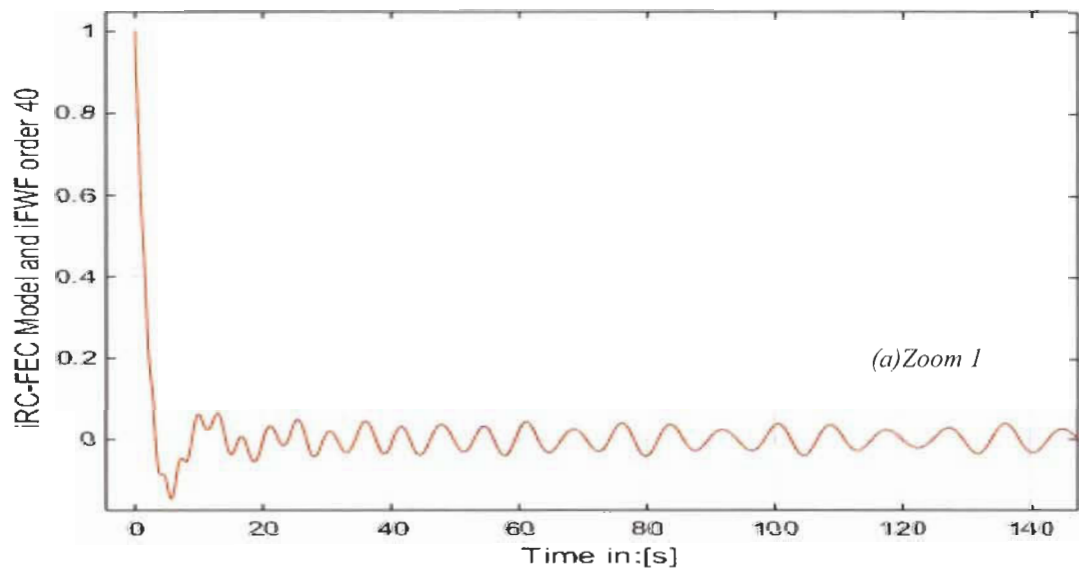


Table 7. 3: Pascal's triangle general form Inverse with multiplication coefficients(K, x_c).



Simulations of $(\frac{V_o}{I_i})_{-40}^{(1,1)} = \frac{1}{c} * g_{-40}^{(1,1)}(s)$ iFWF and iRC-FEC Matlab-Simulink electrical circuit order 40 are illustrated in figure 7.6.



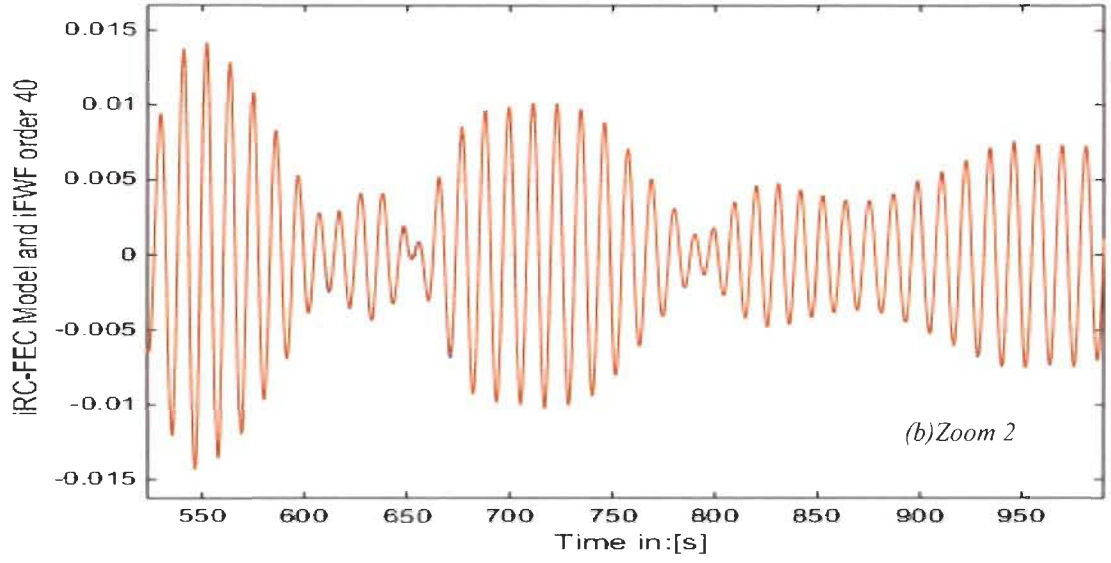
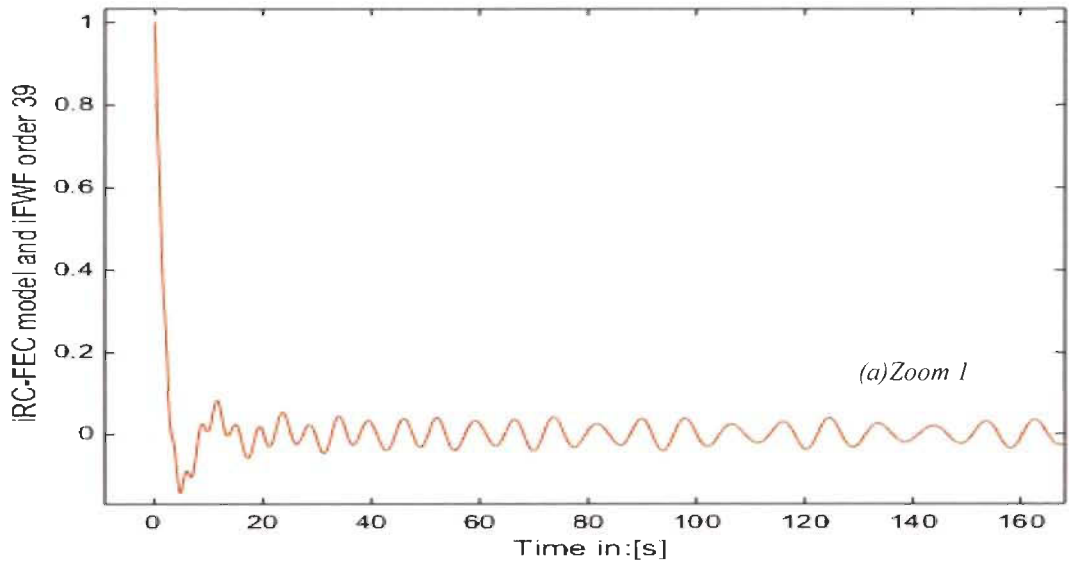


Figure 7. 6: iRC-FEC $(\frac{v_o}{I_i})_{-40}^{(1,1)} = \frac{1}{c} * g_{-40}^{(1,1)}(s)$ with $I_i = 1A$

The $(\frac{l_o}{V_i})_{-39}^{(K,x_c)} = \frac{1}{L} * g_{-39}^{(K,x_c)}(s)$, which is of odd order, will be determined using Pascal's triangle table 2.

Simulation results of $(\frac{l_o}{V_i})_{-39}^{(1,1)} = \frac{1}{L} * g_{-39}^{(1,1)}(s)$ and iRC-FEC electrical circuit order 39 are identical as illustrated in figure 7.7.



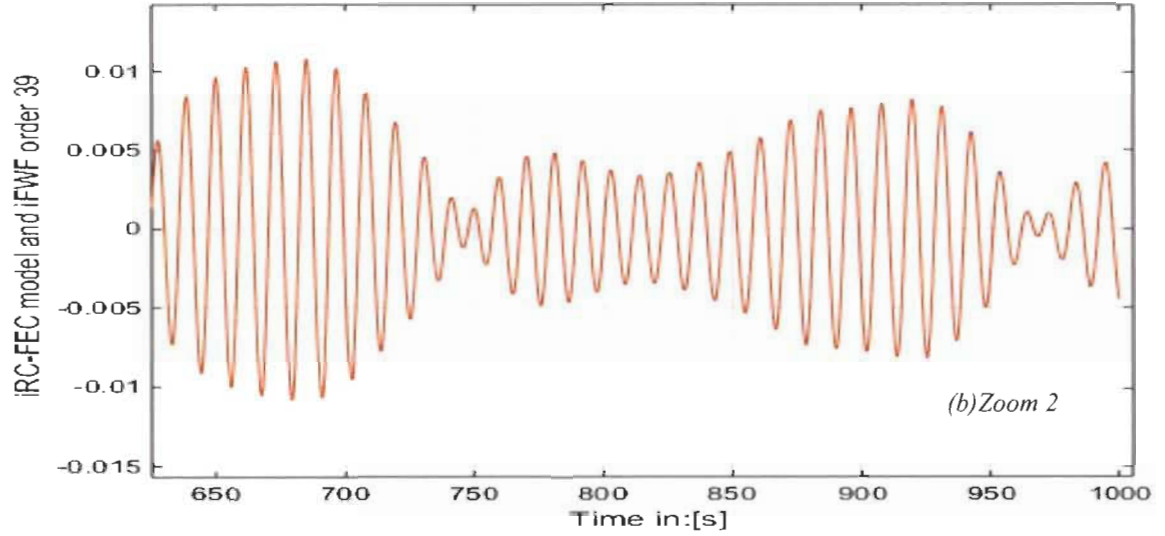


Figure 7. 7: RC-FEC $\left(\frac{I_o}{V_i}\right)_{-39}^{(1,1)} = \frac{1}{L} * g_{-39}^{(1,1)}(s)$ with $V_i = 1V$

7.4 Inverse RL Fibonacci electrical circuit (iRL-FEC)

iRL-FEC is determined in the same way as RC-FEC. The first order circuit in figure 7.8 and its iFWF is presented in (7.10).

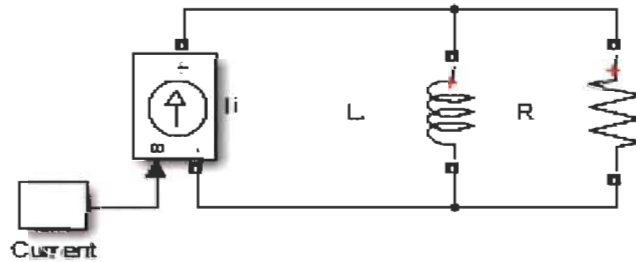


Figure 7. 8: First order iRL-FEC

$$\frac{V_o}{I_i} = \frac{sL}{s^{-1} + \frac{L}{R}} = \frac{1}{C} \frac{LC}{s^{-1} + \frac{L}{R}} = \frac{1}{C} \frac{K}{s^{-1} + x_L} = \frac{1}{C} g_{-1}^{(K, x_L)}(s)$$

$$\left(\frac{CV_o}{I_i}\right)_{-1}^{(K, x_L)} = \frac{K}{s^{-1} + x_L} = g_{-1}^{(K, x_L)}(s) \quad (7.10)$$

$$K = LC \quad \text{and} \quad x_L = 2 \xi_{Lf} \omega_f = \frac{L}{R}$$

$$K = LC = x_c x_L = 4 \xi_{cf} \xi_{Lf} \omega_f^2$$

$$\xi_{cf} \xi_{Lf} = \frac{1}{4}$$

The 2nd order RL-FEC will be defined with current input and voltage output (figure 7.9) and its iFWF expressed in (7.11).

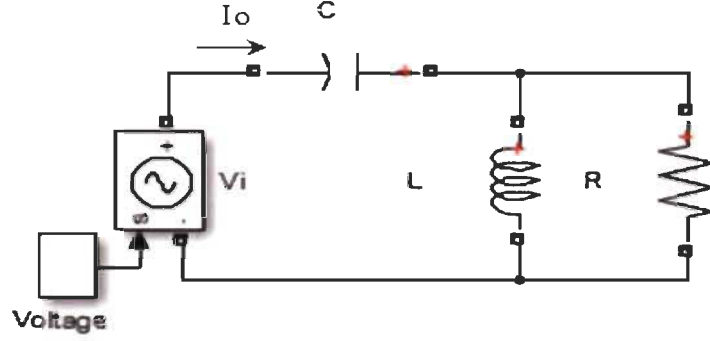


Figure 7. 9: Second order iRL-FEC

$$V_i = \frac{1}{C} \left(g_{-1}^{(K, x_L)}(s) + s^{-1} \right) I_o = \frac{L \left(s^{-1} + g_{-1}^{(K, x_L)}(s) \right) I_o}{LC} \quad (7.11)$$

$$\left(\frac{L I_o}{V_i} \right)_{-2}^{(K, x_L)} = \frac{K}{s^{-1} + \frac{K}{s^{-1} + x_L}} = g_{-2}^{(K, x_L)}(s)$$

The third order iRL-FEC will be defined with an input voltage and output current (Figure 7.10) and its iFWF in (7.12).

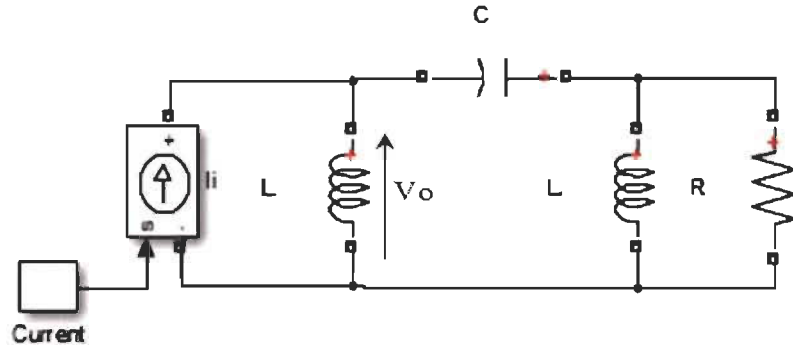


Figure 7. 10: Third order iRL-FEC

$$I_i = \frac{1}{L} \left(g_{-2}^{(K, x_L)}(s) + s^{-1} \right) V_o = \frac{C \left(s^{-1} + g_{-2}^{(K, x_L)}(s) \right) V_o}{LC} \quad (7.12)$$

$$\left(\frac{CV_o}{I_i}\right)_{-3}^{(K,x_L)} = \frac{K}{s^{-1} + \frac{K}{s^{-1} + \frac{K}{s^{-1} + x_L}}} = g_{-3}^{(K,x_L)}(s)$$

In general, iRL-FEC with an even n^{th} order in figure 7.11 has voltage as input and current as output. We have.

$$n = n_c + n_L$$

where n_c is the total number of capacitors in the circuit, and n_L is the total number of inductance in the circuit.

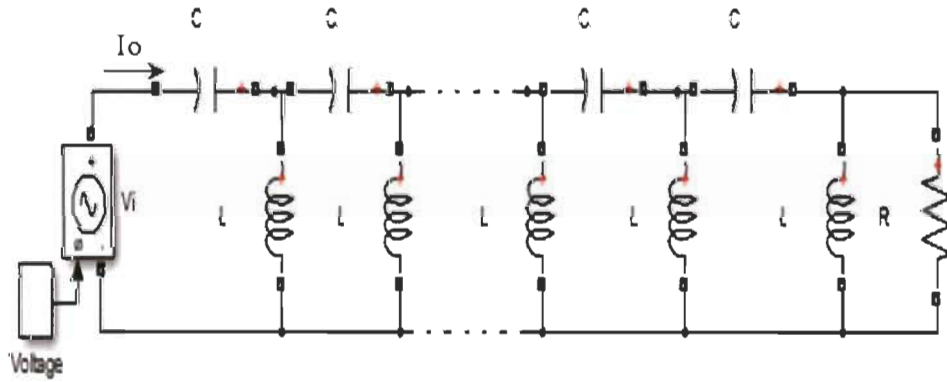


Figure 7. 11: n^{th} even order iRL-FEC

The wave function is:

$$\left(\frac{LI_o}{V_i}\right)_{-n}^{(K,x_L)} = \frac{K}{s + g_{-(n-1)}^{(K,x_L)}(s)} = g_{-n}^{(K,x_L)}(s) \quad (7.13)$$

iRL-FEC with n^{th} odd order (Figure 7.12) has current as input and voltage as output and its wave function is expressed in (7.14).

$$\left(\frac{CV_o}{I_i}\right)_{-n}^{(K,x_L)} = \frac{K}{s^{-1} + g_{-(n-1)}^{(K,x_L)}(s)} = g_{-n}^{(K,x_L)}(s) \quad (7.14)$$

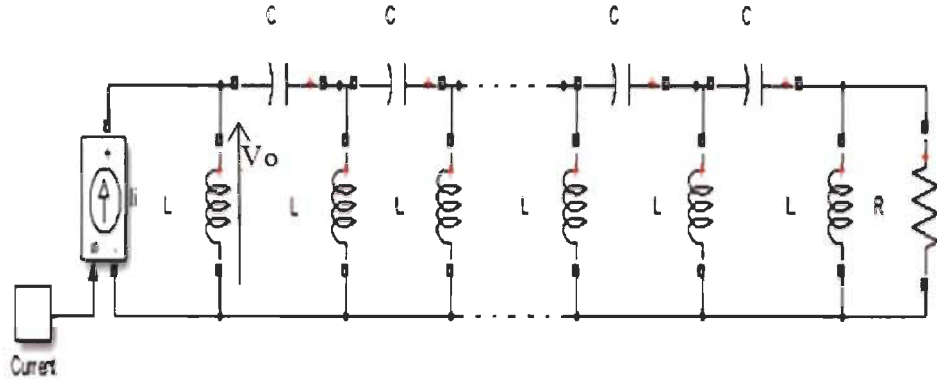


Figure 7. 12: n^{th} odd order iRL-FEC

Table 7.4 shows the iFWFs in the case of a RL-FEC.

Table 7. 4: iRL-FEC Fibonacci wave functions

$(\frac{CV_o}{I_i})_{-1}^{(K,x_L)} = g_{-1}^{(K,x_L)} = \frac{K}{s^{-1} + x_L}$	$(\frac{CV_o}{I_i})_{-1}^{(K,x_L)} = g_{-1}^{(K,x_L)} = \frac{K}{1s^{-1} + 1x_L}$
$(\frac{LI_o}{V_i})_{-2}^{(K,x_L)} = g_{-2}^{(K,x_L)} = \frac{K}{s^{-1} + \frac{K}{s^{-1} + x_L}}$	$(\frac{LI_o}{V_i})_{-2}^{(K,x_L)} = g_{-2}^{(K,x_L)} = \frac{Ks + Kx_L}{1s^{-2} + 1x_Ls + 1K}$
$(\frac{CV_o}{I_i})_{-3}^{(K,x_L)} = g_{-3}^{(K,x_L)}$ $= \frac{K}{s^{-1} + \frac{K}{s^{-1} + \frac{K}{s^{-1} + x_L}}}$	$(\frac{CV_o}{I_i})_{-3}^{(K,x_L)} = g_{-3}^{(K,x_L)}$ $= \frac{Ks^{-2} + Kx_Ls^{-1} + K^2}{1s^{-3} + 1x_Ls^{-2} + 2Ks^{-1} + 1Kx_L}$
$(\frac{LI_o}{V_i})_{-4}^{(K,x_L)} = g_{-4}^{(K,x_L)}$ $= \frac{K}{s^{-1} + \frac{K}{s^{-1} + \frac{K}{s^{-1} + \frac{K}{s^{-1} + x_L}}}}$	$(\frac{LI_o}{V_i})_{-4}^{(K,x_L)} = g_{-4}^{(K,x_L)}$ $= \frac{Ks^{-3} + Kx_Ls^{-2} + 2K^2s^{-1} + K^2x_L}{1s^{-4} + 1x_Ls^{-3} + 3Ks^{-2} + 2Kx_Ls^{-1} + 1K^2}$
$(\frac{LI_o}{V_i})_{-n}^{(K,x_L)} = g_{-n}^{(K,x_L)} = \frac{K}{s^{-1} + g_{-(n-1)L}(s)}$ $n \text{ even}$ $(\frac{CV_o}{I_i})_{-n}^{(K,x_L)} = g_{-n}^{(K,x_L)} = \frac{K}{s^{-1} + g_{-(n-1)L}(s)}$ $n \text{ odd}$	$g_n^{(K,x_L)}(s) = \frac{Kden_{-(n-1)}^{(K,x_L)}(s)}{s^{-1}den_{-(n-1)}^{(K,x_L)}(s) + num_{-(n-1)}^{(K,x_L)}(s)}$ $g_{-n}^{(K,x_L)}(s) = \frac{Kden_{-(n-1)}^{(K,x_L)}(s)}{den_{-n}^{(K,x_L)}(s)}$

7.5 Simulation of iRL-FEC and iFWFs

Simulations will be made with the same values as iRC-FEC in the previous paragraph

A. Case #1: $R=1\Omega$; $L=1H$; $C=1F$; $(K, x_L) = (1,1)$.

$$x_L = \frac{L}{R} = 1 ; \quad K = LC = 1$$

Simulations of the iFWF $\left(\frac{Ll_o}{v_i}\right)_{-40}^{(1,1)} = g_{-40}^{(1,1)}(s)$ and iRL-FEC Matlab-Simulink electrical circuit of order 40 are shown in figure 7.13. Results are identical in iFWF and iRL-FEC

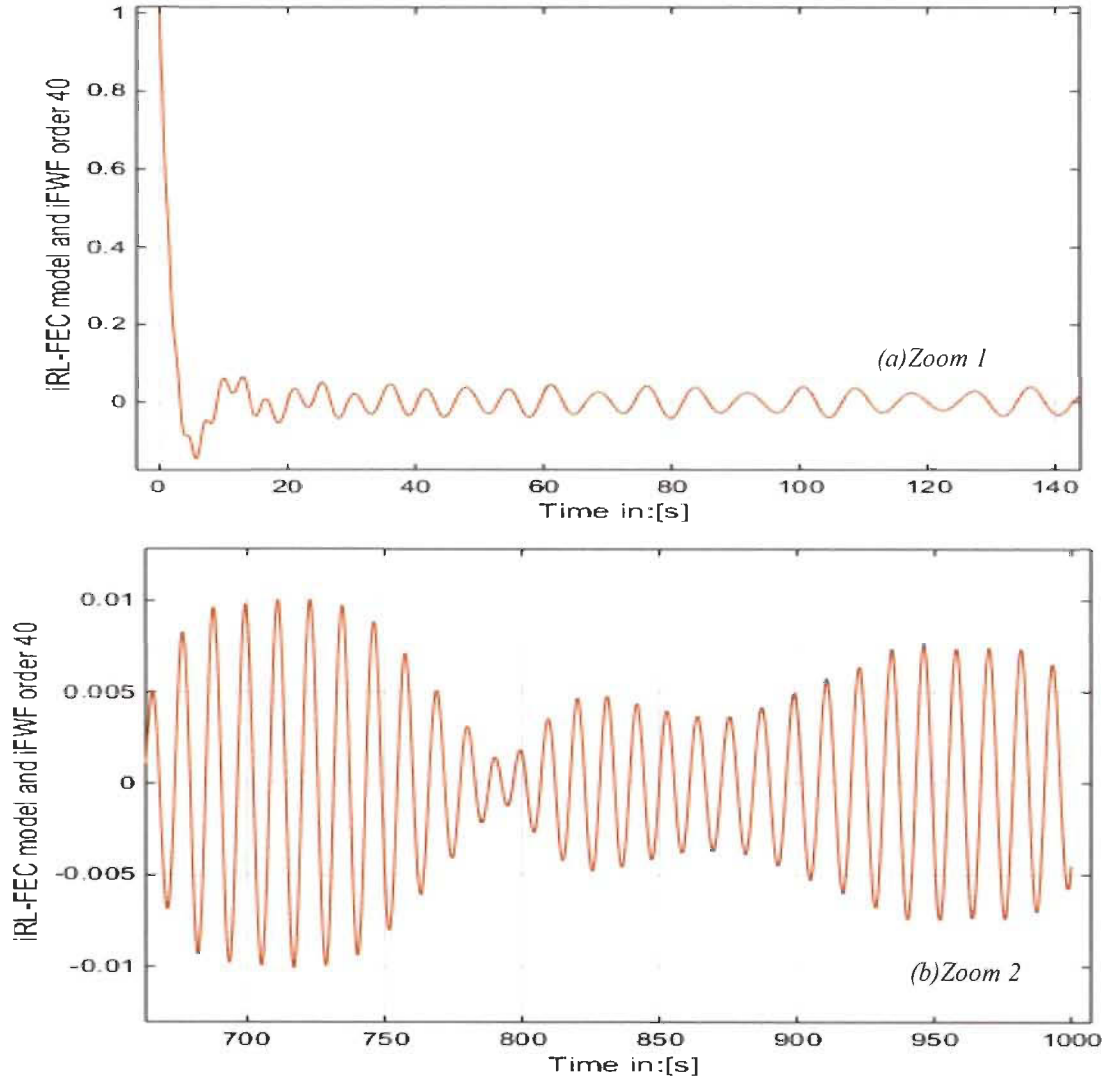


Figure 7. 13: iRL-FEC $\left(\frac{Ll_o}{v_i}\right)_{-40}^{(1,1)} = \frac{1}{L}g_{-40}^{(1,1)}(s)$, $V_i = 1V$

The iFWF $\left(\frac{V_o}{I_i}\right)_{-39}^{(1,1)} = \frac{1}{c} g_{-39}^{(1,1)}(s)$, is shown in figure 7.14 with its equivalent Matlab-Simulink electrical circuit iRL-FEC order 39. Again, simulation results are identical between iFWF and iRL-FEC.

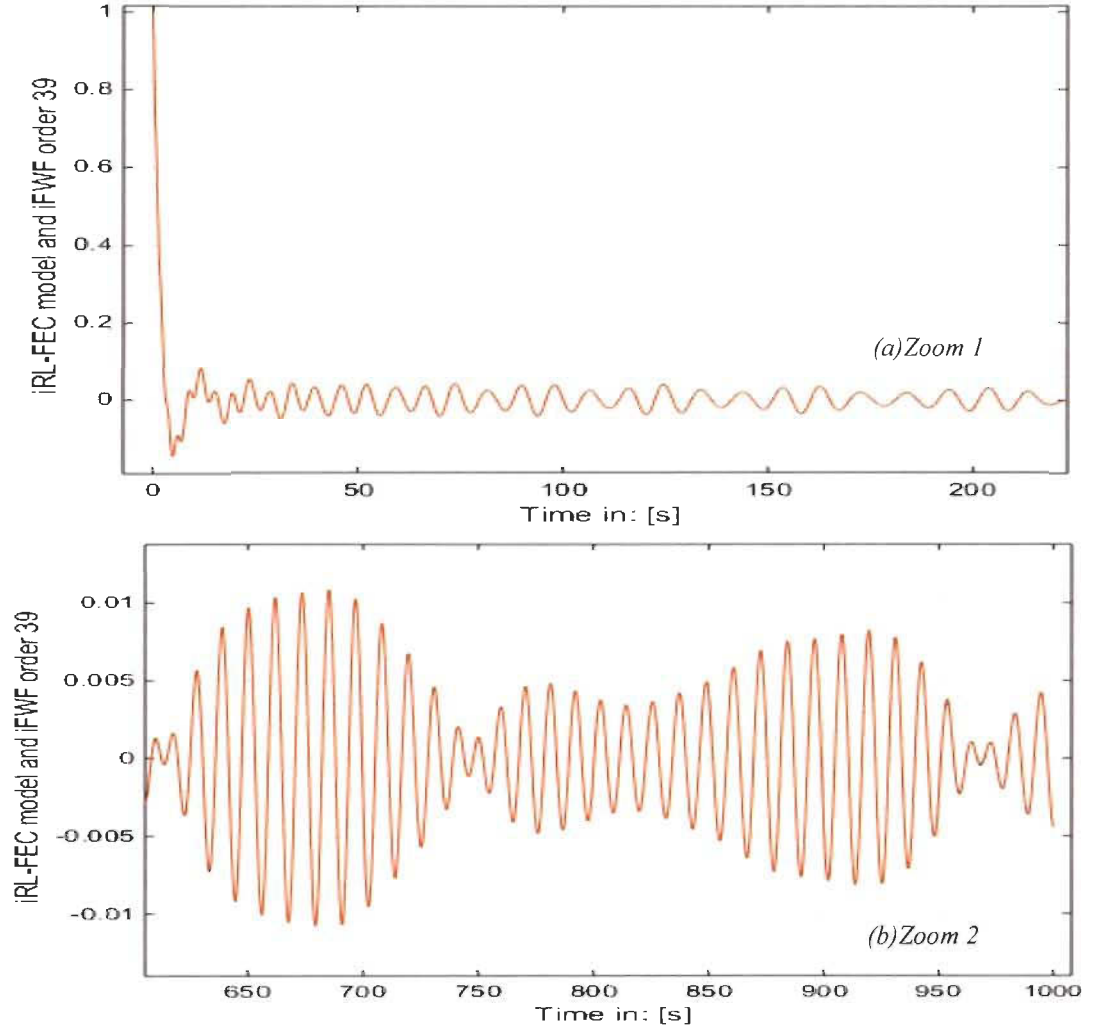


Figure 7. 14: iRL-FEC $\left(\frac{V_o}{I_i}\right)_{-39}^{(1,1)} = \frac{1}{c} g_{-39}^{(1,1)}(s)$ with $I_i = 1A$

An n^{th} order iRL-FEC and its iFWF behaves exactly the same way as an n^{th} order RC-FEC and its iFWF only if $x_L = x_c$.

$$\left(\frac{CV_o}{I_i}\right)_{-n}^{(K,x_L)} = g_{-n}^{(K,x_L)} = \left(\frac{LI_o}{V_i}\right)_{-n}^{(K,x_c)} = g_{-n}^{(K,x_c)} \text{ with } x_L = x_c$$

$$x_L = x_c = \frac{L}{R} = RC \quad (7.15)$$

$$R = \sqrt{\frac{L}{C}} ; K = \omega_f^2 ; x_L = x_c = \omega_f = \sqrt{LC}$$

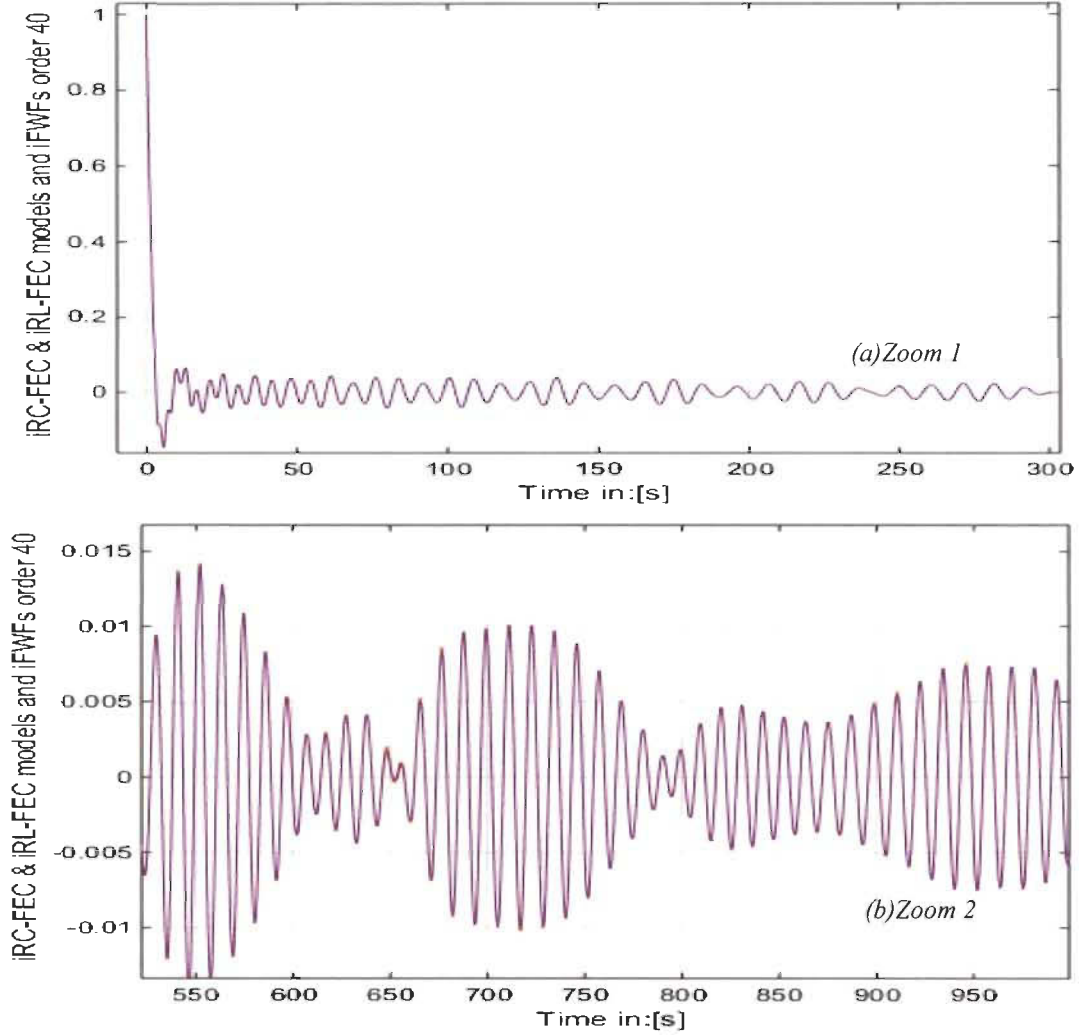


Figure 7. 15: iRL-FEC and iRC-FEC order 40 ; $((\frac{I_o}{V_i})_{-40}^{(1,1)} = \frac{1}{L} g_{-40}^{(1,1)}(s), V_i = 1V)) ((\frac{V_o}{I_i})_{-40}^{(1,1)} = \frac{1}{C} * g_{-40}^{(1,1)}(s), I_i = 1A))$

7.6 N^{th} order inverse LC ladder iRC-FEC and iRL-FEC general model

The n^{th} order iRC-FEC and iRL-FEC are perfectly modeled. All voltages through each inductor and currents through each capacitor are perfectly determined by inverse Fibonacci wave functions illustrated in section II. The model is illustrated in figure 7.17 for $n = 40$ and

can be extended to an infinite order knowing that each iFWF can be determined using Pascal's triangle general form in table 7.2 or 7.3.

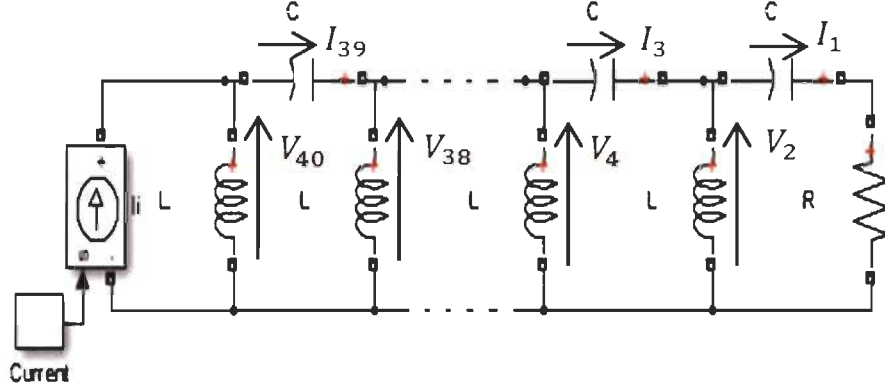


Figure 7.16: n^{th} even order iRC-FEC

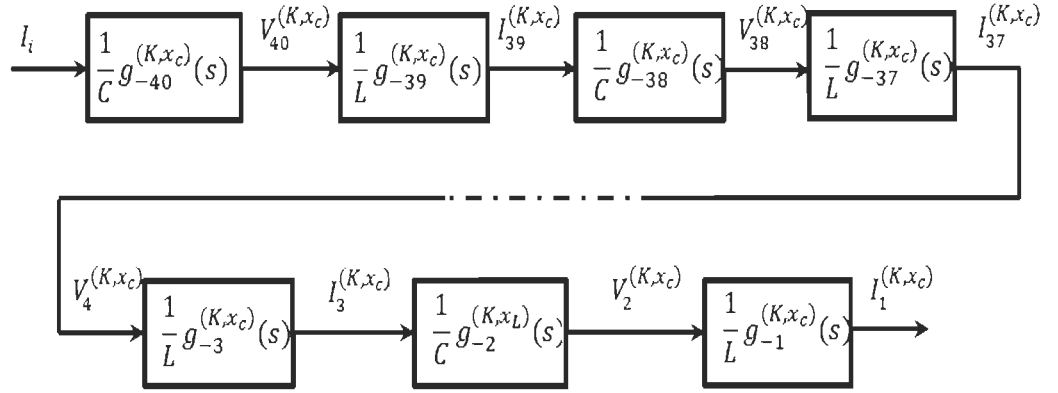


Figure 7.17: n^{th} even order iRC-FEC Model using iFWFs for each current and voltage branch.

In the same way, the iRL-FEC model is illustrated in figure 7.19 below for $n = 40$.

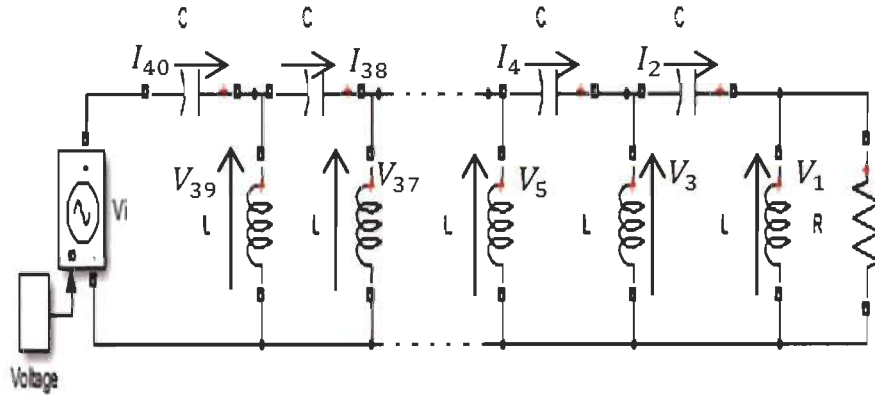


Figure 7.18: n^{th} even order iRL-FEC

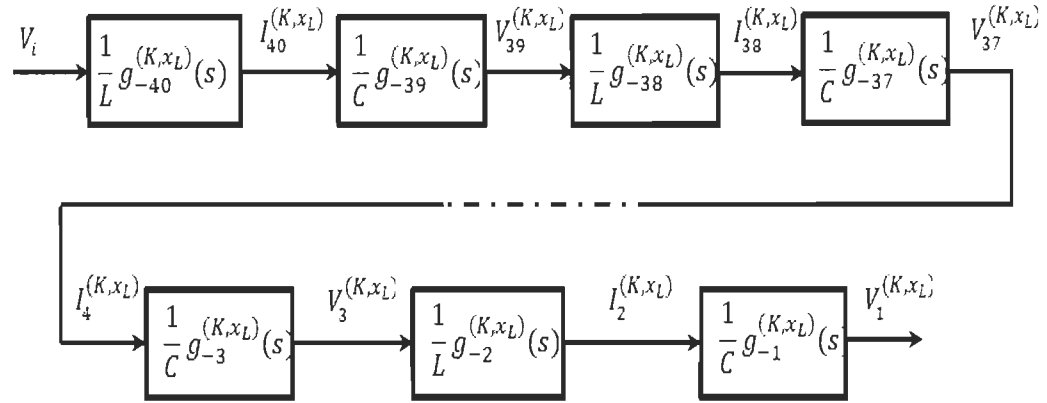


Figure 7. 19: n^{th} even order iRL-FEC Model using IFWFs for each current and voltage branch.

Simulation was conducted for iRC-FEC Matlab-Simulink circuit model and the corresponding general model for $n = 40$ to confirm the accuracy of the proposed model for all currents and voltages. Note that the general model can be applied to any order n of the iRC-FEC and any order n of iRL-FEC.

A. Case #2: $(K, x_c) = (1, 4)$, $R=10\Omega$.

$$K = LC = \omega_f^2 = x_L x_c$$

$$C = \frac{x_c}{R} = 0.4F \quad (7.16)$$

$$L = \frac{K}{C} = 2.5H$$

$$x_L = \frac{L}{R} = 0.25$$

The figures 7.20 and 7.21 show simulation of the general model and Matlab-Simulink iRC-FEC for voltage $V_{40}^{(1,4)}$ and the current $I_{40}^{(1,4)}$ through the inductor for the case $(K, x_c) = (1, 4)$. The figures 7.22 and 7.23 show simulation of the current $I_{39}^{(1,4)}$ and the voltage $V_{39}^{(1,4)}$ through the capacitor.

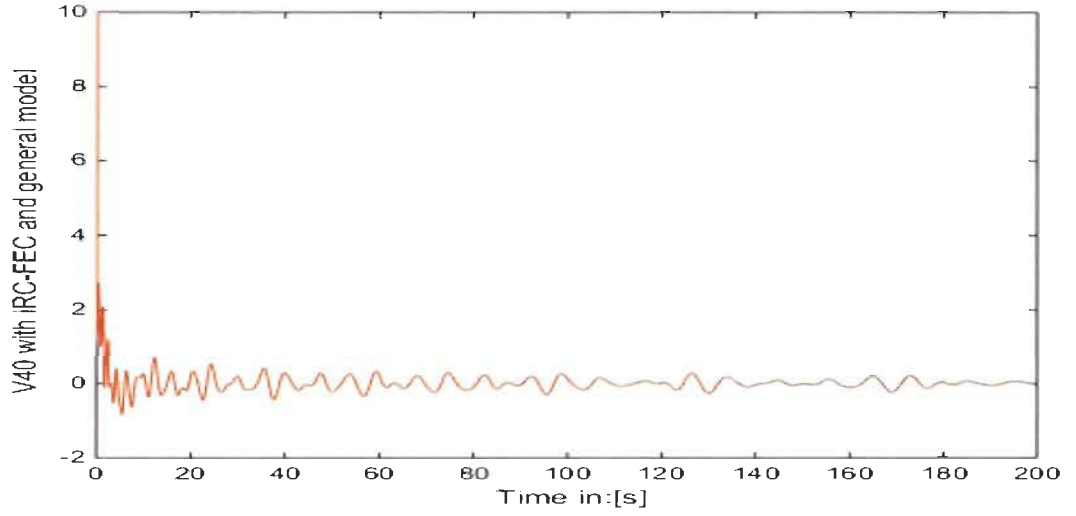


Figure 7. 20: iRC-FEC circuit and general model for $V_{40}^{(1,4)}$ with input $I_i = 1A$

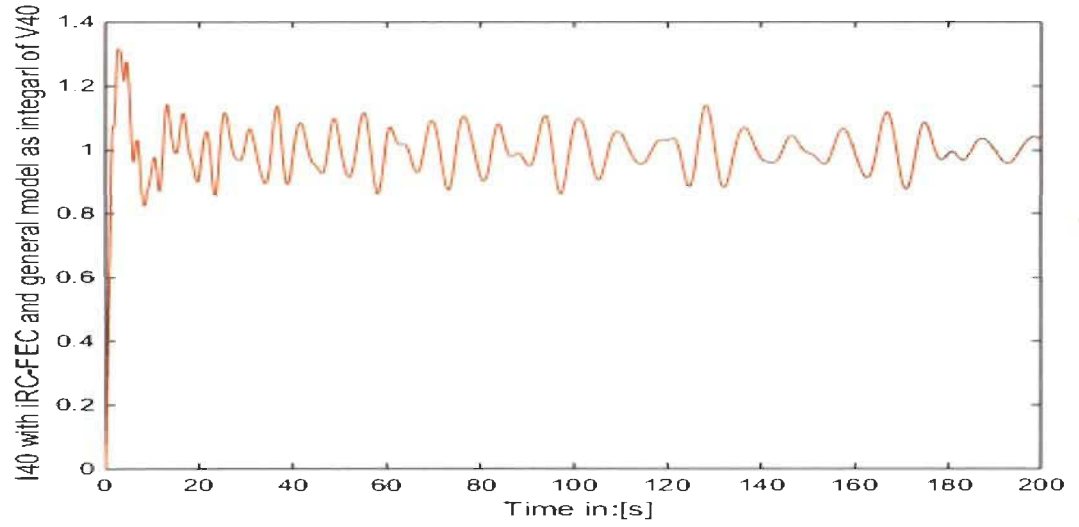


Figure 7. 21: iRC-FEC circuit and general model for $I_{40}^{(1,4)}$ as integral of $V_{40}^{(1,4)}$ with input $I_i = 1A$

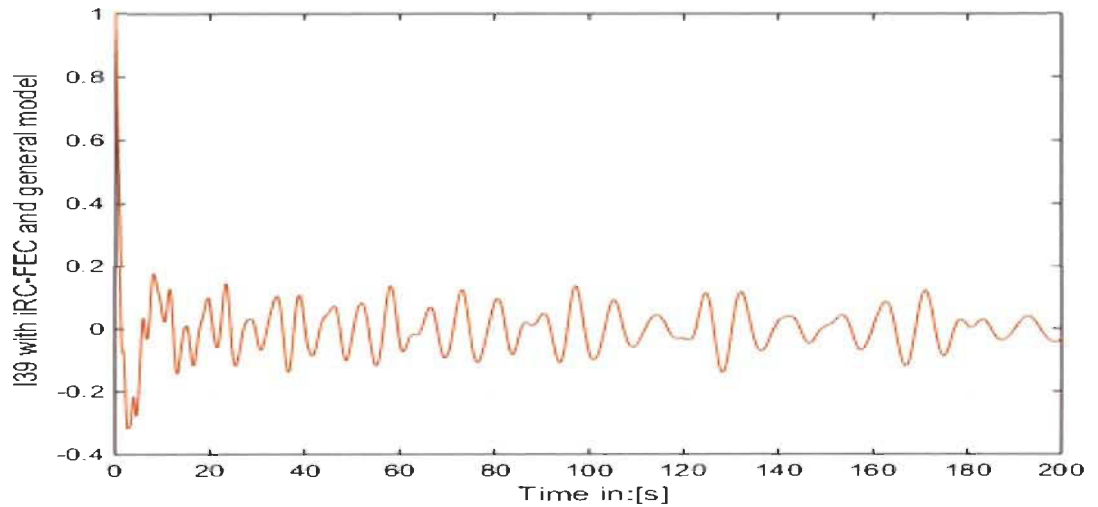


Figure 7. 22: iRC-FEC circuit and general model for $I_{39}^{(1,4)}$ with input $I_i = 1A$

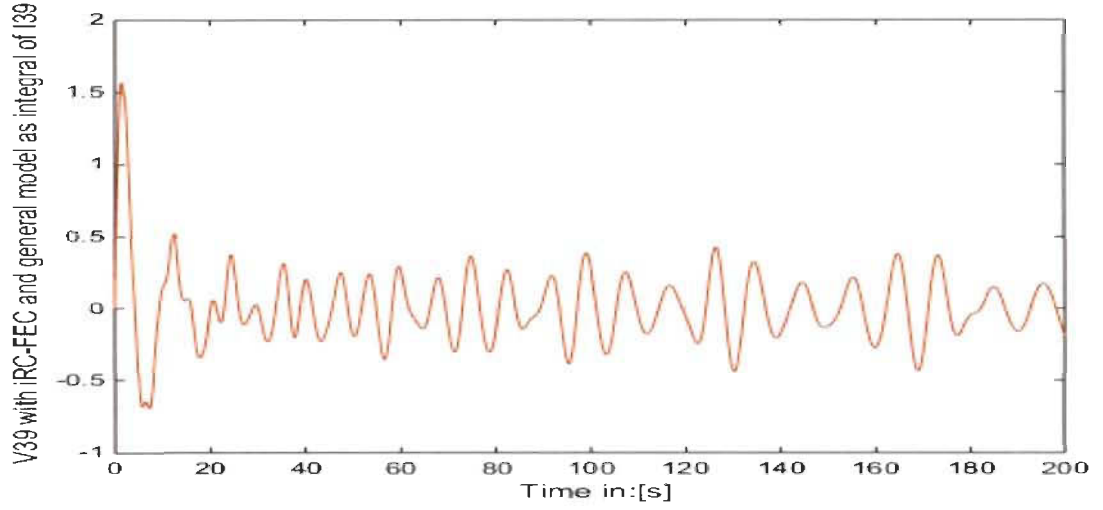


Figure 7. 23: iRC-FEC circuit and general model for $V_{39}^{(1,4)}$ as integral of $I_{39}^{(1,4)}$ with input $I_i = 1A$

iFWFs model presented in figures 7.24 and 7.25 are exactly the same as the iRC-FEC Matlab-Simulink circuit model of all inductors voltages and all capacitors currents and its corresponding iFWF. Thus the iRC-FEC and iRL-FEC can be shaped for any order due to the fact that every order is well defined with its inverse Fibonacci wave function precisely determined from Pascal's triangle general form table 7.2 and table 7.3.

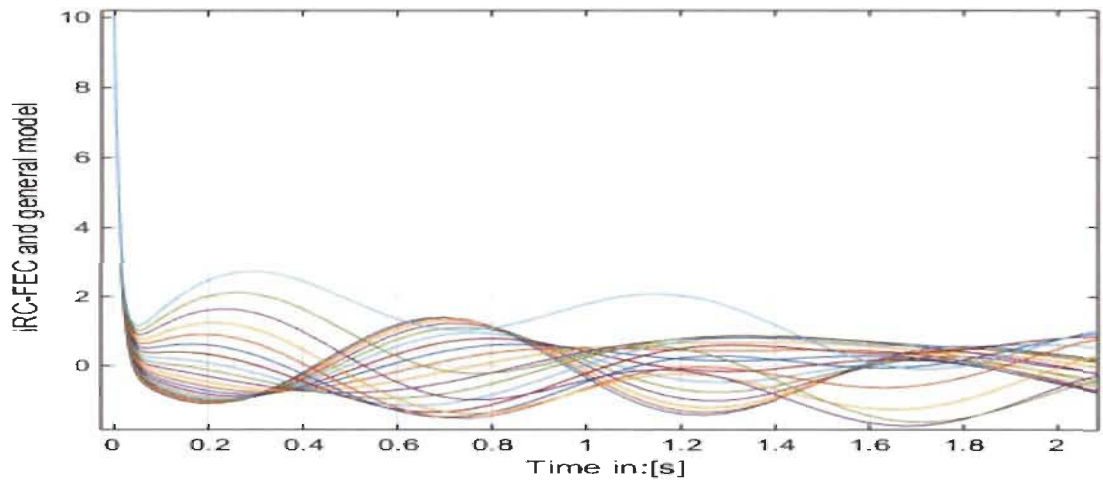


Figure 7. 24: Matlab-Simulink iRC-FEC and general model ($V_2^{(1,4)}, V_4^{(1,4)}, \dots, V_{40}^{(1,4)}$) across inductors

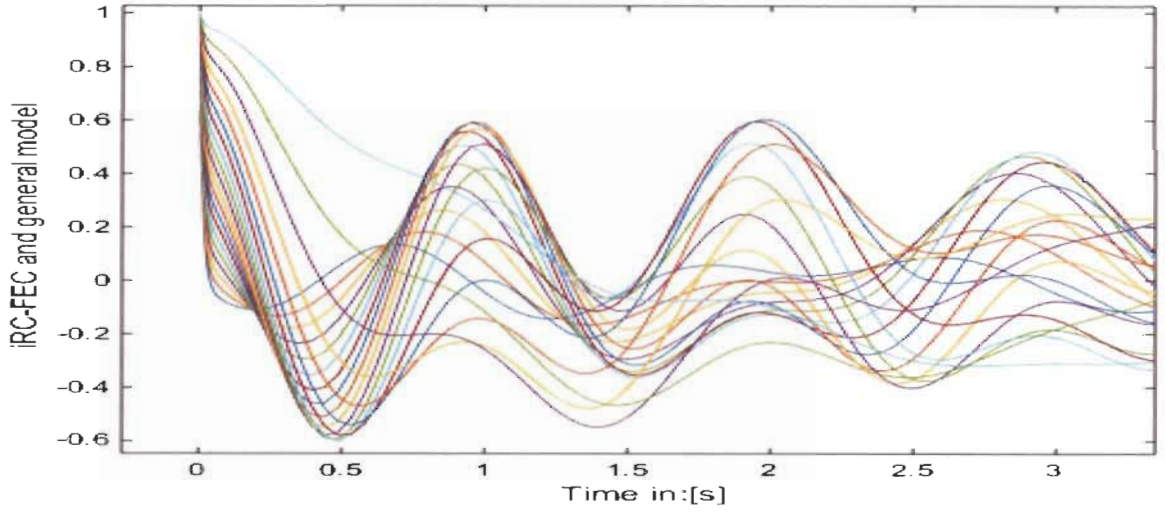


Figure 7. 25: Matlab-Simulink iRC-FEC and general model ($I_1^{(1,4)}, I_3^{(1,4)}, \dots, I_{39}^{(1,4)}$) across capacitors

For the case where both iRC-FEC and iRL-FEC with the same time constant $x_c = x_L$. Simulation was conducted to confirm the accuracy of the iFWF general model proposed in figures 7.17 and 7.20.

B. Case #1: $R=1\Omega$; $L=1H$; $C=1F$; $(K, x_c) = (1,1)$;

$$\begin{aligned}
 C &= \frac{1}{R * x_c} = 1F \\
 L &= \frac{1}{K * C} = 1H \\
 x_L &= \frac{L}{R} = x_c = RC = 1 \\
 R &= \sqrt{\frac{L}{C}} = 1 \\
 K &= LC = \omega_f^2 = x_L x_c = x_L^2 = x_c^2 \\
 x_c &= 2\xi_{cf}\omega_f = x_L = 2\xi_{Lf}\omega_f ; \xi_{Lf} = \xi_{cf} = \frac{1}{2}
 \end{aligned} \tag{7.17}$$

Simulation in figures 7.26 and 7.27 for the iRC-FEC and its model for order 40 show no difference between the general model and Matlab-Simulink iRC-FEC for voltage $V_{40}^{(1,1)}$ and the current $I_{40}^{(1,1)}$ through the inductor for the case $(K, x_c) = (1,1)$

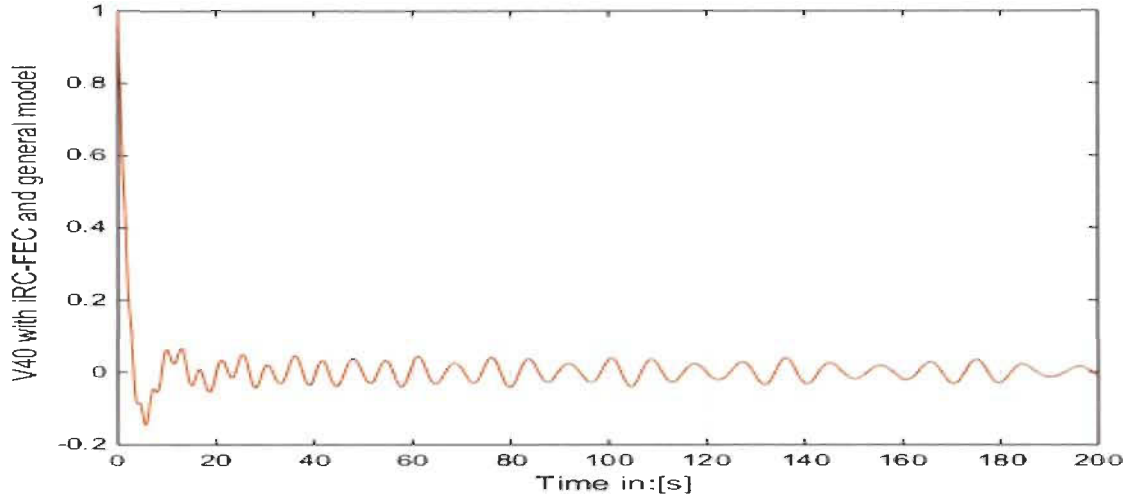


Figure 7. 26: Matlab-Simulink iRC-FEC and general model ($V_{40}^{(1,1)}$, $I_i = 1A$, $R = \sqrt{\frac{L}{C}}$)

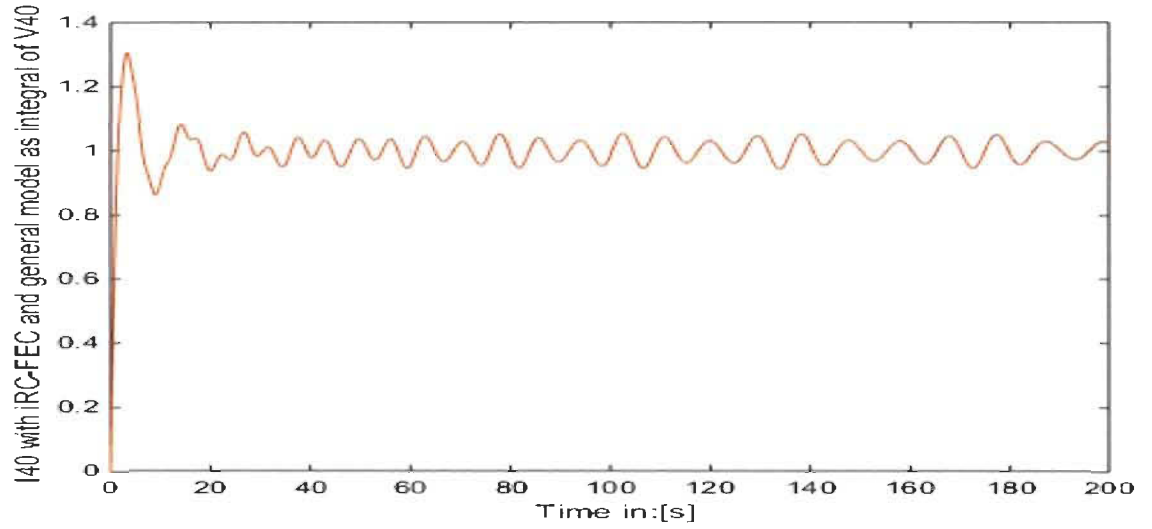


Figure 7. 27: Matlab-Simulink iRC-FEC and general model ($I_{40}^{(1,1)}$, $I_i = 1A$, $R = \sqrt{\frac{L}{C}}$) as integral of $V_{40}^{(1,1)}$

Simulation in figure 7.28 and 7.29 for the iRC-FEC and its model for order 40 also show no difference between the general model and Matlab-Simulink iRC-FEC for the current $I_{39}^{(1,1)}$ and the voltage $V_{39}^{(1,1)}$ through the capacitor for the case $(K, x_c) = (1,1)$

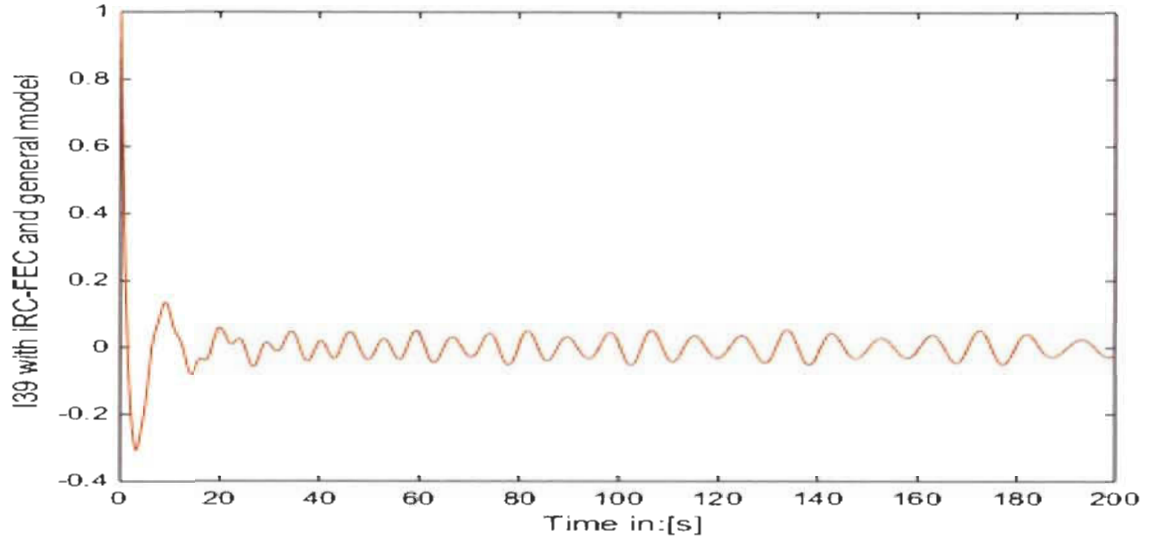


Figure 7. 28: Matlab-Simulink iRC-FEC and general model ($I_{39}^{(1,1)}$, $I_i = 1A$, $R = \sqrt{\frac{L}{C}}$)

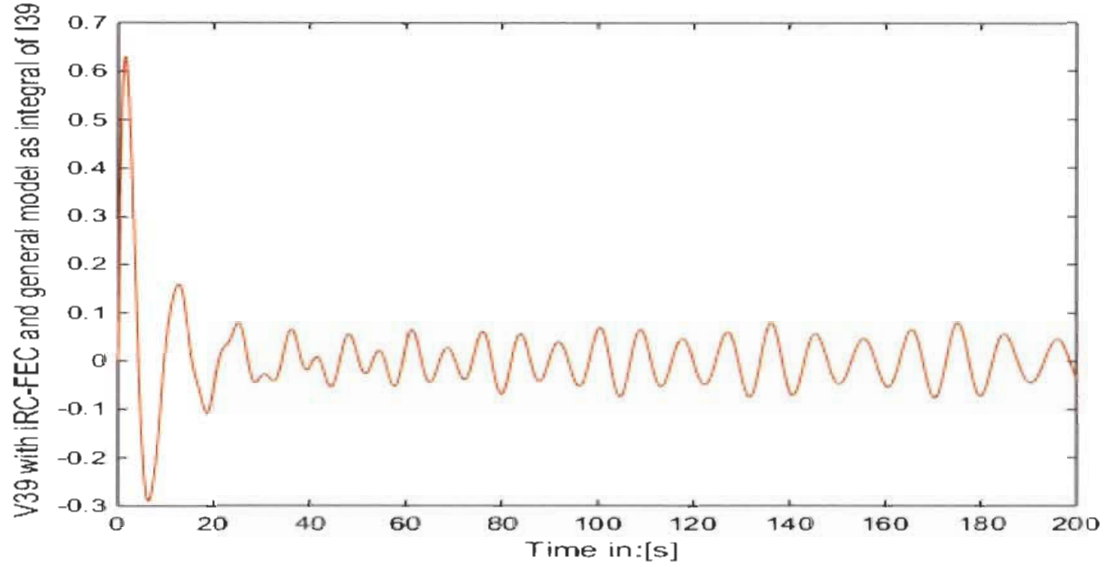


Figure 7. 29: Matlab-Simulink iRC-FEC and general model ($V_{39}^{(1,1)}$, $I_i = 1A$, $R = \sqrt{\frac{L}{C}}$) as integral of $I_{39}^{(1,1)}$

Simulation in figure 7.30 and 7.31 for the iRC-FEC and its model for order 40 show no difference between the general model and Matlab-Simulink iRC-FEC for the voltage

$V_{30}^{(1,1)}$ and the current $I_{30}^{(1,1)}$ through the inductor for the case $(K, x_c) = (1, 1)$

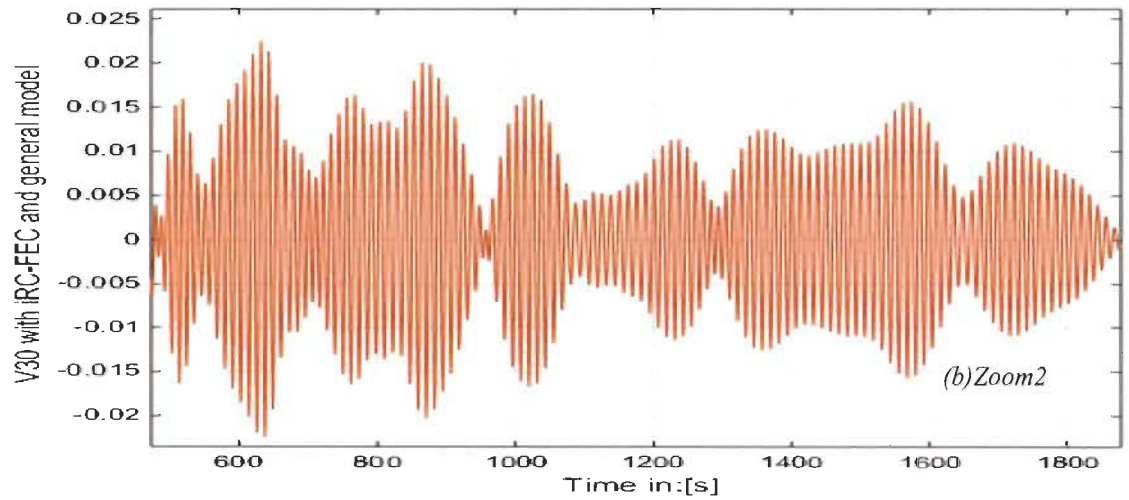
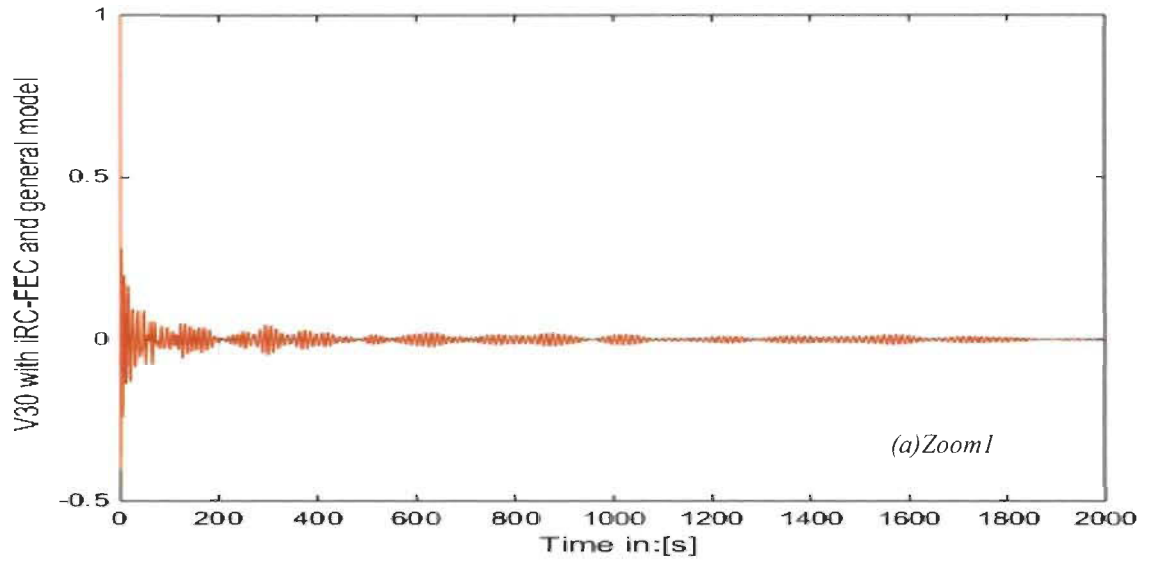
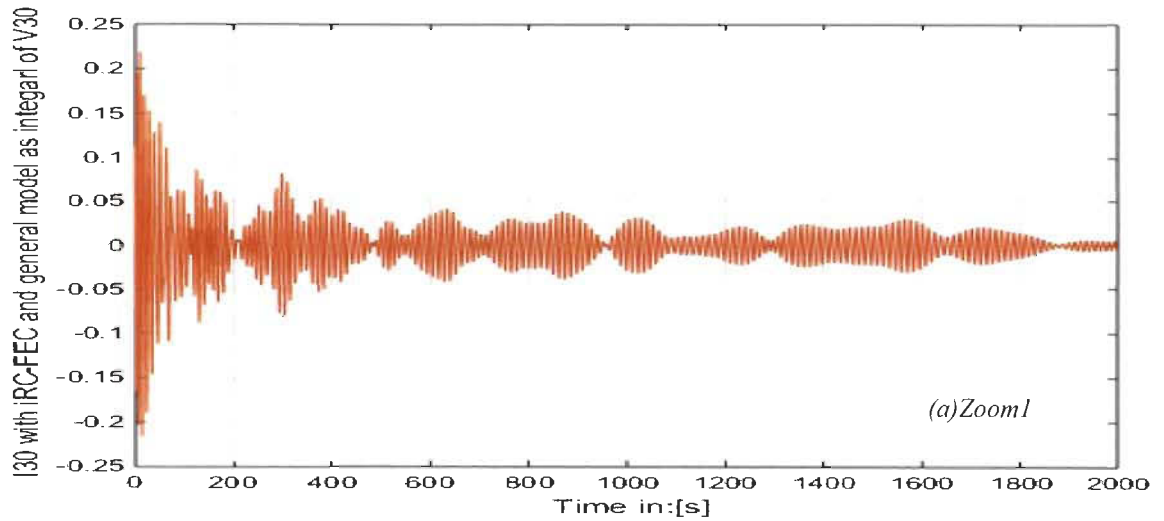


Figure 7. 30: Matlab-Simulink iRC-FEC and general model ($V_{30}^{(1,1)}$, $I_i = 1A$, $R = \sqrt{\frac{L}{C}}$) as integral of $I_{30}^{(1,1)}$



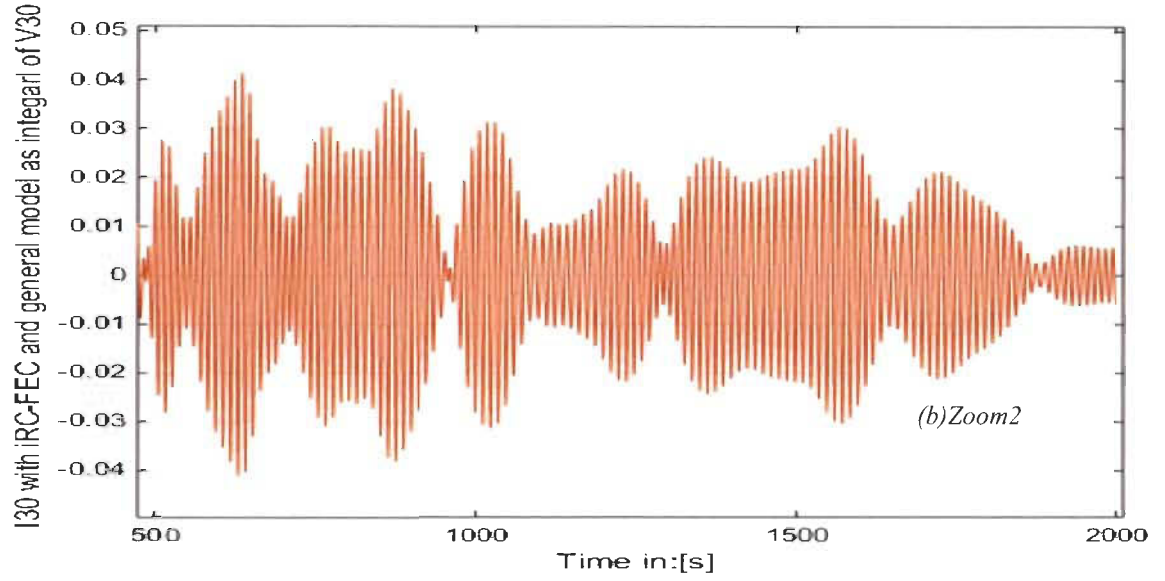


Figure 7.31: Matlab-Simulink iRC-FEC and general model ($I_{30}^{(1,1)}$, $I_i = \mathbf{1A}$, $R = \sqrt{\frac{L}{c}}$) as integral of $V_{30}^{(1,1)}$

Figures 7.32 and 7.33 show the behavior of all voltages in each inductor (even order) and all currents of each capacitor (odd order) using general model of figure 7.17 and compared with iRC-FEC circuit (figure 7.16) for $(K, x_c) = (1,1)$.

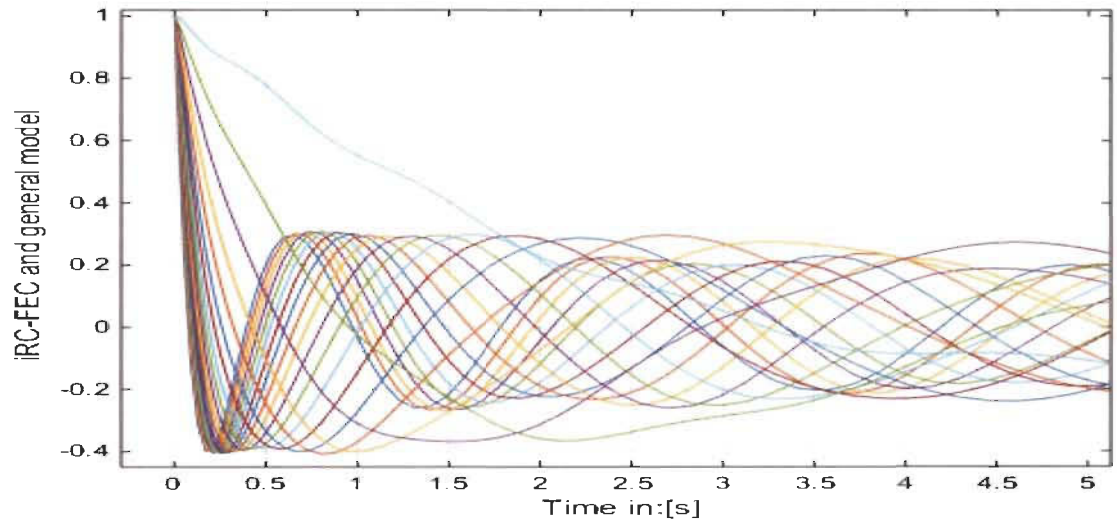


Figure 7.32: Matlab-Simulink iRC-FEC and general model ($V_2^{(1,1)}, V_4^{(1,1)}, \dots, V_{40}^{(1,1)}$, $R = \sqrt{\frac{L}{c}}$) across inductors

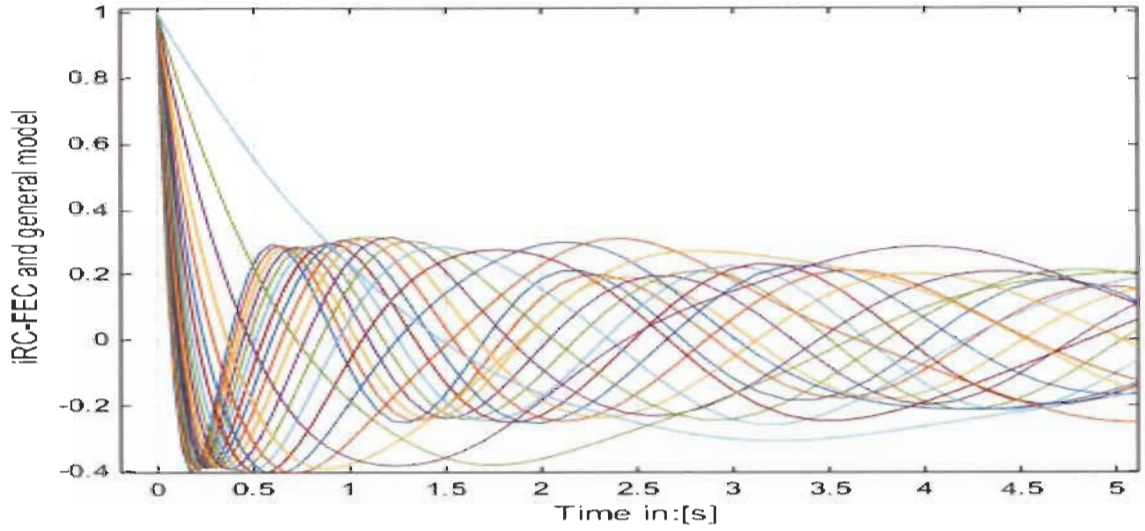


Figure 7.33: Matlab-Simulink iRC-FEC and general model $(I_1^{(1,1)}, I_3^{(1,1)}, \dots, I_{39}^{(1,1)}, R = \sqrt{\frac{L}{C}})$ across capacitors

7.8 Controller Design new Approach applied to iFWFs

The controller design new approach developed in chapter 3 will be applied to these iFWFs based on their first order transfer function source.

$$g_{-1}^{(k,x)}(s) = \frac{K}{s^{-1} + x} = \frac{s(\frac{K}{x})}{s + \frac{1}{x}}$$

$$x = x_c = RC \text{ or } x = x_L = \frac{L}{R}$$

$$\frac{g_{-1}^{(k,x)}(s)}{s} = \frac{(\frac{K}{x})}{s + \frac{1}{x}} \quad (7.18)$$

From equation (4.10), coefficients K_p , K_i will be determined based on the first order of equation (7.18).

$$K_p = \frac{2\xi\omega_n - (\frac{1}{x})}{(\frac{K}{x})} \quad ; \quad K_i = \frac{\omega_n^2}{(\frac{K}{x})} \quad (7.19)$$

This controller will be designed for the two cases studied previously $(K, x) = (1,1)$ and $(K, x) = (1,4)$ and applied to all recursive inverse Fibonacci wave functions.

The closed loop transfer function controller based on equation (7.18) will be.

$$C(s) = (K_p + \frac{K_i}{s}) \frac{1}{s} \quad (7.20)$$

A. Case #1: $(K, x) = (1,1)$.

The choice of ω_n should be outside the resonance and anti-resonance frequencies. The chosen ω_n is 100 rad/s. For $\xi = 2$, the coefficients of the controller using (7.19) are :

$$K_p = 399 \quad ; \quad K_i = 10000 \quad (7.21)$$

Simulation was conducted in closed loop of all iFWFs systems $g_{-1}^{(1,1)}(s), \dots, g_{-40}^{(1,1)}(s)$, the outputs are exactly the same as shown in figure 7.34.

B. Case #2: $(K, x) = (1,4)$.

From bode figure 4.20, the choice of ω_n should be outside the frequencies of resonance and anti-resonances. The choice of ω_n is 250 rad/s and $\xi = 2$, and the coefficients of the controller using (29) are :

$$K_p = 3999 \quad ; \quad K_i = 250000 \quad (7.22)$$

A simulation was made in closed loop of all FWFs systems $g_1^{(1,4)}(s), \dots, g_{40}^{(1,4)}(s)$, the outputs are exactly the same as it is in figure 7.34.

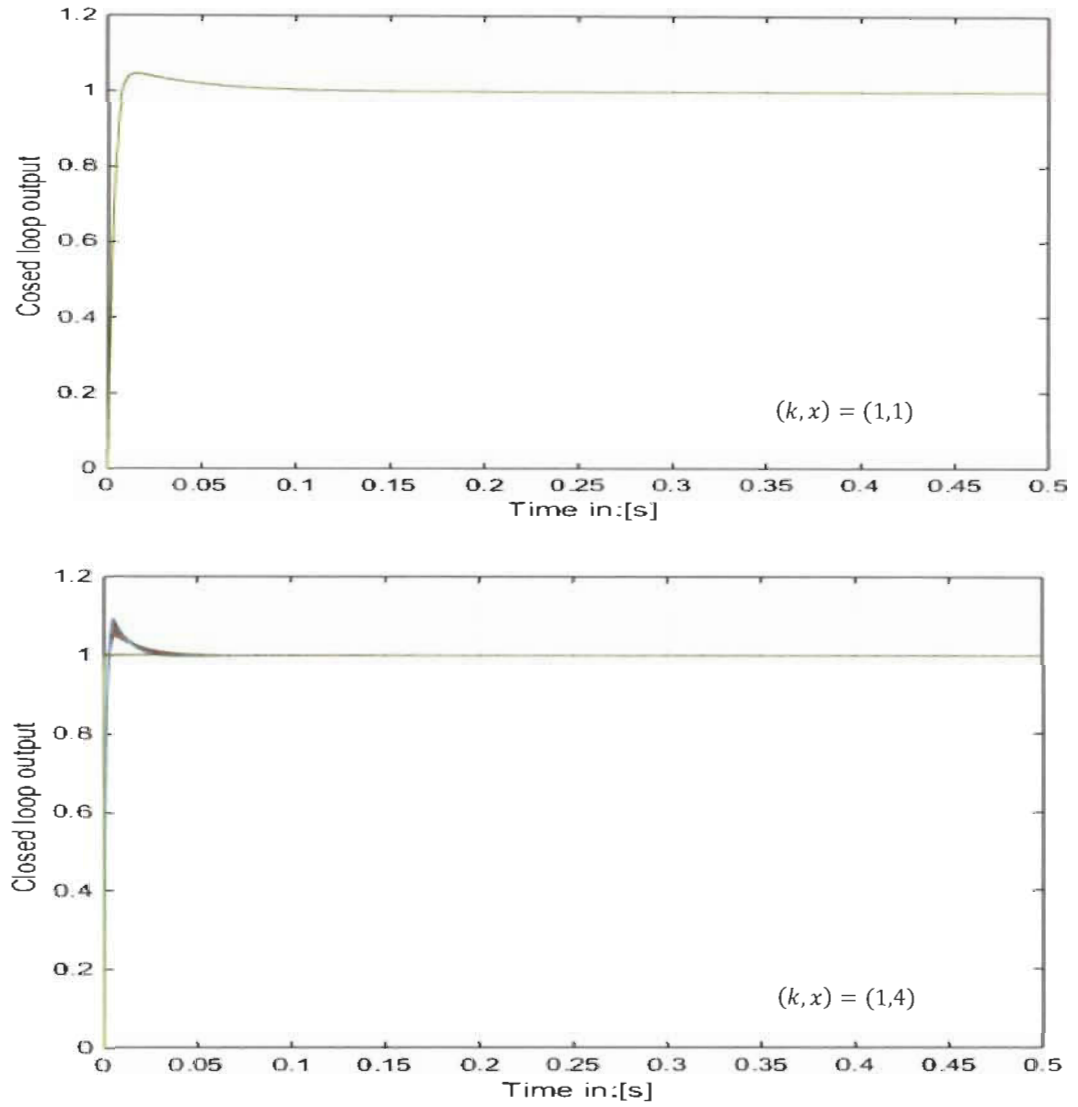


Figure 7. 34: Output response in closed loop of FWFs $g_1^{(1,1)}(s), \dots, g_{40}^{(1,1)}(s), g_1^{(1,4)}(s), \dots, g_{40}^{(1,4)}(s)$.

7.9 Inverse Fibonacci boundary wave functions

In the same way as LC ladder network presented in chapter 5 and spring mass chain presented in chapter 6, the inverse LC ladder network wave functions can be determined easily from Pascal triangle general form. Below is an example of $g_{-14}^{(k,x)}$ using Pascal's triangle in table 7.2.

$$\begin{aligned}
den_{-14}^{(k,x)} &= 1s^{-14} + 1xs^{-13} + 13Ks^{-12} + 12Kxs^{-11} + 66K^2s^{-10} + 55K^2xs^{-9} \\
&\quad + 165K^3s^{-8} + 120K^3xs^{-7} + 210K^4s^{-6} + 126K^4xs^{-5} + 126K^5s^{-4} \\
&\quad + 56K^5xs^{-3} + 28K^6s^{-2} + 7K^6xs^{-1} + 1K^7 \\
den_{-13}^{(k,x)} &= 1s^{-13} + 1xs^{-12} + 12Ks^{-11} + 11Kxs^{-10} + 55K^2s^{-9} + 45K^2xs^{-8} + 120K^3s^{-7} \\
&\quad + 84K^3xs^{-6} + 126K^4s^{-5} + 70K^4xs^{-4} + 56K^5s^{-3} + 21K^5xs^{-2} + 7K^6s^{-1} \\
&\quad + 1K^6x \\
den_{-12}^{(k,x)} &= 1s^{-12} + 1xs^{-11} + 11Ks^{-10} + 10Kxs^{-9} + 45K^2s^{-8} + 36K^2xs^{-7} + 84K^3s^{-6} \\
&\quad + 56K^3xs^{-5} + 70K^4s^{-4} + 35K^4xs^{-3} + 21K^5s^{-2} + 6K^5xs^{-1} + 1K^6
\end{aligned} \tag{7.23}$$

For iRL-FEC in figure 7.19 for order 13 and 14.

$$\begin{aligned}
\left(\frac{CV_o}{I_i}\right)_{-13}^{(K,x_L)} &= g_{-13}^{(K,x_L)}(s) = \frac{Kden_{-12}^{(K,x_L)}(s)}{den_{-13}^{(K,x_L)}(s)} \\
\left(\frac{LI_o}{V_i}\right)_{-14}^{(K,x_L)} &= g_{-14}^{(K,x_L)}(s) = \frac{Kden_{-13}^{(K,x_L)}(s)}{den_{-14}^{(K,x_L)}(s)} \\
x = x_L &= \frac{L}{R}
\end{aligned} \tag{7.24}$$

For iRC-FEC circuit in figure 7.16 for order 13 and 14.

$$\begin{aligned}
\left(\frac{CV_o}{I_i}\right)_{-14}^{(K,x_c)} &= g_{-14}^{(K,x_c)}(s) = \frac{Kden_{-13}^{(K,x_c)}(s)}{den_{-14}^{(K,x_c)}(s)} \\
\left(\frac{LI_o}{V_i}\right)_{13}^{(K,x_L)} &= g_{13}^{(K,x_c)}(s) = \frac{Kden_{-12}^{(K,x_c)}(s)}{den_{-13}^{(K,x_c)}(s)} \\
x = x_c &= RC
\end{aligned} \tag{7.25}$$

Note that based on which Fibonacci circuit, either iRC-FEC or iRL-FEC, one can easily determine the input impedance or input admittance for any order n and for both short-circuit and open-circuit using only Pascal's triangle general form.

For a short-circuit ($R = 0\Omega$), $x_c = 0$ using iRC-FEC and $x_L = \infty$ using iRL-FEC. Equations (7.23), (7.24) and (7.25) become.

$$\begin{aligned}
\left(\frac{LI_o}{V_i}\right)_{-14L}^{(K,\infty)} &= g_{-14L}^{(K,\infty)}(s) = K * \frac{1s^{-12} + 11Ks^{-10} + 45K^2s^{-8} + 84K^3s^{-6} + 70K^4s^{-4} + 21K^5s^{-2} + 1K^6}{1s^{-13} + 12Ks^{-11} + 55K^2s^{-9} + 120K^3s^{-7} + 126K^4s^{-5} + 56K^5s^{-3} + 7K^6s^{-1}} \\
\left(\frac{CV_o}{I_i}\right)_{-13L}^{(K,\infty)} &= g_{-13L}^{(K,\infty)}(s) = K * \frac{1s^{-11} + 10Ks^{-9} + 36K^2s^{-7} + 56K^3s^{-5} + 35K^4s^{-3} + 6K^5s^{-1}}{1s^{-12} + 11Ks^{-10} + 45K^2s^{-8} + 84K^3s^{-6} + 70K^4s^{-4} + 21K^5s^{-2} + 1K^6} \\
\left(\frac{LI_o}{V_i}\right)_{-13c}^{(K,0)} &= g_{-13c}^{(K,0)}(s) = K * \frac{1s^{-12} + 11Ks^{-10} + 45K^2s^{-8} + 84K^3s^{-6} + 70K^4s^{-4} + 21K^5s^{-2} + 1K^6}{1s^{-13} + 12Ks^{-11} + 55K^2s^{-9} + 120K^3s^{-7} + 126K^4s^{-5} + 56K^5s^{-3} + 7K^6s^{-1}} \\
\left(\frac{CV_o}{I_i}\right)_{-14c}^{(K,0)} &= g_{-14c}^{(K,0)}(s) = K * \frac{1s^{-13} + 12Ks^{-11} + 55K^2s^{-9} + 120K^3s^{-7} + 126K^4s^{-5} + 56K^5s^{-3} + 7K^6s^{-1}}{1s^{-14} + 13Ks^{-12} + 66K^2s^{-10} + 165K^3s^{-8} + 210K^4s^{-6} + 126K^5s^{-4} + 28K^6s^{-2} + 1K^7}
\end{aligned} \tag{7.26}$$

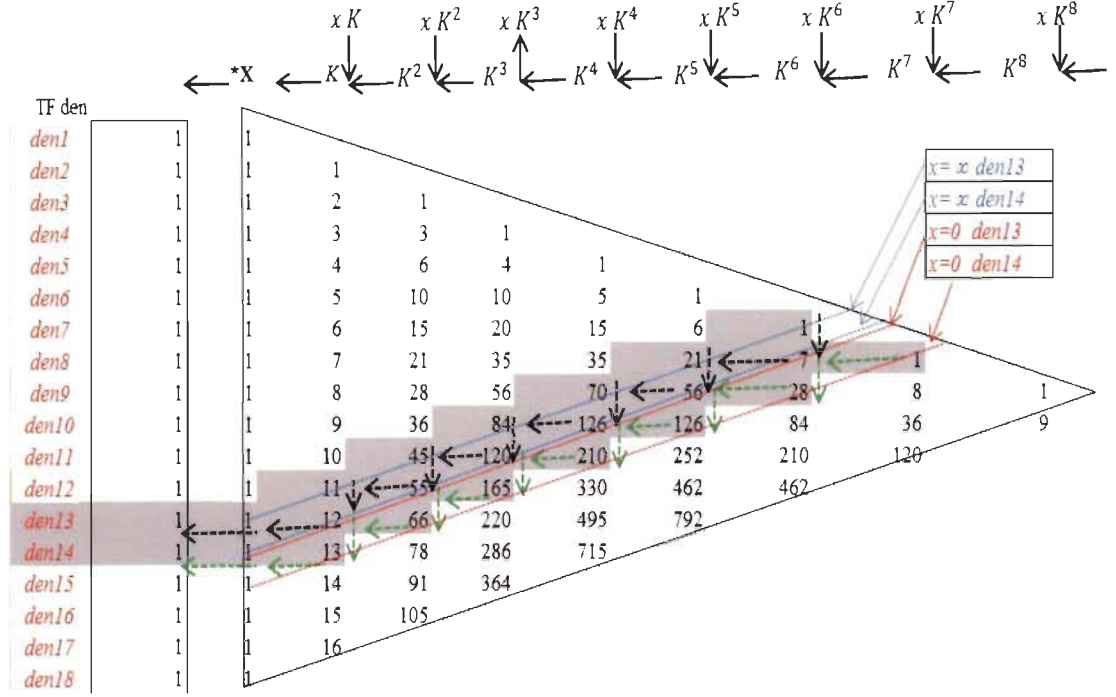
For an open-circuit ($R = \infty, \Omega$), $x_c = \infty$ using iRC-FEC and for iRL-FEC $x_L = 0$.

Equations (7.23), (7.24) and (7.25) become.

$$\begin{aligned}
\left(\frac{CV_o}{I_i}\right)_{-14c}^{(K,\infty)} &= g_{-14c}^{(K,\infty)}(s) = K * \frac{1s^{-12} + 11Ks^{-10} + 45K^2s^{-8} + 84K^3s^{-6} + 70K^4s^{-4} + 21K^5s^{-2} + 1K^6}{1s^{-13} + 12Ks^{-11} + 55K^2s^{-9} + 120K^3s^{-7} + 126K^4s^{-5} + 56K^5s^{-3} + 7K^6s^{-1}} \\
\left(\frac{LI_o}{V_i}\right)_{-13c}^{(K,\infty)} &= g_{-13c}^{(K,\infty)}(s) = K * \frac{1s^{-11} + 10Ks^{-9} + 36K^2s^{-7} + 56K^3s^{-5} + 35K^4s^{-3} + 6K^5s^{-1}}{1s^{-12} + 11Ks^{-10} + 45K^2s^{-8} + 84K^3s^{-6} + 70K^4s^{-4} + 21K^5s^{-2} + 1K^6} \\
\left(\frac{CV_o}{I_i}\right)_{-13L}^{(K,0)} &= g_{-13L}^{(K,0)}(s) = K * \frac{1s^{-12} + 11Ks^{-10} + 45K^2s^{-8} + 84K^3s^{-6} + 70K^4s^{-4} + 21K^5s^{-2} + 1K^6}{1s^{-13} + 12Ks^{-11} + 55K^2s^{-9} + 120K^3s^{-7} + 126K^4s^{-5} + 56K^5s^{-3} + 7K^6s^{-1}} \\
\left(\frac{LI_o}{V_i}\right)_{-14L}^{(K,0)} &= g_{-14L}^{(K,0)}(s) = K * \frac{1s^{-13} + 12Ks^{-11} + 55K^2s^{-9} + 120K^3s^{-7} + 126K^4s^{-5} + 56K^5s^{-3} + 7K^6s^{-1}}{1s^{-14} + 13Ks^{-12} + 66K^2s^{-10} + 165K^3s^{-8} + 210K^4s^{-6} + 126K^5s^{-4} + 28K^6s^{-2} + 1K^7}
\end{aligned} \tag{7.27}$$

These Boundary wave functions can be also derived easily from Pascal triangle general form as shown in the table below.

Table 7. 5: Pascal's triangle general form Inverse for boundary iFWF with $(k, 0)$ & (k, ∞) .



Simulation for short and open circuit were conducted using general model, iRC-FEC and iRL-FEC for $n = 40$. $V_{33}^{(1,x_L=0)}$, $I_{32}^{(1,x_L=0)}$, $V_{40}^{(1,x_c=0)}$, $I_{29}^{(1,x_c=0)}$ with their respective integral $I_{33}^{(1,x_L=0)}$, $V_{32}^{(1,x_L=0)}$, $I_{40}^{(1,x_c=0)}$, $V_{29}^{(1,x_c=0)}$ are shown in figures 7.35, 7.36, 7.37, 7.38, 7.39, 7.40, 7.41 and 7.42.

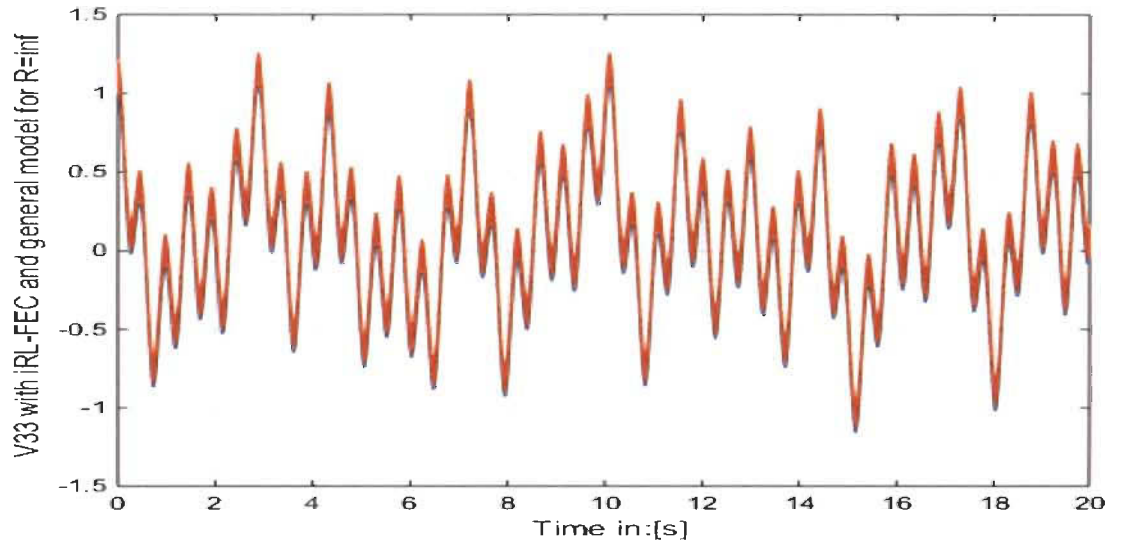


Figure 7. 35: iRL-FEC and general model ($V_{33}^{(1,0)}$, $V_i = 1V$, $R = \infty\Omega$)

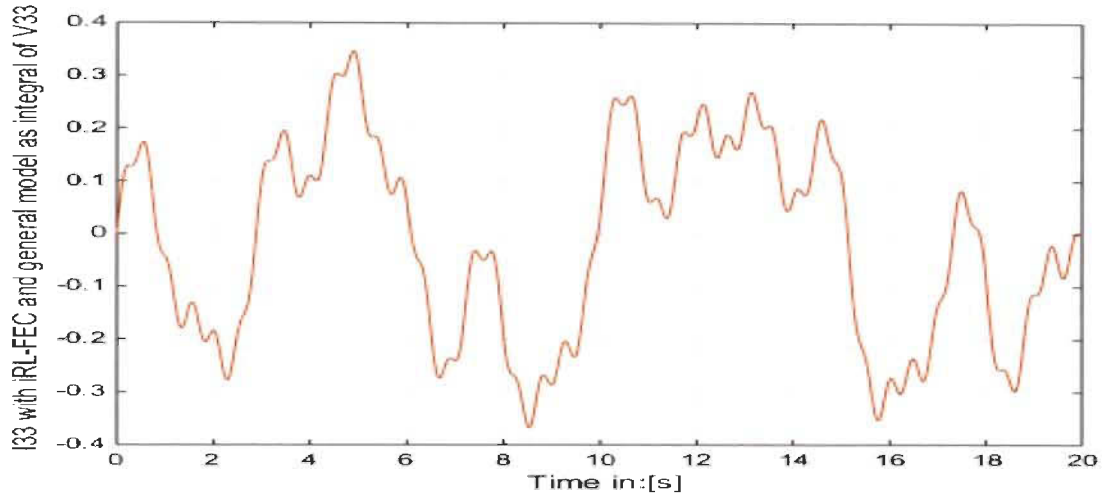


Figure 7.36: iRL-FEC and general model ($I_{33}^{(1,0)}$, $V_i = 1V$, $R = \infty\Omega$) as integral of $V_{33}^{(1,0)}$

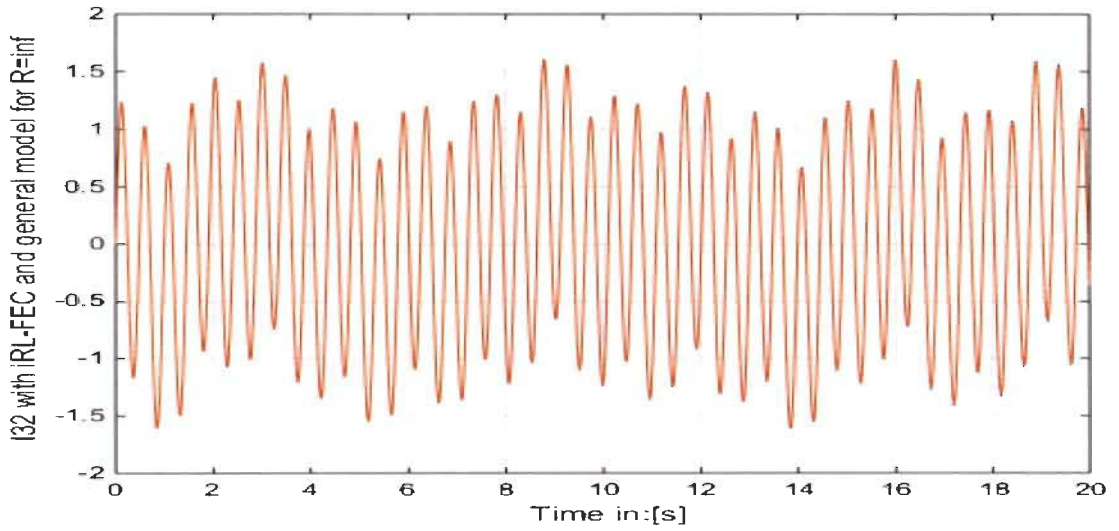


Figure 7.37: iRL-FEC and general model ($I_{32}^{(1,0)}$, $V_i = 1V$, $R = \infty\Omega$)

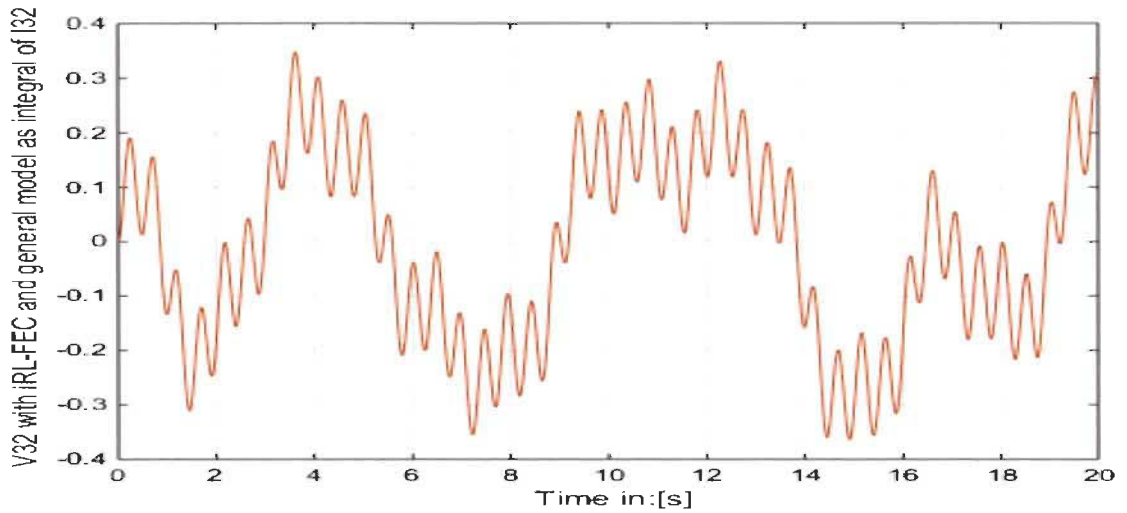


Figure 7.38: iRL-FEC and general model ($V_{32}^{(1,0)}$, $V_i = 1V$, $R = \infty\Omega$) as integral of $I_{32}^{(1,0)}$

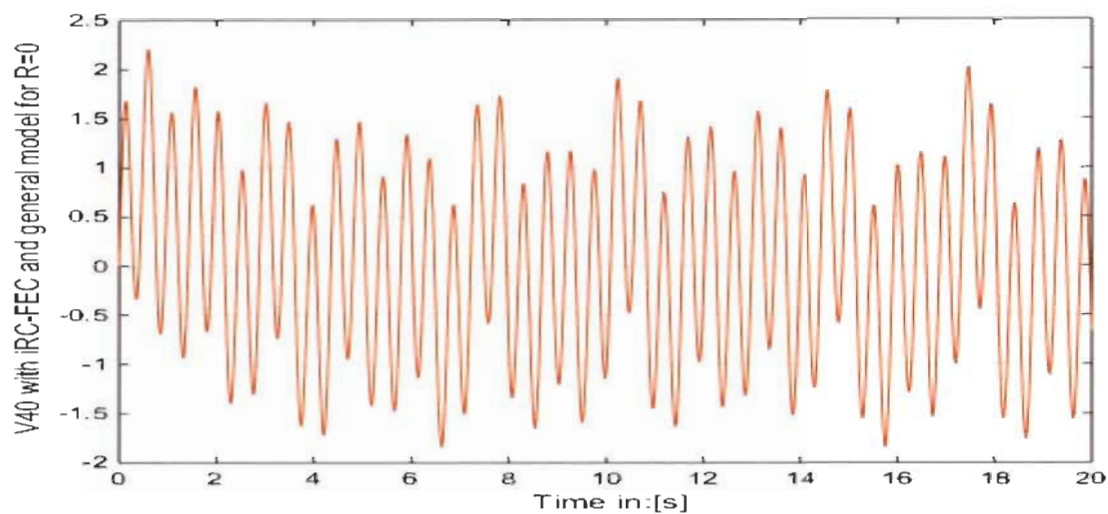


Figure 7. 39: iRC-FEC and general model ($V_{40}^{(1,0)}$, $I_i = 1A$, $R = 0\Omega$)

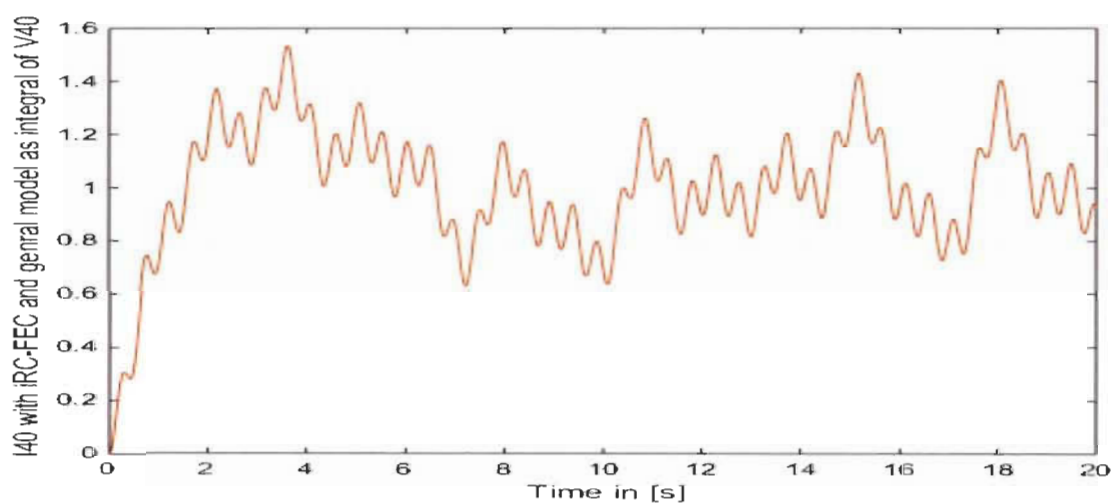


Figure 7. 40: iRC-FEC and general model ($I_{40}^{(1,0)}$, $I_i = 1A$, $R = 0\Omega$) as integral of $V_{40}^{(1,0)}$

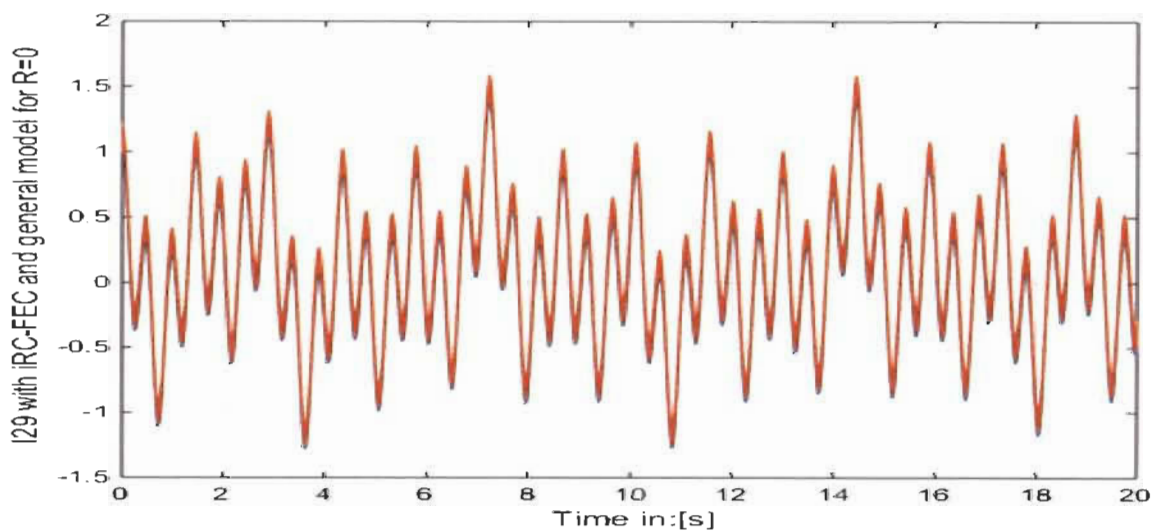


Figure 7. 41: iRC-FEC and general model ($I_{29}^{(1,0)}$, $I_i = 1A$, $R = 0\Omega$)

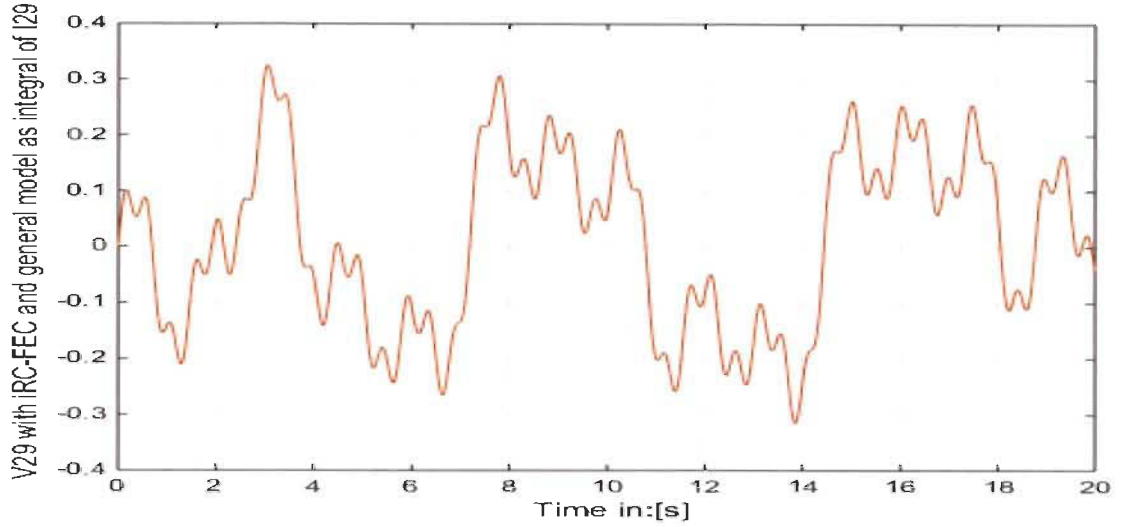


Figure 7. 42: iRC-FEC and general model ($V_{29}^{(1,0)}$, $I_i = 1A$, $R = 0 \Omega$) as integral of $I_{29}^{(1,0)}$

7.10 Conclusion

In this chapter, a complete inverse LC ladder general model based on Fibonacci wave functions iFWFs was introduced. The importance for inverse LC ladder comes from its application that can be found in the literature like piezoelectric. The detailed model that is proposed for each inverse LC ladder branch with precise inverse Fibonacci wave functions shows that the simulation and the model are perfectly the same for each inductor voltage and capacitor current.

The inverse LC ladder input impedance or admittance can be derived using Pascal's triangle general form presented in two forms in Table 7.2 and Table 7.3 with defined coefficients K , x_L and x_C .

Short-circuit and open-circuit were studied and simulated for both inverse Fibonacci boundary wave functions and its Fibonacci electrical circuit to show that these cases are particular cases of the general model and their Fibonacci wave functions are easy to determine based on Pascal's triangle presented in table 7.3 for short load ($x_C = \infty$ and $x_L = 0$) and for open load ($x_L = \infty$ and $x_C = 0$).

Chapter 8: General conclusion

8.1 General conclusion

This research presents new reduction method based on first order transfer function approximation. It can be extended to all systems with different type of outputs having different type of overshoot and oscillations. The concept of similar systems was introduced for the first time to overcome all mathematical equations needed to model the complex systems and to avoid classical reduction methods that are based on the knowledge of the transfer function of the real system. These classical reduction methods use different mathematical theories to reduce the original systems to an identical reduced system like pade approximation [3], [8], pole clustering [4], [17] and integral square error (ISE) [1], [6] and many others in the literature [2], [5], [10], [14-19].

The proposed new reduction method is based on predefined elements $\psi_1, \psi_2, \psi_3, \psi_4, \psi_5$ and ψ_6 that characterize the real and the approximated system. These weighted elements are determined only from the complex system output response.

Simulation results in closed loop for the five investigated case studies show the performance of the new reduction method even if the approximate system is not identical. The fact that both real and approximated systems are similar in their significant weighted elements, allows designing controllers based on the approximated first order system. The design and the implementation of a PI controller using this approach and applied to the real system show impressive results. The PI controller was chosen because of its simplicity to design and implement when applied to a first order system. Another controller type could be

chosen to control these complex systems since it will be based on this approximated first order.

Specific systems called Fibonacci systems FWFs with high degree of their transfer functions have been highlighted from a source of first order transfer function. These FWFs have interesting behaviors.

- ✓ The coefficients of their denominators perfectly follow the golden triangle or Pascal's triangle and they also respect the golden ratio $\phi = 1.618$
- ✓ Their poles are located in harmony with each other following the Fibonacci pattern and specific distribution for their real and imaginary parts.
- ✓ Frequency spectrum of these FWFs present resonance and anti-resonance frequencies perfectly ordered in harmony with each other.
- ✓ Their output responses present multiple intermediate steady states. Their final steady states have continuous oscillations with low amplitudes.
- ✓ These Fibonacci systems are irreducible. It is impossible to reduce their transfer functions to a second or third order degree.
- ✓ Each FWF system $g_n^{(K,x)}(s)$ has two Fibonacci boundaries $g_n^{(K,0)}(s)$ and $g_n^{(K,\infty)}(s)$ that can be determined from Pascal's triangle.

The application of any reduction method in the literature as Pade approximation method, the integral square error (ISE) or other methods cannot reduce such systems to a second or third order system.

By applying the controller design new approach to these systems based on their source of first-order transfer function, the simulation results in closed loop are very impressive for the fact that all output responses are perfectly same.

In this research, a complete LC ladder general model based on Fibonacci wave functions FWFs was introduced. The importance for LC ladder comes from its application that can be found in the literature like lossless transmission lines model, the sound propagation model in the ear and in quantum mechanics to understand the interaction between the particles. The detailed model that is proposed for each LC ladder branch with precise Fibonacci transfer functions shows that the simulation and the model are perfectly same for each inductor current and capacitor voltage. The general model using the charge in the capacitor and the flux in the inductor for each branch is also presented for all charge and flux LC ladder branches.

The LC ladder input impedance or admittance can be derived using Pascal's triangle general form presented in section VII with defined coefficients K , x_L and x_c .

Transmission lines, short-circuit and open-circuit were studied and simulated for both Fibonacci model and Fibonacci electrical circuit to show that these cases are particular cases of general model and their Fibonacci transfer functions are easy to determine based on Pascal's triangle for short load ($x_c = \infty$ and $x_L = 0$) and for open load ($x_L = \infty$ and $x_c = 0$) and Table 3.1.

The inverse LC ladder network was introduced with its general model using inverse Fibonacci wave function (iFWF). The study shown how these wave functions can be determined easily from Pascal triangle general form using the inverse steps path for any order. The input impedance or admittance can be also found for the three cases (with, without or infinite load).

The LC ladder general model for energy transfer between L and C in each section can be used for many other applications that use lossless LC recursive circuit as model for more research and analysis especially, in quantum mechanics, biology and communication.

Fibonacci spring mass chain (FSMC) was also introduced and modelled by these theoretical FWFs. The FSMC is very important based on their application in quantum mechanics and fluid mechanics to analyze the behavior of particles from motion point of view. A combination of LC ladder general model related to charge and flux and FSMC general model related to momentum and position can help understand the relationship between electrical and mechanical behavior of particles.

References

- [1] S. K. Agrawal, Dinesh Chandra and Irfan Ali Khan “Controller design based on ISE Minimization and Dominant Pole Retention Method”, *International Journal on Computer Science and Engineering*, Vol. 02, No. 07, 2010, pp 2242-2245.
- [2] P. Ponmurugan and G. Prakash “Controller Design for Linear Time Invariant System with Improved Pade Approximation”, *International Journal of Micro and Nano-Electronics, Circuits and Systems*, 3(1), 2011, pp 17-22.
- [3] C. B. Vishwakarma “Order Reduction using Modified Pole Clustering and Pade Approximations”, *International Journal of Electrical, Computer, Energetic, Electronic and Communication Engineering*, Vol. 5, No. 8, 2011.
- [4] G.Vasu, P.Murari, R.Prasanna Kumar “Reduction of Higher Order Linear Dynamic SISO and MIMO Systems Using the Advantages of Improved Pole Clustering and PSO”, *International Conference on Advances in Computer, Electronics and Electrical Engineering*, 2012 pp 6-11.
- [5] J. C. Basilio and S. R. Matos “Design of PI and PID Controllers With Transient Performance Specification”, *IEEE Transactions on Education*, Vol. 45, No 4, 2002, pp 364-370.
- [6] Singh, V, Chandra, Dinesh, and Kar “Optimal Routh Approximants Through Integral Squared Error Minimization : Computer- aided approach, “*IEE Proc., Control Theory Appl.*, Vol. 151, pp. 53-58, 2004.

- [7] P O Gutman, C F Mannerfelt and P Molander “Contributions to the Model Reduction Problems”, *IEEE Transactions on Automatic Control*, Vol. 27, No. 2, pp. 454-455, 1982.
- [8] Y Shamash, “Model Reduction Using the Routh Stability Criterion and the Pade Approximation Technique”, *International Journal of Control*, Vol. 21, No. 3, pp. 475-484, 1975.
- [9] T. Manigandan, N. Devarajan, S.N. Sivanandam, “Design of PID Controller using Reduced Order Model”, *Academic Open Internet Journal*, Volume 15, 2005.
- [10] Y. Dolgin, E. Zeheb “On Routh-Pade Model Reduction of Interval Systems”, *IEEE Transaction on Automation Control*, Vol. 48, pp. 1610-1612, 2003.
- [11] N. S. Tanwar, R. Bhatt and G. Parmar “Order Reduction of Interval Systems using Big Bang Big Crunch and Routh Approximation”, *1st Inter. Conference on Power Electronics, Intelligent Control and Energy Systems*, Vol. 1, pp. 1-5, 2016.
- [12] B. Bandyopadhyay “ γ - δ Routh Approximations for Interval Systems”, *IEEE Transactions on Automatic Control*, 42, 1127-1130, 1997.
- [13] G.D. Howitt, and R. Luus “Model reduction by minimization of integral square error performance indices”, *Journal of Franklin Inst.*, Vol. 327, pp. 343-357, 1990.
- [14] Y. Dolgin, E. Zeheb “On Routh-Pade Model Reduction of Interval Systems”, *IEEE Transactions on. Automatic Control*, Vol. 48, pp. 1610-1612.
- [15] Y. Bistritz, G. Langholz, “Model Reduction by Chebyshev polynomial techniques”, *IEEE Transactions on Automatic Control*, Vol. AC-25, No.5, pp. 741-747.

- [16] S. Mukherjee, Satakshi, R.C Mittal “Model Error Reduction using response matching”, *Journal of Franklin Inst.* Vol. 342, No.5, pp. 503-519. 2005.
- [17] C.B. Vishwakama, R. Prasad “MIMO System Reduction using Modified Pole Clustering and Genetic Algorithm”, *Modelling and Simulation in Engineering, Hindawi Pub. Corp., USA*, Vol. 2009, pp. 1-6. 2009.
- [18] R. Mansouri, M. Bittayeb, S. Djennoine “Approximation of High Order Integer System By Fractional Order Reduced-Parameters Models”, *Mathematical & Computer Modelling Journal*, Vol. 51(2010), pp. 53-62. 2010.
- [19] K. Mohamed Hussain, R. Allwyn Rajendran Zepherin², M. Shantha Kumar “Comparison of Tuning Methods of PID Controllers for FOPTD System”, *International Journal of Innovative research in Electrical, Electronics, Instrumentation and Control Engineering*, Vol. 2, Issue 3, March 2014, pp 1177-1180.
- [20] S. Hissem, M. L. Doumbia “New Fibonacci Recurrent Systems Applied to Transmission Lines Input Impedance and Admittance”, *IEEE Conference on Advances Science and Engineering Technology (ASET), March 2019*.
- [21] Joshua W. Phinney, David J. Perreault and Jeffrey H. Lang, "Synthesis of Lumped Transmission Line Analogs", *37th IEEE Power Electronics Specialists Conference*, June 2006, pp. 2967-2978.
- [22] A. D'Amico, C. Falconi, M. Bertsch, G. Ferri, R. Lojacono, M. Mazzotta, M. Santonico and G. Pennazza, "The Presence of Fibonacci Numbers in Passive Ladder Networks: The Case of Forbidden Bands", *IEEE Antennas and Propagation Magazine*, Vol. 56, No. 5, pp. 275-287, 2014.

- [23] N. Naggai and T. Yahagi, "Symmetric Lossless Circuit Constituted with Image Connection of Asymmetric Circuits", *Journal of Signal Processing*, Vol. 21, No. 2, pp. 81-87, March 2017.
- [24] Clara M. Ionescu, "Phase Constancy in a Ladder Model of Neural Dynamics", *IEEE Transactions on Systems. Man & Cybernetics*, Vol. 42, No. 6, pp. 1543-1551, 2012
- [25] Ana Flavia G. Greco, Joaquim J. Barroso, Jose O. Rossi, "Modelling and Analysis of Ladder-Network Transmission Lines with Capacitive and Inductive Lumped Elements", *Journal of Electromagnetic Analysis and Applications*, 2013, 5, pp. 213-218
- [26] Clara Ionescu, Aain Oustaloup, Francois Levron, Pierre Melchior, Jocelyn Sabatier, Robin De Keyser, "A Model of Lungs Based on Fractal Geometrical and Structural Properties", *Proceedings of the 15th IFAC Symposium on System Identification*, July 2019, pp. 994-999.
- [27] S. J. Van Enk, "Paradoxical Behavior of an Infinite Ladder Network of Inductors and Capacitors", *American Journal of Physics*, Vol. 68, No. 9, September 2000, pp. 854-856.
- [28] T. C. Scott, P. Marketos, "On the Origin of Fibonacci Sequence", *Mac Tutor History of Mathematics*, March 2014.
- [29] W. Sriratana, R. Murayama and L. Tanachaikhan, "Synthesis and Analysis of PZT using Impedance method of Reactance Estimation", *Advances in Materials Physics and Chemistry*, 2013, 3, pp. 62-70.

- [30] R. Lojacono, C. Falconi, G. Ferri, E. Lo Castro, M. Salmeri, A. Mencattini, M. Santonic, G. Pennazza and A. D'Amico, "The Role of the Characteristic Load Impedance in Passive Ladder Networks: Again the Presence of Fibonacci Sequence", *World Journal of Research and Review*, Vol. 3, No. 6, Dec 2016, pp. 21-29.
- [31] Petr Augusta and Zdeněk Hurák, "Distributed stabilisation of spatially invariant systems: positive polynomial approach", *Multidimensional Systems and Signal Processing*, pages 1–19, 2013.
- [32] H. Ojima, K. Nagase, and Y. Hayakawa, "Wave-based analysis and wave control of damped mass-spring systems—characterization from the propagation constants", *Transactions of the Society of Instrument and Control Engineers*, 38(3):239–246, 2002.
- [33] William J. O'Connor and Ming Zhu, "Travelling waves in boundary controlled, non-uniform, cascaded lumped systems", *Mechanical Systems and Signal Processing*, 39(1–2):108–118, August 2013.
- [34] Yoram Halevi, "Control of Flexible Structures Governed by the Wave Equation Using Infinite Dimensional Transfer Functions", *Journal of Dynamic Systems, Measurement, and Control*, Vol. 127, No. 4, pp. 579-588, December 2004.
- [35] Zdenek Hurak and Michael Sebek, "2d polynomial approach to stability of platoons of vehicles", In *Proceedings of the 2nd IFAC Workshop on Distributed Estimation and Control in Networked Systems*, volume 2, Centre de Congres de L'Imperial Palace, Annecy, France, 2010.

- [36] Zdenek Hurak and Michael Sebek, "Travelling Wave and Scattering in Control of Chains", Advanced Algorithm for Control and communication, Technical Reports Publication, 2015.
- [37] H. Ojima, K. Nagase, and Y. Hayakawa, "Wave-based analysis and wave control of damped mass-spring systems characterization from the propagation constants", Transactions of the Society of Instrument and Control Engineers, Vol. 38, No. 3, pp. 239-246, 2002.
- [38] S. S. Ge, L. Huang and T. H. Lee, "Position Control of Chained Multiple Mass-Spring-Damper Systems Adaptive Output Feedback Control Approaches", International Journal of Control and Systems Vol. 2, No. 2, pp. 144-155, June 2004.

Appendix A: Résumé étendu

A.1 Introduction

Dans la littérature, la majorité des méthodes de réduction des systèmes complexes sont basées sur la connaissance de leurs fonctions de transfert. Ces méthodes de réduction ont différentes approches pour réduire ces fonctions de transfert en une fonction de transfert de second ordre identique. Ces méthodes ont une particularité commune, leurs approches sont basées sur beaucoup d'équations mathématiques. Une fois le système réduit est identifié, la conception du contrôleur est mise au point en se basant sur ce système réduit. Ce contrôleur sera ensuite appliqué au système réel.

A.1.1 Problématique de recherche

La problématique de recherche consiste à mettre au point un contrôleur d'un système de type boîte noire sans avoir à déterminer sa fonction de transfert. A cet effet, il est nécessaire de développer une approche de réduction ne nécessitant pas beaucoup d'équations mathématiques en se basant seulement sur la réponse de sortie du système de type boîte noire.

La notion de systèmes similaires sera la colonne vertébrale de cette approche. Cette notion de similarité entre systèmes sera définie en utilisant les éléments de poids qui caractérisent chaque système. Ces éléments de poids doivent être identiques pour que les deux systèmes soient similaires. Ces éléments seront déterminés seulement à partir de la réponse du système de type boîte noire sans avoir à déterminer sa fonction de transfert.

A.1.2 Objectif de recherche

A.1.2.1 Contribution de recherche

La première contribution de cette thèse est de développer une approche de réduction basée sur le concept de similarité. Cette technique utilisera uniquement la caractéristique de la réponse du système complexe ou en boîte noire. Cette réponse de sortie sera obtenue soit par expérimentation, soit par simulation. Basé sur cette notion de similitude, il y aura toujours un système similaire de premier ordre qui coïncide avec le système réel seulement dans ces éléments de poids. Pour cela, ces éléments doivent être bien définis.

Une fois que le système de premier ordre est identifié, la conception du contrôleur sera mise au point et sera appliquée au système réel.

La deuxième contribution de cette thèse est d'introduire des systèmes théoriques complexes qui ont la particularité d'avoir des fonctions de transfert irréductibles et que les méthodes de réduction classiques ne peuvent pas les réduire à des systèmes de second ordre. Ceci mettra en évidence leurs limitations. Par contre, la nouvelle approche basée sur le système similaire de premier ordre sera toujours valide même si elle est appliquée à ces systèmes irréductibles et nous permettra la mise au point du contrôleur pour ce type de système.

La dernière contribution de cette thèse est de mettre en évidence des applications concrètes de ces systèmes théoriques irréductibles dits de Fibonacci.

Des circuits électriques récurrents qui ont exactement les mêmes fonctions irréductibles de Fibonacci sont identifiés. Ces circuits inductifs-capacitifs (LC) récurrents sont très utilisés dans la modélisation des lignes de transmission ([21], [22], [25]); en biologie pour modéliser la dynamique des neurones [24] et en mécanique quantique pour modéliser les particules infiniment petites en utilisant les circuits LC récurrents [23].

Des systèmes mécaniques récurrents (masse-ressort) ont été aussi identifiés comme étant des systèmes de Fibonacci avec des fonctions de transfert irréductibles. Ces systèmes mécaniques sont aussi très utilisés dans la modélisation des phénomènes mécaniques des particules surtout en mécanique des fluides et en mécanique quantique pour pouvoir analyser le comportement de ces particules du point de vue des vibrations.

A.1.2.1 Structure de la thèse

Cette thèse est structurée en huit chapitres. Le premier chapitre est une introduction mettant en évidence la problématique de recherche dans la littérature des méthodes de réduction classiques. Le chapitre deux évalue deux méthodes de réduction très connues, l'intégral de l'erreur quadratique (ISE) et l'approximation pade ainsi que leurs approches de conception de contrôleurs. Le chapitre trois est dédié à la nouvelle approche de conception de contrôleurs des systèmes de types boîte noire ainsi qu'une comparaison du point de vue performance avec les deux méthodes classiques du chapitre deux. Le chapitre quatre est dédié aux systèmes irréductibles de Fibonacci. Le chapitre cinq est une application des circuits récurrents LC comme systèmes irréductibles de Fibonacci. Le chapitre six est une application des systèmes mécaniques récurrents masse-ressort qui sont aussi des systèmes irréductibles de Fibonacci. Le chapitre sept traite une autre application des circuits électriques récurrents LC inverse. Enfin, la conclusion générale de cette thèse sera au huitième chapitre.

A.2 Méthodes classiques de réduction

A.2.1 Intégral de l'erreur quadratique (ISE)

La méthode fondée sur l'intégral de l'erreur quadratique (ISE) présenté dans [3] et détaillée dans [4] est l'une des méthodes de réduction connues dans la littérature qui minimise l'erreur quadratique entre la réponse de sortie du système réel avec sa fonction de transfert bien déterminée et le modèle réduit inconnu avec une fonction de transfert de second ordre dont les coefficients sont déterminés en utilisant la théorie de l'ISE.

Définissons un système stable ayant une fonction de transfert d'ordre élevé n de la forme

$$F(s) = \frac{c_0 + c_1s + \dots + c_{n-1}s^{n-1}}{d_0 + d_1s + \dots + d_ns^n} \quad (\text{A.31})$$

Pour simplicité $c_0 = d_0$ le gain du système est 1.

Supposons $F(s)$ à p_1, p_2, \dots, p_n comme pôles qui peuvent être réels ou complexes. Le modèle de réduction est choisi pour être une fonction de transfert de second ordre, soit avec les pôles réels ou complexes (A.2).

$$G_R(s) = \frac{as + bc}{(s + b)(s + c)} \quad (\text{A.32})$$
$$G_C(s) = \frac{\alpha s + \beta^2 + \gamma^2}{s^2 + 2\beta s + \beta^2 + \gamma^2} = \frac{\alpha s + \beta^2 + \gamma^2}{(s + \beta + j\gamma)(s + \beta - j\gamma)}$$

Les paramètres $a, b, c, \alpha, \beta, \gamma$ de ces deux fonctions $G_R(s)$ et $G_C(s)$ qui sont normalement inconnus seront déterminés par la technique ISE. L'index de performance défini par ISE en (A.3) doit être au minimum pour pouvoir déterminer les paramètres du modèle réduit.

$$I_R = \int_0^\infty (g_R(t) - f(t))^2 dt = \int_0^\infty (g_R(t)^2 - 2g_R(t)f(t) + f(t)^2) dt$$

$$I_C = \int_0^\infty (g_C(t) - f(t))^2 dt = \int_0^\infty (g_C(t)^2 - 2g_C(t)f(t) + f(t)^2) dt$$
(A.3)

A.2.2 Approximation Pade

La technique d'approximation Pade est une autre méthode de réduction de fonctions de transfert d'ordre élevé en une réduite, de préférence de deuxième ordre afin de concevoir un contrôleur qui sera appliqué au système réel.

La technique de Pade repose essentiellement sur la réduction de toute fonction $f(x)$ comme étant un rapport de deux polynômes $P_N(x)$ and $Q_M(x)$ avec des degrés N et M respectifs, $R_{N,M}(x)$ sera défini comme un rapport entre ces deux polynômes.

$$R_{N,M}(x) = \frac{P_N(x)}{Q_M(x)} \quad \text{avec } a \leq x \leq b$$
(A.4)

Le but est de minimiser l'erreur entre la fonction $f(x)$ originale et $R_{N,M}(x)$. Nous allons définir les deux polynômes comme suit

$$P_N(x) = p_0 + p_1x + p_2x^2 + \dots + p_Nx^N$$

$$Q_M(x) = q_0 + q_1x + q_2x^2 + \dots + q_Mx^M \quad q_0 = 1$$
(A.5)

Dans le cas particulier $Q_M(x) = 1$, l'approximation Pade est simplement la série de Maclaurin-Taylor de $f(x)$.

Assumons la fonction $f(x)$ continue, analytique et ses dérivées sont aussi continues à l'origine $x = 0$. La série de Taylor-Maclaurin peut être écrite sous la forme :

$$f(x) = a_0 + a_1x + a_2x^2 + \dots + a_kx^k + \dots$$
(A.6)

$$f(x)Q_M(x) - P_N(x) = Z(x)$$

$$\left(\sum_{j=0}^{\infty} a_j x^j\right) \left(\sum_{j=0}^M q_j x^j\right) - \sum_{j=0}^N p_j x^j = \sum_{j=M+N+1}^{\infty} c_j x^j$$

De cette équation, on peut déterminer les coefficients q_j et p_j ce qui nous permet de trouver $R_{N,M}(x)$ dans (A.4).

A.2.3 Autres méthodes de réduction

La méthode des pôles dominants [1], regroupement de pôles [3], la méthode de réduction Big Bang Big Crunch [11] et beaucoup d'autres [14-18] ont le même objectif, trouver un système réduit identique avec la nécessité de connaître la fonction de transfert originale. L'objectif de toutes ces méthodes de réduction n'est pas de trouver un système identique réduit seulement, mais de concevoir un contrôleur en boucle fermée qui contrôle parfaitement le système réel de la même manière que le modèle approximatif.

A.3 Nouvelle approche de réduction

En mathématiques, il est bien connu que deux ensembles A et B sont identiques si :

$$\forall x \in A, x \in B \text{ et } \forall x \in B, x \in A$$

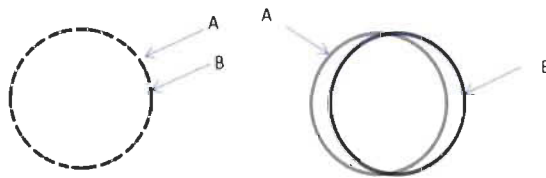


Figure A. 1: a) Ensembles identiques b) Ensembles similaires

Deux ensembles similaires sont présentés dans la figure A.1(b). Dans ce cas, tout élément appartenant à l'intersection de A et B doit d'abord être un élément de poids des deux ensembles A et B. Les éléments de faibles poids peuvent appartenir ou pas à cette intersection.

$$\left(\begin{array}{l} \forall x; x \text{ est élément de poids} \\ x \in A \cap B \end{array} \right) \Rightarrow A \text{ et } B \text{ sont similaires}$$

Dans chaque ensemble ou système, les éléments de poids doivent être bien définis afin de pouvoir conclure sur la similitude entre deux systèmes.

Les systèmes réels qui peuvent être mécanique, électrique, etc., seront définis par leurs éléments de poids qui les caractérisent. Dans le cas d'un système stable, les éléments de poids seront définis comme suit :

ψ_1 : Valeur d'entrée appliquée au système

ψ_2 : Valeur d'état d'équilibre du système

ψ_3 : Temps du régime transitoire estimé de la réponse de la sortie

ψ_4 : Réponse de sortie en régime transitoire

ψ_5 : Gain du système

ψ_6 : Temps de retard initial de la réponse de sortie

Deux systèmes sont semblables si tous les éléments de poids sont communs des deux systèmes, alors les deux systèmes seront dits similaires (figure A.2).

$$\left(\begin{array}{l} \forall x; x \text{ est élément de poids} \\ x \in A \cap B \end{array} \right) \Rightarrow A \text{ et } B \text{ sont similaires}$$

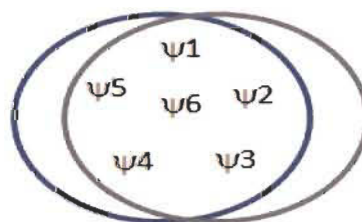


Figure A. 2: Deux systèmes similaires A et B

A.3.1 Application de l'approche des systèmes similaires aux boîtes noires

L'approche présentée est appliquée au système réel pris comme une boîte noire et ayant accès seulement à sa réponse d'entrée et de sortie.

Une valeur unitaire appliquée à l'entrée du système, la réponse sera enregistrée comme indiqué dans les figures A.3, A.4, A.5 qui sont les trois possibilités qu'un système stable peut avoir (réponse sans dépassement, réponse avec dépassement et sans oscillations et réponse avec dépassement et oscillations)

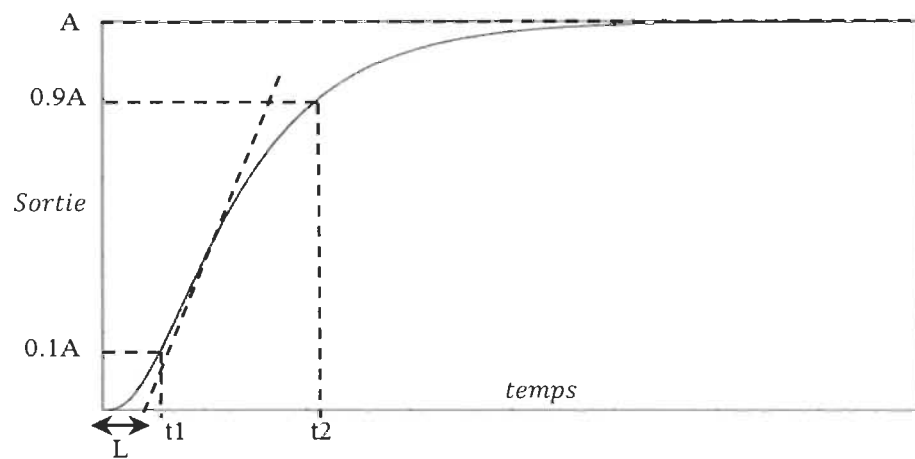


Figure A. 3: Réponse de sortie du système réel sans dépassement

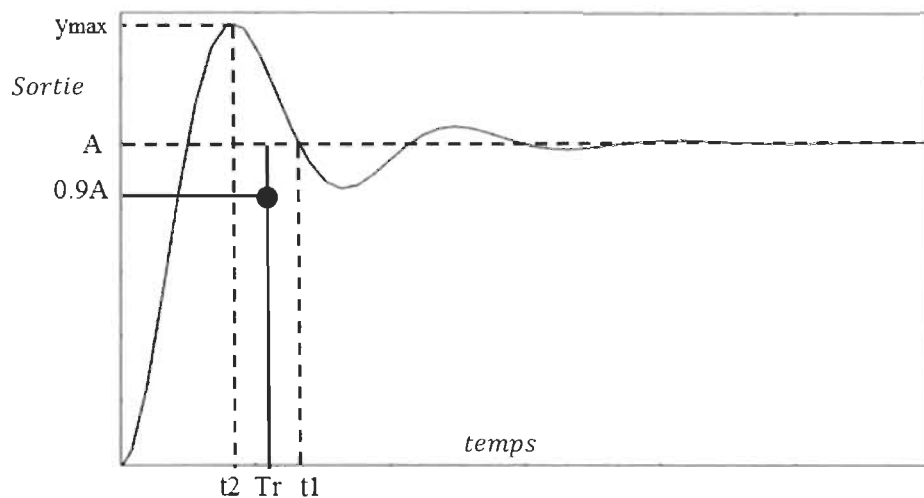


Figure A. 4: Réponse de sortie du système réel avec dépassement et oscillations.

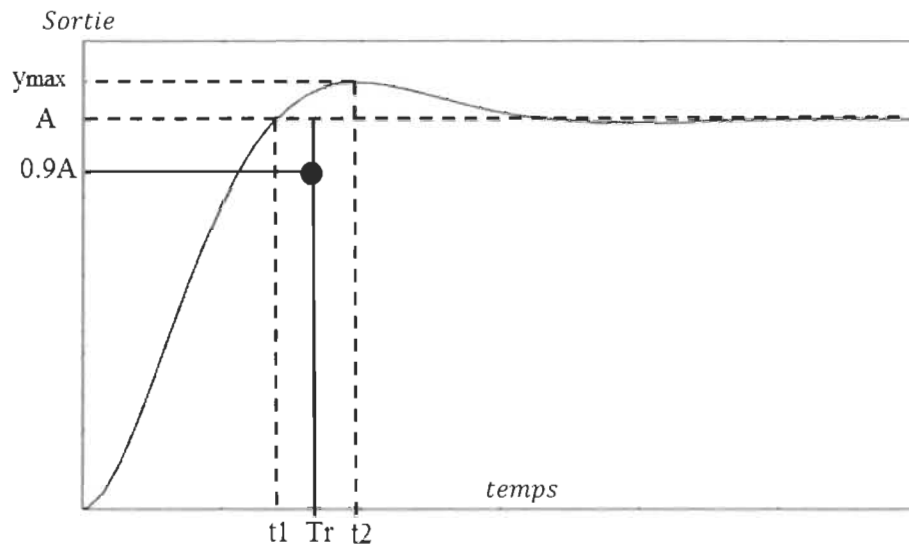


Figure A. 5: Réponse de sortie du système réel avec dépassement et sans oscillations.

Après l'enregistrement de la valeur d'entrée et la réponse de sortie, les éléments de poids du système en boîte noire peuvent être déterminés en utilisant l'approche des systèmes similaires pour approximer le système réel avec un système à déterminer réduit similaire de premier ordre. Ce système similaire doit avoir les mêmes éléments de poids. Un contrôleur sera conçu en se basant sur ce simple système de premier ordre, ensuite ce contrôleur sera appliqué au système réel en boîte noire.

A.4 Systèmes irréductibles et limitations des méthodes classiques

Des nouveaux systèmes appelés systèmes de Fibonacci sont introduits. Les fonctions de transfert de ces systèmes sont irréductibles, c'est-à-dire qu'ils ne peuvent être approximés ou réduits à un modèle d'ordre inférieur. Leurs fonctions de transfert de Fibonacci ont de multiples régimes stationnaires intermédiaires. Ces systèmes ne peuvent jamais être réduits en un système de second ordre en utilisant les méthodes classiques comme ISE et Pade ce qui montrera leurs limitations. L'emplacement de pôles de ces systèmes de Fibonacci suit la spirale connue de Fibonacci et leurs réponses en fréquence présentent de multiples fréquences de résonances et antirésonance bien ordonnées. Les coefficients de leurs fonctions de transfert

sont exactement ceux du triangle de Pascal et suivent une distribution bien spécifique en relation avec le nombre d'or $\Phi=1.618034$. Ces fonctions de transfert appelées *Fibonacci wave functions* ou *fonctions d'ondes de Fibonacci* (FWFs) sont créées avec un simple processus récurrent basé sur un simple système source de premier ordre (Figure A.6).

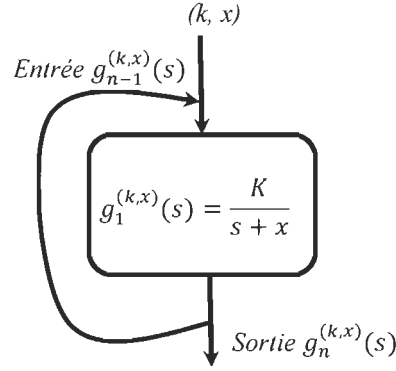


Figure A. 6: FWFs processus récurrent

La table A.1 présente les dénominateurs de toutes les fonctions de transfert suite au processus récurrent de la figure A.6 avec les facteurs (k,x).

Table A. 1: Coefficients des dénominateurs des FWFs avec (K, x)

$g_1^{(k,x)}(s) = \frac{K}{s + x}$	$g_1^{(k,x)}(s) = \frac{K}{\mathbf{1}s + \mathbf{1}x}$
$g_2^{(k,x)}(s) = \frac{K}{s + \frac{K}{s + x}}$	$g_2^{(k,x)}(s) = \frac{1Ks + 1Kx}{\mathbf{1}s^2 + \mathbf{1}xs + \mathbf{1}K}$
$g_3^{(k,x)}(s) = \frac{K}{s + \frac{K}{s + \frac{K}{s + x}}}$	$g_3^{(k,x)}(s) = \frac{1Ks^2 + 1Ksx + 1K^2}{\mathbf{1}s^3 + \mathbf{1}xs^2 + \mathbf{2}Ks + \mathbf{1}Kx}$
$g_4^{(k,x)}(s) = \frac{K}{s + \frac{K}{s + \frac{K}{s + \frac{K}{s + x}}}}$	$g_4^{(k,x)}(s) = \frac{1Ks^3 + 1Kxs^2 + 2K^2s + 1K^2x}{\mathbf{1}s^4 + \mathbf{1}xs^3 + \mathbf{3}Ks^2 + \mathbf{2}Kxs + \mathbf{1}K^2}$
$g_n^{(k,x)}(s) = \frac{K}{s + g_{n-1}^{(k,x)}(s)}$	$g_n^{(k,x)}(s) = \frac{Kden_{n-1}^{(k,x)}(s)}{sden_{n-1}^{(k,x)}(s) + num_{n-1}^{(k,x)}(s)}$

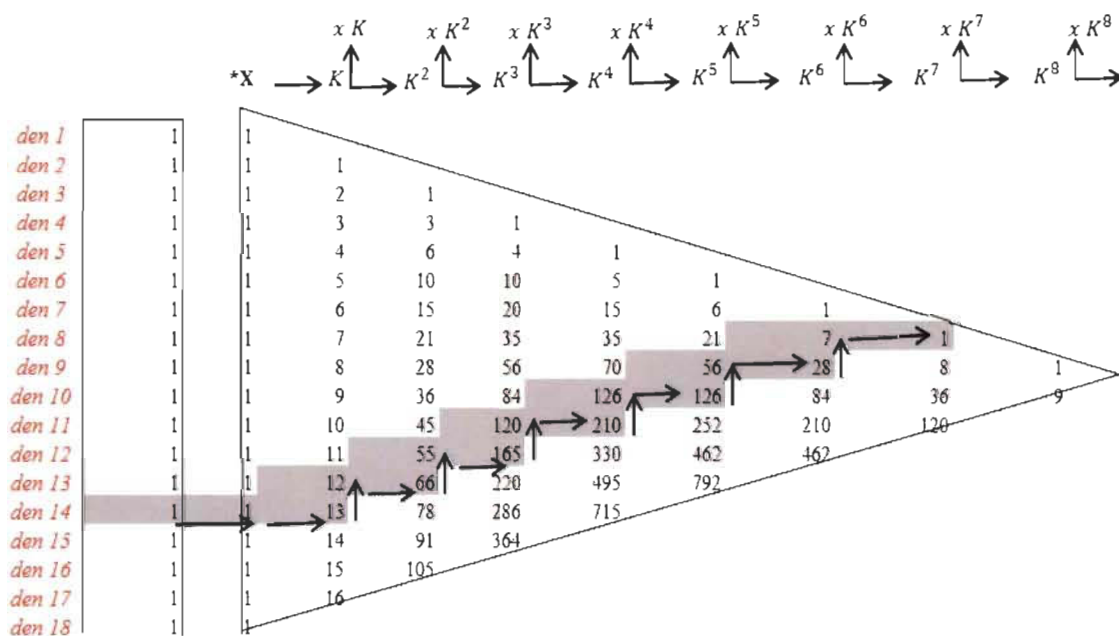
Dans le tableau A.1 les nombres surlignés en rouge sont exactement les coefficients des dénominateurs du cas $(K,x)=(1,1)$ multiplier par des coefficients.

$$x; K; xK; K^2; xK^2; K^3; xK^3; K^4; xK^4; etc$$

Tableau A.2 est la forme générale du triangle de Pascal avec les coefficients de multiplication à partir des valeurs de K et x .

- En se déplaçant horizontalement, le nombre de Fibonacci est multiplié par K^i .
- En se déplaçant verticalement, le nombre de Fibonacci est multiplié par xK^i .

Table A. 2: Triangle de Pascal pour les $den_n^{(k,x)}$ des fonctions de transfert de Fibonacci.



Ci-dessous un exemple de calcul de $g_{14}^{(K,x)}(s)$ utilisant la table A.2.

$$\begin{aligned} den_{13}^{(K,x)}(s) = & \mathbf{1}s^{13} + \mathbf{1}xs^{12} + \mathbf{12}Ks^{11} + \mathbf{11}Kxs^{10} + \mathbf{55}K^2s^9 + \mathbf{45}K^2xs^8 + \mathbf{120}K^3s^7 \\ & + \mathbf{84}K^3xs^6 + \mathbf{126}K^4s^5 + \mathbf{70}K^4xs^4 + \mathbf{56}K^5s^3 + \mathbf{21}K^5xs^2 + \mathbf{7}K^6s + \mathbf{1}K^6x \end{aligned}$$

$$\begin{aligned} den_{14}^{(K,x)}(s) = & \mathbf{1}s^{14} + \mathbf{1}xs^{13} + \mathbf{13}Ks^{12} + \mathbf{12}Kxs^{11} + \mathbf{66}K^2s^{10} + \mathbf{55}K^2xs^9 + \mathbf{165}K^3s^8 \\ & + \mathbf{120}K^3xs^7 + \mathbf{210}K^4s^6 + \mathbf{126}K^4xs^5 + \mathbf{126}K^5s^4 + \mathbf{56}K^5xs^3 + \mathbf{28}K^6s^2 \\ & + \mathbf{7}K^6xs + \mathbf{1}K^7 \end{aligned} \quad (\text{A.7})$$

$$g_{14}^{(1,1)}(s) = K \frac{den_{13}^{(K,x)}(s)}{den_{14}^{(K,x)}(s)}$$

L'approximation pade [8], [10], ISE [10] et beaucoup d'autres [11], [12], [13] ne peuvent pas réduire ces systèmes en un système de deuxième ou troisième ordre à cause de leurs régimes stationnaires intermédiaires. Ces caractéristiques rendent ces systèmes FWFs irréductibles.

A.5 Étude de cas et simulations

Les simulations de toutes les FWFs sont présentées ci-dessous dans deux études de cas pour mettre en évidence leur comportement très particulier ainsi que leurs irréductibilités.

Cas #1: $(K, x) = (1, 1)$;

Ces FWFs sont déterminées jusqu'à $g_{40}^{(1,1)}(s)$ en utilisant le triangle de pascal et Matlab. Figure A.7 ci-dessous.

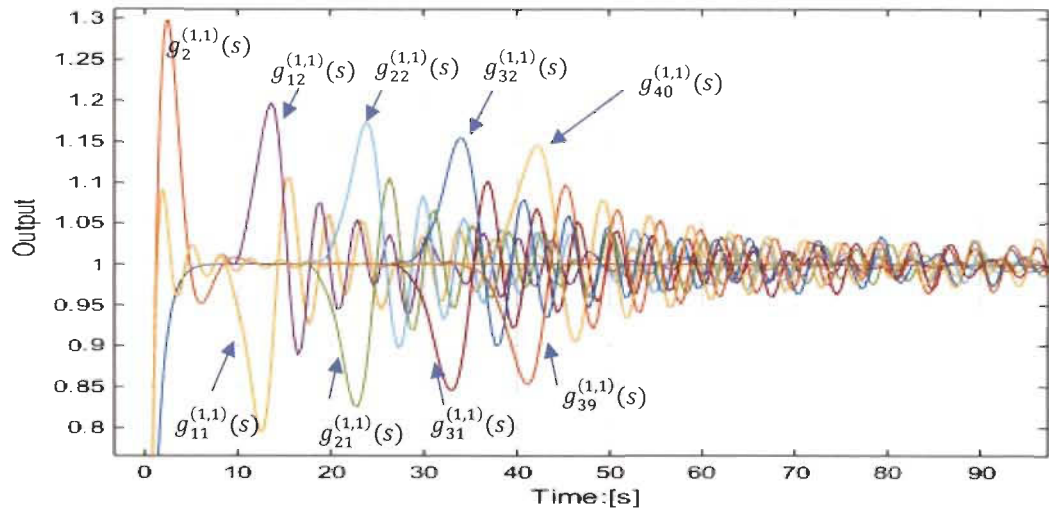


Figure A. 7: Réponses de sortie en boucle ouverte des FWFs $g_1^{(1,1)}(s)$, $g_{11}^{(1,1)}(s)$, $g_{21}^{(1,1)}(s)$, $g_{31}^{(1,1)}(s)$, $g_{39}^{(1,1)}(s)$, $g_2^{(1,1)}(s)$, $g_{12}^{(1,1)}(s)$, $g_{22}^{(1,1)}(s)$, $g_{32}^{(1,1)}(s)$, $g_{40}^{(1,1)}(s)$.

Cas #2: $(K, x) = (1, 4)$;

Ces FWFs sont déterminées jusqu'à $g_{40}^{(1,4)}(s)$ et illustrées sur la figure A.8 et A.9.

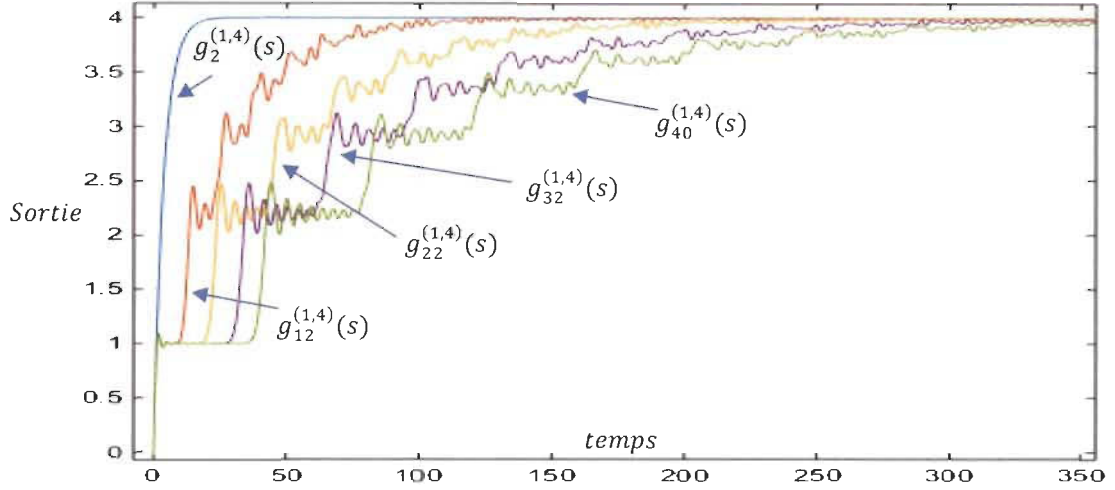


Figure A. 8: Réponses de sortie en boucle ouverte des FWFs $g_2^{(1,4)}(s)$, $g_{12}^{(1,4)}(s)$, $g_{22}^{(1,4)}(s)$, $g_{32}^{(1,4)}(s)$, $g_{40}^{(1,4)}(s)$.

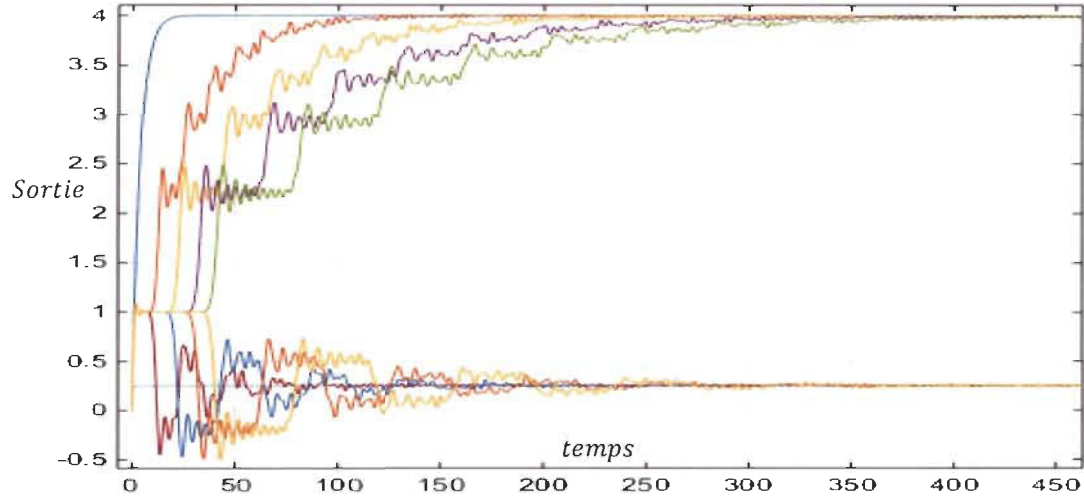


Figure A. 9: Réponses de sortie en boucle ouverte des FWFs $g_1^{(1,4)}(s)$, $g_{11}^{(1,4)}(s)$, $g_{21}^{(1,4)}(s)$, $g_{31}^{(1,4)}(s)$, $g_{39}^{(1,4)}(s)$, $g_2^{(1,4)}(s)$, $g_{12}^{(1,4)}(s)$, $g_{22}^{(1,4)}(s)$, $g_{32}^{(1,4)}(s)$, $g_{40}^{(1,4)}(s)$.

A.6 Nouvelle approche de conception de contrôleur appliquée aux systèmes de Fibonacci

Nous avons développé une nouvelle approche pour concevoir un contrôleur pour les systèmes de boîte noire ou systèmes de fonctions de transfert à haut degré. Cette nouvelle approche est appliquée à ces systèmes de Fibonacci sachant que leur source est une fonction de transfert

du premier ordre (figure A.6). Le contrôleur PI sera conçu selon ce système simple et s'appliquera à tous les systèmes de Fibonacci récurrents.

Connaissant la fonction de transfert du premier ordre, on peut déterminer directement les coefficients K_p et K_i du contrôleur proportionnel-intégral pour un coefficient d'amortissement ξ et une fréquence naturelle ω_n .

$$\begin{aligned} K_p &= \frac{2\xi\omega_n - x}{K} & ; & \quad K_i = \frac{\omega_n^2}{K} ; \\ K_p &= \frac{2\xi\omega_n - 2\xi_f\omega_f}{\omega_f^2} & ; & \quad K_i = \frac{\omega_n^2}{\omega_f^2} \end{aligned} \quad (A.8)$$

Cas #1: $(K, x) = (1, 1)$.

Le choix de ω_n doit être à l'extérieur des fréquences de résonances et antirésonances. Dans ce cas le choix de ω_n est 80 rad/s pour $\xi = 2$, les coefficients du contrôleur utilisant (A.8) sont:

$$K_p = 319 \quad ; \quad K_i = 6400 \quad (A.9)$$

Simulation a été réalisée en boucle fermée de tous les systèmes de FWFs. $g_1^{(1,1)}(s), \dots, g_{40}^{(1,1)}(s)$, les réponses de sorties sont exactement les mêmes pour tous les FWFs, figure A.10.

B. Case #2: $(K, x) = (1, 4)$.

Dans ce cas aussi, le choix de ω_n devrait être dehors les fréquences de résonance et antirésonance. Ce choix de ω_n est 500 rad/s pour un coefficient d'amortissement $\xi = 2$, les coefficients du contrôleur utilisant (A.8) sont:

$$K_p = 395 ; \quad K_i = 10000 \quad (\text{A.10})$$

La simulation a été réalisée en boucle fermée pour tous les systèmes de FWFs $g_1^{(1,4)}(s), \dots, g_{40}^{(1,4)}(s)$, les réponses de sorties sont exactement les mêmes pour tous les FWFs, figure A.10.

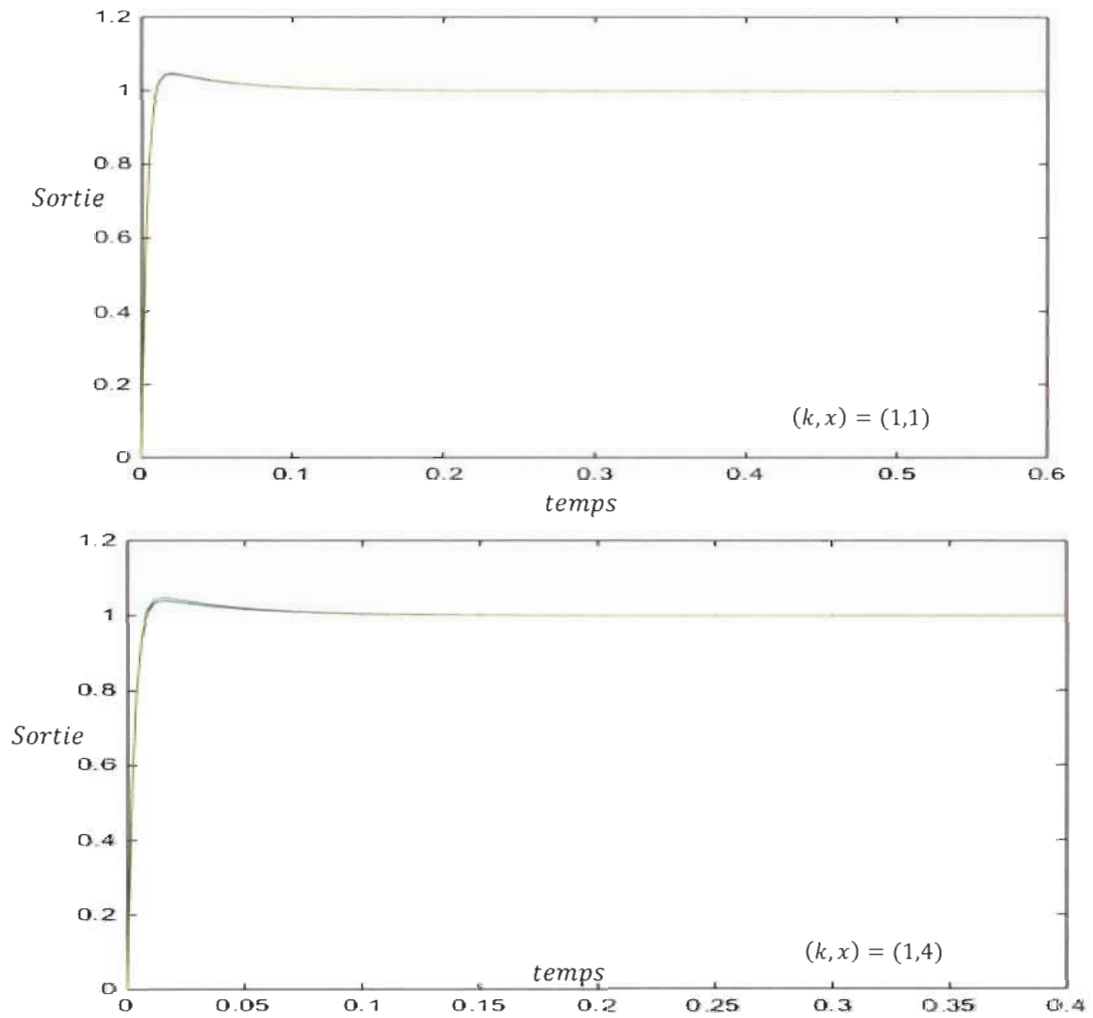


Figure A. 10: Réponses de sortie en boucle fermée des FWFs $g_1^{(1,1)}(s), \dots, g_{40}^{(1,1)}(s), g_1^{(1,4)}(s), \dots, g_{40}^{(1,4)}(s)$.

A.7 Systèmes de Fibonacci appliqués aux Systèmes électriques et mécaniques

A.7.1 Réseau récurrent LC de Fibonacci

En tant qu'application, réseau récurrent LC va s'inspirer de ces FWFs et il servira à modéliser et analyser l'impédance ou admittance des lignes de transmission sans perte, ainsi que le comportement de ces lignes de transmission dans le cas de la charge infinie (circuit ouvert) ou nulle (circuit fermée). Les coefficients du nième ordre du dénominateur et du numérateur de la fonction d'onde de Fibonacci d'un réseau LC sont facilement déterminés à partir de la nouvelle forme générale du triangle de Pascal (Table A.2). Figure A.11 et A.12 montrent le circuit électrique de Fibonacci RC-FEC avec ordre pair et impair, leurs fonctions de transfert de Fibonacci sont illustrées dans la table A.3 à partir de la première fonction source de premier ordre 1.

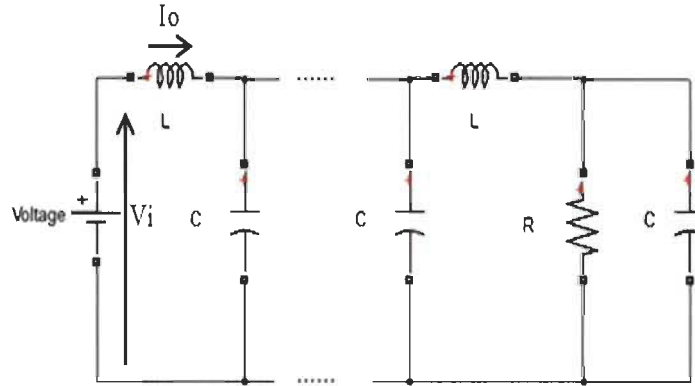


Figure A. 11: n^{ieme} ordre pair RC-FEC

La fonction d'onde de Fibonacci FWF de ce circuit est.

$$\left(\frac{I_o}{CV_i}\right)_n^{(K,x_c)} = \frac{K}{s + g_{n-1}^{(K,x_c)}(s)} = g_n^{(K,x_c)}(s) \quad (A.9)$$

Pour un ordre n impair, la fonction d'onde est.

$$\left(\frac{V_o}{Ll_i}\right)_n^{(K,x_c)} = \frac{K}{s + g_{n-1}^{(K,x_c)}(s)} = g_n^{(K,x_c)}(s) \quad (\text{A.10})$$

$$K = \frac{1}{LC} \quad \text{et} \quad x_c = \frac{1}{RC}$$

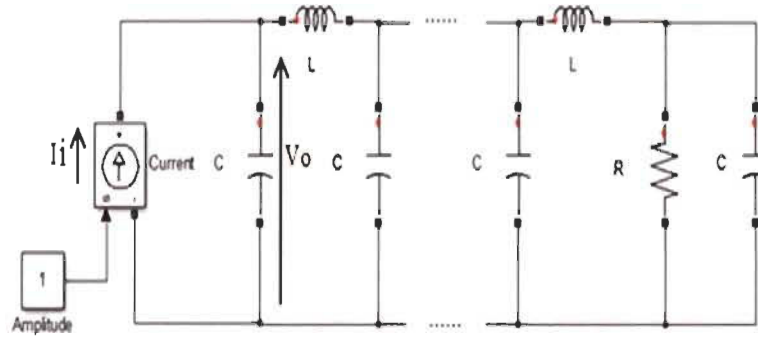


Figure A. 12: n^{ieme} ordre impair RC-FEC

Table A. 3: Fonctions d'onde de Fibonacci RC-FEC

$\left(\frac{V_o}{Ll_i}\right)_1^{(K,x_c)} = g_1^{(K,x_c)} = \frac{K}{s + x_c}$	$\left(\frac{V_o}{Ll_i}\right)_1^{(K,x_c)} = g_1^{(K,x_c)} = \frac{K}{1s + 1x_c}$
$\left(\frac{I_o}{CV_i}\right)_2^{(K,x_c)} = g_2^{(K,x_c)} = \frac{K}{s + \frac{K}{s + x_c}}$	$\left(\frac{I_o}{CV_i}\right)_2^{(K,x_c)} = g_2^{(K,x_c)} = \frac{Ks + Kx_c}{1s^2 + 1x_cs + 1K}$
$\left(\frac{V_o}{Ll_i}\right)_3^{(K,x_c)} = g_3^{(K,x_c)} = \frac{K}{s + \frac{K}{s + \frac{K}{s + x_c}}}$	$\left(\frac{V_o}{Ll_i}\right)_3^{(K,x_c)} = g_3^{(K,x_c)} = \frac{Ks^2 + Ksx_c + K^2}{1s^3 + 1x_cs^2 + 2Ks + 1Kx_c}$
$\left(\frac{I_o}{CV_i}\right)_4^{(K,x_c)} = g_4^{(K,x_c)} = \frac{K}{s + \frac{K}{s + \frac{K}{s + \frac{K}{s + x_c}}}}$	$\left(\frac{I_o}{CV_i}\right)_4^{(K,x_c)} = g_4^{(K,x_c)} = \frac{Ks^3 + Kx_cs^2 + 2K^2s + K^2x_c}{1s^4 + 1x_cs^3 + 3Ks^2 + 2Kx_cs + 1K^2}$
$\left(\frac{I_o}{CV_i}\right)_n^{(K,x_c)} = g_n^{(K,x_c)} = \frac{K}{s + g_{n-1}^{(K,x_c)}(s)}$ $n \text{ even}$ $\left(\frac{V_o}{Ll_i}\right)_n^{(K,x_c)} = g_n^{(K,x_c)} = \frac{K}{s + g_{n-1}^{(K,x_c)}(s)}$ $n \text{ odd}$	$g_n^{(K,x_c)}(s) = \frac{Kden_{n-1}^{(K,x_c)}(s)}{sden_{n-1}^{(K,x_c)}(s) + num_{n-1}^{(K,x_c)}(s)}$ $g_n^{(K,x_c)}(s) = \frac{Kden_{n-1}^{(K,x_c)}(s)}{den_n^{(K,x_c)}(s)}$

A.7.2 Chaîne de masse-ressort de Fibonacci

Les chaîne de masse-ressort de Fibonacci (FSMC) est une autre application dont les fonctions de transfert sont exactement les mêmes que celles des fonctions d'ondes de Fibonacci. La chaîne de masse-ressort de Fibonacci (FSMC) peut être utilisée pour modéliser l'interaction entre de petites particules dans la mécanique quantique, mécanique des fluides à l'aide de ce nouveau modèle général FSMC.

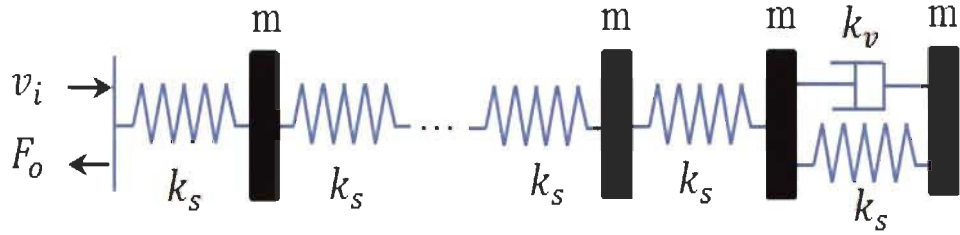


Figure A. 13: n^{ieme} ordre pair de FSMC

La fonction d'onde de Fibonacci sera :

$$\left(\frac{F_o}{mv_i}\right)_n^{(k,x_m)} = \frac{K}{s + g_{(n-1)}(s)} = g_n^{(k,x_m)}(s) \quad (A.11)$$

$$K = \frac{k_s}{m} \quad et \quad x_m = \frac{k_v}{m}$$

Dans le cas où le circuit est d'ordre n avec n impair, la fonction d'onde de Fibonacci sera.

$$\left(\frac{k_s v_o}{F_i}\right)_n^{(k,x_m)} = \frac{K}{s + g_{(n-1)}(s)} = g_n^{(k,x_m)}(s) \quad (A.12)$$

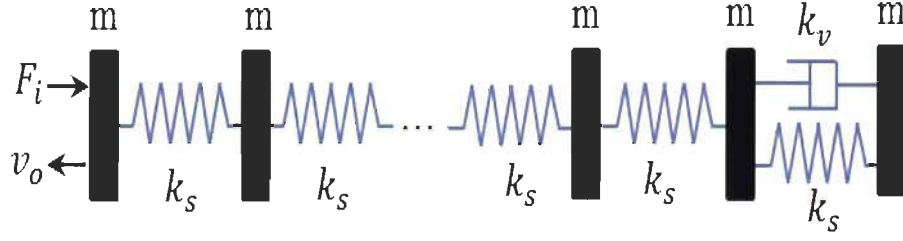


Figure A. 14: n^{ieme} ordre impair de FSMC

Le tableau ci-dessous illustre tous les ordres des FWFs de FSMC.

Table A. 4: Fonctions d'onde de Fibonacci de la chaine FSMC

$(\frac{k_s v_o}{F_i})_1^{(k, x_m)} = g_1^{(k, x_m)}(s) = \frac{K}{s + x_m}$	$(\frac{k_s v_o}{F_i})_1^{(k, x_m)} = g_1^{(k, x_m)}(s) = \frac{K}{1s + 1x_m}$
$(\frac{F_o}{m v_i})_2^{(k, x_m)} = g_2^{(k, x_m)}(s) = \frac{K}{s + \frac{K}{s + x_m}}$	$(\frac{F_o}{m v_i})_2^{(k, x_m)} = g_2^{(k, x_m)}(s) = \frac{Ks + Kx_m}{1s^2 + 1x_m s + 1K}$
$(\frac{k_s v_o}{F_i})_3^{(k, x_m)} = g_3^{(k, x_m)}(s) = \frac{K}{s + \frac{K}{s + \frac{K}{s + x_m}}}$	$(\frac{k_s v_o}{F_i})_3^{(k, x_m)} = g_3^{(k, x_m)}(s) = \frac{Ks^2 + Ks x_m + K^2}{1s^3 + 1x_m s^2 + 2Ks + 1K x_m}$
$(\frac{F_o}{m v_i})_4^{(k, x_m)} = g_4^{(k, x_m)}(s) = \frac{K}{s + \frac{K}{s + \frac{K}{s + \frac{K}{s + x_m}}}}$	$(\frac{F_o}{m v_i})_4^{(k, x_m)} = g_4^{(k, x_m)}(s) = \frac{Ks^3 + Kx_m s^2 + 2K^2 s + K^2 x_m}{1s^4 + 1x_m s^3 + 3Ks^2 + 2Kx_m s + 1K^2}$
$(\frac{F_o}{m v_i})_n^{(k, x_m)} = g_n^{(k, x_m)}(s) = \frac{K}{s + g_{n-1}^{(k, x_m)}(s)}$ $n \text{ even}$ $(\frac{k_s v_o}{F_i})_n^{(k, x_m)} = g_n^{(k, x_m)}(s) = \frac{K}{s + g_{n-1}^{(k, x_m)}(s)}$ $n \text{ odd}$	$g_n^{(k, x_m)}(s) = \frac{K den_{n-1}^{(k, x_m)}(s)}{s den_{n-1}^{(k, x_m)}(s) + num_{n-1}^{(k, x_m)}(s)}$ $g_n^{(k, x_m)}(s) = \frac{K den_{n-1}^{(k, x_m)}(s)}{den_n^{(k, x_m)}(s)}$

A.7.3 Réseau récursif inverse LC de Fibonacci

Une autre application de circuits électriques appelée circuits électriques inverses de Fibonacci (iFECs) est introduite pour modéliser parfaitement le réseau récursif LC inverse. Ces iFECs peuvent être utilisées pour modéliser le réseau piézoélectrique [3], les fonctions de transfert de ces circuits sont parfaitement déterminées en utilisant les fonctions inverse d'onde de Fibonacci.

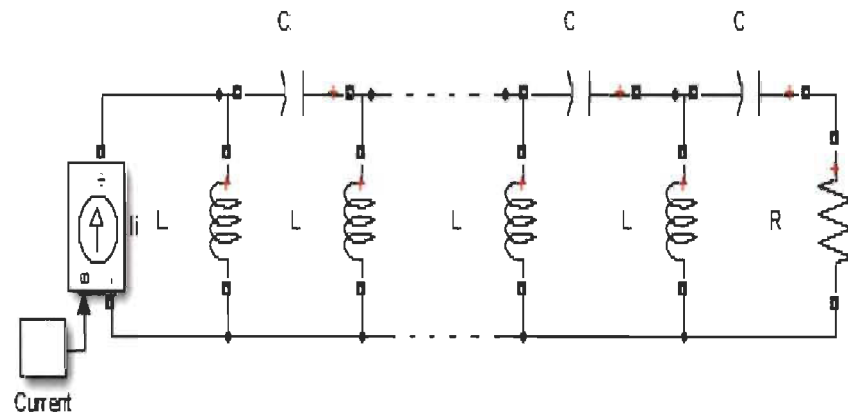


Figure A. 15: n^{ieme} ordre pair de iRC-FEC

L'iFWF de ce circuit est.

$$\left(\frac{CV_o}{I_i}\right)_{-n}^{(K,x_c)} = \frac{K}{s^{-1} + g_{-(n-1)}^{(K,x_c)}(s)} = g_{-n}^{(K,x_c)}(s) \quad (A.13)$$

$$K = LC \quad et \quad x_c = RC$$

Pour un ordre n impair, la fonction d'onde est.

$$\left(\frac{LI_o}{V_i}\right)_{-n}^{(K,x_c)} = \frac{K}{s^{-1} + g_{-(n-1)}^{(K,x_c)}(s)} = g_{-n}^{(K,x_c)}(s) \quad (A.14)$$

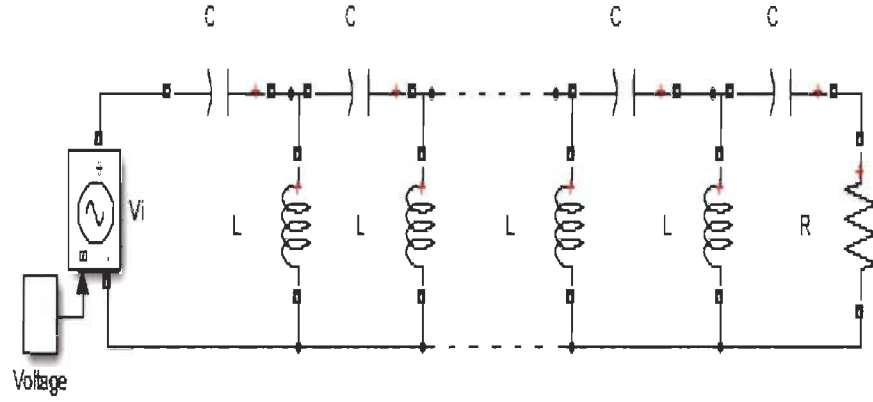


Figure A. 16: n^{ieme} ordre impair de iRC-FEC

Le tableau A.5 présente toutes les fonctions d'onde de Fibonacci inverse du iRC-FEC.

Table A. 5: Fonctions d'onde de Fibonacci du iRC-FEC

$\left(\frac{LI_o}{V_i}\right)_{-1}^{(K,x_c)} = g_{-1}^{(K,x_c)} = \frac{K}{s^{-1} + x_c}$	$\left(\frac{LI_o}{V_i}\right)_{-1}^{(K,x_c)} = g_{-1}^{(K,x_c)} = \frac{K}{1s^{-1} + 1x_c}$
$\left(\frac{CV_o}{I_i}\right)_{-2}^{(K,x_c)} = g_2^{(K,x_c)} = \frac{K}{s^{-1} + \frac{K}{s^{-1} + x_c}}$	$\left(\frac{CV_o}{I_i}\right)_{-2}^{(K,x_c)} = g_2^{(K,x_c)} = \frac{Ks^{-1} + Kx_c}{1s^{-2} + 1x_cs^{-1} + 1K}$
$\left(\frac{LI_o}{V_i}\right)_{-3}^{(K,x_c)} = g_3^{(K,x_c)}$ $= \frac{K}{s^{-1} + \frac{K}{s^{-1} + \frac{K}{s^{-1} + x_c}}}$	$\left(\frac{LI_o}{V_i}\right)_{-3}^{(K,x_c)} = g_3^{(K,x_c)}$ $= \frac{Ks^{-2} + Kx_cs^{-1} + K^2}{1s^{-3} + 1x_cs^{-2} + 2Ks^{-1} + 1Kx_c}$
$\left(\frac{CV_o}{I_i}\right)_{-4}^{(K,x_c)} = g_{-4}^{(K,x_c)}$ $= \frac{K}{s^{-1} + \frac{K}{s^{-1} + \frac{K}{s^{-1} + \frac{K}{s^{-1} + x_c}}}}$	$\left(\frac{CV_o}{I_i}\right)_{-4}^{(K,x_c)} = g_{-4}^{(K,x_c)}$ $= \frac{Ks^{-3} + Kx_cs^{-2} + 2K^2s^{-1} + K^2x_c}{1s^{-4} + 1x_cs^{-3} + 3Ks^{-2} + 2Kx_cs^{-1} + 1K^2}$
$\left(\frac{CV_o}{I_i}\right)_{-n}^{(K,x_c)} = g_{-n}^{(K,x_c)} = \frac{K}{s^{-1} + g_{-(n-1)}^{(K,x_c)}(s)}$ $n \text{ even}$	$g_{-n}^{(K,x_c)}(s) = \frac{Kden_{-(n-1)}^{(K,x_c)}(s)}{s^{-1}den_{-(n-1)}^{(K,x_c)}(s) + num_{-(n-1)}^{(K,x_c)}(s)}$
$\left(\frac{LI_o}{V_i}\right)_{-n}^{(K,x_c)} = g_{-n}^{(K,x_c)} = \frac{K}{s^{-1} + g_{-(n-1)}^{(K,x_c)}(s)}$ $n \text{ odd}$	$g_{-n}^{(K,x_c)}(s) = \frac{Kden_{-(n-1)}^{(K,x_c)}(s)}{den_{-n}^{(K,x_c)}(s)}$

A.8 Conclusion

Cette recherche présente une nouvelle méthode de réduction basée sur l'approximation des systèmes de types boîte noire, en utilisant le concept des systèmes similaires. Un système similaire de premier ordre sera déterminé pour n'importe quel système de type boîte noire. Ce concept a été introduit pour la première fois et a pour but d'éviter toutes les équations mathématiques nécessaires pour modéliser les systèmes complexes. Leurs fonctions de transfert qui sont nécessaires pour les méthodes de réduction classiques ne sont pas requises par la nouvelle méthode basée sur la similitude des systèmes. Ces méthodes de réduction utilisent différentes théories mathématiques pour réduire des systèmes complexes en un système réduit identique pour pouvoir mettre au point un contrôleur.

La nouvelle approche de réduction proposée, repose principalement sur les éléments de poids prédéfinis qui caractérisent le système réel et similaire. Ces éléments de poids sont déterminés uniquement à partir de la réponse de sortie du système complexe.

Les résultats de simulation en boucle fermée montrent les performances de cette nouvelle méthode de réduction. Le fait que les systèmes réels et approximatifs sont similaires dans leurs éléments poids significatifs, permet de concevoir un contrôleur basé sur ce système de premier ordre. La conception et la mise en œuvre d'un contrôleur PI en utilisant cette approche et appliquée au système réel donne des résultats très satisfaisant. Le contrôleur PI a été choisi en raison de sa simplicité dans sa conception et son implémentation.

Des systèmes spécifiques appelés systèmes de Fibonacci ayant un degré élevé de leurs fonctions de transfert ont été introduits à partir d'une fonction de transfert de premier ordre. Ces fonctions appelées fonctions d'onde de Fibonacci (FWFs) ont des comportements intéressants et leurs fonctions de transfert sont irréductibles et ne peuvent pas être réduit en

un système équivalent de second ordre identique. Ces systèmes sont une limitation des méthodes de réduction classiques.

L'application d'une méthode de réduction dans la littérature comme la méthode d'approximation $pade$, ISE ou d'autres ne peuvent pas réduire ces systèmes FWFs. Par contre la nouvelle approche nous permet toujours de concevoir un contrôleur à partir de la fonction de premier ordre source. Ce contrôleur est alors appliqué à tous les systèmes récurrents de Fibonacci avec des résultats très satisfaisants.

Dans cette recherche, un modèle général complet du circuit récurrent LC a été mis au point avec des fonctions d'onde de Fibonacci (FWFs). L'importance du circuit récursif LC provient de son application que l'on retrouve dans la littérature comme modèle de lignes de transmission sans perte, le modèle de propagation du son dans l'oreille et en mécanique quantique pour comprendre l'interaction entre les particules.

Le réseau récurrent LC inverse a été aussi introduit avec son modèle général à l'aide des fonctions d'onde inverses de Fibonacci (iFWF). Ces fonctions d'ondes peuvent être déterminées facilement à partir de la forme générale de triangle de Pascal. L'impédance ou admittance d'entrée peut aussi être trouvée dans les trois cas (circuit avec charge, sans charge ou avec charge infinie).

La chaîne de masse-ressort de Fibonacci (FSMC) a été également introduite et modélisée par ces FWFs théoriques. Le FSMC est très important, grâce à son utilisation en mécanique quantique et mécanique des fluides pour analyser le comportement des particules du point de vue vibration.

Ces trois applications ont la particularité d'avoir les mêmes fonctions d'onde de Fibonacci qui ont la particularité d'être irréductibles et par conséquent, elles sont des exemples pratiques de limitations des méthodes de réduction classiques.